Exchange Representations in Kohn–Sham Theory

Andrew M. Teale

2006

Submitted in conformity with the requirements
for the degree of Doctor of Philosophy

Declaration

The material contained within this thesis has not previously been submitted for a degree at the University of Durham or any other university. The research reported within this thesis has been conducted by the author unless indicated otherwise.

Copyright Notice

Abstract

Exchange Representations in Kohn–Sham Theory

Kohn–Sham density functional theory (DFT) is the most widely used method in quantum chemistry. It has the potential to provide accurate results at low computational cost. The quality of a DFT calculation is determined by the exchange–correlation energy functional. Hybrid functionals, which contain a fraction of exact orbital exchange, are extensively used due to their accuracy in a variety of applications. However, as commonly implemented, these functionals are outside the Kohn–Sham scheme, since the exchange operator is not a local multiplicative potential. In order to handle orbital dependent functionals correctly, schemes which determine a local multiplicative potential must be employed. The implementation and application of several such methods is the focus of this thesis.

In Chapter 1 we outline the Hartree–Fock scheme, which defines the exchange energy, and overview wavefunction based procedures that recover correlation energy. Alternative theories based on the electron density are then considered and the foundations of modern DFT are reviewed. The formalism of the optimized effective potential (OEP) method is introduced, which is the rigorous way to handle orbital dependent functionals.

A number of approximations to the exchange only OEP method are outlined in Chapter 2 and their implementation is described. The methods are applied to the calculation of NMR shielding constants, highlighting differences between the approximations; their use in the construction of multiplicative hybrid functionals is also considered. In Chapter 3 these approximations are further investigated in the calculation of excited states and structural perturbations.

In Chapter 4, the theory and implementation of a direct optimization procedure to determine OEPs is outlined, along with an implementation of the constrained search procedure, which allows the determination of the Kohn–Sham exchange–correlation potential from any input density. Chapter 5 compares the performance of the approximate exchange potentials with those of OEP, highlighting the presence of correlated character in some of the approximate methods.

The OEP implementation is extended to include hybrid exchange–correlation functionals in Chapter 6. The performance of these methods for the calculation of NMR shielding constants, rotational g tensors and transition metal NMR chemical shifts is investigated. In all cases, substantial improvements over conventional results are obtained. In Chapter 7 DFT is used to investigate an interaction of relevance in organic chemistry. Concluding remarks are given in Chapter 8.

Acknowledgements

I would like to express my sincere gratitude to David Tozer for his support and encouragement throughout my PhD. His entertaining company and endless enthusiasm have helped make the past three years exceptionally enjoyable. Special thanks also goes to Tom Keal and Michael Peach for always being willing to put aside their own work and offer help and advice.

It has also been my good fortune to collaborate with a number of people; I am grateful to Ola Lutnæs, Aron Cohen, David O'Hagan for valuable discussions, and also to Trygve Helgaker for his kind invitation to attend the Sostrup summerschool in Denmark.

Having spent the last seven years in Durham I have made a great many friends and I must especially offer my thanks to JF, RRT, JAG, MSE, MJP, JDMcG, NJV, NC, TS and RLD. All of them have provided entertaining company and helped keep the author happy and motivated throughout the writing of this thesis.

"...the only people for me are the mad ones, the ones who are mad to live, mad to talk, mad to be saved, desirous of everything at the same time, the ones who never yawn or say a commonplace thing, but burn, burn, burn, like fabulous yellow roman candles exploding like spiders across the stars and in the middle you see the blue centerlight pop and everybody goes 'Awww!' " - Jack Kerouac, *On the Road*

For my friends and family

Contents

Selected Definitions

Below is a summary of abbreviations pertinent to the work presented in this thesis.

AC	Asymptotic correction
AN	Approximate Newton optimization scheme
B3LYP	Becke-3-Lee–Yang–Parr hybrid functional
B97-*N*	Becke 1997 hybrid exchange-correlation functionals
BD	Brueckner-Doubles coupled cluster method
BFGS	Broyden-Fletcher-Goldfarb-Shanno optimization procedure
BLYP	Becke 1988 exchange functional with Lee–Yang–Parr correlation
CC	Coupled Cluster method
CEDA	Common-Energy-Denominator Approximation
CI	Configuration Interaction method
GIAO	Gauge Including Atomic Orbitals
HCTH	Hamprecht–Cohen–Tozer–Handy exchange–correlation functional
HK	Hohenberg–Kohn
IGLO	Individual Gauges for Localized orbitals
KLI	Krieger–Li–Iafrate exchange approximation
KT*N*	Keal–Tozer exchange–correlation functionals
LDA	Local Density approximation
LHF	Localized Hartree–Fock method
LORG	Localized Orbitals / Localized Origins
MKS	Multiplicative Kohn–Sham method
MP2	Second order Møller–Plesset perturbation theory
OEP	Optimized effective potential approach
PBE0	Perdew–Burke–Ernzerhof hybrid exchange–correlation functional
RKR	Rydberg–Klein–Rees procedure
RPA	Random Phase approximation
TDDFT	Time Dependent Density Functional Theory
TKLI	Transformation Krieger–Li–Iafrate method
TLHF	Transformation Localized Hartree–Fock method
TSVD	Truncated Singular Value Decomposition
WY	Wu–Yang Constrained search approach
ZMP	Zhao–Morrison–Parr constrained search approach
ZPVC	Zero-Point Vibrational Corrections

Chapter 1

Introduction and Background

In this chapter many key concepts relevant to the work in this thesis are introduced. The techniques necessary to approximately solve the time-independent Schrödinger equation for molecular systems are outlined. The wavefunction-based Hartree–Fock theory is briefly reviewed before describing methods for introducing the electron correlation missing in the Hartree–Fock scheme. Kohn–Sham density functional theory is introduced as a formally exact, density based, computationally efficient, alternative. The approximations required for its practical application to molecular systems are discussed with special reference to the exchange–correlation representation. The chapter concludes with an outline of the optimized effective potential (OEP) method, which is one of the central topics of this thesis.

1.1 The Schrödinger Equation

In 1926 Schrödinger presented his non-relativistic wave equation [1–6],

$$\hat{H}\Psi = i\hbar\frac{\partial\Psi}{\partial t} \tag{1.1.1}$$

This equation provides a mathematical model powerful enough to describe all non-relativistic chemical systems. The equation was not derived but rather postulated from a consideration of the classical Hamilton–Jacobi equation. The operator $\hat{H}$ is the Hamiltonian operator and is the sum of operators corresponding to all energy contributions in the system. For a molecule with N electrons and M nuclei the Hamiltonian, in atomic units, may be written as

$$\hat{H} = -\frac{1}{2}\sum_{i=1}^{N}\nabla_i^2 - \frac{1}{2}\sum_{A=1}^{M}\frac{1}{M_A}\nabla_A^2 - \sum_{i=1}^{N}\sum_{A=1}^{M}\frac{Z_A}{r_{iA}} + \sum_{i=1}^{N}\sum_{j>i}^{N}\frac{1}{r_{ij}} + \sum_{A=1}^{M}\sum_{B>A}^{M}\frac{Z_A Z_B}{R_{AB}} \tag{1.1.2}$$

The first two operators describe the kinetic energy contributions of the electrons and nuclei, respectively. The third term describes the electron-nuclear Coulombic interactions and the last two describe the electron-electron and nuclear-nuclear repulsion. The masses of the nuclei are M_A and their atomic numbers are Z_A; the nuclear-nuclear separations are described by R and the inter-electronic distances by r.

The wavefunction Ψ which satisfies the Schrödinger equation must be everywhere single valued, finite and continuously differentiable up to second order. The wavefunction is a complex quantity, depending on the spatial and spin coordinates of all the particles in the system, as well as time. Whilst the wavefunction itself has no physical meaning, the Born interpretation [7] shows that its square is a probability density, with the caveat that the wavefunction is normalised. This interpretation leads to the constraint for finite systems that the wavefunction must be square integrable

$$\int |\Psi|^2 \, d\tau < \infty \tag{1.1.3}$$

since there must be a finite probability of finding the particles somewhere in space. This also implies that far from the system Ψ approaches zero.

The time-dependent form of the Schrödinger Eqn. (1.1.1) with a Hamiltonian of the form of Eqn. (1.1.2) may be simplified by a separation of variables since the Hamiltonian is independent of time. Applying this separation the wavefunction may be written as

$$\Psi(t) = \Psi e^{-iEt/\hbar} \tag{1.1.4}$$

and the time-independent Schrödinger equation is

$$\hat{H}\Psi = E\Psi \tag{1.1.5}$$

For a given $\hat{H}$ there may be an infinite number of Ψ's, each with their corresponding eigenvalues, E; the eigenstate with lowest energy, E_0, is described by the groundstate wavefunction, Ψ_0.

In choosing the Schrödinger equation as the mathematical model a number of approximations have already been introduced. By negelecting relativity the concept of electron spin does not arise (a deficiency which is corrected by the Dirac equation [8, 9]). However, for any reasonable theoretical description of a molecular system spin must be included. In order to achieve this for the electrons without explicitly considering relativity, spin is introduced as a new degree of freedom with two states. The Pauli principle [10] states that the wavefunction must be symmetric under the exchange of two identical bosons and antisymmetric under the exchange of two identical fermions.

The introduction of spin also leads to terms in the Hamiltonian of the system that describe the interactions of the spin of the particles with the magnetic moments due to the orbital motion of the electrons. These terms are required if spin orbit coupling and hyperfine splitting effects are to be considered. However in general these terms are not included. The Schrödinger equation is extremely difficult to solve for all but the simplest systems. In order to attempt its solution for molecular systems a number of further approximations must be made.

1.2 The Born–Oppenheimer Approximation

In 1927 Born and Oppenheimer [11] introduced a method to make possible the approximate solution of the non-relativistic time-independent Schrödinger equation. Their approximation allowed the separation of the Schrödinger Eqn. (1.1.5) into nuclear and electronic parts. The complete solution to the equation is then obtained by solving the electronic equation at fixed nuclear geometries and inserting the resulting potential into the nuclear equation. The electronic Schrödinger equation may be written as

$$\hat{H}_{\mathrm{e}}(\mathbf{R})\Psi_i(\mathbf{R},\mathbf{r}) = E_i(\mathbf{R})\Psi_i(\mathbf{R},\mathbf{r}) \tag{1.2.1}$$

where Ψ_i is now the electronic wavefunction and the electronic Hamiltonian is

$$\hat{H}_{\mathrm{e}} = -\frac{1}{2}\sum_{i=1}^{N}\nabla_i^2 - \sum_{i=1}^{N}\sum_{A=1}^{M}\frac{Z_A}{r_{iA}} + \sum_{i=1}^{N}\sum_{j>i}^{N}\frac{1}{r_{ij}} \tag{1.2.2}$$

The solutions to Eqn. (1.2.1) enter the nuclear Schrödinger equation

$$\left(-\frac{1}{2}\sum_{A=1}^{M}\frac{1}{M_A}\nabla_A^2 + \hat{V}_j(\mathbf{R})\right)\Psi_{nj}(\mathbf{R}) = E_{\mathrm{total}}\Psi_{nj}(\mathbf{R}) \tag{1.2.3}$$

in the form of the potential energy surface $V_j(\mathbf{R})$ constructed from the electronic energy E_j and the nuclear-nuclear repulsion energy at each geometry. In the Born–Oppenheimer approximation the total wavefunction may be considered as consisting of two parts, one which describes the nuclear motion and a second which describes the motion of the electrons as though the nuclei were fixed in their instantaneous positions. The electrons are then described as following the nuclear motion adiabatically, which means that the electrons do not make transitions from one state to another but instead the electronic state is progressively deformed by the nuclear displacements. In certain circumstances such as the description of photochemical processes it is necessary

to go beyond the Born–Oppenheimer approximation because more than one electronic energy surface must be considered. In the majority of calculations, and all of those in this thesis, the Born–Oppenheimer approximation is sufficiently accurate for chemical application.

1.3 Hartree–Fock Theory

A simple mathematical form for the electronic wavefunction is now required to enable the approximate solution of the electronic Schrödinger equation. To this end the orbital approximation to the many electron wavefunction is now introduced. Ψ is written in terms of one electron functions called spin orbitals, $\chi_j(\mathbf{x}_i)$, where $\mathbf{x}_i$ is a combined space and spin coordinate. Each spin orbital may then be written as a product of spatial and spin parts

$$\chi_j(\mathbf{x}) = \begin{cases} \psi_j(\mathbf{r})\alpha(s) \\ \psi_j(\mathbf{r})\beta(s) \end{cases} \tag{1.3.1}$$

where $\psi_j(\mathbf{r})$ corresponds to the spatial function and the spin functions are $\alpha(s)$ (spin up) and $\beta(s)$ (spin down).

If the electronic Hamiltonian of Eqn. (1.2.2) consisted purely of one electron operators, $\hat{h}_i$, then a set of one electron equations could be derived, which take the form

$$\hat{h}(i)\chi_j(\mathbf{x}_i) = \varepsilon_j\chi_j(\mathbf{x}_i) \tag{1.3.2}$$

where we have defined the spin orbital, $\chi_j(\mathbf{x}_i)$, as a one electron wavefunction. The total wavefunction, Ψ, could then be written as the Hartree product [12–14] of these one electron spin orbitals

$$\Psi(\mathbf{x}_1, \mathbf{x}_2, \ldots, \mathbf{x}_N) = \chi_1(\mathbf{x}_1)\chi_2(\mathbf{x}_2)\ldots\chi_N(\mathbf{x}_N) \tag{1.3.3}$$

However, even if the Hamiltonian could be written as a sum of one electron terms the Hartree product would not be a suitable form for the wavefunction since it distinguishes between different electrons and the wavefunction is not antisymmetric with respect to the interchange of the space and spin coordinates of any two electrons. To introduce the antisymmetry condition for the wavefunction, as required by the Pauli principle, we can apply an antisymmetrisation operator

$$\hat{A} = (N!)^{-\frac{1}{2}} \sum_P (-1)^p P \tag{1.3.4}$$

to the Hartree product, where p is the parity of the permutation P. This operator selects the antisymmetric component of the Hartree product and gives the Slater determinant (SD) [15, 16]

$$\Psi(\mathbf{x}_1, \mathbf{x}_2, \ldots, \mathbf{x}_N) = (N!)^{-\frac{1}{2}} \det\{\chi_k\} \tag{1.3.5}$$

This determinant has the desired properties for the wavefunction; interchanging the coordinates of any two electrons corresponds to interchanging two rows of the determinant which results in a change of sign for the wavefunction.

The Hartree–Fock scheme [12–14, 17, 18] is defined by approximating the wavefunction as a single Slater determinant and finding the expectation value of the true electronic Hamiltonian with this wavefunction. This expectation value

$$E_{\mathrm{SD}} = \langle \Psi_{\mathrm{SD}} | \hat{H}_{\mathrm{e}} | \Psi_{\mathrm{SD}} \rangle = \sum_{i=1}^{N} (i|\hat{h}|i) + \frac{1}{2} \sum_{i=1}^{N} \sum_{j=1}^{N} [(ii|jj) - (ij|ji)] \tag{1.3.6}$$

is a functional of the spin orbitals from which the single determinant is constructed. The first term consists of the kinetic and nuclear-electron contributions to the energy which are evaluated as one electron integrals

$$(i|\hat{h}|i) = \int \chi_i^*(\mathbf{x}_1) \hat{h}(\mathbf{x}_1) \chi_i(\mathbf{x}_1) d\mathbf{x}_1 \tag{1.3.7}$$

The second term contains the Coulomb and exchange energies which arise naturally when a single determinant is used to approximate the wavefunction, and are calculated as two electron integrals

$$(ii|jj) = \iint \chi_i^*(\mathbf{x}_1) \chi_i(\mathbf{x}_1) \frac{1}{r_{12}} \chi_j^*(\mathbf{x}_2) \chi_j(\mathbf{x}_2) d\mathbf{x}_1 d\mathbf{x}_2 \tag{1.3.8}$$

$$(ij|ji) = \iint \chi_i^*(\mathbf{x}_1) \chi_j(\mathbf{x}_1) \frac{1}{r_{12}} \chi_j^*(\mathbf{x}_2) \chi_i(\mathbf{x}_2) d\mathbf{x}_1 d\mathbf{x}_2 \tag{1.3.9}$$

Following the variational principle the Hartree–Fock equations are then derived by minimising E_{SD} with respect to the spin orbitals under the constraint that they remain orthonormal. This is achieved by the multiplier method of Lagrange, and results in

$$\hat{F} \chi_i = \sum_{j=1}^{N} \varepsilon_{ij} \chi_j \tag{1.3.10}$$

where ε_{ij} is the matrix of Lagrange multipliers and $\hat{F}$ is the Fock operator given by

$$\hat{F} = \hat{h} + \sum_{j=1}^{N} \hat{J}_j - \hat{K}_j \tag{1.3.11}$$

in which the first term consists of the kinetic and nuclear-electron one electron operators

$$\hat{h}_i = -\frac{1}{2}\nabla_i^2 - \sum_{A=1}^{M} \frac{Z_A}{r_{iA}} \tag{1.3.12}$$

The second term consists of the Coulomb and exchange operators which are defined by their effect when operating on spin orbital $\chi_i(\mathbf{x}_1)$ as,

$$\hat{J}_j\chi_i(\mathbf{x}_1) = \left[\int \chi_j^*(\mathbf{x}_2) r_{12}^{-1} \chi_j(\mathbf{x}_2) d\mathbf{x}_2\right] \chi_i(\mathbf{x}_1) \tag{1.3.13}$$

$$\hat{K}_j\chi_i(\mathbf{x}_1) = \left[\int \chi_j^*(\mathbf{x}_2) r_{12}^{-1} \chi_i(\mathbf{x}_2) d\mathbf{x}_2\right] \chi_j(\mathbf{x}_1) \tag{1.3.14}$$

Eqn. (1.3.10) is not in the form an eigenvalue problem. It can be shown that there will always exist a unique set of spin orbitals such that the matrix of Lagrange multipliers is diagonal. This defines the canonical Hartree–Fock equations

$$\hat{F}\chi_i = \varepsilon_i\chi_i \tag{1.3.15}$$

The Hartree–Fock equations have been presented in terms of the general one electron spin orbitals which are the product of spatial and spin parts. To derive matrix equations two approaches can be adopted, either the spatial parts of the α and β spin orbitals are allowed to be different (Unrestricted Hartree–Fock), or they are constrained to be the same (Restricted Hartree–Fock).

1.3.1 Unrestricted Hartree–Fock (UHF) Theory

In the UHF case the spatial functions corresponding to electrons of α and β spin are allowed to be different

$$\chi_j(\mathbf{x}) = \begin{cases} \psi_j^\alpha(\mathbf{r})\alpha(s) \\ \psi_j^\beta(\mathbf{r})\beta(s) \end{cases} \tag{1.3.16}$$

In order to derive a set of equations for the spatial orbitals the above expressions for the spin orbitals are inserted into the Hartree–Fock equations and the spin is integrated out, giving

$$\hat{F}^\sigma\psi_j^\sigma = \varepsilon_j^\sigma\psi_j^\sigma \tag{1.3.17}$$

where σ is a spin label and the Fock operators are defined by

$$\hat{F}^{\sigma} = \hat{h} + \sum_{i=1}^{N^{\sigma}} \left[\hat{J}_i^{\sigma} - \hat{K}_i^{\sigma} \right] + \sum_{i=1}^{N^{\sigma'}} \hat{J}_i^{\sigma'} \tag{1.3.18}$$

The Coulomb and exchange operators are analogous to those defined previously but with the orbitals restricted to one spin. Since any given electron in the molecule experiences Coulombic repulsion from all of the other electrons, irrespective of spin, the Fock operators and hence the spatial equations for each spin are not independent. The two equations must therefore be solved simultaneously.

To solve the UHF equations the spatial orbitals are expanded in terms of a basis set. Basis sets are typically defined for each nucleus. Basis functions in common use fall into two types; Slater-type atomic orbitals (STOs) [19] and Gaussian-type atomic orbitals (GTOs) [20]. For a nucleus centred at $\mathbf{A} = (A_x, A_y, A_z)$ the STO radial functions are

$$\phi_i(\mathbf{r}) = N(x - A_x)^k (y - A_y)^l (z - A_z)^m e^{-\alpha|\mathbf{r}-\mathbf{A}|} \tag{1.3.19}$$

where α is a nucleus dependent exponent, N is the normalisation constant, and the angular momentum of the function, $L = k + l + m$.

Whilst the STOs have desirable properties in that they can closely resemble the exact hydrogenic wavefunctions, having cusps at the nuclei and decaying exponentially, integrals over these functions are difficult to compute. In 1950 Boys [20] suggested that GTO basis functions could be used in their place

$$\phi_i(\mathbf{r}) = N(x - A_x)^k (y - A_y)^l (z - A_z)^m e^{-\alpha|\mathbf{r}-\mathbf{A}|^2} \tag{1.3.20}$$

since integrals over these functions are computationally simple and efficient to evaluate. However since they have incorrect nuclear cusps and decay too quickly, many more of them must be used to achieve accurate results. This is offset by the large reduction in effort required to evaluate their integrals. Typical basis sets attempt to reproduce STO type behaviour by using contractions of several GTO functions

$$\phi_i(\mathbf{r}) = N \sum_{p=1}^{P_A} C_{ip} (x - A_x)^k (y - A_y)^l (z - A_z)^m e^{-\alpha_p|\mathbf{r}-\mathbf{A}|^2} \tag{1.3.21}$$

where P_A defines the depth of contraction and C_{ip} are the contraction coefficients. Commonly used examples are the correlation consistent sets of Dunning [21] and the split-valence sets of Pople [22–24]. In the calculation of molecular properties a judicious

choice of basis set can be essential to obtain converged results. For example, in the calculation of nuclear magnetic shielding constants or spin-spin coupling constants it is essential that the basis set contains high exponent functions, whereas for the calculation of excitation energies it is essential that the basis set contains many diffuse (low exponent) functions.

The basis set expansion of the molecular orbitals in terms of the chosen basis functions, ϕ, is

$$\psi_i^\sigma = \sum_\mu C_{\mu i}^\sigma \phi_\mu \tag{1.3.22}$$

This can be substituted into the Hartree–Fock equations and then multiplying from the left by another basis function and integrating gives the Pople–Nesbet [25] matrix equations

$$\sum_\mu \left(F_{\lambda\mu}^\sigma - \varepsilon_i S_{\lambda\mu}\right) C_{\mu i}^\sigma = 0 \tag{1.3.23}$$

The indices λ and μ label the basis functions, $\mathbf{S}$ is the overlap matrix and $\mathbf{F}$ is the matrix representation of the Fock operator. The Pople–Nesbet equations are solved using the self-consistent field (SCF) procedure in which a starting set of orbitals are chosen, the corresponding Fock matrix is constructed and a new set of orbitals (the eigenfunctions of the Fock matrix) are computed. This procedure is then iterated until the orbitals no longer change between iterations; this is termed self consistency. The convergence of the SCF procedure can be difficult and so several methods have been proposed for acceleration of the process. Common implementations use the direct inversion in the iterative subspace (DIIS) method of Pulay [26] and the level shifting scheme [27].

1.3.2 Restricted Hartree–Fock (RHF) Theory

The RHF equations can be obtained from the UHF equations by forcing $N^\alpha = N^\beta$ and $\psi_j^\alpha = \psi_j^\beta$ so that all the spatial orbitals are now doubly occupied with two electrons of opposing spin. The spatial orbital one electron equations can be written as

$$\hat{F}\psi_j = \varepsilon_j \psi_j \tag{1.3.24}$$

where the Fock operator now becomes

$$\hat{F} = \hat{h} + \sum_{i=1}^{N/2} \left[2\hat{J}_i - \hat{K}_i\right] \tag{1.3.25}$$

with the sum running to $N/2$ since the orbitals are now doubly occupied. Introducing the basis set expansion results in the Roothaan–Hall [28, 29] matrix equations

$$\sum_{\mu} \left(F_{\lambda\mu} - \varepsilon_i S_{\lambda\mu}\right) C_{\mu i} = 0 \tag{1.3.26}$$

The Hartree–Fock method is exact for one electron systems. However for general many electron systems the Hartree–Fock solutions are approximate. In the next section methods which improve upon the Hartree–Fock wavefunction are considered.

1.4 Introducing Electron Correlation

The broadest definition of electron correlation is to say that at a given moment in time the motion of any one electron is dependent on the motion of all of the other electrons. The Hartree–Fock scheme includes the exchange interaction which arises due to the Pauli principle and keeps electrons of like spin apart, resulting in a lowering of the electronic energy. The Hartree–Fock energy is however still above that of the exact energy since the wavefunction is approximate. This leads to the Löwdin definition [30] that "the correlation energy for a certain state with respect to a specified Hamiltonian is the difference between the exact eigenvalue of the Hamiltonian and its expectation value in the Hartree–Fock approximation for the state under consideration."

$$E_{\mathrm{c}} = E_{\mathrm{exact}} - E_{\mathrm{HF}} \tag{1.4.1}$$

The correlation energy can be further broken down into dynamic and non-dynamic contributions. Dynamic correlation is due to the short range instantaneous interaction of the electrons which cannot be modelled by the average nature of the Hartree–Fock approximation. Non-dynamic correlation is a long range effect which is a result of the fundamental failure of a single Slater determinant to adequately describe the wavefunction. The lack of non-dynamic correlation is especially important when describing the dissociation of molecules. There are several wavefunction based approaches for recovering the correlation energy and these are now outlined.

1.4.1 Configuration Interaction

In order to describe electronic correlation accurately it is necessary to include the interelectronic distance. One conceptually simple way to achieve this is the configuration interaction (CI) approach. In CI theory the wavefunction is expanded as a linear com-

bination of all possible excited determinants from some reference determinant, Ψ_0, in the form

$$\Phi = c_0\Psi_0 + \sum_{ia} c_i^a \Psi_i^a + \sum_{j>i,b>a} c_{ij}^{ab}\Psi_{ij}^{ab} + \ldots \tag{1.4.2}$$

where for example Ψ_i^a represents a Slater determinant created by a single excitation from the reference state. The CI scheme is variational and the optimal expansion parameters may be determined by a minimisation of the energy. When all possible excited state determinants are included the scheme is called full CI (FCI) and gives the exact correlation energy within a given basis set. FCI is impractical for all but the smallest systems so the series must be truncated, but the calculations are then no longer size consistent [31–33]. This means that the energy of an infinitely separated system will not be equal to the sum of the energies of its individual components. For the CISD method (using only singly- and doubly-excited determinants) the Davidson correction [34] was proposed to approximately fix this problem. A better solution to the size-consistency problem is the quadratic configuration interaction method, in which additional higher excitation terms which are quadratic in the expansion coefficients are added [35].

1.4.2 Coupled Cluster Theory

In coupled cluster (CC) methods [36–38] the size consistency is restored at all levels of truncation. The wavefunction is represented by

$$\Psi_{\mathrm{CC}} = \exp(\hat{T}).\Psi_{\mathrm{HF}} \tag{1.4.3}$$

where

$$\exp(\hat{T}) = 1 + \hat{T} + \frac{1}{2}\hat{T}^2 + \frac{1}{6}\hat{T}^3 + \ldots = \sum_{k=0}^{\infty}\frac{1}{k!}\hat{T}^k \tag{1.4.4}$$

and $\hat{T}$ is the cluster operator which generates the excited determinants. The most widely used coupled cluster approach is the CCSD method in which only single and double excitations are included. Other schemes exist which attempt to include higher terms in an approximate fashion, for example CCSD(T) which includes a perturbative treatment of the triply excited contributions. The CC method is not variational, although its application over the past two decades has demonstrated its accuracy.

A variant of the coupled cluster approach, which is closely related to the CCSD scheme, is the Brueckner Doubles (BD) scheme [39–41] in which rather than using a Hartree–Fock single determinant as the reference a new set of orbitals are calculated, defined such that the single excitation amplitudes for the resulting determinant are

zero. These orbitals are determined at each step of the coupled cluster calculation and as such the procedure is slightly more computationally demanding. In most cases the use of Brueckner orbitals offers little advantage. However in cases where the Hartree–Fock wavefunction may exhibit instabilities, such as molecular dissociation, the use of the Brueckner scheme is preferred since the reference on which the coupled cluster calculation is based may not suffer from the instabilities.

1.4.3 Møller–Plesset Perturbation Theory

The Hartree–Fock wavefunction is an approximate eigenfunction of the exact Hamiltonian. However there exists a system for which the Hartree–Fock wavefunction is exact. The Hamiltonian for this system is

$$\hat{H}_0 = \sum_i \hat{F}_i \tag{1.4.5}$$

and is referred to as the Hartree–Fock non-interacting system. The difference between $\hat{H}_0$ and the exact Hamiltonian may be regarded as a perturbation. This is the basis of Møller–Plesset theory which applies Rayleigh–Schrödinger perturbation theory to the electronic structure problem. The Hartree–Fock energy is recovered at first order and so correlation is introduced at higher orders. For example the second order energy is,

$$E_2 = -\frac{1}{4}\sum_{ijab} \frac{\left[(ai\,|bj) - (aj|\,bi)\right]^2}{\varepsilon_a + \varepsilon_b - \varepsilon_i - \varepsilon_j} \tag{1.4.6}$$

This level of perturbation theory is called MP2 [42] theory and typically recovers 70-80% of the correlation energy. Unfortunately convergence of the Møller–Plesset series is not guaranteed. In fact it can diverge and display oscillatory behaviour, especially when the Hartree–Fock determinant is a poor reference. As such most applications of Møller–Plesset theory are limited to the MP2 level. The MP2 method is not variational but is size consistent.

The problem with the above wavefunction based methods is that they are computationally much more expensive than the Hartree–Fock scheme, which scales as N^4 where N is a measure of system size. For example the CISD, CCSD and BD methods scale as N^6 and inclusion of higher excitations makes the situation worse; for CCSD(T) the scaling is N^7 and rises to N^8 for CCSDT. The MP2 approach scales as N^5 and represents the least computationally demanding way to introduce electron correlation. However, all of these methods are difficult to apply to large chemically and biologically relevant systems.

1.5 Early Theories Based on the Electron Density

An attractive alternative is to develop a theory based on the electron density,

$$\rho(\mathbf{r}) = N \int \cdots \int |\Psi(\mathbf{x}_1, \mathbf{x}_2, \ldots, \mathbf{x}_N)|^2 \, ds_1 d\mathbf{x}_2 \ldots d\mathbf{x}_N \tag{1.5.1}$$

which is the probability of finding an electron in volume element $d\mathbf{r}$ with arbitrary spin, whilst the other $N-1$ electrons have arbitrary positions and spins in the state represented by Ψ. The function $\rho(\mathbf{r})$ is dependent on only three spatial variables, is non-negative, vanishes at infinity and when integrated gives the total number of electrons

$$\int \rho(\mathbf{r}) d\mathbf{r} = N \tag{1.5.2}$$

At the positions of the nuclei the density displays cusps which are related to the nuclear charge, Z, by

$$\lim_{r_{iA} \to 0} \left[\frac{\partial}{\partial r} + 2Z_A \right] \rho(\mathbf{r}) = 0 \tag{1.5.3}$$

These properties of the electron density suggest that it may provide enough information to form the basis of an electronic structure theory. The relatively simple nature of the electron density compared to the wavefunction inspired several early attempts at a density functional theory (DFT).

1.5.1 The Thomas–Fermi Model

In 1927, Thomas and Fermi [43, 44] independently derived a method for calculating the electron distributions and fields in heavy atoms. The Thomas–Fermi and related schemes may be regarded as first generation density functional methods. For a uniform gas distribution of electrons the kinetic energy is given by

$$T[\rho] = \frac{3}{10}(3\pi^2)^{2/3} \int \rho^{5/3}(\mathbf{r}) d\mathbf{r} \tag{1.5.4}$$

Then by adding the classical expressions for the nuclear-electron and electron-electron potentials the energy of an atom can be written as a functional of the density

$$E[\rho] = \frac{3}{10}(3\pi^2)^{2/3} \int \rho^{5/3}(\mathbf{r}) d\mathbf{r} - Z \int \frac{\rho(\mathbf{r})}{r} d\mathbf{r} + \frac{1}{2} \iint \frac{\rho(\mathbf{r})\rho(\mathbf{r}')}{|\mathbf{r} - \mathbf{r}'|} d\mathbf{r} d\mathbf{r}' \tag{1.5.5}$$

However the approximation to the kinetic energy is poor and the effects of exchange and correlation are completely negelected. Energies predicted by the Thomas–Fermi model are typically too low by around 20%. The density obtained from the model

also shows serious defects. There is no shell structure present and it is infinite at the nucleus. Furthermore when the model is applied to molecules, none are stable with respect to dissociation [45, 46]. As such the model is completely unsuitable for chemical systems.

1.5.2 The Thomas–Fermi–Dirac Model

A number of refinements to the Thomas–Fermi model were proposed, the first of which was the addition of an approximate exchange energy term

$$E_{\mathrm{x}}[\rho] = -C_{\mathrm{x}} \int \rho^{4/3}(\mathbf{r}) d\mathbf{r} \tag{1.5.6}$$

to give Thomas–Fermi–Dirac Theory [47]. This model was also unsuccessful when applied to chemical systems. The energies that were already too low in the original model are further lowered and the shortcomings of the original model remain. However this idea of deriving a functional for the exchange energy of a uniform electron gas and applying it to non-uniform electron densities in atoms and molecules still finds use in modern density functional theory.

1.5.3 The Thomas–Fermi–Dirac–Weizsacker Model

In 1935 Weizsacker [48] suggested a correction to the Thomas–Fermi kinetic energy functional of the form

$$T_{\mathrm{W}}[\rho] = \frac{1}{8} \int \frac{|\nabla \rho(\mathbf{r})|^2}{\rho(\mathbf{r})} d\mathbf{r} \tag{1.5.7}$$

This correction attempts to take account of the inhomogeneity of the electron density and is the first example of a gradient correction to a density functional. The total kinetic energy can then be written as

$$T_{\mathrm{TF}\lambda\mathrm{W}}[\rho] = T_{\mathrm{TF}}[\rho] + \lambda T_{\mathrm{W}}[\rho] \tag{1.5.8}$$

where λ is an adjustable parameter. In Weizsacker's original work $\lambda = 1$. However from gradient expansion techniques a value of $\frac{1}{9}$ is proposed [49] and from fitting to the energies of hydrogenic atoms a value of $\frac{1}{5}$ is proposed [50]. Inclusion of this correction term can lead to energies much closer to the Hartree–Fock energy for atoms and the density no longer diverges at the nucleus. Molecular binding is also possible but the method is still not accurate enough for chemical application.

1.5.4 The Slater X_α Method

In 1951 Slater [51] proposed replacing the complicated non-multiplicative Hartree–Fock exchange operator with a multiplicative potential. The Hartree–Fock equations can be written

$$\left[\hat{h}(\mathbf{r}) + \sum_{j=1}^{N} \int \frac{\varphi_j^*(\mathbf{r}')\varphi_j(\mathbf{r}')}{|\mathbf{r}-\mathbf{r}'|} d\mathbf{r}' - \frac{\sum_{j=1}^{N} \int \frac{\varphi_i^*(\mathbf{r})\varphi_j^*(\mathbf{r}')\varphi_j(\mathbf{r})\varphi_i(\mathbf{r}')}{|\mathbf{r}-\mathbf{r}'|} d\mathbf{r}'}{\varphi_i^*(\mathbf{r})\varphi_i(\mathbf{r})}\right] \varphi_i(\mathbf{r}) = \varepsilon_i \varphi_i(\mathbf{r}) \tag{1.5.9}$$

where the exchange operator has been replaced by an equivalent potential acting on the ith orbital. In order to obtain a single potential common to all of the one electron equations Slater proposed replacing the exchange operator with an average over all of the orbitals according to the density, resulting in

$$\left[\hat{h}(\mathbf{r}) + \sum_{j=1}^{N} \int \frac{\varphi_j^*(\mathbf{r}')\varphi_j(\mathbf{r}')}{|\mathbf{r}-\mathbf{r}'|} d\mathbf{r}' - \frac{\sum_{i=1}^{N}\sum_{j=1}^{N} \int \frac{\varphi_i^*(\mathbf{r})\varphi_j^*(\mathbf{r}')\varphi_j(\mathbf{r})\varphi_i(\mathbf{r}')}{|\mathbf{r}-\mathbf{r}'|} d\mathbf{r}'}{\sum_{i=1}^{N} \varphi_i^*(\mathbf{r})\varphi_i(\mathbf{r})}\right] \varphi_i(\mathbf{r}) = \varepsilon_i \varphi_i(\mathbf{r}) \tag{1.5.10}$$

The Slater exchange potential can be written more succinctly as

$$v_{\mathrm{x}}^{\mathrm{Slater}}(\mathbf{r}) = -\frac{n_s}{\rho(\mathbf{r})} \int \frac{\rho(\mathbf{r}', \mathbf{r})\rho(\mathbf{r}, \mathbf{r}')}{|\mathbf{r}-\mathbf{r}'|} d\mathbf{r}' \tag{1.5.11}$$

where n_s is the spin degeneracy.

Slater suggested further simplification by replacing the averaged exchange charge density with that of a uniform electron gas, in which case the exchange potential becomes

$$v_{\mathrm{x}}^{X_\alpha}(\mathbf{r}) = -\alpha \frac{3}{2} \left(\frac{3}{\pi}\right)^{\frac{1}{3}} \rho^{\frac{1}{3}}(\mathbf{r}) \tag{1.5.12}$$

Here the adjustable exchange parameter α has been introduced, which was equal to 1 in Slater's original work. Taking α to be $\frac{2}{3}$ gives the local density approximation to the exchange potential derived by Dirac. Using the potential of Eqn. (1.5.12) with a chosen value of α to solve approximate Hartree–Fock equations is called the Slater X_α method. Although this approach found widespread application in physics it did not make much impact in chemical applications.

1.6 Modern Density Functional Theory

In 1964 Hohenberg and Kohn (HK) [52] gave a sound foundation for a theory based on the electronic density, $\rho(\mathbf{r})$, and showed that the density associated with the ground

state of a molecule may be determined variationally. In 1965 Kohn and Sham (KS) [53] derived a set of equations that can be solved self-consistently and include the effects of electron correlation. These two key papers form the basis of all modern density functional theory (DFT) schemes.

1.6.1 The Hohenberg–Kohn Theorems

Consider a group of electrons moving under the influence of a time-independent external potential, $v(\mathbf{r})$. For non-degenerate ground states, Ψ, Hohenberg and Kohn showed that for a given $v(\mathbf{r})$ there exists one unique corresponding electron density $\rho(\mathbf{r})$ and vice versa. Mathematically this is expressed by saying that $v(\mathbf{r})$ is a unique functional of $\rho(\mathbf{r})$. The proof of this proceeds by considering the case of two potentials, $v(\mathbf{r})$ and $v'(\mathbf{r})$, with corresponding ground states Ψ and Ψ'. The potentials are subject to the condition that $v(\mathbf{r}) \neq v'(\mathbf{r}) + \text{constant}$, so that $\Psi \neq \Psi'$ since the wavefunctions must satisfy different Schrödinger equations. This means that there are two different Hamiltonians, $\hat{H}$ and $\hat{H}'$, with different ground state energies E_0 and E_0'.

Assume that Ψ and Ψ' correspond to the same electron density. Using Ψ' as a trial wavefunction with the Hamiltonian $\hat{H}$, evaluating its expectation value and using the variational principle gives the inequality

$$E_0 < E_0' + \int \rho(\mathbf{r})[v(\mathbf{r}) - v'(\mathbf{r})]d\mathbf{r} \tag{1.6.1}$$

Similarly using Ψ as a trial wavefunction for $\hat{H}'$ gives the inequality

$$E_0' < E_0 + \int \rho(\mathbf{r})[v'(\mathbf{r}) - v(\mathbf{r})]d\mathbf{r} \tag{1.6.2}$$

The addition of these two relations cancels the integral terms and we obtain the contradiction that

$$E_0 + E_0' < E_0' + E_0 \tag{1.6.3}$$

Hence $v(\mathbf{r})$ is to within an additive constant a unique functional of $\rho(\mathbf{r})$. This important result is the first Hohenberg–Kohn theorem (HK1). Bright–Wilson gave an elegant explanation of why $\rho(\mathbf{r})$ determines $v(\mathbf{r})$. He stated that the cusps of the electron density give us the positions of the nuclei and their slopes allow us to determine their atomic numbers. Hence $\rho(\mathbf{r})$ determines $v(\mathbf{r})$. Since $\rho(\mathbf{r})$ also integrates to the number of electrons, N, then it follows that $\rho(\mathbf{r})$ determines the complete electronic Hamiltonian and all properties which may be determined from it. This establishes a firm foundation for a theory of electronic structure based on the density rather than

the wavefunction.

The second Hohenberg–Kohn theorem (HK2) gives a variational principle in terms of the density. HK1 establishes that the exact $\rho(\mathbf{r})$ may be uniquely associated with a $v(\mathbf{r})$ and hence determine $\hat{H}$ and Ψ. Let us also consider a trial density $\tilde{\rho}(\mathbf{r})$ which is associated with $\tilde{v}(\mathbf{r})$, $\tilde{\hat{H}}$ and $\tilde{\Psi}$. From the variational principle we have

$$\langle\tilde{\Psi}|\hat{H}|\tilde{\Psi}\rangle \geqslant \langle\Psi|\hat{H}|\Psi\rangle \tag{1.6.4}$$

giving the variational principle in terms of the energy as a functional of the density

$$E[\tilde{\rho}] \geqslant E[\rho] \tag{1.6.5}$$

The variational principle requires that for the true density the energy is a minimum subject to the constraint that the integral of the density is equal to the number of electrons

$$\delta E[\rho] - \mu\delta\left[\int \rho(\mathbf{r})d\mathbf{r} - N\right] = 0 \tag{1.6.6}$$

which gives the Euler–Lagrange equation

$$\mu = v(\mathbf{r}) + \frac{\delta T[\rho]}{\delta\rho(\mathbf{r})} + \frac{\delta V_{\text{ee}}[\rho]}{\delta\rho(\mathbf{r})} \tag{1.6.7}$$

If the exact form of $T[\rho]$ and $V_{\text{ee}}[\rho]$ were known then the solution of this equation would yield the exact density $\rho(\mathbf{r})$.

1.6.2 The v-representability Problem

The Hohenberg–Kohn theorems assume that $\rho(\mathbf{r})$ is associated with a ground state wavefunction of some Hamiltonian, $\hat{H}$, of the form

$$\hat{H} = \hat{T} + \hat{V}_{\text{ee}} + \sum_i v(\mathbf{r}_i) \tag{1.6.8}$$

with the external potential $v(\mathbf{r})$. This is termed v-representability. It has been shown that certain reasonable trial densities are not v-representable [54, 55]. It is also assumed that there is no degeneracy in the ground state. Levy was able to solve both of these issues by reformulation of the proof into a constrained search over trial wavefunctions yielding a chosen electron density such that only the N-representability of ρ is required [54, 56]. He noted that the true ground state wavefunction could be distinguished from the set of wavefunctions yielding the exact ground state density by the

minimisation of the expectation value of $\hat{T} + \hat{V}_{ee}$ and so defined the universal (in the sense that it is independent of the external potential) functional

$$F[\rho] = \min_{\Psi \to \rho} \left\langle \Psi \left| \hat{T} + \hat{V}_{\mathrm{ee}} \right| \Psi \right\rangle \tag{1.6.9}$$

The energy in terms of this functional can then be written as

$$\begin{aligned} E &= \min_{\rho \to N} \left[F[\rho] + \int v(\mathbf{r})\rho(\mathbf{r}) d\mathbf{r} \right] \\ &= \min_{\rho \to N} E[\rho] \end{aligned} \tag{1.6.10}$$

and the search only requires the N-representability of the density, the conditions for which are known, namely that the density should be everywhere positive, integrate to the number of electrons and $\int |\nabla \rho^{\frac{1}{2}}|^2 d\mathbf{r} < \infty$, which are satisfied by all reasonable trial densities. The restriction to a non-degenerate ground state is also lifted since the proof now focuses on the wavefunctions which yield a selected density, and so only the wavefunction giving the required density will be selected from a degenerate set. The N-representability condition is a weaker constraint than v-representability and all v-representable densities are N-representable by definition.

1.6.3 The Kohn–Sham Equations

Kohn and Sham [53] were able to work from the HK theorems to derive a set of equations that could be solved self consistently and include the effects of electron correlation. They began by further partitioning the energy as

$$E = \int v_{\mathrm{ext}}(\mathbf{r})\rho(\mathbf{r}) d\mathbf{r} + \frac{1}{2} \iint \frac{\rho(\mathbf{r})\rho(\mathbf{r}')}{|\mathbf{r} - \mathbf{r}'|} d\mathbf{r} d\mathbf{r}' + T_s[\rho] + E_{\mathrm{xc}}[\rho] \tag{1.6.11}$$

The first term corresponds to the interaction of the electrons with the fixed nuclear framework and the second is the classical Coulombic repulsion of an electron density with itself. The third term is the kinetic energy for a system of non-interacting electrons with the same density as the real system and the final term is the Kohn–Sham definition of the exchange–correlation energy. Using this partitioning only the final term is unknown and consists of the exchange and correlation energies along with a kinetic energy contribution to account for the difference between the kinetic energy of the real system and the non-interacting system. The fact that T_s gives a good approximation to the kinetic energy of the interacting system is important since the kinetic contribution to the electronic energy is by far the largest. Functional differentiation of

the above energy expression with respect to the density subject to the constraint,

$$\int \rho(\mathbf{r})d\mathbf{r} - N = 0 \tag{1.6.12}$$

yields

$$\left[v_{\text{ext}}(\mathbf{r}) + \int \frac{\rho(\mathbf{r}')}{|\mathbf{r}-\mathbf{r}'|}d\mathbf{r}' + \frac{\delta T_s[\rho]}{\delta\rho(\mathbf{r})} + \frac{\delta E_{\text{xc}}[\rho]}{\delta\rho(\mathbf{r})}\right] = \mu \tag{1.6.13}$$

where μ is the Lagrange multiplier. This is exactly the same as the Euler–Lagrange equation for a non-interacting system with a density equal to that of the interacting one moving in the effective potential $v_s(\mathbf{r}) = v_{\text{ext}}(\mathbf{r}) + v_J(\mathbf{r}) + v_{xc}(\mathbf{r})$

$$\left[v_s(\mathbf{r}) + \frac{\delta T_s[\rho]}{\delta\rho(\mathbf{r})}\right] = \mu \tag{1.6.14}$$

A single Slater determinant is an exact eigenfunction of the Hamiltonian for a non-interacting system and so the Kohn–Sham scheme is in principle exact but with a machinery similar to that of the Hartree–Fock method. Following the derivation of the HF scheme we can write a set of one electron equations for this system as

$$\left[-\frac{1}{2}\nabla^2 - \sum_A^M \frac{Z_A}{r_{iA}} + \int \frac{\rho(\mathbf{r}')}{|\mathbf{r}-\mathbf{r}'|}d\mathbf{r}' + \frac{\delta E_{\text{xc}}[\rho]}{\delta\rho(\mathbf{r})}\right]\varphi_i = \varepsilon_i\varphi_i \tag{1.6.15}$$

where the term in square brackets defines the Kohn–Sham operator and consists of kinetic, nuclear-electron, Coulomb and exchange-correlation terms. The Coulomb, exchange-correlation and external potentials are all local multiplicative operators defined as the functional derivatives of the corresponding energy contributions with respect to the density. The density may be obtained via

$$\rho(\mathbf{r}) = \sum_{i=1}^{N} |\varphi_i(\mathbf{r})|^2 \tag{1.6.16}$$

where N is the number of electrons and φ_i are the Kohn–Sham single particle orbitals. The energy is calculated in a similar way to the Hartree–Fock scheme, but with the exchange–correlation energy in place of the exchange energy

$$E^{\text{KS}} = \sum_{i=1}^{N}(i|\hat{h}|i) + \frac{1}{2}\sum_{i=1}^{N}\sum_{j=1}^{N}(ii|jj) + E_{\text{xc}}[\rho] \tag{1.6.17}$$

These equations can be solved self-consistently in the same fashion as the Hartree–Fock equations discussed in Section 1.3. However, since the single determinant in the Kohn–

Sham scheme is not used to approximate the wavefunction of the interacting system but rather to describe a non-interacting system with the same density, the equations are formally exact and can in principle include all effects of electron correlation if an accurate form for E_{xc} is known.

1.6.4 Applying the Constrained Search to the Kohn–Sham System

It is also possible to employ the Levy constrained search formalism [56] within the Kohn–Sham scheme. This allows the determination of the Kohn–Sham exchange–correlation potential, orbitals and eigenvalues associated with an input electron density. In the Kohn–Sham partitioning of the total energy of Eqn. (1.6.11), all terms except the non-interacting kinetic energy are explicit functionals of the density and so for a given input density are fixed. However the non-interacting kinetic energy is an implicit density functional since it depends on the orbitals which are themselves functionals of the density. As shown by Levy and Perdew [57] the Kohn–Sham orbitals are returned from the minimisation

$$T_s[\rho] = \min_{\Psi_{SD}\to\rho_0} \left\langle \Psi_{SD} \left| \hat{T} \right| \Psi_{SD} \right\rangle \tag{1.6.18}$$

where Ψ_{SD} is the Slater determinant constructed from the Kohn–Sham orbitals, T_s is the kinetic energy of the non-interacting reference system and the sum of the squares of the occupied orbitals is constrained to give the input electronic density, ρ_0. Thus the constrained search distinguishes the closed shell determinant which gives the lowest energy from the set of determinants that give the input density.

There are several schemes in the literature which attempt to implement this approach. In Chapter 4 the implementation of the Wu–Yang (WY) procedure [58] is described in detail and in later chapters its performance in application to various problems is examined. An alternative approach is the procedure of Zhao, Morrison and Parr (ZMP) [59] which is outlined here and applied in Chapter 2.

In order to force the calculated density to be equal to the input density, $\rho_0(\mathbf{r})$, ZMP introduced a constraint of the form

$$C[\rho,\rho_0] = \frac{1}{2}\int\int \frac{[\rho(\mathbf{r})-\rho_0(\mathbf{r})][\rho(\mathbf{r}')-\rho_0(\mathbf{r}')]}{|\mathbf{r}-\mathbf{r}'|} d\mathbf{r}d\mathbf{r}' = 0 \tag{1.6.19}$$

where $\rho(\mathbf{r})$ is the density used during the minimisation. Introducing a Lagrange multiplier, λ, the potential associated with the constraint may be written as,

$$v_c^{\lambda}(\mathbf{r}) = \lambda \int \frac{\rho(\mathbf{r}')-\rho_0(\mathbf{r}')}{|\mathbf{r}-\mathbf{r}'|} d\mathbf{r}' \tag{1.6.20}$$

Minimisation of T_s with respect to the orbitals then gives the differential equations,

$$\left[-\frac{1}{2}\nabla^2 + v_c^\lambda(\mathbf{r})\right]\varphi_i^\lambda(\mathbf{r}) = \varepsilon_i^\lambda\varphi_i^\lambda(\mathbf{r}) \tag{1.6.21}$$

The form of Eqn. (1.6.21) is not particularly useful for implementation since it puts a large burden on the constraint potential. This may be reduced by adding to it the nuclear-electron and Coulomb potentials. Modifying the Coulomb potential by the Fermi–Amaldi factor $(1 - 1/N)$ also ensures the correct $-1/r$ long range behaviour of the exchange–correlation potential. This results in the equation

$$\left[-\frac{1}{2}\nabla^2 + v_{\text{ext}}(\mathbf{r}) + \left(1 - \frac{1}{N}\right)v_J^\lambda(\mathbf{r}) + v_c^\lambda(\mathbf{r})\right]\varphi_i^\lambda = \varepsilon_i^\lambda\varphi_i^\lambda(\mathbf{r}) \tag{1.6.22}$$

As $\lambda \to \infty$, Eqn. (1.6.22) gives the Kohn–Sham orbitals and so represents the Kohn–Sham equations. The exchange–correlation potential, $v_{\text{xc}}(\mathbf{r})$, can be identified as

$$v_{\text{xc}}(\mathbf{r}) = \lim_{\lambda\to\infty}\left[v_c^\lambda(\mathbf{r}) - \frac{1}{N}v_J^\lambda(\mathbf{r})\right] \tag{1.6.23}$$

In the application of the ZMP procedure to molecular calculations we employ Gaussian basis sets to represent the orbitals. The use of a finite basis set in ZMP calculations can cause a problem since it is not always possible to exactly describe a high quality input density in terms of N orbitals, so the solution point $\rho^\lambda(\mathbf{r}) = \rho_0(\mathbf{r})$ may not be obtainable. As a consequence, when the value of λ becomes large the exchange–correlation potential exhibits unphysical oscillatory structure and so a choice must be made for a finite value of λ which gives the best approximation to $v_{\text{xc}}(\mathbf{r})$ [60].

1.7 Exchange Correlation Functionals

If $E_{\text{xc}}[\rho]$ were exactly known then the KS-DFT scheme would be exact within the Born–Oppenheimer approximation. However no exact mathematical form is known for $E_{\text{xc}}[\rho]$ and so it must be approximated. The quality of this approximation is the limiting factor in the accuracy of results that can be obtained within the KS-DFT method. Unfortunately no systematic strategy exists for the development of $E_{\text{xc}}[\rho]$ functionals. Several different types of approximation are available and the development of new approximations is an active area of research.

1.7.1 The Local Density Approximation

In their initial paper, Kohn and Sham proposed the first approximation to $E_{\mathrm{xc}}[\rho]$, which is now known as the local density approximation (LDA). The LDA is based on the uniform electron gas. In this model electrons are evenly distributed on a positive background charge. It is possible to derive a highly accurate expression for $\varepsilon_{\mathrm{xc}}$, the exchange–correlation energy per electron in a uniform electron gas. The form of the LDA is

$$E_{\mathrm{xc}}^{\mathrm{LDA}}[\rho] = \int \rho(\mathbf{r})\varepsilon_{\mathrm{xc}}[\rho(\mathbf{r})]d\mathbf{r} \tag{1.7.1}$$

This is essentially $\varepsilon_{\mathrm{xc}}$ weighted by the probability of finding an electron at the point, $\rho(\mathbf{r})$. The quantity $\varepsilon_{\mathrm{xc}}[\rho(\mathbf{r})]$ may then be further divided into the exchange contribution $\varepsilon_{\mathrm{x}}[\rho(\mathbf{r})]$ and the correlation contribution $\varepsilon_{\mathrm{c}}[\rho(\mathbf{r})]$. The exchange part can be treated by the simple expression due to Dirac [47] as discussed for the Thomas–Fermi model. However the treatment of the correlation contribution is more difficult since there is no corresponding simple expression known for ε_{c}. Following the high accuracy quantum Monte-Carlo simulation results of Ceperley and Alder [61], several analytic forms were proposed by Vosko, Wilk and Nussair (VWN) [62] in 1980 and remain the most commonly used today. Despite the severe approximations involved in the application of the LDA to molecular systems, the results obtained from it are surprisingly good, in most cases comparable with those of the Hartree–Fock scheme. It is possible to achieve good vibrational frequencies, equilibrium structures and dipole moments. However bond energies are significantly too high giving a consistent overbinding of molecules. This has been rationalised in terms of the treatment of the exchange energy in the LDA by Ernzerhof, Perdew and Burke [63].

1.7.2 Generalised Gradient Approximation

In order to improve over the accuracy of the LDA, new functionals which include the gradient of the density, $\nabla\rho(\mathbf{r})$, were developed. The LDA can be thought of as the first term in a Taylor expansion. The full expression is the gradient expansion approximation (GEA) which models a system where the density is slowly varying

$$E_{\mathrm{xc}}^{\mathrm{GEA}}[\rho_\alpha, \rho_\beta] = \int \rho\ \varepsilon_{\mathrm{xc}}[\rho_\alpha, \rho_\beta]d\mathbf{r} + \sum_{\sigma,\sigma'} \int C_{\mathrm{xc}}^{\sigma,\sigma'}[\rho_\alpha, \rho_\beta] \frac{\nabla\rho_\sigma}{\rho_\sigma^{2/3}} \frac{\nabla\rho_{\sigma'}}{\rho_{\sigma'}^{2/3}} d\mathbf{r} + \ldots \tag{1.7.2}$$

The GEA however performs in general no better and often worse than the LDA. The reasons for this can be explained in terms of exact relations for the exchange–correlation hole which are not satisfied by the GEA but are satisfied by the LDA; consequently

the GEA potential diverges at long range. The solution to this problem with the GEA has been to apply corrections which force the functionals to obey the relations for the true exchange–correlation hole. The new functionals derived in this fashion are then called generalised gradient approximations (GGA's) and have the general form

$$E_{\mathrm{xc}}^{\mathrm{GGA}}[\rho_\alpha, \rho_\beta] = \int f(\rho_\alpha, \rho_\beta, \nabla\rho_\alpha, \nabla\rho_\beta)d\mathbf{r} \tag{1.7.3}$$

Normally $E_{\mathrm{xc}}^{\mathrm{GGA}}$ is split into exchange and correlation contributions which are derived separately. Two approaches to the development of GGA functionals have evolved. The first is to derive the functionals from first principles based on relations that are known to be true for the exact exchange–correlation functional. The second approach is to develop functionals by fitting to semi-empirical parameters. Some argument about the validity of the semi-empirical approach exists, but Becke [64] has argued in its defence that since we are approximating an exact but unknown functional $E_{\mathrm{xc}}[\rho]$ then either approach is equally valid to shed light on the underlying functional form. Commonly used examples of semi-empirical GGA functionals are BLYP [64, 65] and HCTH [66], whilst non-empirical examples include PW91 [67] and PBE [68]. Many GGA functionals have been designed specifically for the accurate calculation of certain chemical properties, for example the KT series of functionals [69, 70] derived with a focus on magnetic response properties. The use of GGA functionals can lead to significantly improved calculations of thermochemical properties compared with the LDA and the BLYP functional [64, 65] did a great deal to popularise density functional theory in chemistry.

1.7.3 Failures of the LDA and GGA Exchange Functionals

The exchange energy accounts for the bulk (~90%) of the exchange–correlation energy and its functional form is defined by the Hartree–Fock approximation. Unfortunately the LDA and GGA exchange functionals in current use have deficiencies in the form of their exchange potentials. Firstly since the Coulomb potential, $v_J(\mathbf{r}) = \int \frac{\rho(\mathbf{r}')}{|\mathbf{r}-\mathbf{r}'|}d\mathbf{r}'$, is the classical repulsive potential of the electron density with itself there is a spurious self repulsion contribution for each electron. In the Hartree–Fock method (which defines the exchange energy) this self interaction error is neatly cancelled by the non-local Hartree–Fock exchange potential

$$-\sum_{j=1}^{N}\int \frac{\varphi_i^*(\mathbf{r})\varphi_j^*(\mathbf{r}')\varphi_j(\mathbf{r})\varphi_i(\mathbf{r}')}{|\mathbf{r}-\mathbf{r}'|}d\mathbf{r}' \Big/ \varphi_i^*(\mathbf{r})\varphi_i(\mathbf{r}) \tag{1.7.4}$$

which for the case where $i = j$ becomes exactly the negative of the Coulomb potential. Thus an electron in an occupied orbital experiences repulsion from only the other $N - 1$ electrons. The case is different however for the unoccupied orbitals. Since the summation over j in Eqn. (1.7.4) runs over only the occupied orbitals then for an unoccupied orbital this cancellation cannot occur. Thus if an electron were placed into one of these orbitals it would experience repulsion from all N electrons. As a consequence the Hartree–Fock unoccupied orbitals generally have positive eigenvalues and are unbound.

In contrast the Kohn–Sham exchange operator is a local multiplicative potential, $v_{\mathrm{x}}(\mathbf{r})$, which acts on both the occupied and unoccupied orbitals equally. The exact Kohn–Sham exchange potential should ensure that all orbitals are self interaction free, correcting the deficiency of the Hartree–Fock approximation for the unoccupied orbitals, and hence must exhibit a $-1/r$ asymptotic behaviour. Unfortunately the LDA and commonly used GGAs are not self interaction free and because they are based on the density and its gradient they are unable to reproduce the correct asymptotic potential, instead decaying exponentially to zero. This leads to potentials which give a reasonable approximation to the shape of the true exchange potential in valence regions but are poor in asymptotic regions. Consequently only a few of the unoccupied orbitals are bound and properties such as excitation energies which depend sensitively on the unoccupied orbital eigenvalue spectrum are often poor. Although a method has been proposed by Perdew and Zunger to correct for the self interaction error explicitly in these functionals, it has not found widespread use [71].

A second way in which the LDA and GGAs are deficient is that they fail to exhibit the discontinuous behaviour of the derivative of the electronic energy with respect to particle number. As the particle number passes through an integer from the electron deficient side to the electron abundant side, the exact Kohn–Sham potential should 'jump' upwards [72]. Since neither the external or Coulomb contributions to the potential display this behaviour it must be introduced by the exchange–correlation potential. The LDA and GGA potentials are the derivatives of exchange–correlation energies which are continuous with respect to the variation in particle number and so they do not display this property. It may be argued that these so called continuum functionals average over the discontinuity, and so the resulting eigenvalues in the valence regions are shifted upwards by approximately half of the discontinuity.

To apply a correction to the shape of the GGA or LDA potentials in the asymptotic regions as $r \longrightarrow \infty$ the potential could be altered to approach a positive value as $-1/r$. Such a correction was proposed by Tozer and Handy [73] in which the potential in the

asymptotic region is replaced by

$$v_{\mathrm{xc}} = -\frac{1}{r} + \varepsilon_{\mathrm{HOMO}} + I \tag{1.7.5}$$

where $\varepsilon_{\mathrm{HOMO}}$ is the HOMO eigenvalue and I is the ionisation energy of the system, which may be obtained from separate calculations; the sum of the two terms approximates half of the derivative discontinuity. Unfortunately this scheme is not variational, although energies remain close to those of the original functionals employed since changes in the asymptotic potential have little effect on the electronic energy. This approach is employed in Chapter 3. Similar procedures have been proposed by other authors, see for example Refs. [74–76]

Whilst the asymptotic correction may be effective in correcting the shape of the Kohn–Sham potential it still averages over this discontinuity. This may have severe implications when GGA or LDA potentials are applied to the calculation of time-dependent properties involving well separated subsystems such as dissociation, ionisation [77] or charge transfer [78, 79] processes since the GGA and LDA exchange–correlation kernels (the derivative of the exchange–correlation potential with respect to the density) fail to display the required discontinuity. One way in which the above mentioned shortcomings of the LDA and GGA exchange potentials may be overcome in DFT is the use of orbital dependent functionals.

1.7.4 Meta-Generalised Gradient Approximations

An obvious next step to improve over the generalised gradient approximation functionals is to include higher order gradient corrections. A number of functionals have been developed which include the Laplacian, $\nabla^2\rho$ [80–82]. However the inclusion of the Laplacian can cause computational difficulties arising from the numerical sensitivity of the exchange–correlation Kohn–Sham matrix elements when this term is introduced [83]. An alternative approach is to include the non-interacting kinetic energy density

$$\tau_\sigma = \frac{1}{2}\sum_{i}^{N} |\nabla\varphi_{i,\sigma}(\mathbf{r})|^2 \tag{1.7.6}$$

Functionals which include either the Laplacian or the non-interacting kinetic energy density are called meta-GGAs. Examples include PKZB [84], TPSS [85] and VSXC [86]. This class of functionals is still in the relatively early stages of development and improvements over conventional GGA functionals in chemical applications have yet to be fully explored.

1.7.5 Hybrid Functionals

The exchange energy is defined by the Hartree–Fock scheme. It is also possible to use this orbital dependent form within the KS-DFT scheme by replacing the HF orbitals in the HF exchange energy expression by the KS orbitals. This could then be combined with a correlation functional effectively resulting in a version of the HF scheme which is corrected for the effects of electron correlation. This was proposed by Kohn and Sham [53] in their original paper and has been studied more recently and denoted as HF-KS theory. However the results obtained using the HF-KS scheme have been disappointing [87], owing to the difficulty of deriving a correlation functional appropriate for use with the non-local exchange energy, although recently some progress has been made in this direction [88].

Motivated by the adiabatic connection [89–92], an alternative to treating the full exchange contribution exactly is to include only a fraction of orbital exchange in combination with a GGA exchange–correlation functional. The resulting class of functionals are called hybrid functionals and represent the most successful and widely used functionals in KS-DFT. In genreal hybrid functionals have the form

$$E_{\mathrm{xc}}^{\mathrm{HYBRID}} = E_{\mathrm{x}}^{\mathrm{GGA}} + E_{\mathrm{c}}^{\mathrm{GGA}} + c_{\mathrm{x}} E_{\mathrm{x}}^{0} \tag{1.7.7}$$

where E_{x}^{0} is the orbital dependent exchange energy expression of the Hartree–Fock scheme

$$E_{\mathrm{x}}^{0} = -\sum_{ij} \iint \frac{\varphi_i^*(\mathbf{r})\varphi_j^*(\mathbf{r}')\varphi_j(\mathbf{r})\varphi_i(\mathbf{r}')}{|\mathbf{r}-\mathbf{r}'|} d\mathbf{r} d\mathbf{r}' \tag{1.7.8}$$

evaluated with the Kohn–Sham orbitals. The first such approximation was the 'Half and Half' functional of Becke [93] containing 50% orbital dependent Hartree–Fock exchange. It was recognised however that this amount of exchange is far from optimal and a number of semi-empirical hybrid functionals soon followed. The most popular and widely available of all is the B3LYP functional of Stevens *et al.* [94]. This functional has the form

$$E_{\mathrm{xc}}^{\mathrm{B3LYP}} = (1-a)E_{\mathrm{x}}^{\mathrm{LSDA}} + aE_{\mathrm{x}}^{0} + bE_{\mathrm{x}}^{\mathrm{LYP}} + cE_{\mathrm{c}}^{\mathrm{LYP}} + (1-c)E_{\mathrm{c}}^{\mathrm{LSDA}} \tag{1.7.9}$$

where $a = 0.20$, $b = 0.72$, and $c = 0.81$. The success of this functional in many applications including transition metal chemistry has lead to its enormous popularity. Other popular semi-empirical hybrid functionals follow the B97 form proposed by Becke [95]. Examples are the B97-1 [66], and B97-2 [96] functionals, the latter of which is used ex-

tensively throughout this thesis. It is notable that hybrid functionals generally contain 20-25% of exact exchange. This observation has been rationalized by Burke, Ernzerhof and Perdew [97] in the context of perturbation theory.

1.8 The Optimized Effective Potential Method

In the Kohn–Sham scheme the exchange–correlation potential is defined as the derivative of the exchange–correlation energy with respect to the density. However in most standard implementations, the potential corresponding to the orbital dependent part of hybrid functionals is evaluated as the derivative with respect to the orbitals. It can therefore be argued that these approaches are outside the Kohn–Sham formalism. In order to bring these approximations back into the Kohn–Sham scheme it is necessary to employ the optimized effective potential (OEP) method which delivers the lowest energy state for an orbital dependent functional subject to the constraint that the exchange–correlation operator is a local multiplicative potential.

Like many of the ideas discussed in this introduction, the optimized effective potential approach was suggested long before the beginning of Kohn–Sham theory. Stimulated by Slater's 1951 paper [51] proposing a simplification of the Hartree–Fock problem, Sharp and Horton [98] suggested the following variational problem. Find the potential, the same for all electrons, with respect to which the energy is stationary. Sharp and Horton presented integral equations for the problem and proposed an approximate way to solve them. It was not until 1976 that Talman and Shadwick [99] first solved the OEP problem numerically for atoms using the Hartree–Fock energy functional. The exchange potential arising from the solution of the exchange-only OEP equation may be identified as the exact exchange potential in the Kohn–Sham scheme [100].

The OEP scheme is now outlined. The Kohn–Sham potential may be written as

$$v_s(\mathbf{r}) = v_{\text{ext}}(\mathbf{r}) + v_{\text{J}}(\mathbf{r}) + v_{\text{xc}}(\mathbf{r}) \tag{1.8.1}$$

which is the sum of the external, Coulomb and exchange–correlation potentials. The exchange–correlation potential is defined as the derivative of the exchange–correlation energy with respect to the density

$$v_{\text{xc}}(\mathbf{r}) = \frac{\delta E_{\text{xc}}}{\delta \rho(\mathbf{r})} \tag{1.8.2}$$

In the OEP approach a form for the exchange–correlation energy which is orbital

dependent is chosen. Using the chain rule for functional derivatives twice, we can write the exchange–correlation potential as

$$v_{\mathrm{xc}}(\mathbf{r}) = \sum_i \int d\mathbf{r}' \int d\mathbf{r}'' \left[\frac{\delta E_{\mathrm{xc}}}{\delta \varphi_i(\mathbf{r}')} \frac{\delta \varphi_i(\mathbf{r}')}{\delta v_s(\mathbf{r}'')} + \frac{\delta E_{\mathrm{xc}}}{\delta \varphi_i^*(\mathbf{r}')} \frac{\delta \varphi_i^*(\mathbf{r}')}{\delta v_s(\mathbf{r}'')} \right] \frac{\delta v_s(\mathbf{r}'')}{\delta \rho(\mathbf{r})} \tag{1.8.3}$$

The last term is the inverse of the density response function for a system of non-interacting particles, $\chi_s^{-1}(\mathbf{r}'', \mathbf{r})$, which relates changes in the density with changes in the Kohn–Sham effective potential

$$\delta\rho(\mathbf{r}) = \int d\mathbf{r}' \chi_s(\mathbf{r}, \mathbf{r}') \delta v_s(\mathbf{r}') \tag{1.8.4}$$

Acting with the response operator on both sides of Eqn. (1.8.3) gives

$$\int d\mathbf{r}' v_{\mathrm{xc}}(\mathbf{r}') \chi_s(\mathbf{r}', \mathbf{r}) = \sum_i \int d\mathbf{r}' \left[\frac{\delta E_{\mathrm{xc}}}{\delta \varphi_i(\mathbf{r}')} \frac{\delta \varphi_i(\mathbf{r}')}{\delta v_s(\mathbf{r})} + \frac{\delta E_{\mathrm{xc}}}{\delta \varphi_i^*(\mathbf{r}')} \frac{\delta \varphi_i^*(\mathbf{r}')}{\delta v_s(\mathbf{r})} \right] \tag{1.8.5}$$

From first order perturbation theory the the functional derivative of the orbitals with respect to the potential is known [101]

$$\frac{\delta \varphi_i(\mathbf{r}')}{\delta v_s(\mathbf{r})} = \sum_{j \neq i} \varphi_i(\mathbf{r}) \frac{\varphi_j^*(\mathbf{r}) \varphi_j(\mathbf{r}')}{\varepsilon_i - \varepsilon_j} \tag{1.8.6}$$

The density response function of the non-interacting system can also be expressed in terms of the orbitals and eigenvalues as [101]

$$\chi_s(\mathbf{r}, \mathbf{r}') = \sum_i \sum_a \frac{\varphi_i^*(\mathbf{r}) \varphi_a(\mathbf{r}) \varphi_a^*(\mathbf{r}') \varphi_i(\mathbf{r}')}{\varepsilon_i - \varepsilon_a} + \text{c.c.} \tag{1.8.7}$$

Substituting these into Eqn. (1.8.5) gives the OEP integral equation

$$\sum_i \int d\mathbf{r}' \left[v_{\mathrm{xc}}(\mathbf{r}') - u_{\mathrm{xc}i}(\mathbf{r}') \right] G_{si}(\mathbf{r}', \mathbf{r}) \varphi_i(\mathbf{r}) \varphi_i^*(\mathbf{r}') + \text{c.c.} = 0 \tag{1.8.8}$$

where

$$u_{\mathrm{xc}i}(\mathbf{r}) = \frac{1}{\varphi_i^*(\mathbf{r})} \frac{\delta E_{\mathrm{xc}}}{\delta \varphi_i(\mathbf{r})} \tag{1.8.9}$$

$$G_{si}(\mathbf{r}, \mathbf{r}') = \sum_{j \neq i} \frac{\varphi_j(\mathbf{r}) \varphi_j^*(\mathbf{r}')}{\varepsilon_i - \varepsilon_j} \tag{1.8.10}$$

The same expression can be reached by demanding that the energy is stationary with respect to the potential. The orbital dependent energy functional has not been specified

in these equations. Originally in the literature the exchange-only case was considered since the form of the orbital dependent exchange energy is known by definition from the Hartree–Fock scheme. In Chapter 6 the OEP scheme is applied to other orbital dependent energy functionals.

The solution of Eqn. (1.8.8) must be carried out at each iteration of the Kohn–Sham calculation. Many different strategies have been devised to attempt this; most use a finite basis set to discretise the OEP equation and then solve it algebraically. These methods have been developed for solids [102–104] and molecules [105–108]. Recently an iterative scheme for the calculation of the OEP potential was developed by Kümmel and Perdew [109]. However most of these approaches are not suitable for application to larger chemically relevant systems.

An alternative approach is to ensure that the effective potential depends on a set of scalar parameters and directly optimize the energy with respect to these parameters. Several implementations of this type have been suggested [110–112] and of these the approach due to Yang and Wu [112] is particularly applicable to molecular systems. The implementation and application of this method forms a significant part of this thesis.

In Chapter 2 the implementation of several approximations to the OEP exchange potential are described and applied to the calculation of NMR shielding constants. Chapter 3 extends the investigation to excitation energies and structural perturbations. The implementation and testing of the Yang–Wu OEP procedure [112] and WY constrained search [58] methods are described in Chapter 4. A comparison of the approximate exchange only methods of Chapter 2 with the exchange-only OEP is presented in Chapter 5, paying particular attention to the potential, frontier orbitals, density, eigenvalues and electronic energies from each approach. In Chapter 6 the OEP implementation is extended to include hybrid functionals and these are applied to the calculation of rotational g tensors and particularly challenging transition metal NMR chemical shifts. Chapter 7 describes the application of DFT methods to a problem of relevance to organic chemistry. Conclusions are presented in Chapter 8.

Chapter 2

Approximate Exchange: Magnetic Response

In this chapter we describe our implementation of several approximations to the exact OEP exchange potential and apply them to the calculation of magnetic response properties. Their use in multiplicative hybrid functionals is explored and the potentials from these approaches are compared with those obtained using the Zhao–Morrison–Parr procedure.

2.1 Exchange Only Methods

In exchange only Kohn–Sham theory the Born–Oppenheimer electronic energy may be written as

$$E = T_{\mathrm{s}} + E_{\mathrm{ext}} + E_{\mathrm{J}} + E_{\mathrm{x}} \tag{2.1.1}$$

where T_s is the non-interacting kinetic energy, E_{ext} describes the interaction between the density and the external potential due to the nuclei, E_{J} is the classical electrostatic Coulomb repulsion of the density, and E_{x} is the exchange energy. These energy contributions are evaluated from the exchange only Kohn–Sham orbitals $\varphi_i(\mathbf{r})$ which are the solutions to exchange only Kohn–Sham equations of the form

$$\left[-\frac{1}{2}\nabla^2 + v_{\mathrm{ext}}(\mathbf{r}) + v_{\mathrm{J}}(\mathbf{r}) + v_{\mathrm{x}}(\mathbf{r})\right]\varphi_i(\mathbf{r}) = \varepsilon_i\varphi_i(\mathbf{r}) \tag{2.1.2}$$

where $v_{\mathrm{ext}}(\mathbf{r})$ and $v_{\mathrm{J}}(\mathbf{r})$ are the external and Coulomb potentials, $v_{\mathrm{x}}(\mathbf{r})$ is the multiplicative exchange potential

$$v_{\mathrm{x}}(\mathbf{r}) = \frac{\delta E_{\mathrm{x}}}{\delta\rho(\mathbf{r})} \tag{2.1.3}$$

and ε_i are the Kohn–Sham one electron eigenvalues.

The exchange energy is defined by the Hartree–Fock scheme and may be calculated by the orbital dependent energy functional of Eqn. (1.7.8). If this functional is to be used in Kohn–Sham theory then the evaluation of the exchange potential according to Eqn. (2.1.3) is non-trivial and the optimized effective potential (OEP) scheme outlined in Section 1.8 must be employed. The solution of the OEP Eqn. (1.8.8) is difficult and a number of simplifications have been proposed to allow the determination of approximate exchange potentials. The implementation and application of several such schemes is described in this chapter.

2.2 The Slater Exchange Potential

The first approximate exchange potential considered is the Slater potential (also known as the average Fock approximation) [51]. Although this potential was proposed some 14 years prior to the advent of Kohn–Sham theory it may be regarded as a Kohn–Sham exchange potential [113]. It displays the correct $-1/r$ asymptote and occurs as the leading term in many approximations to the exact exchange potential. In this section we outline our implementation and testing of the Slater exchange potential as suggested by Della Sala and Görling [114]. The Slater potential may be written in the form

$$v_{\mathrm{x}}^{\mathrm{Slater}}(\mathbf{r}) = -\frac{n_s}{\rho(\mathbf{r})} \sum_{i \leqslant j} j_{ij} \varphi_i(\mathbf{r}) \varphi_j(\mathbf{r}) \int d\mathbf{r}' \frac{\varphi_j(\mathbf{r}') \varphi_i(\mathbf{r}')}{|\mathbf{r} - \mathbf{r}'|} \tag{2.2.1}$$

where $j_{ij} = 2$ for $i \neq j$ and $j_{ij} = 1$ for $i = j$. To evaluate this expression would require calculation of the electrostatic potential of the overlap density for all products of occupied orbitals at each point on the quadrature grid. This is computationally demanding and so instead, following Della Sala and Görling [114], we employ the resolution of the identity in the basis set and evaluate the Slater potential as

$$v_{\mathrm{x}}^{\mathrm{Slater}}(\mathbf{r}) = \frac{n_s}{\rho(\mathbf{r})} \mathrm{Tr}\left[\mathbf{Q}\mathbf{X}(\mathbf{r})\right] \tag{2.2.2}$$

where $\mathbf{X}(\mathbf{r}) = \chi(\mathbf{r})\chi^T(\mathbf{r})$ and $\chi(\mathbf{r})$ contains the basis functions. The matrix $\mathbf{Q}$ is defined by $\mathbf{Q} = \frac{1}{2}\mathbf{S}^{-1}\mathbf{K}\mathbf{P} + \frac{1}{2}\mathbf{P}\mathbf{K}\mathbf{S}^{-1}$ where $\mathbf{P} = \sum_i \mathbf{u}_i \mathbf{u}_i^T$ is the density matrix, $\mathbf{u}$ contains the molecular orbital coefficients and the matrix $\mathbf{S}$ is the basis function overlap matrix. We have implemented this method in the CADPAC quantum chemistry code [115].

2.3 The Localized Hartree-Fock Method

The Slater potential provides a link between the local exchange potential in the Kohn–Sham scheme and the non-local exchange potential in the Hartree–Fock scheme by carrying out a weighted average according to the density. In 2001 Della Sala and Görling [114] suggested a derivation of an approximate Kohn–Sham exchange potential by considering the link between the single determinants in the two theories. They began from the assumption that the Kohn–Sham exchange only and Hartree–Fock determinants are the same. Hence there would exist one Slater determinant which could simultaneously satisfy the Kohn–Sham and Hartree–Fock non-interacting equations

$$\left[\hat{T} + \hat{V}_{\text{ext}} + \hat{V}_{\text{J}} + \hat{V}_{\text{x}}^{\text{NL}}\right] \Phi = E_s^{\text{HF}} \Phi \tag{2.3.1}$$

$$\left[\hat{T} + \hat{V}_{\text{ext}} + \hat{V}_{\text{J}} + \hat{V}_{\text{x}}\right] \Phi = E_s^{\text{KS}} \Phi \tag{2.3.2}$$

where the operators in square brackets are the sum of the corresponding one electron operators for the HF and KS formalisms respectively.

To derive an expression for the exchange potential, Eqns. (2.3.1) and (2.3.2) are multiplied by the Hermitian adjoint of the Slater determinant, $\Phi^{\dagger}$, and the two are subtracted. Integration over the spatial variables of all but one electron and summation over all the spin variables gives

$$\begin{aligned}
&\frac{1}{N} \quad \sum_i \varphi_i(\mathbf{r}) v_{\text{x}}(\mathbf{r}) \varphi_i(\mathbf{r}) - \varphi_i(\mathbf{r}) \left[\hat{v}_{\text{x}}^{\text{NL}} \varphi_i\right](\mathbf{r}) + \frac{n_s}{N} \sum_{i,j} \varphi_i(\mathbf{r}) \varphi_i(\mathbf{r}) \left\langle \varphi_j \left| \hat{v}_{\text{x}} - \hat{v}_{\text{x}}^{\text{NL}} \right| \varphi_j \right\rangle \\
-&\frac{1}{N} \quad \sum_{i,j} \varphi_i(\mathbf{r}) \varphi_j(\mathbf{r}) \left\langle \varphi_j \left| \hat{v}_{\text{x}} - \hat{v}_{\text{x}}^{\text{NL}} \right| \varphi_i \right\rangle \\
=&\frac{1}{N} \quad \sum_j \left\langle \varphi_j \left| \hat{v}_{\text{x}} - \hat{v}_{\text{x}}^{\text{NL}} \right| \varphi_j \right\rangle \rho(\mathbf{r})
\end{aligned} \tag{2.3.3}$$

The second term of this equation is equal to the right hand side and so cancels it. Division of the resulting equation by the electron density and rearranging gives an expression for the exchange potential

$$\begin{aligned}
v_{\text{x}}(\mathbf{r}) \;=\; & \frac{n_s}{\rho(\mathbf{r})} \sum_i \varphi_i(\mathbf{r}) \left[\hat{v}_{\text{x}}^{\text{NL}} \varphi_i\right](\mathbf{r}) + \frac{n_s}{\rho(\mathbf{r})} \sum_{i,j} \varphi_i(\mathbf{r}) \varphi_j(\mathbf{r}) \left\langle \varphi_j \left| \hat{v}_{\text{x}} \right| \varphi_i \right\rangle \\
- \; & \frac{n_s}{\rho(\mathbf{r})} \sum_{i,j} \varphi_i(\mathbf{r}) \varphi_j(\mathbf{r}) \left\langle \varphi_j \left| \hat{v}_{\text{x}}^{NL} \right| \varphi_i \right\rangle
\end{aligned} \tag{2.3.4}$$

which is the key expression in the LHF scheme. The first term may be identified as the Slater potential [51], allowing us to write the exchange potential as a sum of the

Slater potential and a correction term

$$\begin{aligned} v_{\mathrm{x}}(\mathbf{r}) &= v_{\mathrm{x}}^{\mathrm{Slater}}(\mathbf{r}) + v_{\mathrm{x}}^{\mathrm{cor}}(\mathbf{r}) \\ &= \frac{n_s}{\rho(\mathbf{r})} \sum_i \varphi_i(\mathbf{r}) \left[\hat{v}_{\mathrm{x}}^{\mathrm{NL}} \varphi_i\right](\mathbf{r}) \\ &+ \frac{n_s}{\rho(\mathbf{r})} \sum_{i \leqslant j} j_{ij} \varphi_i(\mathbf{r}) \varphi_j(\mathbf{r}) \left\langle \varphi_j \left| \hat{v}_{\mathrm{x}} - \hat{v}_{\mathrm{x}}^{\mathrm{NL}} \right| \varphi_i \right\rangle \end{aligned} \tag{2.3.5}$$

This equation now determines the exchange potential up to an additive constant. The constant is fixed by inserting the KS canonical orbitals and ensuring that for the highest occupied orbital

$$\left\langle \varphi_N \left| \hat{v}_{\mathrm{x}} - \hat{v}_{\mathrm{x}}^{\mathrm{NL}} \right| \varphi_N \right\rangle = 0 \tag{2.3.6}$$

The exchange potential then has the same asymptotic behaviour as the Slater potential and approaches zero as $-1/r$. If the KS and HF determinants were in fact equal then the potential of Eqn. (2.3.5) could replace the complex non-multiplicative operator in the HF scheme without altering the resulting orbitals. However since the non-multiplicative exchange operator can never be replaced exactly by a multiplicative counterpart (in a complete basis set) the determinants can never be exactly equal and hence the LHF potential represents an approximation to the operator. To implement the above scheme in the CADPAC quantum chemistry code the LHF equations must be transformed to a set of matrix equations.

In matrix form the Slater potential is given by Eqn. (2.2.2), which uses the resolution of the identity. Hence whilst this is exact in a complete basis set it becomes only approximately so in a finite one. We will discuss the effect that this has on practical calculations later. The correction potential may be re-written in matrix form as

$$\begin{aligned} v_{\mathrm{x}}^{\mathrm{cor}}(\mathbf{r}) &= \frac{n_s}{\rho(\mathbf{r})} \mathrm{Tr}[(\mathbf{U}\mathbf{C}\mathbf{U}^T)\chi(\mathbf{r})\chi^T(\mathbf{r})] \\ &= \frac{n_s}{\rho(\mathbf{r})} \mathrm{Tr}[\mathbf{R}\mathbf{X}(\mathbf{r})] \end{aligned} \tag{2.3.7}$$

where $\mathbf{R} = \mathbf{U}\mathbf{C}\mathbf{U}^T$ and $\mathbf{U}$ is constructed from the N column vectors for the occupied orbitals in the basis set. The elements of the $N \times N$ matrix $\mathbf{C}$ are given by

$$c_{ij} = \left\langle \varphi_j \left| \hat{v}_{\mathrm{x}} - \hat{v}_{\mathrm{x}}^{\mathrm{NL}} \right| \varphi_i \right\rangle \tag{2.3.8}$$

except when $i = j = N$, in which case we choose $c_{ij} = 0$. All of the expressions required to efficiently evaluate the LHF potential in a self consistent scheme are now in place. At each iteration in the LHF method the following steps are performed, starting from

the orbitals and exchange potential of the cycle before.

1. The Coulomb potential is calculated as in standard codes;
2. A new Slater potential is calculated according to Eqn. (2.2.2);
3. The correction term is assembled according to Eqn. (2.3.7) and the correction potential calculated;
4. The new KS exchange potential is calculated by summation of the two terms;
5. A new Hamiltonian operator is constructed and diagonalized to give a new set of orbitals.

On the first iteration, only the Slater potential is calculated since the correction term requires the multiplicative exchange potential of the previous cycle for its construction. The LHF scheme can be implemented by constructing the LHF potential at each iteration of the SCF cycle. Although in practice this scheme does converge to give the LHF exchange potential, the number of iterations required is excessive, making even simple calculations very time consuming.

2.3.1 Accelerating the Convergence of the LHF Method

As an alternative to the iterative LHF scheme, a second scheme exists in which the local KS exchange potential is calculated directly using the canonical HF orbitals. This non-iterative approach effectively transforms the HF orbitals and eigenvalues into KS orbitals and is called the transformation LHF (TLHF) scheme [114]. In the TLHF scheme the canonical HF orbitals, ψ_i, are used and the requirement

$$\left\langle \psi_N \left| \hat{v}_\mathrm{x} - \hat{v}_\mathrm{x}^\mathrm{NL} \right| \psi_N \right\rangle = 0 \tag{2.3.9}$$

is imposed. The expression for the TLHF exchange potential is analogous with Eqn. (2.3.5) for the LHF potential but with the Kohn–Sham orbitals replaced by the Hartree–Fock ones. Defining the quantity

$$c_{ij} = \sqrt{j_{ij}} \left\langle \psi_j \left| \hat{v}_\mathrm{x} - \hat{v}_\mathrm{x}^\mathrm{NL} \right| \psi_i \right\rangle \tag{2.3.10}$$

allows the TLHF exchange potential to be written as

$$v_\mathrm{x}(\mathbf{r}) = v_\mathrm{x}^\mathrm{Slater}(\mathbf{r}) + v_\mathrm{x}^\mathrm{cor}(\mathbf{r}) = \frac{n_s}{\rho(\mathbf{r})} \sum_i \psi_i(\mathbf{r}) \left[\hat{v}_\mathrm{x}^\mathrm{NL} \psi_i\right](\mathbf{r}) + \frac{n_s}{\rho(\mathbf{r})} \sum_{i \lessdot j} \sqrt{j_{ij}} c_{ij} \psi_i(\mathbf{r}) \psi_j(\mathbf{r}) \tag{2.3.11}$$

To calculate the TLHF exchange potential via this equation the coefficients c_{ij} are required. In order to find these coefficients the above expression is manipulated into a set of linear equations which can be solved for c_{ij}. This is achieved by multiplying Eqn. (2.3.11) by the product $\psi_k(\mathbf{r})\psi_l(\mathbf{r})$ then integrating over $\mathbf{r}$, subtracting $\langle \psi_k | \hat{v}_x^{NL} | \psi_l \rangle$ from both sides of the equation and multiplication by $\sqrt{j_{kl}}$. This results in the set of matrix equations

$$[\mathbf{I} - \mathbf{M}]\,\mathbf{c} = \mathbf{t} \tag{2.3.12}$$

in which

$$M_{kl,ij} = n_s \sqrt{j_{kl} j_{ij}} \int d\mathbf{r}\, \frac{\psi_k(\mathbf{r})\psi_l(\mathbf{r})\psi_i(\mathbf{r})\psi_j(\mathbf{r})}{\rho(\mathbf{r})} \tag{2.3.13}$$

$$t_{kl} = \sqrt{j_{kl}} \langle \psi_k | \hat{v}_x^{Slater} - \hat{v}_x^{NL} | \psi_l \rangle \tag{2.3.14}$$

and the vector $\mathbf{c}$ contains the coefficients c_{kl}. The solution of these matrix equations is most efficient, especially in the case of larger systems, if the conjugate gradient procedure is used. The factors $\sqrt{j_{ij}}$ and $\sqrt{j_{kl}}$ are included in the definition of c_{ij} and t_{kl} in order to ensure that the matrix $\mathbf{M}$ is symmetric. This allows the selection of a subroutine designed to work only for symmetric matrices [116]. This is more efficient because the computationally expensive product $\mathbf{Mc}$ is then required only once per conjugate gradient step. In our implementation of the TLHF scheme in CADPAC we set the initial guess at the solution by constructing a matrix $\mathbf{C}$ whose elements are given by

$$c_{ij}^{(0)} = \frac{2}{3} \langle \psi_i | \hat{v}_x^{Slater} | \psi_j \rangle - \langle \psi_i | \hat{v}_x^{NL} | \psi_j \rangle \tag{2.3.15}$$

A vector $\mathbf{c}$ is then constructed from the lower triangle of this matrix. The matrix $\mathbf{T}$ is constructed according to Eqn. (2.3.14) and its lower triangle stored as the vector $\mathbf{t}$. At each step of the conjugate gradient procedure we require the vector $\mathbf{c}$-$\mathbf{Mc}$ which for its construction requires the product $\mathbf{Mc}$. In order to evaluate this product we do not explicitly construct the matrix elements of $\mathbf{M}$ but rather we determine the correction potential of Eqn. (2.3.7), ${}^{(n)}v_x^{cor}$, using the coefficients at that stage of the conjugate gradient procedure $c_{ij}^{(n)}$. Then the matrix elements $\langle \psi_k | {}^{(n)}v_x^{cor} | \psi_l \rangle$ are calculated and multiplied by the factors $\sqrt{j_{kl}}$ which gives the required product $\mathbf{Mc}^{(n)}$. The set of matrix equations can be solved provided that the matrix $\mathbf{M}$ does not have an eigenvalue equal to 1. This is the case in all practical applications and so no problem arises with the evaluation of the TLHF potential. The TLHF scheme therefore consists of the following steps,

1. Carry out a HF calculation;

2. Calculate the Slater potential from the HF orbitals according to Eqn. (2.2.2);

3. Calculate t_{kl} according to Eqn. (2.3.14) and determine the coefficients c_{ij} by solving Eqn. (2.3.12) using the conjugate gradient procedure. Construct the correction potential according to Eqn. (2.3.7);

4. Calculate the TLHF exchange potential;

5. Construct a new Hamiltonian operator and diagonalise to give a new set of orbitals.

The potential and orbitals resulting from the TLHF scheme as described above are not quite the same as those obtained from the LHF scheme introduced earlier. The reasons for this can be traced to the fact that the asymptotic behaviour of the Hartree–Fock orbitals is different to the Kohn–Sham orbitals. However if we iterate steps 2–5 of the TLHF procedure then the LHF solutions are obtained but in significantly fewer iterations. The final set of coefficients c_{ij} from each iteration is used as the starting guess for the next, which leads to progressively fewer conjugate gradient iterations as the calculation converges. This procedure allows the application of the LHF scheme to a much wider range of molecules.

2.3.2 The Asymptotic Behaviour of the LHF Potential

Examination of Eqns. (2.2.2) and (2.3.7) shows that the LHF potential will be subject to numerical problems in asymptotic regions. This arises due to dividing through by an almost vanishing density, which cannot be accurately held within machine precision. To circumvent this problem Della Sala and Görling suggested [114] replacing the potential in regions where the density falls below 10^{-7}a.u. with the potential from the multipole expansion

$$v_{\mathrm{x}}^{\mathrm{asymp}}(\mathbf{r}) = -\frac{1}{(n_s N)} \int \frac{\rho(\mathbf{r}')}{|\mathbf{r} - \mathbf{r}'|} d\mathbf{r}' \tag{2.3.16}$$

This expression is already routinely evaluated in the CADPAC code for KS calculations using the asymptotic correction scheme of Tozer and Handy [73].

By forcing the LHF potential to approach zero as $-1/r$ asymptotically we may introduce an approximation because for regions that are on the nodal plane of the HOMO, the exact exchange potential can be shown to approach a constant value [117, 118]. This behaviour is lost by artificially enforcing the asymptotic potential of Eqn. (2.3.16). Görling has presented a method which allows the calculation of the LHF potential in asymptotic regions whilst maintaining this behaviour [118]. At present this is not implemented in our LHF code and so throughout this thesis we restrict our LHF calculations to molecules in which the HOMO has no nodal plane.

2.3.3 The Resolution of the Identity and Basis Sets

The derivation of the Slater potential in Eqn. (2.2.2) involves the resolution of the identity. An alternative is to evaluate the Slater potential numerically. This approach has been taken by Della Sala and Görling [114], however calculations of properties using either approach give very similar results for even moderately large basis sets. Recently other schemes for the efficient evaluation of the Slater potential have been suggested which employ density fitting techniques [119].

The evaluation of the Slater potential according to Eqn. (2.2.2) relies on the expansion of $[\hat{v}_{\mathrm{x}}^{\mathrm{NL}}\varphi_i]$ in the orbital basis set. When basis sets are derived they often contain core functions which are contractions of several Gaussian functions. This helps to keep the basis sets small and so improves computational efficiency. The contractions are usually optimized so that the representation of the Hartree–Fock orbitals is as accurate as possible. Unfortunately these contractions are far from optimal for the basis set expansion of the quantity $[\hat{v}_{\mathrm{x}}^{\mathrm{NL}}\varphi_i]$, degrading the quality of the Slater potential calculated.

For first row atoms basis sets generally contain few contracted functions and so the Slater potential calculated using standard basis sets may be reasonably accurate. However for atoms after the first row, basis sets contain progressively more contractions as the core becomes larger. This can lead to serious defects in the Slater potential. Evaluating the Slater potential numerically is one solution to this problem, although it is computationally demanding. Alternatively we can remove the contractions from the basis sets completely so that they become sufficiently flexible to represent both the orbitals and the quantity $[\hat{v}_{\mathrm{x}}^{\mathrm{NL}}\varphi_i]$. This is the approach taken in the current work.

2.4 The KLI Method

After the work of Talman and Shadwick [99] to enable the solution of the numerical OEP equation for atoms, it was not until the early 1990's that interest in the OEP approach was further stimulated by the implementation of a simple approximation to the OEP exchange potential by Kreiger, Li, and Iafrate (KLI) [120]. The KLI potential retains many of the key features of the true exchange only OEP. It reduces to the LDA in the uniform electron gas limit; for finite systems as $r \longrightarrow \infty$ it behaves as $-1/r$; the highest occupied orbital eigenvalue satisfies the generalised Koopmans theorem; and it displays the integer discontinuity of Section 1.7.3.

The KLI potential is derived by making an approximation which was originally

proposed by Sharp and Horton [98]. In the OEP integral Eqn. (1.8.8) the replacement

$$G_{si}(\mathbf{r},\mathbf{r}') = \sum_{j\neq i} \frac{\varphi_j(\mathbf{r})\varphi_j^*(\mathbf{r}')}{\varepsilon_i - \varepsilon_j} \simeq \frac{1}{\Delta\varepsilon}\left[\delta(\mathbf{r}-\mathbf{r}') - \varphi_i(\mathbf{r})\varphi_i^*(\mathbf{r}')\right] \tag{2.4.1}$$

is made which leads to the KLI potential

$$v_{\mathrm{xc}}^{\mathrm{KLI}}(\mathbf{r}) = \frac{1}{\rho(\mathbf{r})}\sum_i |\varphi_i(\mathbf{r})|^2 \left[w_{\mathrm{xc}i}(\mathbf{r}) + (\overline{v}_{\mathrm{xc}i} - \overline{w}_{\mathrm{xc}i})\right] \tag{2.4.2}$$

where $w_{\mathrm{xc}i} = \frac{1}{2}(u_{\mathrm{xc}i}(\mathbf{r}) + u_{\mathrm{xc}i}^*(\mathbf{r}))$, with $u_{\mathrm{xc}i}$ of Eqn. (1.8.9), and $\overline{v}_{\mathrm{xc}i}$ and $\overline{w}_{\mathrm{xc}i}$ denote the averaged values of $w_{\mathrm{xc}i}$ and $v_{\mathrm{xc}i}$ over the ith orbital, respectively. That is

$$\overline{w}_{\mathrm{xc}i} = \int d\mathbf{r}\, |\varphi_i(\mathbf{r})|^2 w_{\mathrm{xc}i}(\mathbf{r}) \tag{2.4.3}$$

$$\overline{v}_{\mathrm{xc}i} = \int d\mathbf{r}\, |\varphi_i(\mathbf{r})|^2 v_{\mathrm{xc}i}(\mathbf{r}) \tag{2.4.4}$$

It may be noted that for the exchange-only case the KLI potential can be separated into two contributions. The first may be identified as the Slater potential of Section 1.5.4 and the second is often referred to as the response or correction term. So we may write the KLI potential as

$$v_{\mathrm{xc}}^{\mathrm{KLI}}(\mathbf{r}) = v_{\mathrm{x}}^{\mathrm{Slater}}(\mathbf{r}) + \sum_i \frac{|\varphi_i|^2}{\rho(\mathbf{r})}\left(\overline{v}_{\mathrm{x}i} - \overline{w}_{\mathrm{x}i}\right) \tag{2.4.5}$$

The KLI potential is determined only up to an additive constant, as is the exact potential, and this constant is chosen such that $v_{\mathrm{x}}^{\mathrm{KLI}} \to 0$ as $r \to \infty$. This requires that the $\overline{v}_{\mathrm{x}N} = \overline{w}_{\mathrm{x}N}$ where N denotes the HOMO. This also has the consequence that the generalised Koopmans theorem is satisfied. This requirement determines one of the N constants of Eqn. (2.4.5). The other $N-1$ may be found by multiplying Eqn. (2.4.2) by $|\varphi_j(\mathbf{r})|^2$ and integrating over $\mathbf{r}$, resulting in

$$\overline{v}_{\mathrm{x}j} = \overline{v}_{\mathrm{x}j}^{\mathrm{Slater}} + \sum_{i=1}^{N-1} M_{ij}\left(\overline{v}_{\mathrm{x}i} - \overline{w}_{\mathrm{x}i}\right) \tag{2.4.6}$$

where

$$M_{ij} = \int \frac{\varphi_j^*(\mathbf{r})\varphi_j(\mathbf{r})\varphi_i^*(\mathbf{r})\varphi_i(\mathbf{r})}{\rho(\mathbf{r})} d\mathbf{r} \tag{2.4.7}$$

and

$$\overline{v}_{\mathrm{x}j}^{\mathrm{Slater}} = \int d\mathbf{r}\, |\varphi_j(\mathbf{r})|^2 v_{\mathrm{x}j}^{\mathrm{Slater}}(\mathbf{r}) \tag{2.4.8}$$

giving the matrix equation for the coefficients as

$$\overline{v}_{\mathrm{x}i} = \sum_{j=1}^{N-1} (I - M)^{-1}_{ij} \left(\overline{v}_{\mathrm{x}j}^{\mathrm{Slater}} - M_{ij} \overline{v}_{\mathrm{x}j} \right) \tag{2.4.9}$$

The KLI equations clearly bear a close resemblance to the LHF equations. In fact replacing Eqn. (2.3.10) with

$$c_{ij} = \delta_{ij} \sqrt{j_{ij}} \left\langle \varphi_j \left| \hat{v}_{\mathrm{x}} - \hat{v}_{\mathrm{x}}^{\mathrm{NL}} \right| \varphi_i \right\rangle \tag{2.4.10}$$

causes the TLHF equations to become the TKLI equations which may be solved by the same methods. So we may use our LHF implementation to solve the KLI equations simply by replacing the off diagonal elements of the matrix $\mathbf{C}$ with 0.

2.5 Other Approximate Exchange Potentials

In 2001 Gritsenko and Baerends proposed another approximation to the exchange potential in Kohn–Sham theory [121]. Their approach, denoted CEDA (common-energy-denominator approximation), recognises the fact that the Sharp–Horton replacement for the Green's function used in the KLI scheme levels the eigenvalue differences for the occupied-occupied and occupied-unoccupied orbital pairs, which may be substantially different. The alternative replacement

$$G_{si}(\mathbf{r}, \mathbf{r}') = \sum_{i \neq j} \frac{\varphi_j(\mathbf{r}) \varphi_j^*(\mathbf{r}')}{\varepsilon_i - \varepsilon_j} \simeq \frac{\delta(\mathbf{r} - \mathbf{r}')}{\Delta\varepsilon} - \frac{1}{\Delta\varepsilon} \sum_{j}^{N} \varphi_j(\mathbf{r}) \varphi_j^*(\mathbf{r}') + \sum_{j \neq i}^{N} \frac{1}{\Delta\varepsilon_{ij}} \varphi_j(\mathbf{r}) \varphi_j^*(\mathbf{r}') \tag{2.5.1}$$

is made in the OEP integral Eqn. (1.8.8) which maintains the true eigenvalue differences $\Delta\varepsilon_{ij}$ for the occupied-occupied pairs but replaces the occupied-virtual eigenvalue differences with the common denominator $\Delta\varepsilon$. Following a derivation analogous to the one presented for the KLI potential a set of matrix equations are obtained which are equivalent to those obtained under the LHF approximation for closed shells. This approach gives a more formal insight into the link between the KLI and CEDA/LHF approaches as compared with the OEP equation. The inclusion of the exact occupied-occupied eigenvalue differences in the Green's function of the CEDA approach may be regarded as an improvement over the Sharp–Horton approximation used in the derivation of the KLI potential. The potential which results also has the desirable property that it is invariant with respect to a unitary transformation of the orbitals, which is not the case for the KLI potential.

Table 2.1: Electronic energies and eigenvalues of the Ne atom calculated using exchange-only approaches in E_h

	Slater	KLI	LHF	OEP	HF
E	-128.500679	-128.544832	-128.544808	-128.5454	-128.547094
ε_1	-32.076390	-30.802103	-30.770286	-30.8200	-32.772441
ε_2	-1.751203	-1.707260	-1.707266	-1.7181	-1.930389
$\varepsilon_{3,4,5}$	-0.912020	-0.849401	-0.849559	-0.8507	-0.850409

2.6 Testing the Slater, LHF and KLI Implementations

We have implemented the Slater, LHF and KLI approximate exchange potentials in the CADPAC quantum chemistry code [115], as described above. In order to check the accuracy of our implementation we compare our results with those reported in the literature. For the neon atom, accurate values of the total energy and the occupied orbital eigenvalues have been reported for both the Slater and KLI potentials [109, 113]. For the LHF method, values of the total energy, HOMO eigenvalue and HOMO–LUMO gap have been reported for a large uncontracted basis set in Ref. [114].

To begin with we compute the total electronic energy and occupied eigenvalues for the neon atom using the extensive uncontracted Partridge-3 basis set [122] with each of the three approaches. The results are presented in Table 2.1. For the Slater potential the results reproduce the values in Ref. [113]. For the KLI potential the values reproduce those in Ref. [109]. This indicates that the Partridge-3 basis set is sufficiently saturated to provide an accurate description of the occupied orbitals and gives an accurate total energy. Also presented are the LHF results for the same basis set. The LHF total energy is remarkably close to the KLI value. This may in general be expected since the matrix elements $\langle \varphi_i | \hat{v}_x - \hat{v}_x^{NL} | \varphi_j \rangle$ arising in the evaluation of the LHF correction potential will vanish unless both orbitals belong to the same irreducible representation and those which are non-zero will be small unless they have significant spatial overlap. Hence the neglect of the off-diagonal terms in the KLI approach causes only a small change.

The exchange potentials corresponding to the Slater, KLI and LHF approximations are presented in Figure 2.1. In each case the potentials are compared with the exact exchange only OEP potential [123]. The Slater potential displays the correct asymptotic decay but the 1s-2s intershell peak is described poorly and the potential in the core is significantly too negative. The KLI and LHF methods are very similar and are much closer to the OEP potential. They are very slightly too positive in the core region and slightly underestimate the 1s-2s intershell peak.

We have reproduced the values reported in Ref. [113] for the Slater potential and since this potential is the leading term in the KLI and LHF potentials we now restrict

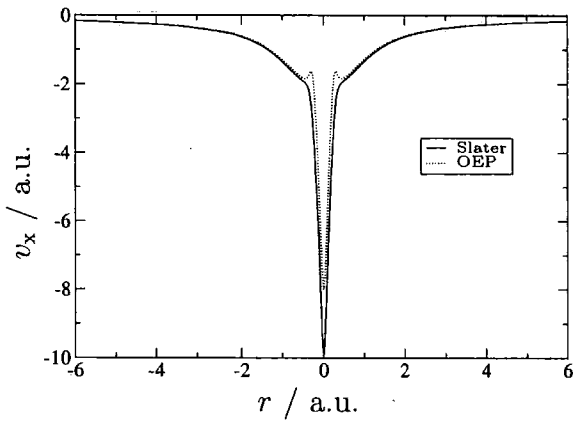

(a) Slater

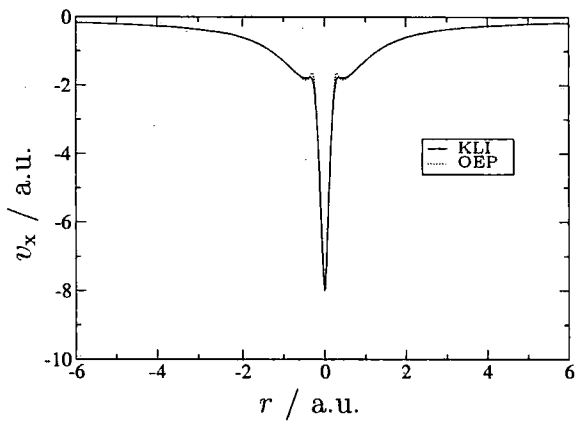

(b) KLI

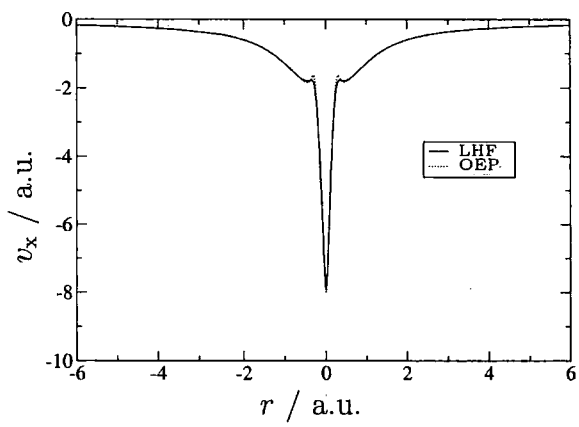

(c) LHF

Figure 2.1: Approximate exchange potentials for the Ne atom calculated using the Partridge-3 basis set (solid lines) compared with the OEP exchange only potential (dotted lines)

ourselves to tests of the latter two approaches. For the Ne atom and CO molecule we used the extensive GEO basis set defined in Ref. [114] to calculate total energies, HOMO eigenvalues and HOMO–LUMO gaps. For both methods the values reproduced those in Ref. [114]. For Ne and CO we note that the total energies and HOMO eigenvalues were also close to the previously reported values in Refs. [124–127]. These tests demonstrate the accuracy of the KLI and LHF implementations and the implied accuracy of the Slater potential.

A more challenging test is to reproduce property calculations that make use of the LHF potential and orbitals. Görling and co-workers calculated excitation energies using the LHF potential in Ref. [128]. They employed the LDA exchange-only kernel in time-dependent density functional theory (TDDFT) calculations with the LHF potential to determine excitation energies for several molecules. For the N_2 molecule Table 2.2 presents excitation energies calculated using our implementation with a 6-311G+(2df) basis set augmented by 2 additional s,p and d functions (whose exponents were determined by continuation of the progression in the original basis). These additional diffuse functions ensure an accurate description of the Rydberg orbitals. It was confirmed that addition of further diffuse functions had minimal effect on the values presented in Table 2.2. Results are also presented using an uncontracted version of this basis set. In regions where the density fell below 10^{-8}a.u. the LHF potential was replaced by the multipole expansion of Section 2.3.2. For comparison the results of Ref. [128] obtained using the XCU1T basis set, containing additional contractions of the primitive functions which are re-optimized to aid calculation of the Slater potential, are also presented. Comparing our results for the contracted basis with the XCU1T values, we see that for the highest electronic state the agreement is relatively poor. This reflects the fact that in a finite basis set the resolution of the identity used in the implementation of the Slater potential can lead to inaccurate results. Uncontracting the basis set removes this problem and agreement with the XCU1T values is better than 0.05 eV. Table 2.3 presents results for the CO molecule. Agreement with the literature values [128] is typically within 0.1 eV for both the uncontracted and XCU1T basis sets. The remaining differences can be attributed to differences in the integration grids. We note that the LHF excitation energies of the valence states are surprisingly close to the experimental values despite the exchange-only nature of the theory as observed in Ref. [128]. The accuracy of the Rydberg states may be expected from the fact that the LHF potential exhibits the correct $-1/r$ asymptote.

Table 2.2: LHF excitation energies for N_2, in eV

State	6-311G+(2df) Contracted	6-311G+(2df) Uncontracted	XCU1T Ref. [128]
$a^1\Pi_g$	9.55	9.58	9.57
$a'^1\Sigma_u^-$	10.23	10.21	10.20
$w^1\Delta_u$	10.81	10.78	10.77
$a''^1\Sigma_g^+$	12.63	12.34	12.31

Table 2.3: LHF excitation energies for CO, in eV

State	6-311G+(2df) Contracted	6-311G+(2df) Uncontracted	XCU1T Ref. [128]
$A^1\Pi$	8.70	8.70	8.78
$I^1\Sigma^-$	10.71	10.71	10.62
$D^1\Delta$	11.16	11.16	11.07
$B^1\Sigma^+$	9.34	10.85	10.93
$C^1\Sigma^+$	10.85	11.85	11.89
$E^1\Pi$	11.71	11.72	11.82

2.7 The Calculation of NMR Shielding Constants

The calculation of magnetic properties is an area in which KS-DFT has not been able to match the accuracy of traditional correlated high level *ab initio* methods. A problem with applying the KS-DFT scheme to the magnetic properties of molecules is that the Hohenberg–Kohn theorems on which the theory is based are no longer strictly valid. This is because for a molecule in a magnetic field, $E_{\rm xc}$ depends not only on the density but also on the current density, $j(\mathbf{r})$. Whilst some attempts have been made at developing functionals which include this dependence, it is thought that the effects of $j(\mathbf{r})$ are relatively small [129, 130]. Thus in most calculations of magnetic properties such as NMR shielding constants, standard functionals are employed using the approximation that $E_{\rm xc}[\rho, j] \approx E_{\rm xc}[\rho]$.

In 1950 Ramsey [131, 132] used perturbation theory to derive an expression for the elements of the shielding tensor. In order to make practical use of the Ramsey expressions in the Hartree–Fock and Kohn–Sham schemes we require a knowledge of how the molecular orbitals respond to the magnetic field. The coupled perturbed equations [133, 134] take a single determinant wavefunction which is optimized, either in the Hartree–Fock or Kohn–Sham sense, and determine the first order changes required in the molecular orbitals such that self consistency is maintained in the presence of a field. The coupled perturbed equations for a magnetic field perturbation may be written as

$$\sum_{bj}(H_2)_{ai,bj}C^{\alpha}_{bj} = -l^{\alpha}_{ai} \tag{2.7.1}$$

$$(H_2)_{ai,bj} = (\varepsilon_a - \varepsilon_i)\delta_{ai,bj} + \xi[(aj|bi) - (ab|ji)] \tag{2.7.2}$$

where $(H_2)_{ai,bj}$ is the magnetic Hessian matrix, l^{α}_{ai} is the angular momentum integral matrix, and ξ is the fraction of orbital dependent exchange. If shielding constants are determined directly from Hartree–Fock orbitals or using Kohn–Sham hybrid functionals the Hessian is non-diagonal and the coupled perturbed equations must be solved. Properties determined in this way are referred to as coupled. If GGA functionals are used then the magnetic Hessian becomes diagonal and the response contribution reduces to

$$C^{\alpha}_{bj} = \frac{-l^{\alpha}_{bj}}{(\varepsilon_b - \varepsilon_j)} \tag{2.7.3}$$

When the response is determined in this fashion the calculation of properties is referred to as uncoupled. In terms of the molecular orbitals and eigenvalues the shielding tensor may be constructed as

$$\sigma^{A}_{\alpha\beta} = \sum_{j}(j|(\mathbf{r}\cdot\mathbf{r}_A\delta^{\alpha\beta} - r^{\alpha}r^{\beta}_A)r_A^{-3}|j) - \sum_{bj} C^{\alpha}_{bj}\left[(j|l^{\beta}_A r_A^{-3}|b) + (b|l^{\beta}_A r_A^{-3}|j)\right] \tag{2.7.4}$$

where j and b are the occupied and virtual molecular orbitals respectively.

In the calculation of magnetic properties such as the shielding tensor extra terms are introduced into the Hamiltonian of the system depending on the magnetic flux density $\mathbf{B}$ and a vector potential $\mathbf{A}$, whose curl is $\mathbf{B}$. One possible solution for the vector potential is

$$\mathbf{A}_{\mathrm{O}} = \frac{1}{2}\mathbf{B}\times(\mathbf{r}-\mathbf{O}) \tag{2.7.5}$$

where $\mathbf{O}$ is an arbitrary origin. This means that the vector potential is not unique since the gradient of any arbitrary function of position may be added to Eqn. (2.7.5) without changing the physical field; such a transformation defines a change of gauge. When the gauge is changed the wavefunction must change its phase such that physical observables are independent of the gauge origin. This behaviour is difficult to reproduce for approximate wavefunctions in finite basis sets. For large basis sets no special consideration of the gauge problem is required [135]. However for large systems where the use of extensive basis sets leads to prohibitive computational costs alternative methods to circumvent the gauge problem have been devised in which gauge factors are introduced either into the atomic orbitals of the basis set or into the molecular orbitals resulting from the solution of the coupled perturbed equations. Many approaches have been developed; examples include individual gauges for localized orbitals (IGLO) [136, 137], gauge including atomic orbitals (GIAO) [138–140], the localized orbitals/localized origins (LORG) [141] method, and the individual gauges for atoms in molecules (IGAIM) [142] approach.

In this thesis we make use of the LORG and GIAO methods. The LORG approach

applies the random phase approximation (RPA) to Ramsey's equations using a set of localized orbitals. Using the properties of the RPA solutions, an expression for the shielding tensor can be derived which avoids the introduction of gauge dependent orbitals. The gauge origin is replaced by local origins relative to the magnetic nuclei which are at the centroids of the localized orbitals. Alternatively, in the GIAO approach gauge factors are included in the atomic orbitals as first proposed by London [138]. The GIAO method is particularly rapidly convergent with respect to the size of the basis set and is currently the preferred method for the evaluation of shielding constants in large systems.

In the next section we use the calculation of isotropic shielding constants (one third of the trace of the shielding tensor) to examine differences between the exchange-only Kohn–Sham potentials. This quantity is a particularly sensitive probe of differences in the exchange potentials since it is governed entirely by the orbitals and eigenvalues through Eqn. (2.7.4). We compare our results with those obtained using the multiplicative Kohn–Sham (MKS) procedure of Ref. [143] via the method of Zhao, Morrison and Parr [59] described in Section 1.6.4. We then extend the application of these approximate exchange potentials to use in hybrid exchange–correlation functionals and examine their behaviour as the fraction of exchange, ξ, is varied from 0 to 1.

2.7.1 Exchange-Only NMR Shielding Constants

Initially we consider the isotropic NMR shielding constants calculated using the LDAX, B88X, Slater, KLI, LHF and MKS(HF) exchange potentials, as well as values from the conventional Hartree–Fock method. The results for a set of 21 small main group molecules are presented in Table 2.4.

In the MKS(HF) approach an approximate exchange potential corresponding to a Hartree–Fock density is calculated via the ZMP method. This potential is then read back into a separate calculation and the NMR shielding constants are computed in an uncoupled fashion. The shielding constants from the LDAX, B88X, Slater, KLI and LHF procedures are also computed in an uncoupled manner. These values can be compared with the Hartree–Fock shieldings which are evaluated in a coupled manner. For all shielding calculations the Huzinaga IGLO IV basis set [144, 145] was employed with the LORG gauge formalism [141]. For molecules of the size considered here with this choice of large orbital basis set, LORG shielding constants have been shown to be very close to those obtained using the GIAO formalism [146]. For the evaluation of the ZMP potential in the MKS procedure a TZ2P basis set [147] was used in order to reduce computational cost. This mixed basis set procedure was justified in Ref. [143]

Table 2.4: Exchange only shielding constants in ppm

Mol	Nucl	LDAX	B88X	Slater	KLI	LHF	MKS(HF)	HF	Expt.
HF	F	416.3	408.4	437.1	431.9	428.0	424.4	414.7	419.7
H_2O	O	337.0	324.8	344.3	344.9	342.9	337.7	328.7	357.6
CH_4	C	195.3	185.4	186.6	195.3	195.5	192.1	195.2	198.4
CO	C	-14.9	-10.4	-80.1	-2.0	2.5	25.6	-23.2	2.8
	O	-87.0	-76.0	-75.9	-7.8	-5.1	42.2	-84.6	-36.7
N_2	N	-86.4	-80.8	-127.7	-54.3	-49.3	-7.9	-109.9	-59.6
F_2	F	-271.5	-265.3	-385.6	-211.5	-217.5	-37.3	-168.4	-192.8
O'OO'	O'	-1495.5	-1449.2	-1473.6	-1103.3	-1135.6	-625.1	-2819.5	-1290.0
	O	-912.0	-897.2	-861.2	-771.9	-760.9	-571.3	-2739.4	-724.0
PN	P	-60.3	-20.2	-68.5	81.0	79.3	227.3	-79.2	53.0
	N	-412.1	-403.8	-379.2	-262.5	-284.8	-194.1	-480.5	-349.0
H_2S	S	748.2	700.8	722.9	761.6	758.4	740.4	722.1	752.0
NH3	N	269.3	257.0	265.2	270.2	270.1	265.4	262.2	273.3
HCN	C	67.5	72.8	40.1	79.1	82.0	95.0	72.1	82.1
	N	-56.0	-43.7	-64.8	0.9	28.6	30.3	-48.4	-20.4
C_2H_2	C	101.4	107.8	86.4	118.9	119.6	126.7	115.8	117.2
C_2H_4	C	42.0	47.1	17.8	65.9	66.7	76.0	59.9	64.5
H_2CO	C	-38.3	-22.7	-90.9	-14.5	-8.4	15.3	-5.8	-4.4
	O	-508.5	-439.1	-409.7	-237.9	-257.7	-154.4	-436.8	-375.0
N'NO	N'	92.9	91.2	53.1	114.6	115.9	127.5	63.8	99.5
	N	-1.9	-3.4	-26.5	17.2	22.4	28.5	-32.5	11.3
	O	184.8	175.6	173.0	217.9	221.0	241.6	175.4	200.5
CO_2	C	51.0	51.4	23.0	63.0	65.1	69.9	52.8	58.8
	O	213.8	214.8	207.3	249.0	249.7	266.8	223.3	243.4
OF_2	O	-656.8	-621.9	-837.9	-527.7	-583.0	-270.8	-440.6	-473.1
H_2CNN'	C	168.1	159.8	143.8	172.5	174.5	169.9	164.9	164.5
	N	-58.3	-62.1	-113.9	-33.2	-26.4	-11.3	-11.2	-43.4
	N'	-155.0	-164.8	-280.0	-102.5	-103.1	-67.5	-298.8	-149.0
HCl	Cl	967.4	937.8	973.0	985.9	980.5	962.0	958.2	952.0
SO_2	S	-60.3	-206.0	-328.4	-133.5	-120.4	-55.3	-312.5	-126.0
	O	-412.1	-272.6	-255.2	-124.4	-129.1	-54.4	-280.7	-205.0
PH_3	P	597.0	557.4	558.2	600.7	600.1	592.8	586.8	599.9
d		-44.9	-42.2	-69.7	18.2	16.2	75.2	-143.1	
$\|d\|$		50.2	42.2	72.1	28.5	28.5	78.5	149.1	
$\|d\|$ %		80.5	57.3	216.3	30.0	27.3	93.4	90.3	
Omitting O_3									
d		-34.8	-33.9	-63.6	14.8	13.4	52.9	-34.4	
$\|d\|$		40.4	33.9	66.2	22.6	24.0	56.5	40.8	
$\|d\|$ %		84.5	59.9	229.6	31.3	28.5	97.2	83.1	

since only a spatial representation of the exchange potential is required.

Relative to experiment the results in Table 2.4 give mean absolute errors, $|d|$, in the order HF > MKS(HF) > Slater > LDAX > B88X > KLI $\approx$ LHF. Since these theories do not include the effects of electron correlation we would expect the results to be poor in comparison with experiment. This is indeed the case for the HF, MKS(HF), and Slater values. The LDAX and B88X values are similar and are closer to experiment. It has been argued previously that these approximations actually introduce some correlation for molecules and so this may not be a surprising result [148]. The LHF and KLI results are again very similar, as was observed for the Ne atom. However they are unexpectedly close to experiment, with mean absolute errors of just 28.5 ppm, making them comparable with the conventional GGA functional HCTH, which for the same set of molecules gives a mean absolute error of 32.4 ppm. This is in spite of the fact that the approximations do not include any consideration of electron correlation. These observations are consistent with the excitation energy calculations of Ref. [128]. The differences between the results indicate significant differences in the various KS exchange representations.

2.7.2 HOMO–LUMO Eigenvalue Differences

For uncoupled shielding constants determined by Eqn. (2.7.4) the paramagnetic contribution depends on the inverse of the occupied-virtual Kohn–Sham eigenvalue differences. If the diamagnetic component remains approximately constant along with the numerator of the paramagnetic term, then methods which yield large occupied-virtual eigenvalue differences will tend to give larger total shielding constants. This behaviour has been widely observed [149–152]. For a subset of the 21 molecules where the variation in the shielding constants is particularly pronounced, the HOMO–LUMO gaps for LDAX, B88X, Slater, KLI, LHF and MKS(HF) are presented in Table 2.5 along with the near exact values of Ref. [152] obtained using the ZMP procedure on Brueckner-Doubles coupled cluster densities. In each case we see that the LDAX and B88X functionals underestimate the gap, consistent with a systematic underestimation of the shielding constants in Table 2.4. The MKS(HF) procedure consistently over estimates the gap leading to shielding constants which are too large. Use of the Slater potential leads to shieldings which do not show a systematic trend. This is because the potential is particularly poor in the core region and so the occupied orbitals are severely degraded (see also Table 2.1), changing the diamagnetic contribution and paramagnetic numerator significantly. The LHF and KLI potential correct the Slater potential in the core region. Both methods lead to HOMO–LUMO gaps which are surprisingly close to

Table 2.5: HOMO–LUMO gaps calculated with exchange-only methods in E_h

Molecule	LDAX	B88X	Slater	KLI	LHF	MKS(HF)	Near Exact[a]
CO	0.251	0.260	0.247	0.266	0.267	0.290	0.27
N_2	0.300	0.307	0.316	0.317	0.319	0.351	0.32
F_2	0.126	0.137	0.144	0.152	0.147	0.234	0.16
PN	0.159	0.163	0.185	0.179	0.175	0.200	0.17
H_2CO	0.122	0.134	0.147	0.156	0.154	0.187	0.15
OF_2	0.121	0.131	0.137	0.155	0.141	0.221	0.16
SO_2	0.134	0.136	0.151	0.153	0.153	0.173	0.15

[a] Ref. [152]

the best estimate values of Ref. [152], rationalising the good performance LHF and KLI approaches. This issue will be investigated further in Chapter 5. Since the occupied-virtual eigenvalue differences are the key quantities in the evaluation of excited states by TDDFT these observations also go some way towards explaining the observations of Ref. [128].

2.8 Extension to Hybrid Functionals

In order improve the accuracy of the NMR shielding constants relative to experiment we must use functionals which include the effects of electron correlation. Wilson and Tozer have demonstrated the high accuracy of uncoupled shielding constants evaluated via the MKS scheme applied to electron densities of hybrid functionals [143]. Subsequently we have confirmed [153] that applying the ZMP procedure to a Hartree–Fock density, scaling the resulting potential and adding it to the GGA component of a hybrid functional yields essentially the same accuracy results, with mean absolute errors for each procedure differing by less than 1 ppm for the B97-2 functional form when applied to the 21 molecules of Table 2.4. This corresponds to solving a Kohn–Sham equation of the form

$$\left[-\frac{1}{2}\nabla^2 + v_{\text{ext}} + v_{\text{J}} + v_{\text{xc}}^{\text{GGA}} + \xi v_{\text{x}}\right]\varphi_i = \varepsilon_i\varphi_i \tag{2.8.1}$$

The MKS results for the B97-2 functional have a mean absolute error of just 15.1 ppm. Unfortunately the MKS procedure requires the evaluation of an exchange potential via the numerically difficult ZMP method. The high quality of the results obtained provides us with the impetus to consider other approximations to the exchange potential of Eqn. 2.8.1, in the calculation of NMR shielding constants, thus avoiding the need to perform a ZMP calculation. Specifically we consider the Slater, KLI and LHF approximations to the exchange potential. A similar approach based on the B3LYP hybrid functional was considered by Hieringer *et al.* in Ref. [154].

Table 2.6 presents multiplicative hybrid shielding constants calculated using the B97-2 hybrid functional [96] form. Conventional coupled results are presented along with uncoupled results from functionals in which the $v_x^{\mathrm{MKS(HF)}}$ (prefixed M), v_x^{Slater} (prefixed S), v_x^{KLI} (prefixed K) and v_x^{LHF} (prefixed L) exchange representations are used. Errors are presented relative to experiment and the mean absolute errors indicate that the quality of the approximations follows the trend M(B97-2)>K(B97-2)≈L(B97-2)>S(B97-2)>B97-2. All of the multiplicative hybrids outperforming the conventional B97-2 functional. The highest quality results are the M(B97-2) values which approach the quality of the best *ab initio* calculations. As expected the L(B97-2) and K(B97-2) results are of similar quality but both are notably worse than the M(B97-2) results, reflecting the differences in the LHF and MKS exchange representations observed in the previous section. This indicates that the amount of exchange included in conventional hybrid functionals is not appropriate for functionals based on these multiplicative potentials.

2.8.1 Varying the Fraction of Orbital Exchange

Wilson and Tozer [152] have demonstrated that for multiplicative hybrids in the MKS scheme, an amount of orbital exchange in the range $0.2 - 0.3$ is optimal for the calculation of NMR shielding constants. This is consistent with the fraction found in conventional hybrid functionals such as B97-2 (0.21), B3LYP (0.20) and PBE0 (0.25). We now consider the behaviour of Slater, KLI and LHF based hybrid functionals as the fraction of orbital exchange is varied between 0 and 1. We employ the functionals of Ref. [152] which take the B97 form and have coefficients that were optimized for amounts of exchange between 0 and 1 in steps of 0.1. Thus zero corresponds to a GGA functional, whilst 1 corresponds to full orbital dependent exchange plus a GGA correlation functional. The shielding constants of the same set of molecules were calculated. Figure 2.2 presents plots of the mean absolute error as a function of the amount of exchange for each representation. The introduction of Slater exchange leads to a steady degradation of the shielding constants relative to experiment as shown by Figure 2.2(a). This again reflects the poor quality of the Slater approximation. When the KLI approximation is employed the mean absolute error minimises at $\xi = 0.5$ as shown in Figure 2.2(b). The use of a larger fraction of LHF exchange was first suggested in Ref. [153] and investigated in detail by Arbuznikov and Kaupp [155], who observed a minimisation in the range $\xi = 0.5 - 0.6$ for a different functional form. Again LHF based hybrids behave in a similar manner to KLI based ones with minimisation of the mean absolute error around $\xi = 0.5$ as shown in Figure 2.2(c). This highlights a dif-

Table 2.6: Multiplicative hybrid shielding constants, in ppm

Mol	Nucl	B97-2	M(B97-2)	S(B972)	K(B972)	L(B972)	*ab initio*	Expt.
HF	F	412.5	415.0	417.4	416.8	415.6	418.6[a]	419.7[a]
H_2O	O	328.3	330.4	331.3	332.0	331.4	337.9[a]	357.6 [a]
CH_4	C	191.3	190.4	189.1	191.2	191.3	198.9[a]	198.4[a]
CO	C	-12.4	-0.6	-22.1	-7.5	-6.5	5.6[a]	2.8[a]
	O	-74.1	-40.7	-70.4	-56.1	-55.4	-52.9[a]	-36.7[a]
N_2	N	-85.9	-60.9	-88.9	-73.7	-72.5	-58.1[a]	-59.6[a]
F_2	F	-242.9	-199.2	-289.5	-253.3	-254.7	-186.5[a]	-192.8[a]
O'OO'	O'	-1660.2	-1162.5	-1450.1	-1360.9	-1370.3	-1208.2[a]	-1290.0[a]
	O	-1099.6	-777.9	-866.5	-846.1	-843.3	-754.6[a]	-724.0[a]
PN	P	-35.9	46.8	-29.2	2.4	1.9	86.0[b]	53.0[b]
	N	-407.4	-332.3	-382.5	-356.5	-361.9	-341.0[b]	-349.0[b]
H_2S	S	722.5	724.7	719.7	730.0	729.2	754.6[c]	752.0[c]
NH_3	N	260.9	261.4	261.0	262.5	262.5	270.7[a]	273.3[a]
HCN	C	73.4	79.5	67.5	75.4	76.1	86.3[a]	82.1[a]
	N	-39.8	-19.3	-42.2	-28.0	-28.0	-13.6[a]	-20.4[a]
C_2H_2	C	111.7	114.9	106.1	112.8	113.0	121.8[d]	117.2[e]
C_2H_4	C	53.8	58.4	45.5	55.5	55.7	71.2[f]	64.5[f]
H_2CO	C	-16.6	-10.4	-32.9	-18.9	-17.2	4.7[a]	-4.4[a]
	O	-425.0	-340.4	-413.3	-373.7	-379.4	-383.1[a]	-375.0[a]
N'NO	N'	86.7	101.4	85.0	97.8	98.1	100.5[g]	99.5[g]
	N	-2.4	11.7	0.2	9.1	10.3	5.3[g]	11.3[g]
	O	173.9	192.2	173.7	184.1	184.9	198.8[g]	200.5[g]
CO_2	C	55.1	59.5	49.9	57.9	58.5	63.5[f]	58.8[f]
	O	215.7	227.7	212.3	221.8	222.0	236.4[h]	243.4[h]
OF_2	O	-556.1	-500.8	-653.3	-589.4	-602.1	-465.5[h]	-473.1[h]
H_2CNN'	C	162.7	163.7	158.2	164.4	164.9	171.9[a]	164.5[a]
	N	-49.9	-41.9	-64.0	-48.0	-46.4	-31.6[a]	-43.4[a]
	N'	-180.2	-135.1	-180.5	-145.3	-145.4	-142.4[a]	-149.0[a]
HCl	Cl	952.5	952.3	953.4	957.9	956.5	962.3[i]	952.0[i]
SO_2	S	-227.5	-163.2	-222.1	-183.8	-180.3	-134.2[c]	-126.0[c]
	O	-274.1	-206.9	-262.8	-232.0	-233.4	-170.4[c]	-205.0[c]
PH_3	P	580.0	579.2	572.1	582.1	581.9	594.0[b]	599.9[i]
d		-50.4	-2.6	-41.6	-22.6	-23.3	4.5	
$\|d\|$		50.4	15.1	41.6	23.2	23.8	11.2	
$\|d\|$ %		54.9	13.4	77.9	35.9	33.0	19.5	
Omitting O_3								
d		-28.9	-5.3	-34.2	-17.6	-18.2	3.1	
$\|d\|$		28.9	10.0	34.3	18.3	18.8	8.2	
$\|d\|$%		55.9	13.7	82.0	37.5	34.4	20.4	

[a] Ref. [156], GIAO-CCSD(T), experimental values include rovibrational corrections (except HCN)
[b] Ref. [157], SOLO
[c] Ref. [158], IGLO-CASSCF
[d] Ref. [159], GIAO-CCSD
[e] Ref. [145]
[f] Ref. [160], GIAO-MP2
[g] Ref. [161], GIAO-CCSD
[h] Ref. [162], GIAO-MP2
[i] Ref. [163], GIAO-MP3

ference between the KLI/LHF and ZMP exchange potentials which will be examined in further detail in Chapter 5.

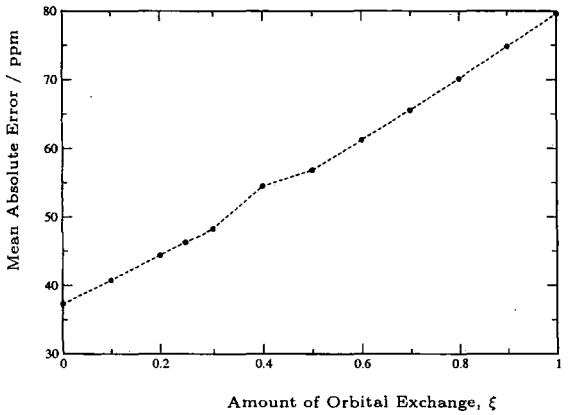

(a) Slater

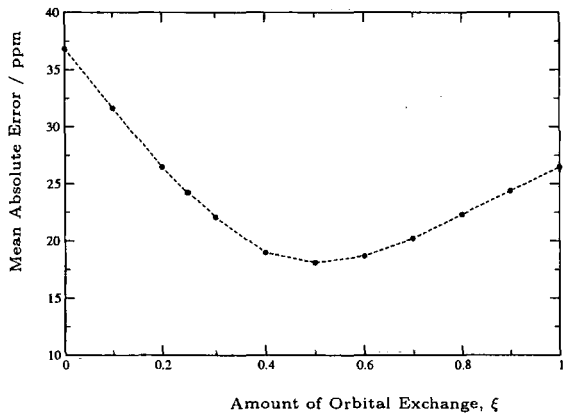

(b) KLI

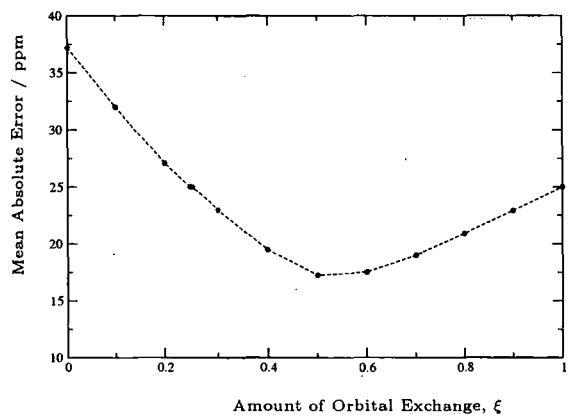

(c) LHF

Figure 2.2: The mean absolute error, in ppm, as a function of the amount of exchange for shielding constants calculated using hybrid functionals containing approximate exchange potentials

Chapter 3

Approximate Exchange: Excited States and Nuclear Perturbations

In this chapter we consider the application of LHF-based approaches to excited states and structural perturbations. Specifically we consider excitation energies, ground and excited state optimized geometries, vibrational levels and potential energy curves. We compare LHF and multiplicative hybrid results with HF and conventional hybrid DFT to assess the influence of the alternative exchange treatment. In light of the observations in Section 2.8.1, relating to the optimal amount of exchange in LHF based hybrids, we consider both standard (0.21) and increased (0.60) amounts of orbital exchange. We also consider the HCTH GGA functional with no orbital exchange and, where required, investigate the influence of the asymptotic correction (AC) to the potential.

3.1 Optimized Geometries

We commence by considering the performance of LHF exchange-based methods for the calculation of ground state properties. Specifically we calculate the optimized geometries of 45 diatomic molecules. Since analytic derivatives are not available for the LHF methods, the bond lengths were optimized numerically. The multiplicative hybrid Kohn–Sham equations were solved self-consistently, as described in Section 2.3.1, by iterating the TLHF equations which were solved at each step of the SCF cycle by the conjugate gradient procedure. In asymptotic regions when the density falls below 10^{-8}a.u., the LHF potential was replaced with a multipole representation of $-1/r$ as discussed in Section 2.3.2. This procedure is only formally correct when the highest occupied molecular orbital (HOMO) does not exhibit a nodal surface. However, changes to the asymptotic region have minimal effect on the ground state electronic

energy and hence their potential energy curves.

In Table 3.1 we present the optimized bond lengths of 45 diatomic molecules (arranged according to the periodic grouping of each atom). The methods considered are the Hartree–Fock and LHF exchange only methods, the conventional hybrid B97-2 and B97(0.6) functionals (the latter is the $\xi = 0.6$ functional of Ref. [152]), the HCTH GGA functional, and the multiplicative hybrid functionals L(B97-2) and L(B97(0.6)) in which the Hartree–Fock exchange contribution is replaced by the LHF exchange potential as in Eqn. (2.8.1).

Following Ref. [164], the 6-311G+(2df) basis set was initially used for the calculation of the optimized geometries. However, for the alkali metal (1-1) diatomic molecules, the LHF potential energy curves exhibited small oscillations making the location of the minimum to the precision of ± 0.0005 Å impossible. For the other molecules this problem was not observed. The origin of this problem can be traced to the resolution of the identity employed in our implementation of the LHF method. To improve the flexibility of the basis set and hence remove the oscillations, the 6-311G+(2df) set was uncontracted. This resulted in smooth potential energy surfaces on which minima could be located to the required precision. Uncontraction of the basis set had minimal effect on the results computed with the non-LHF based methods.

The results presented in Table 3.1 are compared with the experimental results of Ref. [164] and MP2 wavefunction values. The mean, d, mean absolute, $|d|$, and mean absolute percentage, $|d|$ %, errors are reported relative to experiment. The results demonstrate that the bond lengths are relatively insensitive to the choice of exchange treatment. The HF, B97-2 and B97(0.6) results are very close to those of LHF, L(B97-2) and L(B97(0.6)) respectively. As in Ref. [164], errors are reported both including and excluding the difficult (1-1) diatomics. In both cases the conventional approaches give very similar errors to their LHF based counterparts. This is not surprising since the goal of the LHF approach is to find the multiplicative operator, $v_x(\mathbf{r})$, which may as accurately as possible replace the non-local Hartree–Fock exchange operator, and hence the energies of the two approaches are close and have a similar response to structural perturbations. One surprising observation is that the B97(0.6)/L(B97(0.6)) and B97-2/L(B97-2) errors are comparable over the full set of molecules. When the (1-1) combination is omitted, the errors from the B97(0.6)/L(B97(0.6)) functionals barely change indicating that these systems present no special difficulties for the functionals with larger fractions of orbital exchange. In contrast for B97-2/L(B97-2) the errors reduce significantly when these systems are removed. As is commonly observed the hybrid functionals outperform the HCTH GGA functional in the calculation of optimized geometries, for main group molecules. The MP2 method provides a consistent

Table 3.1: Optimized bond lengths, in Å, for diatomic molecules

Molecule	HF	LHF	B97-2	L(B97-2)	B97(0.6)	L(B97(0.6))	HCTH	MP2	Expt.[a]
(1-1)									
Li_2	2.784	2.788	2.746	2.745	2.690	2.689	2.759	2.725	2.673
LiNa	3.001	3.007	2.956	2.954	2.861	2.863	2.985	2.923	2.885
LiK	3.509	3.517	3.413	3.413	3.322	3.329	3.456	3.332	3.319
Na_2	3.194	3.204	3.138	3.143	3.011	3.014	3.185	3.103	3.079
NaK	3.693	3.702	3.589	3.591	3.464	3.465	3.641	3.499	3.497
K_2	4.199	4.205	4.056	4.056	3.924	3.920	4.127	3.890	3.924
(15-15)									
N_2	1.066	1.065	1.090	1.090	1.077	1.076	1.098	1.110	1.098
NP	1.448	1.447	1.480	1.481	1.461	1.460	1.494	1.519	1.491
NAs	1.570	1.569	1.604	1.603	1.581	1.581	1.618	1.662	1.618
P_2	1.854	1.853	1.885	1.885	1.862	1.863	1.900	1.922	1.893
PAs	1.958	1.958	1.988	1.989	1.966	1.966	2.005	2.027	1.999
As_2	2.058	2.058	2.089	2.089	2.064	2.064	2.108	2.128	2.103
(17-17)									
F_2	1.327	1.322	1.378	1.378	1.345	1.343	1.398	1.397	1.412
FCl	1.590	1.587	1.628	1.628	1.601	1.601	1.645	1.637	1.628
FBr	1.717	1.715	1.759	1.759	1.728	1.727	1.777	1.761	1.759
Cl_2	1.982	1.982	1.990	1.991	1.974	1.974	2.001	1.993	1.988
ClBr	2.128	2.128	2.139	2.139	2.115	2.115	2.152	2.133	2.136
Br_2	2.278	2.277	2.289	2.289	2.260	2.260	2.306	2.279	2.281
(1-17)									
LiF	1.557	1.559	1.571	1.568	1.542	1.543	1.586	1.574	1.564
LiCl	2.036	2.037	2.028	2.029	1.999	2.002	2.038	2.025	2.021
LiBr	2.196	2.198	2.186	2.183	2.151	2.151	2.197	2.179	2.170
NaF	1.930	1.933	1.949	1.947	1.909	1.903	1.975	1.951	1.926
NaCl	2.391	2.395	2.383	2.387	2.340	2.342	2.402	2.377	2.361
NaBr	2.544	2.547	2.529	2.527	2.482	2.480	2.552	2.525	2.502
KF	2.212	2.223	2.174	2.175	2.159	2.164	2.190	2.197	2.171
KCl	2.742	2.756	2.680	2.678	2.654	2.663	2.698	2.682	2.667
KBr	2.910	2.923	2.839	2.843	2.811	2.814	2.861	2.848	2.821
(13-17)									
BF	1.246	1.244	1.264	1.264	1.245	1.244	1.273	1.264	1.263
BCl	1.720	1.716	1.725	1.725	1.707	1.705	1.734	1.710	1.716
BBr	1.902	1.898	1.901	1.901	1.878	1.876	1.911	1.878	1.888
AlF	1.647	1.646	1.672	1.671	1.648	1.648	1.687	1.671	1.654
AlCl	2.149	2.148	2.152	2.152	2.128	2.129	2.166	2.141	2.130
AlBr	2.332	2.331	2.327	2.327	2.300	2.300	2.343	2.316	2.295
GaF	1.769	1.768	1.793	1.793	1.770	1.772	1.813	1.789	1.774
GaCl	2.227	2.234	2.221	2.222	2.196	2.200	2.240	2.206	2.202
GaBr	2.395	2.403	2.380	2.381	2.352	2.355	2.400	2.361	2.352
(14-16)									
CO	1.103	1.102	1.124	1.124	1.111	1.111	1.132	1.135	1.128
CS	1.512	1.508	1.533	1.534	1.515	1.514	1.544	1.537	1.535
CSe	1.654	1.648	1.673	1.673	1.655	1.653	1.685	1.676	1.676
SiO	1.479	1.478	1.510	1.510	1.489	1.489	1.523	1.527	1.510
SiS	1.912	1.910	1.933	1.933	1.916	1.914	1.947	1.941	1.929
SiSe	2.044	2.042	2.064	2.064	2.041	2.040	2.080	2.069	2.058
GeO	1.592	1.591	1.622	1.622	1.601	1.601	1.637	1.643	1.625
GeS	1.996	1.995	2.014	2.014	1.997	1.996	2.029	2.021	2.012
GeSe	2.122	2.121	2.140	2.140	2.118	2.118	2.158	2.141	2.135
d	0.018	0.019	0.016	0.017	-0.019	-0.018	0.035	0.012	
$\|d\|$	0.047	0.050	0.021	0.021	0.020	0.020	0.036	0.015	
$\|d\|$ %	2.0	2.1	0.9	0.9	1.1	1.1	1.4	0.8	
Omitting 1-1 Group;									
d	-0.005	-0.005	0.006	0.006	-0.019	-0.019	0.021	0.012	
$\|d\|$	0.029	0.031	0.011	0.011	0.019	0.019	0.022	0.014	
$\|d\|$ %	1.6	1.7	0.6	0.6	1.1	1.1	1.1	0.7	

[a] Experimental values taken from Ref. [164]

treatment for all the molecules considered, with accuracy intermediate between the B97(0.6) and B97-2 functionals when the (1-1) molecules are omitted.

Next, we extend our investigation to consider potential energy curves for both ground and excited states, and use them to determine bond lengths and vibrational energy levels. It is not feasible to consider all the molecules in Table 3.1. We therefore concentrate on the N_2 and CO molecules, for which ample experimental data is available. Excitation energies are calculated by time-dependent density functional theory (TDDFT) calculations.

3.2 Time-Dependent Density Functional Theory

Up until now we have considered the time-independent version of Kohn–Sham theory where the first Hohenberg–Kohn theorem established a one to one mapping between the potential $v(\mathbf{r})$ and the density $\rho(\mathbf{r})$. We now consider the time-dependent case, in which both the potential and the density depend on the time, t.

In 1984 Runge and Gross [165] proved that there is a one to one correspondence between $v(\mathbf{r}t)$ and $\rho(\mathbf{r}t)$ for many body systems, analogous to the Hohenberg–Kohn theorem for the time-independent case [165]. With this theorem in place a time-dependent density functional theory (TDDFT) scheme can be constructed in a similar fashion to the time-independent case. We introduce a system of non-interacting electrons moving subject to a time-dependent external potential. So we have the time-dependent Kohn–Sham equation

$$i\frac{\partial}{\partial t}\varphi_i(\mathbf{r}t) = \hat{H}_{\mathrm{KS}}(\mathbf{r}t)\varphi_i(\mathbf{r}t) \tag{3.2.1}$$

where the time-dependent Kohn–Sham Hamiltonian is

$$\hat{H}_{\mathrm{KS}}(\mathbf{r}t) = -\frac{1}{2}\nabla^2 + v_{\mathrm{ext}}(\mathbf{r}t) + v_{\mathrm{J}}(\mathbf{r}t) + v_{\mathrm{xc}}(\mathbf{r}t) \tag{3.2.2}$$

The unknown term in this equation, $v_{\mathrm{xc}}(\mathbf{r}t)$, is now even more complex than in the time-independent case since it has functional dependence on the time-dependent density which at a given position may depend on the density at all other positions and all previous times. The v-representability problem discussed in Section 1.6.2 is still present in the time-dependent case. In using the Kohn–Sham scheme we have assumed the interacting time-dependent density is non-interacting v-representable. Although it has been suggested that this may be less of a problem than in the time-independent case [166].

In time-dependent systems the total energy is not conserved and so a variational

principle cannot be based upon it. Instead the quantum mechanical action is employed. This means that the exchange–correlation potential should be defined as the derivative of the action with respect to the time-dependent density. This is further complicated by the fact that in order to avoid violating causality, the quantum mechanical action must be reformulated in terms of the Keldysh pseudotime as done by van Leeuwen [167]. The development of time-dependent exchange functionals is still in its very early stages and hence in most practical applications of TDDFT the adiabatic approximation is employed in which we simply replace the time-dependent potential $v_{\mathrm{xc}}(\mathbf{r}t)$ by the $v_{\mathrm{xc}}(\mathbf{r})$ of some typical ground state exchange–correlation functional, evaluated using the density at that time.

In order to calculate time-dependent properties we make use of linear response theory in which we consider the response of the non-interacting Kohn–Sham system to a weak time-dependent perturbation. Providing the perturbing potential is relatively weak, as is the case in most spectroscopic experiments, we may obtain accurate results via this route. This technique is used to calculate excitation energies in most computer packages which are available for application to chemical systems. It is important to be aware however that more accurate solutions are required when the perturbations become large, for example to describe an interaction with a strong laser.

3.2.1 Kohn–Sham Linear Response Theory

Consider a system of interacting particles subject to a small time-dependent perturbation, the external potential may be written as $v_{\mathrm{ext}}(\mathbf{r}t) = v_0(\mathbf{r}) + v_1(\mathbf{r}t)$ where $v_0(\mathbf{r})$ is the external potential of the unperturbed system, and $v_1(\mathbf{r}t)$ is the time-dependent perturbation. The response of the density to the perturbation may be written as

$$\chi(\mathbf{r}t, \mathbf{r}'t') = \left.\frac{\delta\rho[v_{\mathrm{ext}}](\mathbf{r}t)}{\delta v_{\mathrm{ext}}(\mathbf{r}'t')}\right|_{v_{\mathrm{ext}}[\rho_0]} \tag{3.2.3}$$

which is evaluated at the static external potential of the unperturbed density, $\rho_0(\mathbf{r})$. The linear density response $\rho_1(\mathbf{r}t)$ is then

$$\rho_1(\mathbf{r}t) = \int dt' \int d\mathbf{r}' \chi(\mathbf{r}t, \mathbf{r}'t') v_1(\mathbf{r}'t') \tag{3.2.4}$$

For a Kohn–Sham system of non-interacting particles moving in some potential $v_s(\mathbf{r}t) = v_{\mathrm{ext}}(\mathbf{r}t) + v_{\mathrm{J}}(\mathbf{r}t) + v_{\mathrm{xc}}(\mathbf{r}t)$, we may similarly write the non-interacting response function

with the same unperturbed density, $\rho_0(\mathbf{r})$,

$$\chi_s(\mathbf{r}t,\mathbf{r}'t') = \left.\frac{\delta\rho[v_s](\mathbf{r}t)}{\delta v_s(\mathbf{r}'t')}\right|_{v_s[\rho_0]} \tag{3.2.5}$$

Since by the Runge–Gross theorem [165] we know that the time-dependent KS potential and density have a one-to-one correspondence and since $\rho_0(\mathbf{r})$ and $\rho(\mathbf{r}t)$ are the same in the interacting and non-interacting cases, the interacting density $\rho[v_{\text{ext}}](\mathbf{r}t)$ uniquely determines the potential $v_s[\rho[v_{\text{ext}}]]$ of the KS system such that $\rho[v_s](\mathbf{r}t) = \rho[v_{\text{ext}}](\mathbf{r}t)$.

The change in the time-dependent exchange–correlation potential when the density is perturbed by a small amount $\delta\rho$ may be written as

$$v_{\text{xc}}[\rho+\delta\rho](\mathbf{r}t) = v_{\text{xc}}[\rho](\mathbf{r}) + \int dt' \int d\mathbf{r}' f_{\text{xc}}[\rho](\mathbf{r}t,\mathbf{r}'t')\delta\rho(\mathbf{r}'t') \tag{3.2.6}$$

where f_{xc} is the exchange–correlation kernel defined as,

$$f_{\text{xc}}[\rho](\mathbf{r}t,\mathbf{r}'t') = \frac{\delta v_{\text{xc}}[\rho](\mathbf{r}t)}{\delta\rho(\mathbf{r}'t')} \tag{3.2.7}$$

Using the chain rule on the interacting response function of Eqn. (3.2.3) and inserting Eqn. (3.2.6) then taking the Fourier transform with respect to time we arrive at the Dyson-like equation

$$\chi(\mathbf{r}\mathbf{r}'\omega) = \chi_s(\mathbf{r}\mathbf{r}'\omega) + \int d\mathbf{r}_1 \int d\mathbf{r}_2 \chi_s(\mathbf{r}\mathbf{r}_1\omega)\left(\frac{1}{|\mathbf{r}_1-\mathbf{r}_2|} + f_{\text{xc}}(\mathbf{r}_1\mathbf{r}_2\omega)\right)\chi(\mathbf{r}_2\mathbf{r}'\omega) \tag{3.2.8}$$

where ω is the frequency and we note that in the adiabatic approximation the exchange–correlation kernel becomes freqency independent. Eqn. (3.2.8) is a formally exact representation of the density response of an interacting system in terms of objects which are all functionals of the ground state density $\rho_0(\mathbf{r})$. The non-interacting response function $\chi_s(\mathbf{r}\mathbf{r}'\omega)$ can be written in terms of the static unperturbed KS orbitals as

$$\chi_s(\mathbf{r}\mathbf{r}'\omega) = \sum_{ia}\left(\frac{\varphi_i(\mathbf{r})\varphi_a^*(\mathbf{r})\varphi_a^*(\mathbf{r}')\varphi_i(\mathbf{r}')}{\omega-(\varepsilon_i-\varepsilon_a)} - \frac{\varphi_i^*(\mathbf{r})\varphi_a(\mathbf{r})\varphi_a(\mathbf{r}')\varphi_i^*(\mathbf{r}')}{\omega+(\varepsilon_i-\varepsilon_a)}\right) \tag{3.2.9}$$

The interacting response function displays poles at the true excitation energies of the system. From Eqn. (3.2.9) we can see that χ_s also displays poles at frequencies corresponding to the Kohn–Sham occupied-virtual eigenvalue differences. In the absence of the Coulomb and exchange–correlation interactions these differences would give the true transition frequencies. In their presence Eqn. (3.2.8) shifts these transitions to their true values by addition of a shift depending on the Coulomb and exchange–

correlation kernels. Unfortunately the solution of Eqn. (3.2.8) is numerically difficult and requires a knowledge of the non-interacting response function which depends on a summation over both the occupied and virtual states and is not guaranteed to be rapidly convergent.

3.2.2 Excited State Calculations

Fortunately for finite systems it is possible to find the poles of the interacting response function by the solution of a pseudo-eigenvalue problem. We begin by considering the Lehmann representation of the density response function

$$\chi(\mathbf{r}\mathbf{r}'\omega) = \lim_{\eta\to 0^+} \sum_m \left[\frac{\langle 0|\hat{\rho}_\sigma(\mathbf{r})|m\rangle\langle m|\hat{\rho}_\sigma(\mathbf{r}')|0\rangle}{\omega - (E_m - E_0) + i\eta} - \frac{\langle 0|\hat{\rho}_\sigma(\mathbf{r}')|m\rangle\langle m|\hat{\rho}_\sigma(\mathbf{r})|0\rangle}{\omega - (E_m - E_0) + i\eta} \right] \tag{3.2.10}$$

where $\hat{\rho}$ is the density operator, $|m\rangle$ form a complete set of states with energies E_m and η is a positive infinitesimal. The interacting density response function has poles at the excitation energies $\Omega = E_m - E_0$. In the exact case the eigenstates may be mixtures of single, double and higher multiple excitations and so the response function can have poles dominated by any number of excitations. However in the case of χ_s only poles at single excitations may be observed. So χ_s exhibits fewer poles than χ. Under the adiabatic approximation (which we employ throughout this thesis) states with significant multiple excitation character cannot be described accurately.

Casida [168] showed that the poles of χ may be found by the solution of a pseudo eigenvalue problem. If we introduce the double index $q = (i, a)$ to represent a single excitation from φ_i to φ_a and define ω_q as the KS eigenvalue difference $\varepsilon_a - \varepsilon_i$ then the squares of the true transition frequencies $\Omega_I = \omega_I^2$ are the eigenvalues of the matrix

$$\tilde{\Omega}(\omega)_{qq'} = \delta_{qq'}\omega_q^2 + 2\sqrt{\omega_q\omega_{q'}}\langle q|f_{\mathrm{hxc}}(\omega)|q'\rangle \tag{3.2.11}$$

in which

$$\langle q|f_{\mathrm{hxc}}(\omega)|q'\rangle = \int d\mathbf{r}\int d\mathbf{r}'\varphi_i^*(\mathbf{r})\varphi_a(\mathbf{r})f_{\mathrm{hxc}}(\mathbf{r}\mathbf{r}'\omega)\varphi_{i'}(\mathbf{r}')\varphi_{a'}^*(\mathbf{r}') \tag{3.2.12}$$

and f_{hxc} is $\frac{1}{|\mathbf{r}-\mathbf{r}'|} + f_{\mathrm{xc}}(\mathbf{r}\mathbf{r}'\omega)$. The oscillator strengths may be obtained from the eigenvectors. In the adiabatic approximation the above equations become a simple matrix equation which may be solved for the excitation energies. Most commonly used quantum chemistry codes contain algorithms for the extraction of the lowest N states.

Table 3.2: Vertical excitation energies of N_2, in eV, calculated at the experimental bond length

State	Transition	HF	LHF	B97-2	L(B97-2)	B97(0.6)	L(B97(0.6))	HCTH	Expt.[a]
$a^1\Pi_g$	$\sigma_g \rightarrow \pi_g$	9.76	9.58	9.32	9.25	9.54	9.41	9.16	9.31
$a'^1\Sigma_u^-$	$\pi_u \rightarrow \pi_g$	7.93	10.21	9.43	9.85	8.74	10.02	9.74	9.92
$w^1\Delta_u$	$\pi_u \rightarrow \pi_g$	8.75	10.78	9.84	10.23	9.47	10.62	10.07	10.27
$a''^1\Sigma_g^+$	$\sigma_g \rightarrow 3s\sigma_g$	14.00	12.34	11.31	11.05	13.29	12.31	10.19	12.20
$b^1\Pi_u$	$\sigma_g \rightarrow 3p\pi_u$	14.56	13.18	11.65	11.35	13.81	12.56	10.52	12.90
$b'^1\Sigma_u^+$	$\sigma_g \rightarrow 3p\sigma_u$	14.84	13.42	11.69	11.39	13.72	12.84	10.50	12.98
$c_3^1\Pi_u$	$\pi_u \rightarrow 3s\sigma_g$	15.10	13.63	12.18	12.35	13.34	13.24	11.44	13.24
d		0.59	0.33	-0.77	-0.76	0.16	0.03	-1.31	
$\|d\|$		1.59	0.33	0.77	0.76	0.72	0.16	1.31	
$\|d\|$ %		13.7	2.9	6.3	6.0	6.4	1.4	10.4	

[a] Ref. [176]

3.3 Excitation Energies of the CO and N_2 Molecules

The calculation of molecular excited state properties is a relatively unexplored application of KS-DFT. The use of TDDFT allows the calculation of excited state potential energy surfaces and implementations of excited-state analytic derivative programs have been reported [169–175]. The calculation of the properties of excited states will clearly be an important area in the future. Since we are considering diatomic molecules we may map out the excited state potential energy curves and calculate the optimized bond lengths and vibrational energy levels of each state. To ensure an accurate description of the excited states, the uncontracted 6-311G+(2df) basis set was further augmented by the addition of 2 extra s, p and d diffuse functions at the bond centres with exponents determined from the geometric progression (the average of the C and O exponents was used for CO).

To begin with we consider vertical excitation energies at the experimental ground state bond lengths in Table 3.1. We compare the Hartree–Fock and LHF methods, the conventional B97-2 functional and its multiplicative counterpart containing LHF exchange denoted L(B97-2), the B97(0.6) hybrid containing a lager fraction of orbital exchange and the corresponding L(B97(0.6)) functional, and the HCTH GGA functional. Following Ref. [128] the LHF excitation energies are determined using the adiabatic approximation of time-dependent linear response theory, with the contribution to the exchange–correlation kernel of Eqn. (3.2.7) being represented by the Dirac exchange kernel. For multiplicative hybrid calculations with a fraction of orbital dependent exchange ξ this contribution is scaled accordingly and added to the kernel of the GGA part of the hybrid functional. The singlet vertical excitation energies are presented in Tables 3.2 and 3.3 for the N_2 and CO molecules respectively, along with experimental values from Refs. [176, 177]. Errors are calculated relative to these values.

Table 3.3: Vertical excitation energies of CO, in eV, calculated at the experimental bond length

State	Transition	HF	LHF	B97-2	L(B97-2)	B97(0.6)	L(B97(0.6))	HCTH	Expt.[a]
$A^1\Pi$	$\sigma \rightarrow \pi^*$	8.78	8.70	8.45	8.41	8.60	8.53	8.29	8.51
$I^1\Sigma^-$	$\pi \rightarrow \pi^*$	9.37	10.71	9.84	10.12	9.58	10.41	9.94	9.88
$D^1\Delta$	$\pi \rightarrow \pi^*$	9.93	11.16	10.15	10.42	10.13	10.88	10.19	10.23
$B^1\Sigma^+$	$\sigma \rightarrow 3s\sigma$	11.88	10.85	9.96	9.79	11.48	10.92	8.97	10.78
$C^1\Sigma^+$	$\sigma \rightarrow 3p\sigma$	12.57	11.85	10.27	10.19	11.99	11.66	9.29	11.40
$E^1\Pi$	$\sigma \rightarrow 3p\pi$	12.60	11.72	10.41	10.25	12.01	11.64	9.29	11.53
$F^1\Sigma^+$	$\sigma \rightarrow 3d\sigma$	13.58	12.95	10.87	10.63	12.63	12.30	9.63	12.40
d		0.57	0.46	-0.68	-0.70	0.24	0.23	-1.30	
$\|d\|$		0.80	0.46	0.68	0.83	0.36	0.26	1.32	
$\|d\|$ %		7.2	4.3	5.9	7.2	3.3	2.5	11.5	

[a] Ref. [177]

If we consider the excitations individually, a smooth variation with the fraction of exchange is observed in moving from HCTH to B97-2 to B97(0.6) to HF and similarly for the multiplicative counterparts (prefixed L). For both molecules the HF results are poor and LHF is a notable improvement, which is consistent with Ref. [128] and Section 2.6. This improvement for the higher excitations results from the $-1/r$ asymptotic behaviour of the LHF potential which leads to an improved virtual eigenvalue spectrum. The B97-2 and L(B97-2) results are of overall similar quality with the errors in both cases being dominated by the Rydberg excitations, which is to be expected since in the first case the HF exchange contribution is scaled by 0.21 and in the latter the exchange–correlation potential exhibits an asymptotic $-0.21/r$ behaviour. The B97(0.6) functional gives excitations intermediate between the B97-2 and HF values as expected, and offers little overall improvement in quality. In contrast the L(B97(0.6)) results represent a substantial improvement over L(B97-2), reflecting the increased proportion of LHF exchange which results in a $-0.6/r$ asymptotic potential and consequently much improved Rydberg excitations. The values for L(B97(0.6)) are intermediate between those of L(B97-2) and LHF which tend to underestimate and overestimate the experimental values respectively. The HCTH error is large, as is commonly observed for GGA functionals, owing to its poor description of the Rydberg excitations due the exponential decay of the HCTH exchange–correlation potential.

The errors in Tables 3.2 and 3.3 are dominated by the poor description of the Rydberg states. It is well established that the asymptotic correction (AC) described in Section 1.7.3 can significantly reduce errors arising from the breakdown of the exchange–correlation potential in asymptotic regions. For the functionals of Table 3.2 we may apply the correction

$$\lim_{r\rightarrow\infty} v_{\mathrm{xc}}(\mathbf{r}) = \frac{-(1-\xi)}{r} + \varepsilon_{\mathrm{HOMO}} + I \tag{3.3.1}$$

where ξ is the fraction of orbital exchange in the functional, and I is the ionisation

Table 3.4: Vertical excitation energies of N_2, in eV, calculated at the experimental bond length with asymptotically corrected methods

State	Transition	B97-2 (AC)	L(B97-2 (AC))	B97(0.6) (AC)	L(B97(0.6) (AC))	HCTH (AC)	Expt.[a]
$a^1\Pi_g$	$\sigma_g \rightarrow \pi_g$	9.33	9.28	9.53	9.41	9.20	9.31
$a'^1\Sigma_u^-$	$\pi_u \rightarrow \pi_g$	9.45	9.87	8.73	10.03	9.78	9.92
$w^1\Delta_u$	$\pi_u \rightarrow \pi_g$	9.86	10.26	9.47	10.62	10.12	10.27
$a''^1\Sigma_g^+$	$\sigma_g \rightarrow 3s\sigma_g$	12.35	12.20	13.13	12.71	11.97	12.20
$b^1\Pi_u$	$\sigma_g \rightarrow 3p\pi_u$	12.97	12.83	13.74	13.45	12.62	12.90
$b'^1\Sigma_u^+$	$\sigma_g \rightarrow 3p\sigma_u$	13.06	13.00	13.66	13.63	12.73	12.98
$c_3^1\Pi_u$	$\pi_u \rightarrow 3s\sigma_g$	13.12	13.34	13.15	14.00	13.11	13.24
d		-0.10	-0.01	0.08	0.43	-0.18	
$\|d\|$		0.19	0.04	0.68	0.43	0.18	
$\|d\|$ %		1.7	0.3	6.0	3.5	1.6	

[a] Ref. [176]

Table 3.5: Vertical excitation energies of CO, in eV, calculated at the experimental bond length with asymptotically corrected methods

State	Transition	B97-2 (AC)	L(B97-2 (AC))	B97(0.6) (AC)	L(B97(0.6) (AC))	HCTH (AC)	Expt.[a]
$A^1\Pi$	$\sigma \rightarrow \pi^*$	8.49	8.46	8.59	8.54	8.39	8.51
$I^1\Sigma^-$	$\pi \rightarrow \pi^*$	9.86	10.14	9.57	10.41	9.99	9.88
$D^1\Delta$	$\pi \rightarrow \pi^*$	10.18	10.45	10.12	10.89	10.24	10.23
$B^1\Sigma^+$	$\sigma \rightarrow 3s\sigma$	10.83	10.63	11.39	10.90	10.48	10.78
$C^1\Sigma^+$	$\sigma \rightarrow 3p\sigma$	11.56	11.56	11.96	11.92	11.36	11.40
$E^1\Pi$	$\sigma \rightarrow 3p\pi$	11.52	11.42	12.02	11.77	11.24	11.53
$F^1\Sigma^+$	$\sigma \rightarrow 3d\sigma$	12.49	12.40	12.98	12.75	12.22	12.40
d		0.03	0.05	0.27	0.35	-0.12	
$\|d\|$		0.06	0.14	0.39	0.35	0.15	
$\|d\|$ %		0.5	1.3	3.5	3.2	1.4	

[a] Ref. [177]

potential calculated separately for each method. This correction is not appropriate for the HF method and is not required for the LHF approach. It is therefore only applied to the B97-2, L(B97-2), B97(0.6) and L(B97(0.6)) functionals. Since our LHF implementation is for closed shell molecules we utilise the B97-2 and B97(0.6) ionisation potentials in calculations involving their multiplicative counterparts. For the multiplicative functionals the combination of the $-(1-\xi)/r$ in Eqn. (3.3.1) and the $-\xi/r$ LHF component gives the overall $-1/r$ behaviour. The resulting excitation energies are presented in Tables 3.4 and 3.5.

For both the CO and N_2 molecules the B97-2(AC) and HCTH(AC) results are a significant improvement over the non-asymptotically corrected values, in line with previous observations. The L(B97-2)(AC) results are also a significant improvement over L(B97-2). The addition of the AC to the B97(0.6) functional does not lead to a similar improvement, which may reflect the fact that the AC was not designed to be used with such a large fraction of HF exchange. Since in L(B97(0.6)) the operator is fully multiplicative we may expect more success. However for both molecules the correction leads to an overestimation of the Rydberg values, which were reasonably

accurate before the correction was applied. This arises because the ionisation potential estimated by the B97(0.6) functional is significantly too large, and so the shift of Eqn. (3.3.1) is too great. Using the experimental value of I leads to much improved Rydberg excitations.

3.4 Calculation of Potential Energy Curves

From the analysis of the bond length and excitation energy data we may conclude that the best overall results are obtained with B97-2(AC), L(B97-2)(AC), and HCTH(AC). We now proceed to use these methods to calculate ground and excited state potential energy curves for N_2 and CO.

The ground state potential curves were determined in steps of 0.005 Å at geometries between 0.5 and 2.5 r_e for each method. These potential energy curves are subject to basis set superposition error (BSSE) which arises when the basis functions on a given atom overlap with those on another. This leads to each centre experiencing a more complete basis than would otherwise be the case and a geometry dependent lowering of the energy is introduced. To remove the lowering we estimate the BSSE via the counterpoise correction approach of Ref. [178].

In order to map out the excited state potential energy curves, TDDFT calculations were performed at each geometry to determine the excitation energies. The ionisation potentials required by the AC for each method were also determined at each geometry. These were then added to the BSSE corrected ground state potential energy curve such that the excited state curves are also indirectly BSSE corrected. For both molecules we examine the ground state, the three valence excited states and a single Rydberg state.

3.4.1 A Comparison with Experiment; The RKR Approach

In order to assess the accuracy of the potential energy curves calculated using each approach we also determined potential energy curves from spectroscopic constants using the semi-classical RKR inversion procedure [179–181]. The RKR method is exact within the Wentzel-Kramer-Brillouin (WKB) approximation [182–184] and is used to determine the potential energy curve for a diatomic molecule from a knowledge of the vibrational energy levels $G(v)$ and the inertial rotational constants $B(v)$ which may be obtained spectroscopically. The method is based on the Bohr-Sommerfeld quantisation condition

$$v + \frac{1}{2} = \left(\frac{1}{\pi\beta}\right) \int_{r_1}^{r_2} dr \, [E - U(r)]^{1/2} \tag{3.4.1}$$

for a diatomic molecule of reduced mass, $\mu = m_1 m_2/(m_1 + m_2)$, bound by a one dimensional potential, $U(r)$. Here $\beta^2 = (\hbar^2/2\mu)$ and $r_1(v)$ and $r_2(v)$ are the inner and outer turning points at the energy, E, defined by $U(r_1) = E = U(r_2)$. From this equation the allowed eigenvalues of the system are the energies at which the right hand side is equal to a half integer. However in the semi-classical approach v is treated as a continuous function of E. Differentiating the quantisation condition then gives

$$\frac{dv}{dE} = \left(\frac{1}{2\pi\beta}\right) \int_{r_1}^{r_2} dr/[E - U(r)]^{1/2} \tag{3.4.2}$$

This expression can be inverted to give an expression for the width of the potential well at $E = E(v)$. The result is

$$r_1(v) - r_2(v) = 2\beta \int_{v_0}^{v} dv'/[E(v) - E(v')]^{1/2} \tag{3.4.3}$$

where v_0 is the value of the vibrational quantum number at the potential minimum.

For a rotating system the potential $U(r)$ also contains a centrifugal term,

$$U(r) = U_J(r) = U_0(r) + J(J+1)\beta^2/r^2 \tag{3.4.4}$$

where J is the rotational quantum number and the energy then depends on both v and J. Differentiating the quantisation condition with respect to $[J(J+1)]$ gives

$$B(v)\frac{dv}{dE} = -\left(\frac{\beta}{2\pi}\right) \int_{r_1}^{r_2} dr/r^2[E - U(r)]^{1/2} \tag{3.4.5}$$

This equation may also be inverted to obtain the relation

$$\frac{1}{r_1(v)} - \frac{1}{r_2(v)} = \left(\frac{2}{\beta}\right) \int_{v_0}^{v} dv' B(v')/[E(v) - E(v')]^{1/2} \tag{3.4.6}$$

Eqns. (3.4.3) and (3.4.6) are the basis of the 1st order RKR method for the determinantion of potential energy curves.

In the 1st order RKR approach the vibrational quantum number at the minimum of the potential, v_0, is taken to have a value of one half. The Kaiser correction [185] adjusts the value of v_0 according to a consideration of higher order semi-classical approaches and is employed in all of our calculations. The RKR method is exact within the 1st order WKB approximation and for heavy molecules the quantum mechanical level spacings calculated from RKR potentials usually agree with experimental values to within experimental error. However for molecules with a small reduced mass larger

discrepancies between experimental vibrational levels and those calculated from RKR potentials may be observed.

The v dependence of the vibrational energies, $G(v)$, and the inertial rotational constants $B(v)$ are represented by Dunham [186] expansions

$$G(v) = \sum_{l=1} Y_{l,0} \left(v + \frac{1}{2}\right)^l = \omega_e \left(v + \frac{1}{2}\right) - \omega_e x_e \left(v + \frac{1}{2}\right)^2 + \omega_e y_e \left(v + \frac{1}{2}\right)^3 + \ldots \tag{3.4.7}$$

$$B(v) = \sum_{l=0} Y_{l,1} \left(v + \frac{1}{2}\right)^l = B_e - \alpha_e \left(v + \frac{1}{2}\right) + \gamma_e \left(v + \frac{1}{2}\right)^2 + \ldots \tag{3.4.8}$$

where the Dunham coefficients Y can be obtained from fitting to spectroscopic data. Since experimental data often defines $G(v)$ with more accuracy than $B(v)$ any non-physical behaviour in calculated RKR potentials is often attributed to inaccuracies in $B(v)$. Using equation (3.3) it is possible to calculate the well width without $B(v)$ and so by extrapolating the inner-wall in regions where non-physical anomalies are present a reasonable estimate of the potential may still be calculated. All of the RKR potential calculations in this work use the `RKR1` code of Le Roy [187] in which this feature is implemented. However in order to ensure that we compare our calculated potentials only with truly experimental ones we do not use any form of extrapolation or smoothing and instead only calculate the potential in regions close to the minima for which the constants are known to be accurate.

For N_2 the ground and valence state Dunham coefficients were taken from Ref. [188] and for the first Rydberg state the vibrational coefficients of Ref. [189] were employed along with the rotational coefficients of Ref. [190]. For CO the coefficients of Ref. [191] were used for the ground state, for all other states the coefficients of Ref. [192] were employed.

3.5 Excited State Optimized Geometries

The optimized bond lengths of each state may be determined from the minima of the potential energy curves. Near exact values are determined from the RKR curves. For each method the results are presented in Tables 3.6 and 3.7 for the N_2 and CO molecules respectively. Errors are calculated relative to the RKR values. For both molecules the B97-2 and L(B97-2) bond lengths are the same for the ground state, in line with the results in Table 3.1. The small differences are due to the addition of extra diffuse functions to the basis set and the application of the counterpoise correction. For excited states, the B97-2(AC) and L(B97-2)(AC) bond lengths differ, reflecting the importance

Table 3.6: Optimized bond lengths, in Å, of ground and excited states of N_2

State	B97-2 (AC)	L(B97-2 (AC))	HCTH (AC)	RKR
$X^1\Sigma_g^+$	1.090	1.090	1.098	1.098
$a^1\Pi_g$	1.207	1.194	1.212	1.220
$a'^1\Sigma_u^-$	1.272	1.259	1.283	1.276
$w^1\Delta_u$	1.265	1.256	1.280	1.269
$a''^1\Sigma_g^+$	1.104	1.104	1.111	1.115
d	-0.008	-0.015	0.001	
$\|d\|$	0.008	0.015	0.006	
$\|d\|$ %	0.7	1.2	0.5	

Table 3.7: Optimized bond lengths, in Å, of ground and excited states of CO

State	B97-2 (AC)	L(B97-2 (AC))	HCTH (AC)	RKR
$X^1\Sigma^+$	1.125	1.125	1.133	1.128
$A^1\Pi$	1.227	1.213	1.233	1.235
$I^1\Sigma^-$	1.354	1.343	1.375	1.391
$D^1\Delta$	1.350	1.342	1.371	1.399
$B^1\Sigma^+$	1.112	1.105	1.118	1.120
d	-0.021	-0.029	-0.009	
$\|d\|$	0.021	0.029	0.011	
$\|d\|$ %	1.6	2.2	0.8	

of the eigenvalue spectrum and choice of kernel in TDDFT calculations. B97-2(AC) tends to underestimate the bond lengths and in moving to L(B97-2)(AC) they tend to shorten further and hence become slightly less accurate. Both give an accuracy comparable with that obtained for the ground state optimized geometries determined in Section 3.1. The HCTH(AC) results are more accurate still with mean absolute errors of 0.006 and 0.011Å for the N_2 and CO molecules respectively. This is not expected to be a general conclusion since HCTH is known to perform particularly well for these two molecules.

3.6 Vibrational Frequencies

The potential energy curves may also be used to determine vibrational energy levels through the solution of the one dimensional Born–Oppenheimer nuclear dynamics Schrödinger equation. We use the LEVEL v7.5 program of Le Roy [193]. This program takes the calculated potential energy curves as input and uses them to solve the radial Schrödinger equation

$$-\frac{\hbar^2}{2\mu}\frac{d^2\Psi_{v,J}(R)}{dR^2} + V_J(R)\Psi_{v,J}(R) = E_{v,J}\Psi_{v,J}(R) \tag{3.6.1}$$

To ensure convergence to better than 0.1 cm^{-1} the potential energy curves consisted of points spaced by 0.005 Å and ten-point piecewise polynomial interpolation was

Table 3.8: Zero Point (ZP), fundamental, and first-overtone vibrational wavenumbers, in cm^{-1}, of ground and excited states of N_2

State		B97-2 (AC)	L(B97-2 (AC))	HCTH (AC)	RKR
$X^1\Sigma_g^+$	ZP	1232	1231	1186	1176
	$v=0\rightarrow v=1$	2443	2443	2351	2330
	$v=0\rightarrow v=2$	4861	4862	4677	4631
$a^1\Pi_g$	ZP	886	930	868	844
	$v=0\rightarrow v=1$	1749	1847	1716	1666
	$v=0\rightarrow v=2$	3471	3669	3404	3341
$a'^1\Sigma_u^-$	ZP	781	813	745	762
	$v=0\rightarrow v=1$	1546	1613	1474	1506
	$v=0\rightarrow v=2$	3072	3207	2929	2989
$w^1\Delta_u$	ZP	797	816	750	777
	$v=0\rightarrow v=1$	1577	1621	1483	1536
	$v=0\rightarrow v=2$	3143	3221	2945	3048
$a''^1\Sigma_g^+$	ZP	1166	1161	1127	1100
	$v=0\rightarrow v=1$	2317	2309	2240	2149
	$v=0\rightarrow v=2$	4607	4601	4466	4259
d_{ZP}		41	59	4	
$\|d\|_{ZP}$		41	59	21	
$\|d\|\,\%_{ZP}$		4.2	6.4	2.4	
$d_{v=0\rightarrow v=1}$		89	129	15	
$\|d\|_{v=0\rightarrow v=1}$		89	129	49	
$\|d\|\,\%_{v=0\rightarrow v=1}$		4.6	7.2	2.7	
$d_{v=0\rightarrow v=2}$		177	259	31	
$\|d\|_{v=0\rightarrow v=2}$		177	259	96	
$\|d\|\,\%_{v=0\rightarrow v=2}$		4.6	7.2	2.6	

used. These criteria were determined following the calculation of vibrational levels using several different spacings and levels of interpolation. DFT and RKR results for the zero point, fundamental and first overtone ($J = 0$) vibrational wavenumbers are presented in Tables 3.8 and 3.9. Errors are calculated relative to the RKR values. The results closely reflect the bond length observations with improvement in the mean absolute errors from L(B97-2)(AC) to B97-2(AC) to HCTH(AC).

The potential energy curves for N_2 and CO calculated using the HCTH GGA functional, which provides the most accurate geometries and vibrational frequencies, are presented in Figure 3.1. The potentials may be compared with the near exact RKR curves and these are presented in Figures 3.2 and 3.3 for the N_2 and CO molecules respectively. Each state is plotted separately for clarity. For both methods the energies are relative to the ground state minimum. The relative energies of the RKR curves were determined from the experimental T_e values of Ref. [194]. For both molecules the HCTH(AC) and RKR curves are in excellent agreement for the ground state. The first excited states ($^1\Pi_g$ in N_2 and $^1\Pi$ in CO) are also well described. For the next two states ($^1\Sigma_u^-$ / $^1\Sigma^-$ and $^1\Delta_u$ / $^1\Delta$), HCTH(AC) is accurate near equilibrium but becomes less accurate with increasing bond length. The agreement for the Rydberg states is not as good, but still a significant improvement over what would be obtained

Table 3.9: Zero Point (ZP), fundamental, and first-overtone vibrational wavenumbers, in cm^{-1}, of ground and exited states of CO

State		B97-2 (AC)	L(B97-2 (AC))	HCTH (AC)	RKR
$X^1\Sigma^+$	ZP	1107	1108	1069	1082
	$v=0\rightarrow v=1$	2196	2197	2119	2143
	$v=0\rightarrow v=2$	4368	4370	4214	4260
$A^1\Pi$	ZP	784	835	774	754
	$v=0\rightarrow v=1$	1545	1651	1541	1481
	$v=0\rightarrow v=2$	3059	3272	3075	2928
$I^1\Sigma^-$	ZP	626	644	585	544
	$v=0\rightarrow v=1$	1239	1275	1154	1071
	$v=0\rightarrow v=2$	2459	2534	2290	2121
$D^1\Delta$	ZP	634	645	588	545
	$v=0\rightarrow v=1$	1254	1277	1160	1074
	$v=0\rightarrow v=2$	2490	2538	2300	2127
$B^1\Sigma^+$	ZP	1120	1180	1103	1055
	$v=0\rightarrow v=1$	2240	2193	2170	2083
	$v=0\rightarrow v=2$	4434	4378	4288	4135
d_{ZP}		59	87	28	
$\|d\|_{ZP}$		59	87	33	
$\|d\|$ $\%_{ZP}$		8.8	12.4	4.8	
$d_{v=0\rightarrow v=1}$		124	148	59	
$\|d\|_{v=0\rightarrow v=1}$		124	148	68	
$\|d\|$ $\%_{v=0\rightarrow v=1}$		9.3	11.5	5.0	
$d_{v=0\rightarrow v=2}$		248	305	119	
$\|d\|_{v=0\rightarrow v=2}$		248	305	138	
$\|d\|$ $\%_{v=0\rightarrow v=2}$		9.5	11.8	5.2	

without an asymptotic correction. The $B^1\Sigma^+$ state of CO exhibits an avoided crossing; the RKR data corresponds only to the principal minimum. The potentials in Figures 3.2 and 3.3 thus neatly summarise the data in Tables 3.6 to 3.9.

Finally, we note that calculating the AC ionisation potential at each bond length is theoretically appropriate and does influence the results. To illustrate this, we determined alternative N_2 HCTH(AC) potential-energy curves using an AC scheme where a fixed ionisation potential that was calculated at the experimental bond length was used throughout. Although valence states were unaffected, the optimized bond length and fundamental vibrational wave number of the $^1\Sigma_g^+$ Rydberg state changed by 0.009 Å and 57 cm^{-1}, respectively, reducing agreement with the RKR values.

In Chapters 2 and 3 we have examined the performance of various approximate exchange potentials. In the next chapter we move on to consider the direct evaluation of the theoretically rigorous optimized effective potentials (OEPs) in a finite basis set.

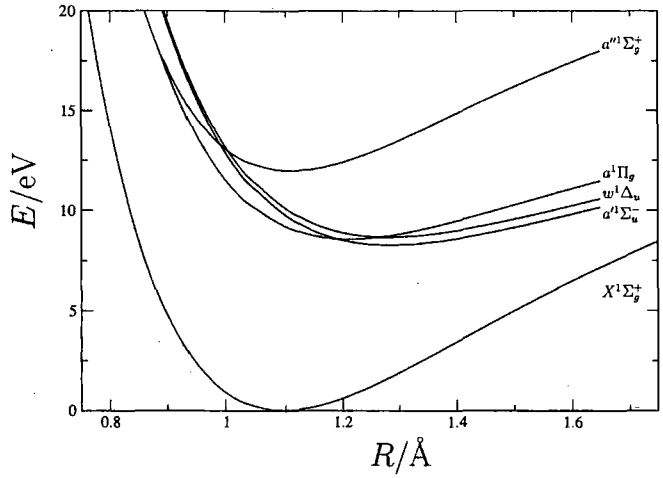

(a) Potential energy curves of N_2

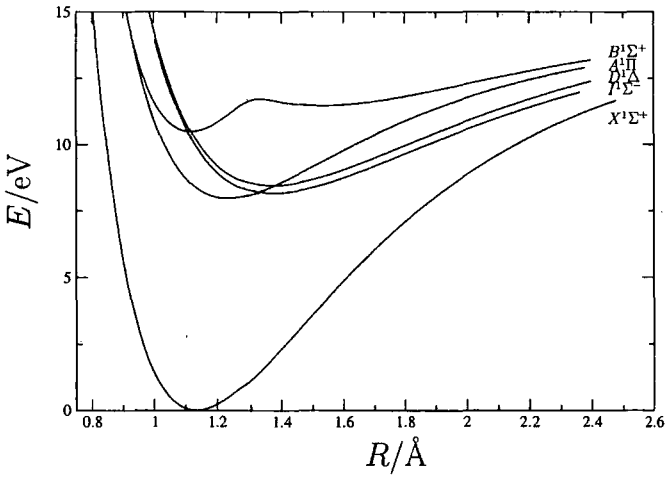

(b) Potential energy curves of CO

Figure 3.1: Potential energy curves calculated using the HCTH(AC) GGA functional

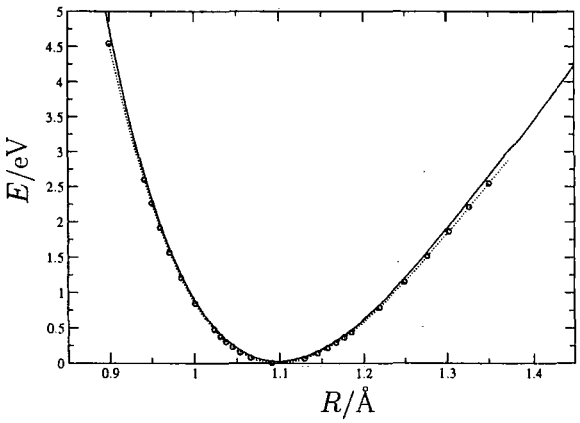

(a) $X^1\Sigma_g^+$ Ground State

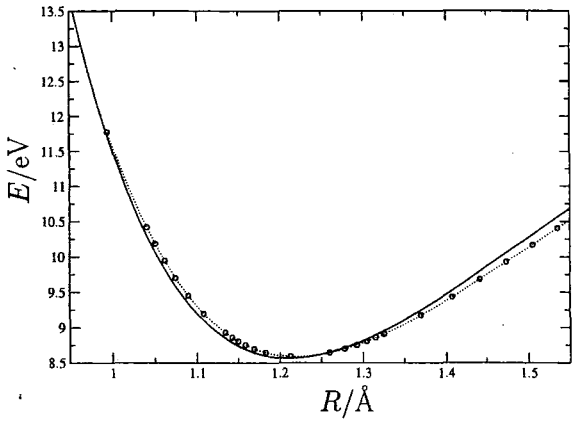

(b) $a^1\Pi_g$

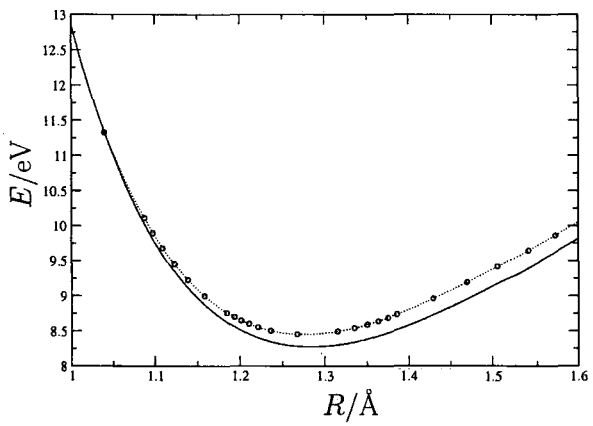

(c) $a'^1\Sigma_u^-$

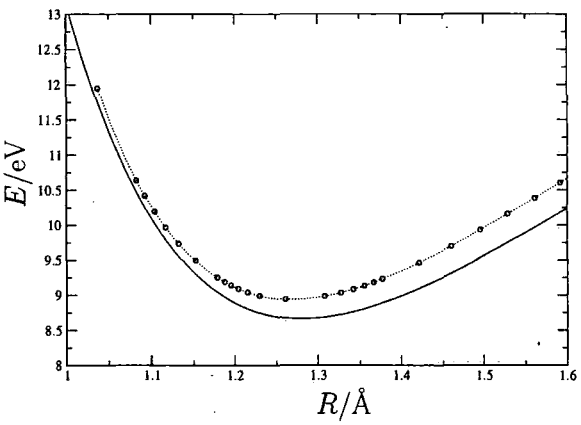

(d) $w^1\Delta_u$

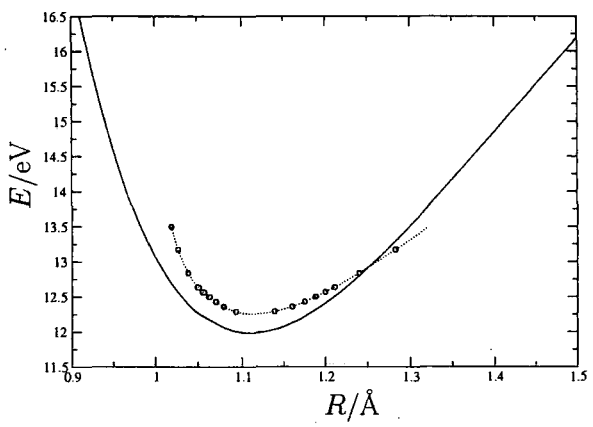

(e) $a''^1\Sigma_g^+$ Rydberg State

Figure 3.2: Potential energy curves of N_2, determined using HCTH(AC) (solid line) and RKR (dotted line with circles)

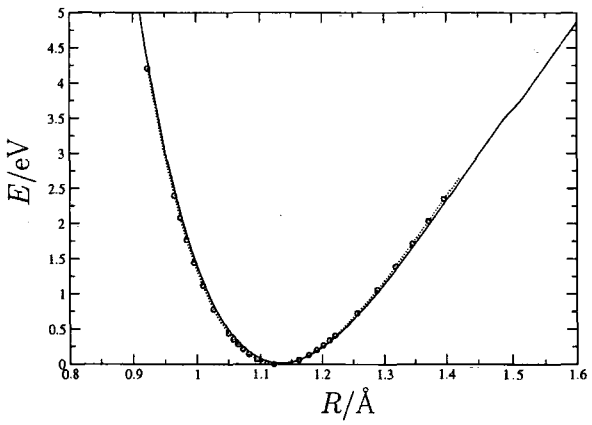

(a) $X^1\Sigma^+$ Ground State

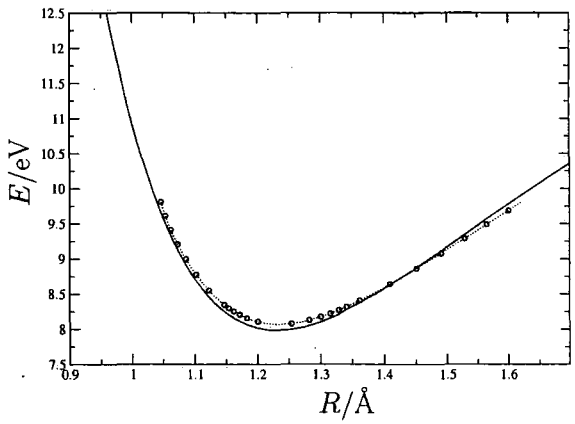

(b) $A^1\Pi$ State

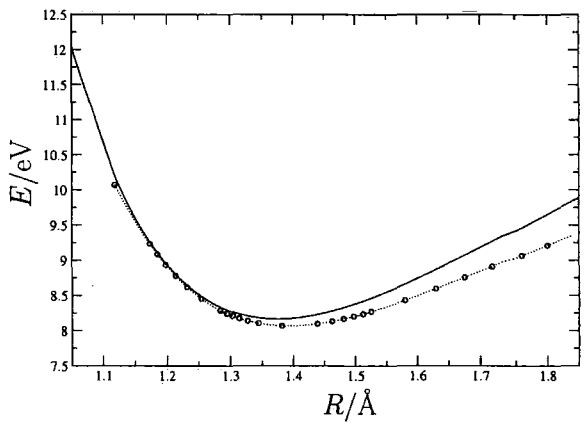

(c) $I^1\Sigma^-$ State

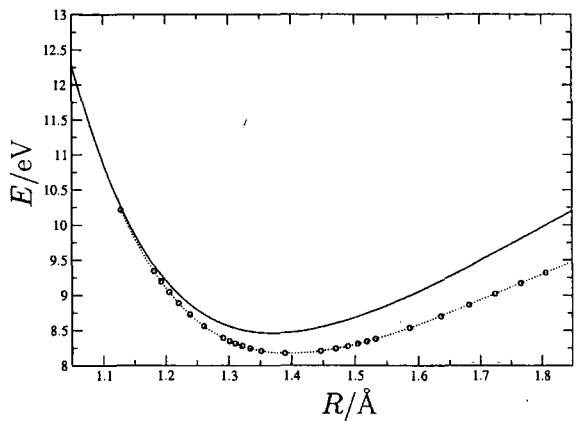

(d) $D^1\Delta$ State

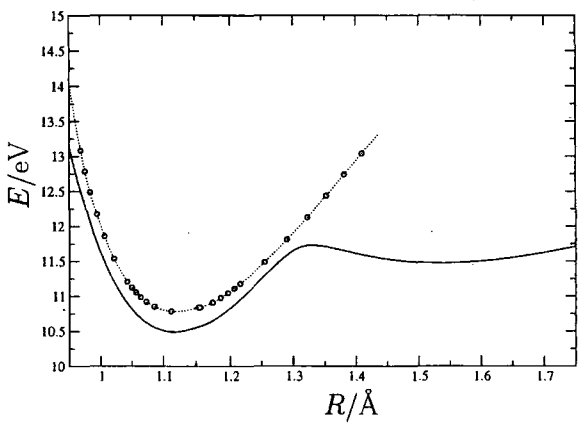

(e) $B^1\Sigma^+$ Rydberg State

Figure 3.3: Potential energy curves of CO, determined using HCTH(AC) (solid line) and RKR (dotted line with circles)

Chapter 4

Exact Exchange: Implementation of the OEP Method

In this chapter we outline the theory, implementation and testing of a method to calculate optimized effective potentials (OEPs) in a finite basis set. The key feature of the method is the expansion of the Kohn–Sham effective potential, $v_s(\mathbf{r})$, as a linear combination of Gaussian functions plus fixed terms. This allows the use of efficient direct optimization methods to calculate theoretically rigorous Kohn-Sham potentials corresponding to orbital dependent energy functionals. A computationally similar implementation of the constrained search procedure is also presented which provides a useful link to high level *ab initio* calculations via the electron density.

4.1 Potential Functionals and v-representability

The first Hohenberg–Kohn theorem establishes the mapping between the external potential $v(\mathbf{r})$ and the density $\rho(\mathbf{r})$. In the second Hohenberg–Kohn theorem a variational principle in terms of the density is established. However, it is assumed the density is v-representable; that is a ground state density for some external potential. Since this cannot be guaranteed for all trial densities the Hohenberg–Kohn functional, $F^{\mathrm{HK}}[\rho] = \hat{T} + \hat{V}_{ee}$, cannot always be used. The conditions for v-representability are unknown and so we cannot easily ensure that the density in the course of a variational calculation remains in this domain. As shown in Section 1.6.2 the v-representability problem can be removed by the Levy constrained search formulation in which the domain of the Hohenberg–Kohn functional is extended to all N-representable densities for which the conditions are known and trivially satisfied for any reasonable trial density.

An alternative solution to the v-representability problem which does not require ex-

tension of the Hohenberg–Kohn functional was suggested by Yang, Ayers and Wu [195]. The second Hohenberg–Kohn theorem establishes a variational principle in terms of the density. However, by virtue of the first Hohenberg–Kohn theorem, it is also possible to establish a variational principle based on the potential. For some trial potential $w(\mathbf{r})$ then following a route analogous to the original proof of Section 1.6.1 we may write the energy as a functional of the potential as

$$\begin{aligned} E[w] &= \left\langle \Psi_w \left| \hat{H}_v \right| \Psi_w \right\rangle \\ &= \left\langle \Psi_w \left| \hat{H}_w \right| \Psi_w \right\rangle + \left\langle \Psi_w \left| \hat{H}_v - \hat{H}_w \right| \Psi_w \right\rangle \\ &= E_{0,w} + \int d\mathbf{r}\, [v(\mathbf{r}) - w(\mathbf{r})]\, \rho_w(\mathbf{r}) \end{aligned} \tag{4.1.1}$$

and from the Rayleigh–Ritz variational principle establish $E_0 \leqslant E[w]$ with the equality holding for the case $w = v + c$ since the potential is defined only up to an additive constant. The subscript w indicates dependence on the trial potential, whilst the subscript v indicates dependence on the true external potential. For details of the proof see Ref. [195].

To make use of this variational principle the Kohn–Sham non-interacting reference system is employed. This assumes that there is a mapping between the ground state of the interacting system and the ground state of a non-interacting system moving under the influence of an effective potential, such that their densities are the same $\rho_{w_s} = \rho_w$. As such ρ_w must be non-interacting ground state v-representable. The density ρ_{w_s} is constructed from the Kohn–Sham orbitals via $\rho_{w_s} = \sum_i |\varphi_{w_s,i}|^2$ where the orbitals are the N lowest eigenstates arising from a one-electron local multiplicative potential $w_s(\mathbf{r})$ through the solution of

$$\left[\hat{T} + w_s(\mathbf{r})\right] \varphi_{w_s,i}(\mathbf{r}) = \varepsilon[w_s]\varphi_{w_s,i}(\mathbf{r}) \tag{4.1.2}$$

and the usual Kohn–Sham partitioning of the energy is employed

$$E^{\mathrm{KS}}[\rho] = T_s[\rho] + J[\rho] + E_{\mathrm{xc}}[\rho] + \int d\mathbf{r}\; v_{\mathrm{ext}}(\mathbf{r})\rho(\mathbf{r}) \tag{4.1.3}$$

where the exchange–correlation energy, $E_{\mathrm{xc}}[\rho]$, is the only unknown term. If the exact form for the exchange correlation energy were known then the solution of Eqn. (4.1.2) would yield $E^{\mathrm{KS}}[\rho] = E_0$, providing ρ is non-interacting ground state v-representable.

In order to obtain the Kohn–Sham energy we must minimise $E[w]$ with respect to variations in the potential, for which purpose we require the functional derivative of

$E[w]$ with respect to w_s

$$\frac{\delta E[w]}{\delta w_s(\mathbf{r})} = \int d\mathbf{r}' \left[v_s(\mathbf{r}') - w_s(\mathbf{r}')\right] \chi_s(\mathbf{r}', \mathbf{r}) \tag{4.1.4}$$

where $\chi_s(\mathbf{r}', \mathbf{r}) = \frac{\delta \rho_{w_s}(\mathbf{r}')}{\delta w_s(\mathbf{r})}$, $v_s = v_{\text{ext}} + v_J + v_{xc}$ (the usual KS effective potential) and the stationary condition is $w_s(\mathbf{r}) = v_s(\mathbf{r}) + c$. In order to ensure that we remain within the set of non-interacting v-representable densities the derivatives of density functionals are evaluated through the Kohn–Sham orbitals (which are eigenstates of the local potential w_s). For an exchange–correlation functional

$$\int d\mathbf{r}' v_{xc}(\mathbf{r}') \chi_s(\mathbf{r}', \mathbf{r}) = \frac{\delta E_{xc}}{\delta w_s(\mathbf{r})} \tag{4.1.5}$$

and so in relation to the original Kohn–Sham scheme

$$v_{xc}(\mathbf{r}) = \int d\mathbf{r}' \frac{\delta E_{xc}}{\delta w_s(\mathbf{r}')} \chi_s^{-1}(\mathbf{r}', \mathbf{r}) \tag{4.1.6}$$

$$= \sum_i \int d\mathbf{r}' d\mathbf{r}'' \frac{\delta E_{xc}[\varphi_{w_s,i}]}{\delta \varphi_{w_s,i}(\mathbf{r}'')} \frac{\delta \varphi_{w_s,i}(\mathbf{r}'')}{\delta w_s(\mathbf{r}')} \frac{\delta w_s(\mathbf{r}')}{\delta \rho_w(\mathbf{r})} = \frac{\delta E_{xc}[\varphi_{w_s,i}]}{\delta \rho_w(\mathbf{r})} \tag{4.1.7}$$

In the Kohn–Sham scheme focussing on the density the exchange–correlation potential is defined as the functional derivative $\delta E_{xc}/\delta\rho(\mathbf{r})$. This definition for a functional which is an explicit functional of the density does not cause any complications since the exchange–correlation potential in terms of this derivative will then be uniquely defined. However for orbital dependent functionals the use of this definition implies extension beyond the domain of v-representable densities. To ensure that we remain within the domain of non-interacting v-representable densities, the derivative is instead taken with respect to the orbitals which are eigenstates of the local potential. Thus by minimising the energy with respect to variations in the potential we can solve the Kohn–Sham self consistent equation without going outside the set of non-interacting ground state v-representable densities.

This approach to Kohn–Sham theory from the point of view of varying the potential is dual to the minimisation of the energy as a functional of the density as Kohn–Sham theory is commonly viewed. The foregoing theory places the optimized effective potential approach proposed by Sharp and Horton [98] on a firm theoretical basis in the context of DFT. The exchange only OEP may be identified as the exact exchange approach in DFT [100], although the OEP approach is the rigorous way to handle any orbital dependent functional.

4.2 The Optimized Effective Potential Approach

In 1950 Slater presented his simplification of the Hartree–Fock method [51] in which he derived an approximate exchange potential under which all electrons move, to replace the more complex exchange contribution to the Hartree–Fock equations where each electron experiences a different exchange interaction. This potential was introduced in Eqn. (1.5.11) of Chapter 1. The publication of this approximation stimulated Sharp and Horton [98] to suggest reformulating the Hartree–Fock equations with an effective multiplicative potential. This leads to the following problem; for a one-electron Schrödinger equation of the form

$$\left[\hat{T} + v_s^\sigma(\mathbf{r})\right] \varphi_{i\sigma}(\mathbf{r}) = \varepsilon_{i\sigma}\varphi_{i\sigma}(\mathbf{r}) \tag{4.2.1}$$

find the potential $v_s^\sigma(\mathbf{r})$ which gives rise to a set of orbitals $\{\varphi_{i\sigma}\}$ such that a Slater determinant formed from the occupied orbitals gives the minimum obtainable value for the Hartree–Fock energy functional. This leads to a set of three-dimensional integral equations for $v_s^\sigma(\mathbf{r})$ that are difficult to solve exactly. Since the exchange energy is defined by the Hartree–Fock method and Kohn–Sham theory requires that the electrons move in a multiplicative effective potential the solution to the exchange-only OEP problem above is identified as exact exchange DFT.

In a finite basis set an algebraic equation for the OEP may be derived. However solution of this equation is beset by numerical difficulties since it involves the inversion of an almost singular matrix. This has hindered the application of the OEP method to molecular systems. However, Yang and Wu [112, 196] have recently proposed an alternative strategy to solve the OEP equation. If one writes down a representation of the potential $v_s^\sigma(\mathbf{r})$ such that it depends on a set of scalars, $\{b_t^\sigma\}$, then it is possible to solve the OEP problem by the direct optimization of these parameters. This approach allows the application of the OEP method to molecules and we now focus on the theory, implementation and testing of this approach in the CADPAC quantum chemistry code.

4.2.1 A Direct Optimization Scheme

The aim of the Yang–Wu method is to recast the OEP problem into a form that is amenable to efficient solution by direct iterative optimization methods. In order to achieve this the Kohn–Sham effective potential is written as

$$v_s^\sigma(\mathbf{r}) = v_{\text{ext}}(\mathbf{r}) + v_0(\mathbf{r}) + \sum_t b_t^\sigma g_t(\mathbf{r}) \tag{4.2.2}$$

where $v_{\text{ext}}(\mathbf{r})$ is the external potential due to the nuclei, $v_0(\mathbf{r})$ is a fixed reference potential and the remaining term is a linear combination of Gaussian basis functions $\{g_t(\mathbf{r})\}$ with coefficients $\{b_t^\sigma\}$. The reference potential is chosen such that it accounts for as much as possible of the potential. This helps the optimization procedure to converge efficiently. Two possible choices of reference potential are the Slater potential [51] of Chapter 2 and the Fermi–Amaldi potential [197], defined in terms of some fixed density as

$$v_0(\mathbf{r}) = \frac{N-1}{N}\int \frac{\rho_0(\mathbf{r}')}{|\mathbf{r}-\mathbf{r}'|}d\mathbf{r}' \tag{4.2.3}$$

which was used by Zhao, Morrison and Parr in their constrained search scheme [59]. Both potentials exhibit $-1/r$ asymptotic decay, which is appropriate for the exchange only case. This is a key requirement of the reference potential since this decay can never be reproduced by a finite set of Gaussian functions.

The coefficients $\{b_t^\sigma\}$ which lead to a potential and set of orbitals that minimise the energy functional $E[\{\varphi_{i\sigma}\}]$, must be determined. To achieve this the derivatives of the energy with respect to $\{b_t^\sigma\}$ are required. Using the chain rule the first derivative of a given energy expression with respect to the coefficients can be written as

$$\frac{\partial E[\{\varphi_{i\sigma}\}]}{\partial b_t^\sigma} = \sum_i \int d\mathbf{r}d\mathbf{r}' \frac{\delta E[\{\varphi_{i\sigma}\}]}{\delta\varphi_{i\sigma}(\mathbf{r})}\frac{\delta\varphi_{i\sigma}(\mathbf{r})}{\delta v_s^\sigma(\mathbf{r}')}\frac{\partial v_s^\sigma(\mathbf{r}')}{\partial b_t^\sigma} + \text{c.c.} \tag{4.2.4}$$

The second term in the chain can be obtained in terms of orbitals and eigenvalues from first order perturbation theory [101]. Substituting it into the above expression and evaluating the last term in the chain gives

$$\begin{aligned}\frac{\partial E[\{\varphi_{i\sigma}\}]}{\partial b_t^\sigma} &= \sum_i \int d\mathbf{r}d\mathbf{r}' \frac{\delta E[\{\varphi_{i\sigma}\}]}{\delta\varphi_{i\sigma}(\mathbf{r})}\sum_{a\neq i}\varphi_{a\sigma}(\mathbf{r})\frac{\varphi_{a\sigma}^*(\mathbf{r}')\varphi_{i\sigma}(\mathbf{r}')}{\varepsilon_{i\sigma}-\varepsilon_{a\sigma}}g_t(\mathbf{r}') + \text{c.c.} \\ &= \sum_{i,a\neq i}\int d\mathbf{r}\frac{\delta E[\{\varphi_{i\sigma}\}]}{\delta\varphi_{i\sigma}(\mathbf{r})}\varphi_{a\sigma}(\mathbf{r})\frac{\langle\varphi_{a\sigma}|g_t|\varphi_{i\sigma}\rangle}{\varepsilon_{i\sigma}-\varepsilon_{a\sigma}} + \text{c.c.}\end{aligned} \tag{4.2.5}$$

In order to accelerate convergence in iterative optimization procedures it is often useful to be able to calculate the second derivative. Unfortunately in this case the second derivative has a complex form [195] which is difficult to compute. In practical optimization schemes we may make use of the following approximation to it [196]

$$\frac{\partial^2 E[\{\varphi_{i\sigma}\}]}{\partial b_u^\sigma \partial b_t^\sigma} \approx -\sum_i\sum_a \frac{\langle\varphi_{a\sigma}|g_u|\varphi_{i\sigma}\rangle\langle\varphi_{a\sigma}|g_t|\varphi_{i\sigma}\rangle}{\varepsilon_{i\sigma}-\varepsilon_{a\sigma}} + \text{c.c.} \tag{4.2.6}$$

which provides an approximate Hessian matrix that is positive definite symmetric. A

variety of well established optimization techniques can be employed to calculate the optimized effective potential using the derivatives of Eqns. (4.2.5) and (4.2.6).

4.3 Optimization Techniques

The most popular optimization techniques are the conjugate gradient, first order quasi-Newton methods and second order quasi-Newton methods. The quasi-Newton methods have a key advantage in that second order information may be used directly and this can lead to significant acceleration in the convergence of the method. As such we will focus on these approaches for calculating the optimized effective potential.

4.3.1 The BFGS quasi-Newton Procedure

The basis of the quasi-Newton methods is to suppose that our function $E(\mathbf{b})$, where $\mathbf{b}$ is a vector of N scalar parameters in the expansion of Eqn. (4.2.2), can be modelled by a quadratic form. Then writing a Taylor series expansion to second order around a given point $\mathbf{b}_n$ where $H_{ij} = \frac{\partial^2 E(\mathbf{b_n})}{\partial b_i \partial b_j}$, the function at a new point $\mathbf{b}_{n+1}$ is given by

$$E(\mathbf{b}_{n+1}) = E(\mathbf{b}_n) + (\mathbf{b}_{n+1} - \mathbf{b}_n) \cdot \nabla E(\mathbf{b}_n) + \frac{1}{2}(\mathbf{b}_{n+1} - \mathbf{b}_n) \cdot \mathbf{H} \cdot (\mathbf{b}_{n+1} - \mathbf{b}_n) \quad (4.3.1)$$

and

$$\nabla E(\mathbf{b}_{n+1}) = \nabla E(\mathbf{b}_n) + \mathbf{H} \cdot (\mathbf{b}_{n+1} - \mathbf{b}_n) \quad (4.3.2)$$

If we wish to find the minimum of $E(\mathbf{b})$ then we set $\nabla E(\mathbf{b}_{n+1}) = 0$, and so the step required to reach the minimum can be determined by

$$\mathbf{b}_{n+1} - \mathbf{b}_n = -\mathbf{H}^{-1} \cdot \nabla E(\mathbf{b_n}) \quad (4.3.3)$$

For a function that is exactly quadratic and where $\mathbf{H}^{-1}$ is known exactly then the step of Eqn. (4.3.3) would lead directly to the minimum. However in general $E(\mathbf{b})$ is not quadratic and $\mathbf{H}^{-1}$ may be unknown or difficult to evaluate. Instead, by using this quadratic model along with an approximation to the inverse of the Hessian, an iterative procedure can be constructed where at each step we move towards the minimum and build up a refined approximation to $\mathbf{H}^{-1}$. This is the aim of the so called quasi-Newton methods.

The 'trick' of the quasi-Newton procedures is to ensure that the approximation to $\mathbf{H}^{-1}$ always leads to a decrease in the function $E(\mathbf{b})$. Consider the directions $\mathbf{p} = \mathbf{b}_{n+1} - \mathbf{b}_n$ along which $E(\mathbf{b})$ decreases, i.e. $\nabla E(\mathbf{b}) \cdot \mathbf{p} < 0$ then multiplying Eqn.

(4.3.3) by $\mathbf{p}$ and rearranging gives the requirement

$$\mathbf{p} \cdot \nabla E(\mathbf{b}_n) = -\mathbf{p} \cdot \mathbf{H} \cdot \mathbf{p} < 0 \tag{4.3.4}$$

which will be satisfied if $\mathbf{H}$ is positive definite symmetric. Thus the quasi-Newton procedure must build up an approximation to $\mathbf{H}^{-1}$ in such a way that $\mathbf{H}$ remains positive definite symmetric. This guarantees that even far from the minimum the calculated step always leads in a downhill direction. However, taking the full Newton step may lead to an increase in the function since we are approximating it by a quadratic form and so it is only guaranteed to decrease initially. To circumvent this problem a line search along the direction $\mathbf{p}$ is performed in which the new point is chosen such that

$$\mathbf{b}_{n+1} = \mathbf{b}_n + \lambda \mathbf{p} \tag{4.3.5}$$

where λ is between 0 and 1. A value of 1 is the full Newton step and is tried first; this will work best in regions close to the minimum where the quadratic model is most valid. If this does not lead to sufficient decrease (or leads to an increase) in $E(\mathbf{b})$ then the value of λ is decreased until the value of $E(\mathbf{b})$ falls by a satisfactory amount. In order to avoid convergence problems we define the sufficient decrease by the condition

$$E(\mathbf{b}_{n+1}) \leqslant E(\mathbf{b}_n) + \alpha \nabla E \cdot (\mathbf{b}_{n+1} - \mathbf{b}_n) \tag{4.3.6}$$

where $0 < \alpha < 1$. In our implementation we choose a value of 10^{-4}. After each step we must update our approximation to $\mathbf{H}^{-1}$. This can be achieved by using the BFGS updating formula for the inverse of the Hessian [198]. The initial approximation to $\mathbf{H}^{-1}$, is usually chosen to be the unit matrix $\mathbf{I}$.

4.3.2 The Approximate Newton Scheme

In the BFGS quasi-Newton procedure we need only evaluate the first derivative of Eqn. (4.2.5) and an approximation to the inverse of the Hessian is constructed iteratively. The convergence of this procedure can be slow, large numbers of iterations being required to minimise the electronic energy. To accelerate convergence the same scheme may be employed but instead of using the BFGS updating formula, the approximate Hessian of Eqn. (4.2.6) is calculated directly. Since this matrix is positive definite symmetric the resulting decent direction is guaranteed to lead to a decrease in the value of the function $E(\mathbf{b})$. The only disadvantage to this approach is that the Hessian must be inverted, which is a numerically difficult procedure. This is especially the case for the OEP problem where the Hessian is near singular, a characteristic of discrete ill

posed problems [199].

In order to obtain the best possible approximation to the inverse of the Hessian, regularisation schemes must be used to filter out the small singular contributions which cause numerical difficulties. The most widely used scheme is the truncated singular value decomposition (TSVD). In this method the approximate Hessian, $\tilde{\mathbf{H}}$, is decomposed into the product of three matrices.

$$\tilde{\mathbf{H}} = \mathbf{U} \cdot \mathbf{W} \cdot \mathbf{U}^T \tag{4.3.7}$$

where $\mathbf{W}$ is a diagonal matrix of singular values w_i and $\mathbf{U}$ is an orthogonal symmetric matrix. The inverse of $\tilde{\mathbf{H}}$ is then given by

$$\tilde{\mathbf{H}}^{-1} = \mathbf{U} \cdot [\mathrm{diag}(1/w_i)] \cdot \mathbf{U}^T \tag{4.3.8}$$

clearly this can cause numerical difficulties if some of the w_i's approach zero. To avoid this, we regularise the Hessian by use of a filter f_i

$$\tilde{\mathbf{H}}^{-1} = \mathbf{U} \cdot [\mathrm{diag}(f_i/w_i)] \cdot \mathbf{U}^T \tag{4.3.9}$$

In the TSVD scheme the filters take a value of either 0 or 1 depending on whether the singular values, w_i, are below or above a cutoff, respectively. This scheme has been implemented in our current approach using the algorithm of Ref. [200].

The use of the TSVD scheme leads to an abrupt cutoff of the singular values. This may not be optimal since the singular values of the approximate Hessian calculated using Eqn. (4.3.7) decay to zero gradually. An alternative is to use Tikhonov regularisation [201] in which the new direction is determined by solving the equation

$$(\tilde{\mathbf{H}}^T \cdot \tilde{\mathbf{H}} + \lambda^2) \cdot \mathbf{p} = \tilde{\mathbf{H}}^T \cdot \nabla E \tag{4.3.10}$$

where λ is a positive weighting factor. The solution of Eqn. (4.3.10) can be regarded as equivalent to performing a TSVD with filter factors chosen equal to

$$f_i = \frac{w_i^2}{w_i^2 + \lambda^2} \tag{4.3.11}$$

The value of the filter as a function of w_i for both TSVD and Tikhonov regularisation is illustrated in Figure 4.1 where a value of 10^{-4} is chosen for the TSVD threshold and λ in the Tikhonov case. We see the abrupt cutoff of the singular values for the TSVD scheme in contrast to the Tikhonov filters which smoothly decay to zero as the singular

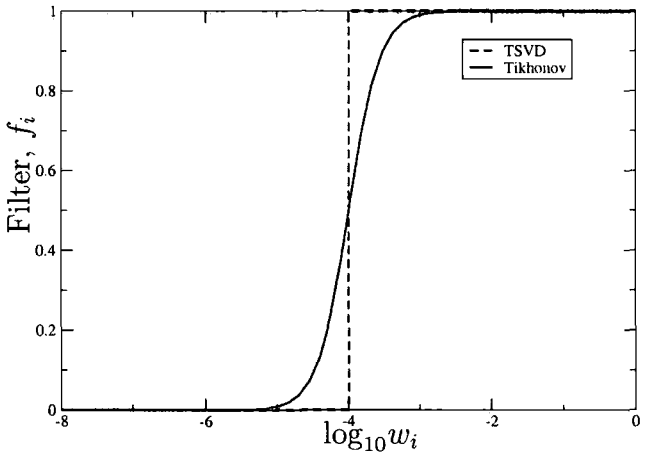

Figure 4.1: The variation of the filter with the singular values, in the TSVD (cutoff 10^{-4}) and Tikhonov ($\lambda = 10^{-4}$) regularisation schemes

values decrease.

4.4 Testing Our Implementation

We have implemented both the BFGS and approximate Newton schemes described above in the CADPAC quantum chemistry code for the restricted and unrestricted Kohn–Sham formalisms. The derivative of Eqn. (4.2.5) was checked by numerical finite difference and the BFGS algorithm of Ref. [200] was initially employed to perform the optimization. This routine was then modified accordingly to allow the use of the alternative approximation to the Hessian of Eqn. (4.2.6) and the Tikhonov and TSVD regularisation schemes were employed to ensure accurate evaluation of its inverse. The OEP calculations then proceed as follows,

1. Calculate the 1 and 2 electron integrals over the basis functions as in standard codes.

2. For a given set of guess orbitals construct a reference density $\rho_0(\mathbf{r})$ and compute the Fermi–Amaldi reference potential of Eqn. (4.2.3).

3. On the first iteration, calculate and store the three centre integrals $\langle \varphi_{a\sigma} | g_t | \varphi_{i\sigma} \rangle$ where $\{g_t\}$ is a set of auxiliary basis functions to be used in the construction of the Kohn–Sham effective potential as defined in Eqn. (4.2.2). The integrals are also required for the calculation of the derivatives on all subsequent iterations.

4. Begin with the set of coefficients $\{b_t^\sigma\}$ set equal to zero.

5. Construct $v_s^\sigma(\mathbf{r})$ of Eqn. (4.2.2) and determine a new set of orbitals and an energy E. Using these orbitals calculate the first derivative of Eqn. (4.2.5).

6. If optimization is to be done by the BFGS procedure then construct the new approximation to the inverse of the Hessian as described in Section 4.3.1. Otherwise calculate the approximate second derivative according to Eqn. (4.2.6) and its inverse after regularisation by either TSVD or Tikhonov methods as described in Section 4.3.2. The descent direction is then determined according to Eqn. (4.3.3).

7. Perform a line search along the descent direction, beginning with a full Newton step and backtracking until the energy decreases by a sufficient amount. At this point a new set of coefficients $\{b_t^\sigma\}$ have been determined.

8. Repeat steps 5 to 7 until the largest element of the first derivative of Eqn. (4.2.5) falls below a desired convergence threshold.

To test our implementation, we consider the 19 atoms and molecules of Ref. [112]. OEP energies are calculated for the Hartree–Fock energy functional using both the BFGS and approximate Newton procedures. For the approximate Newton approach TSVD regularisation is used and two cutoffs are applied, 10^{-4} and 10^{-6}. Convergence of the calculations is determined by a threshold on the largest element of the gradient of 10^{-6}. For the reference potential of Eqn. (4.2.3), a Hartree–Fock density was employed.

In Table 4.1 we present the deviation of the OEP energies from the Hartree–Fock values and compare them with those of Refs. [105, 112]. For the atoms, the extensive uncontracted Partridge-3 basis set was used and for the molecules an uncontracted cc-pVTZ basis set was employed. Molecular geometries were taken from Ref. [105]. In all cases the auxiliary basis set $\{g_t\}$ is chosen to be the same as the orbital basis set. The need to backtrack during the line search in regions where the quadratic model function is a poor approximation means that the number of energy evaluations may be larger than the number of quasi-Newton iterations and so both quantities are presented.

Table 4.1: OEP exchange-only electronic energies calculated using the Hartree–Fock energy functional with BFGS and approximate Newton (AN) optimization schemes. Deviations from Hartree–Fock energies, in mE_h, are compared with those of Refs. [105, 112]

		BFGS			AN Filter 4			AN Filter 6			Ref. [112]	Ref. [105]
Mol / Atom	HF Energy	N It	N E Eval	Dev.	N It	N E Eval	Dev.	N It	N E Eval	Dev.	Dev.	Dev.
Li	-7.43275	262	264	0.26	12	14	0.32	11	14	0.26	0.26	0.24
Be	-14.57302	176	262	0.58	14	17	0.68	11	13	0.58	0.58	0.58
N	-54.40454	466	470	1.15	43	47	1.22	38	40	1.15	1.15	1.14
Ne	-128.54709	219	222	1.68	13	21	1.72	12	19	1.68	1.7	1.7
Ar	-526.81749	306	311	5.13	89	95	6.07	86	91	5.15	5.2	5.1
H_2	-1.13308	1	2	0.00	1	2	0.00	1	2	0.00	0	0
H_2O	-76.05775	464	467	2.30	15	24	2.51	13	21	2.30	2.31	2.3
HF	-100.05850	347	350	1.99	17	26	2.08	15	26	1.99	2	1.99
OH	-75.41967	663	671	2.39	23	34	2.53	21	34	2.39	2.39	2.39
N_2	-108.98468	375	379	5.21	29	41	5.99	28	41	5.22	5.22	5.2
O_2	-149.67646	622	630	6.70	36	67	6.91	35	65	6.66	6.69	6.62
F_2	-198.75244	241	246	8.55	16	27	8.95	15	23	8.55	8.56	8.55
CH_2	-38.89264	468	471	2.89	20	28	3.06	19	28	2.90	2.9	2.89
CH_2	-38.92047	1000	1003	1.87	23	33	2.06	22	30	1.88	1.87	1.87
NH_2	-55.58660	926	930	2.55	23	34	2.76	23	35	2.55	2.55	2.55
NH	-54.98141	746	749	1.96	20	29	2.19	23	31	1.97	1.97	1.97
CO	-112.78160	479	484	5.10	18	35	5.51	16	30	5.10	5.12	5.08
CN^-	-92.33594	483	487	4.50	20	39	5.09	18	34	4.50	4.5	
OH^-	-75.38699	325	327	2.24	15	26	2.34	15	27	2.24	2.24	

The BFGS calculations reproduce accurately those of Yang and Wu [112], with a maximum difference of 0.02 mE_h. In general several hundred iterations are required to achieve convergence. This means that even for the simple molecules and relatively modest uncontracted cc-pVTZ basis sets considered here, the calculations can be time consuming. The notable exception is the H_2 molecule for which only a single iteration is required. This is due to the fact that for a 1 electron or 2 electron spin paired system the Hartree–Fock potential is a local multiplicative potential equal to $-v_\mathrm{J}/N$ and hence is reproduced easily by the OEP method which uses exactly this potential (the Fermi–Amaldi potential) as a reference. The fact that for this molecule the HF energy is reproduced exactly is in itself an important test of the implementation. In most cases the number of iterations required is similar to the number of energy evaluations indicating that during the course of the optimization the quadratic model used for the determination of the descent direction is reasonably accurate. The notable exception is the Be atom which may indicate that the initial guess used in the OEP calculation was particularly poor for this system.

When second order optimization is used the number of iterations is dramatically reduced. However, since TSVD regularisation is used in the calculation of the inverse of the Hessian, which introduces an abrupt cutoff in the singular values, the requested convergence may not always be attainable. In such a case the calculation proceeds as far as possible until with the given approximation to the Hessian the energy no longer decreases sufficiently. In Table 4.1 results for cutoffs of 10^{-4} and 10^{-6} are presented and in all cases the deviations from the Hartree–Fock energy with a cutoff of 10^{-4} are larger than those obtained using BFGS optimization. In order to reach a similar level of convergence it is necessary to reduce the cutoff to a value of 10^{-6} and then the deviations again reproduce those of Ref. [112] with a maximum difference of 0.02 mE_h. These tests indicate that the optimization and regularisation procedures are correctly implemented and that when the $\{g_t\}$ are chosen to be the orbital basis functions we can accurately reproduce values reported previously in the literature. We now move on to consider other possible choices for the set of functions $\{g_t\}$.

4.5 Using an Alternative Auxiliary Basis Set

The set of basis functions $\{g_t\}$ in which the Kohn–Sham effective potential is expanded according to Eqn. (4.2.2) have so far been chosen to be the same as those of the orbital basis set. However, this choice may not be satisfactory, since orbital basis functions are not optimized to represent the Kohn–Sham potential. Typically they will contain contracted functions which are optimized to provide an accurate description

Table 4.2: Exponent ranges used to specify eventempered basis sets

	AUX 1		AUX2		AUX3	
Ang. Mom.	min	max	min	max	min	max
s	-5	5	-10	10	-15	15
p	-4	4	-8	8	-12	12
d	-3	3	-6	6	-9	9
f	-2	2	-4	4	-6	6

Table 4.3: Deviation of the OEP exchange-only energies from Hartree–Fock values for various choices of auxiliary basis set in, mE_h

Mol	AUX 1 Deviation	AUX 2 Deviation	AUX3 Deviation
Base = 3.0			
N	1.14	1.14	1.14
Ne	1.68	1.68	1.68
OH	1.68	1.67	1.67
F_2	7.04	6.94	6.94
N_2	4.68	4.56	4.57
Base = 2.5			
N	1.14	1.14	1.14
Ne	1.69	1.68	1.68
OH	1.69	1.67	1.67
F_2	7.11	6.89	6.88
N_2	4.65	4.60	4.61
Base = 2.0			
N	1.15	1.14	1.14
Ne	1.70	1.68	1.67
OH	1.97	1.65	1.66
F_2	7.32	6.86	6.84
N_2	4.63	4.59	4.56
Base = 1.8			
N	1.18	1.14	1.14
Ne	1.85	1.68	1.67
OH	2.06	1.66	1.65
F_2	7.41	6.77	6.76
N_2	4.91	4.60	4.55

of molecular orbitals and so may not provide sufficient flexibility to be used in the expansion of Eqn. (4.2.2). We are free to choose this set in order to ensure maximum variational flexibility. For a representative subset of atoms and molecules from Table 4.1, namely N, Ne, OH, F_2 and N_2 we now investigate the convergence of the OEP energy with respect to the choice of auxiliary basis set. Even tempered auxiliary basis sets are employed which are the same on each atom; the functions are specified by a universal base N raised to a range of integer powers. Auxiliary functions up to i angular momenta have been implemented but we consider only up to f functions in the present case. Several bases are considered; 3.0, 2.5, 2.0 and 1.8. The three sets of ranges are chosen as specified in Table 4.2 and labelled AUX1, AUX2, and AUX3. To ensure rapid and tight convergence of the energy, the approximate Newton scheme is employed with TSVD regularisation and a cutoff of 10^{-6}.

The deviations of the OEP energies from the Hartree–Fock values are presented in Table 4.3. For each base, moving across the rows increases the range of exponents included in the set. Moving down each column causes a reduction in the base and has the effect of reducing the range of the exponents whilst keeping the same number of functions and so they are more tightly spaced. The most converged results are therefore expected to be at the bottom right of the table where the range is effectively saturated, even for the small base functions, and the exponents are most tightly spaced. This is indeed the case. The deviations for the AUX3 range with a base of 1.8 are 1.14, 1.67, 1.65, 6.76 and 4.55 mE_h for N, Ne, O, F_2, and N_2 respectively. These compare with orbital basis as auxiliary values of 1.15, 1.68, 2.39, 8.55, and 5.22 mE_h. We note that the atomic values are relatively converged even when $\{g_t\}$ are chosen to be the orbital basis functions. This indicates that the Partridge-3 uncontracted basis set is sufficiently flexible to represent both the orbitals and potential accurately. However, when molecules are considered we use an uncontracted version of the cc-pVTZ basis set and when these functions are used for $\{g_t\}$ substantially larger deviations are observed compared with the best eventempered sets. The effect of the compromise between the spacing of the exponents and their range in the auxiliary set on the total energy may be gauged from Table 4.3. Essentially to achieve good convergence the auxiliary functions must be spaced more tightly than is found in commonly used orbital basis sets and the range should be large enough to ensure the energy cannot be lowered further.

4.5.1 The Effect of the Auxiliary Basis Set Choice on the Exchange Potential

The effect of the auxiliary basis on the energy is however only one aspect of the OEP calculations which must be considered. It is also important to establish what effect the use of a large auxiliary basis set has on the exchange potentials calculated in the procedure, since the key idea of the OEP approach is to vary the effective potential, $v_s(\mathbf{r})$, such that E is minimised. In Figure 4.2 we present the OEP exchange potentials of the Ne atom and N_2 molecule. The same orbital basis sets as the previous section were employed and results are presented using the orbital basis set as the auxiliary set and using the AUX3 range defined in Table 4.2 with a base of 1.8, which gives the lowest energy deviations in Table 4.3. In all calculations we employ second order optimization and TSVD regularisation with a cutoff of 10^{-6} on the singular values of the Hessian to ensure good convergence of the energy.

It is clear from Figure 4.2 that the use of a large auxiliary set with the uncontracted Partridge-3 orbital basis set on the Ne atom does not present any special difficulties

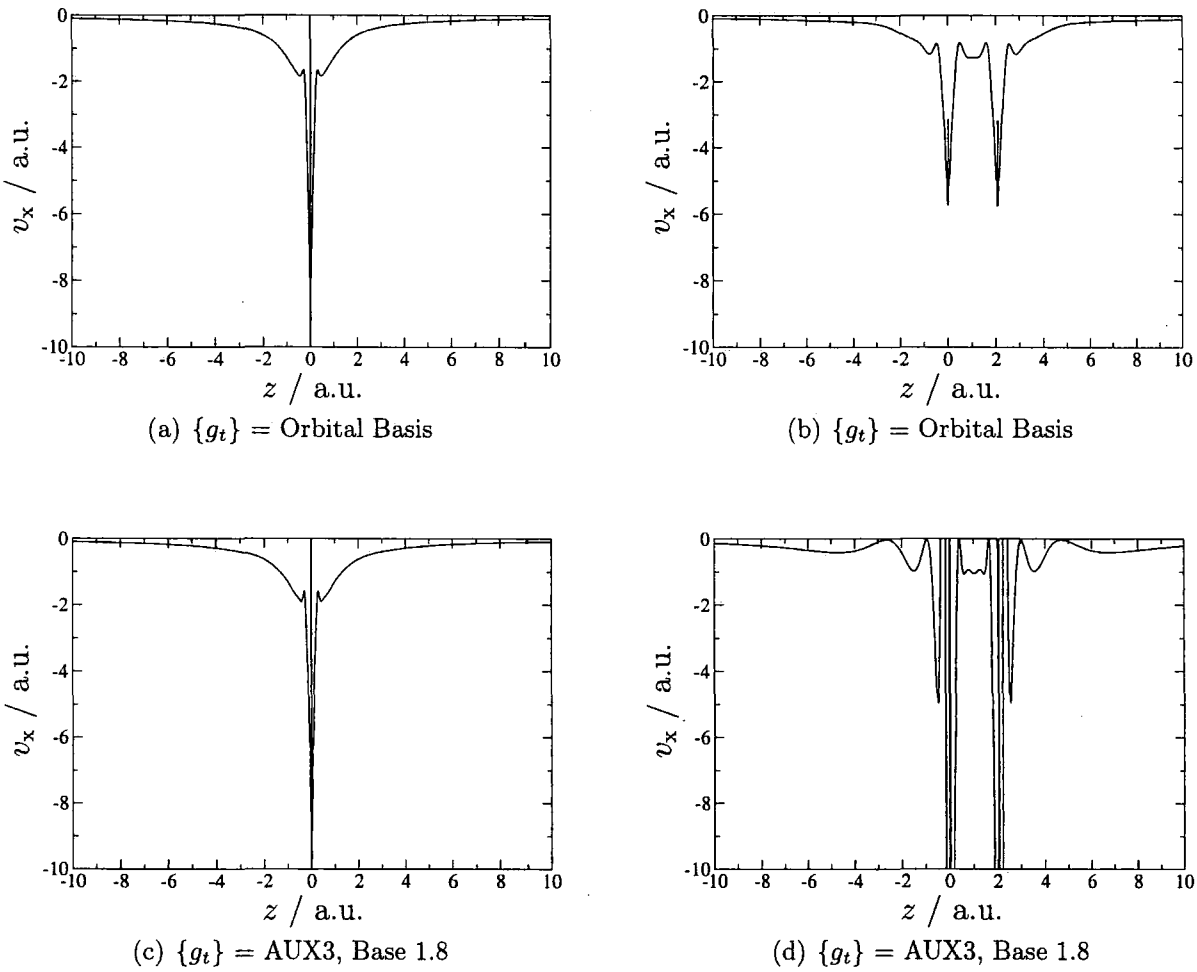

(a) $\{g_t\}$ = Orbital Basis

(b) $\{g_t\}$ = Orbital Basis

(c) $\{g_t\}$ = AUX3, Base 1.8

(d) $\{g_t\}$ = AUX3, Base 1.8

Figure 4.2: Exchange potentials of Ne and N_2 calculated using the orbital basis set in Eqn. (4.2.2) and an alternative eventempered auxiliary set defined by a base of 1.8 and the AUX3 range

in the calculation of the exchange potential, the potential obtained being similar to that obtained using only the primary orbital basis. Both potentials exhibit a spike at the position of the nucleus. This is commonly observed when very large exponents are present in the basis sets, in the case of Partridge 3 the highest exponent is 2598845.0. This is exceptionally large and the difficulty associated with accurately evaluating the required integrals with such a function is likely to be the origin of the observed structure. For the N_2 molecule when the uncontracted cc-pVTZ orbital basis set is used for the potential expansion similar features are observed at the nuclei but are considerably smaller, reflecting the fact that the highest exponent whilst still large has a more modest value of 11420.0. When the large auxiliary set is applied to the N_2 calculation the exchange potential obtained becomes very unphysical, displaying wild oscillations.

To investigate this issue further, we now apply the OEP procedure to the LDA functional, which contains no orbital dependent terms and already corresponds to a rigorous Kohn–Sham equation in its conventional evaluation. In the limit of a complete auxiliary set the OEP solutions should therefore be the same as those of the conventional evaluation. We use the unbalanced orbital / auxiliary basis set combination of uncontracted cc-pVTZ / AUX 3 (base 1.8) with a filter of 10^{-6} and calculate the OEP potential. The results are presented in Figure 4.3 along with the potential from the conventional evaluation for comparison. For the LDA functional the OEP evaluation returns a smooth potential despite the imbalance and the conventional energy is reproduced to within $3 \times 10^{-9} E_\mathrm{h}$. This is particularly impressive given that the Fermi–Amaldi reference potential is used which imposes $-1/r$ asymptotic behaviour on the potential which is not appropriate for the LDA potential and leads to a downward shift of the potential relative to the conventional evaluation.

To quantify the singularity of the Hessian in both the LDA and Hartree–Fock case we may calculate the condition number of the matrix both before and after the regularisation. The condition number is defined by the ratio of the largest and smallest singular values, which are already routinely evaluated in the TSVD procedure. If the logarithm of the condition number approaches ~ 12 then roundoff errors can be introduced due to limitations in the precision to which floating point operations may be carried out. Ideally to ensure accurate computation of the inverse the logarithm of the condition number should be less than 8. The logarithm of the Hessian matrix condition numbers using the Hartree–Fock and LDA energy functionals before regularisation are 26.5 and 27.0 respectively and reduce to 2.3 and 2.3 when the regularisation procedure is applied. This indicates that the Hessian should be difficult to invert accurately in both cases since both have similar values for the logarithm of the condition number

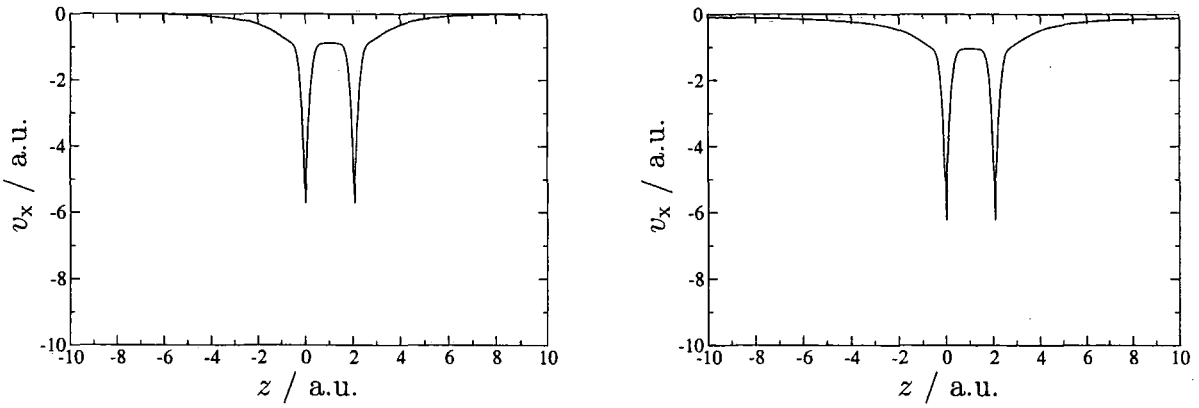

(a) Conventional Evaluation (b) OEP Evaluation

Figure 4.3: The LDA exchange potentials calculated using conventional and OEP evaluations

before the regularisation and similar numbers of singular values below the cutoff (474 for HF and 475 for LDA). Once the regularisation is applied then the calculation of the inverse should be relatively free from numerical problems. However in the Hartree–Fock case the oscillations in the potential remain. This leads to the conclusion that the oscillations are not due to numerical noise but are in fact real features of the finite basis set OEP solution. This is further supported by the fact that similar observations are made with the BFGS procedure which does not require calculation of the inverse of the Hessian directly.

In the next section we investigate the origin of the unphysical undulations present in the OEP solutions when the Hartree–Fock energy functional is used, and ways in which this structure may be avoided.

4.6 Origin of Unphysical Structure in Optimized Effective Potentials

In the limit of a complete basis set the non-multiplicative Hartree–Fock operator cannot be reproduced by a local multiplicative potential [202]. As a consequence the KS and HF orbitals, and the determinants constructed from them, cannot be the same. The only exceptions to this are one electron systems and two electron systems which are spin paired. In these cases the Hartree–Fock exchange operator is a multiplicative potential equal to $-v_J/N$ as can be appreciated from Eqn. (1.5.9).

As shown by Handy and Silverstone [203], for states which do not consist entirely of s orbitals the asymptotic behaviour of the Hartree–Fock and Kohn–Sham orbitals is different. The asymptotic form of the Hartree–Fock orbitals is

$$\varphi_i \sim \sum_j \exp[-(-2\varepsilon_j)^{1/2} r] \tag{4.6.1}$$

where the decay of each orbital depends on the eigenvalues of all other orbitals, although at long range this will be dominated by the HOMO for all the orbitals. In contrast the Kohn–Sham orbitals which arise from a multiplicative operator have the asymptotic form

$$\varphi_i \sim \exp[-(-2\varepsilon_i)^{1/2} r] \tag{4.6.2}$$

and so their decay is governed only by their own eigenvalue ε_i. However, this analysis assumes that we solve the Kohn–Sham and Hartree–Fock equations exactly and so have the exact orbitals. In practice we actually represent the orbitals by a linear combination of basis functions. In that case each orbital does not decay according to either of Eqns. (4.6.1) or (4.6.2) but rather at a rate determined by the most diffuse function in the expansion. This has the consequence that in a finite basis set the Hartree–Fock and Kohn–Sham orbitals may in fact have the same behaviour.

Recently Staroverov *et al.* have demonstrated that it is possible to construct multiplicative potentials which return the Hartree–Fock electronic energy [204]. In their approach the exchange potential is expanded as $v_{\mathrm{x}}(\mathbf{r}) = \sum_{t=1}^{M_\sigma} b_t^\sigma g_t(\mathbf{r})$ and they solve the set of equations

$$\sum_{t=1}^{M_\sigma} \left\langle \varphi_{i\sigma}^{\mathrm{HF}} \left| g_t \right| \varphi_{a\sigma}^{\mathrm{HF}} \right\rangle b_t^\sigma = K_{ia}^\sigma \tag{4.6.3}$$

where K_{ia}^σ is the matrix representation of the non-multiplicative Hartree–Fock exchange operator. This equation may be solved providing that the number of auxiliary functions in the set $\{g_t\}$ is greater than the number of non-zero elements in K_{ia} and the products $\varphi_{i\sigma}^{\mathrm{HF}} g_t \varphi_{a\sigma}^{\mathrm{HF}}$ have no exact linear dependencies. In practice, the authors were able to obtain the Hartree–Fock energy and density to machine precision by solving this equation for an exchange potential and using that potential to evaluate a new set of orbitals. From this set of orbitals the ones which span the occupied HF space are chosen to be occupied. These may not necessarily correspond to the N lowest eigenvalue orbitals. In other words they allow the violation of the Aufbau principle on the grounds that choosing other orbitals leads to the lowest energy. In fact the Hartree–Fock energy is obtained, and the authors argue that this is the global minimum of the exchange only OEP problem in a finite basis set. The potentials obtained using the

prescription of Ref. [204] are not unique and exhibit wildly oscillatory behaviour.

This clearly has severe implications for the practical application of the Yang–Wu OEP scheme described in this chapter. The OEP scheme in a finite basis set can yield a minimum solution which is equivalent to the solution of the Hartree–Fock equations, which could have been achieved with much less computational effort! The fact that any finite basis set with a sufficiently large expansion for the potential yields the Hartree–Fock energy whilst in the limit of a complete basis set the significantly higher numerical OEP energy is obtained has been referred to as the 'OEP paradox'. In Ref. [204] it is noted that the Yang–Wu scheme may also yield the Hartree–Fock energy, although modification to violate the Aufbau principle is required.

When we carry out OEP calculations in a finite basis set we must make a choice of orbital and auxiliary basis sets. How well a non-local operator may be modelled by a local one in conventional calculations has been shown by Harriman to depend on the degree to which the orbital basis function products are linearly dependent [205, 206]. In the extreme case for which the basis function products are completely linearly independent the matrix representation of a non-local operator, for example the Hartree–Fock exchange operator, can be replaced exactly by the matrix representation of a local one, for example a Kohn–Sham exchange potential $v_{\mathrm{x}}(\mathbf{r})$. For the equations of Staroverov et. al. a similar situation is encountered, the ease with which the solutions corresponding to the Hartree–Fock energy can be obtained will depend on the linear dependence of the products $\varphi_{i\sigma}^{\mathrm{HF}} g_t \varphi_{a\sigma}^{\mathrm{HF}}$. As a consequence, to avoid these unphysical solutions a good balance between the orbital and auxiliary basis sets is required. In our implementation of the OEP scheme the Aufbau principle is satisfied and so in most cases we obtain energies above those of the Hartree–Fock method. However the unphysical structure observed in the potentials may represent a situation intermediate between the Hartree–Fock solution and smooth physical potentials, which more closely approximate the numerical OEP potentials.

We now investigate the exchange only OEP procedure for the Ne atom, for which accurate numerical results are available, using the series of cc-pVNZ and cc-pCVNZ orbital basis sets where N is the cardinal number and can be 2, 3, 4, 5, or 6. The introduction of core correlating functions in the cc-pCVNZ sets increases the product linear dependence of the basis sets in areas important for the representation of the occupied orbitals. We investigate the convergence of the electronic energy, eigenvalues and exchange potential with cardinal number in each series. Second order optimization is employed with TSVD regularisation of the Hessian. Two values of the cutoff are considered, a large value of 10^{-4} and a small value of 10^{-8}. We also consider the use of different auxiliary basis sets, $\{g_t\}$; the primary orbital basis is employed initially and

Table 4.4: Finite Basis set OEP and Hartree–Fock electronic energies, in E_h

N	HF E	OEP $\{g_t\}$ = orb cutoff 10^{-4}	OEP $\{g_t\}$ = orb cutoff 10^{-8}	OEP $\{g_t\}$ = large cutoff 10^{-4}	OEP $\{g_t\}$ = large cutoff 10^{-8}
cc-pVNZ					
2	-128.488866	-128.488848	-128.488848	-128.488866	-128.488866
3	-128.532010	-128.531354	-128.531612	-128.531747	-128.532008
4	-128.543513	-128.540437	-128.542667	-128.542890	-128.543466
5	-128.546775	-128.544323	-128.545630	-128.545348	-128.546371
6	-128.547062	-128.545098	-128.545624	-128.545606	-128.545998
cc-pCVNZ					
2	-128.489058	-128.486668	-128.486892	-128.489038	-128.489058
3	-128.532128	-128.530667	-128.530791	-128.531028	-128.531125
4	-128.543771	-128.542083	-128.542092	-128.542094	-128.542163
5	-128.546799	-128.545108	-128.545115	-128.545116	-128.545116
6	-128.547067	-128.545366	-128.545384	-128.545384	-128.545384

then a large eventempered basis set with a base of 1.8 and a range defined by -10 to 7 for each angular momentum. Higher exponents are not included to avoid unphysical structure at the positions of the nuclei.

4.6.1 Convergence of the Finite Basis Set OEP Energy

To begin with we consider the convergence of the electronic energy of the OEP method with respect to N. In Table 4.4 the OEP electronic energies for each basis set series with both choices of filter and the two auxiliary sets are presented. For comparison the Hartree–Fock finite basis set energies are also included. Moving down each column the electronic energies decrease with increasing cardinal number for both choices of orbital basis set as would normally be expected. For each choice of auxiliary basis set, reducing the filter also leads to a reduction in the electronic energy, as expected. There are two unexpected results. Firstly for the cc-pVDZ basis set ($N = 2$) the Hartree–Fock energy is reproduced for the larger choice of auxiliary basis set, and is very nearly reproduced when the orbital basis set is used as the auxiliary basis. For the cc-pCVDZ basis the HF energy is reproduced only when the large auxiliary basis set and very small filter is used. Secondly the numerical OEP energy for Ne is -128.5454 [99] and for the cc-pVNZ basis sets energies *below* this value can be obtained. However, in moving to the larger cc-pCVNZ series no values below the numerical OEP result are observed and the energy approaches the numerical value from above.

This can be rationalised by how well the Hartree-Fock operator in a finite basis set can be reproduced by a local multiplicative operator. As the basis set products approach linear dependence, the HF operator becomes increasingly non-local and so

cannot be replaced by a local operator. This is reflected by the fact that the cc-pV5Z electronic energies are below those of the cc-pV6Z basis set since the latter has greater product linear dependence. Both remain below the numerical OEP value. Adding core correlating functions, resulting in the cc-pCVNZ basis sets, increases the product linear dependence in areas important for the description of the occupied orbitals, which we choose according to the Aufbau principle. The energies reflect this, smoothly approaching the numerical OEP value as the cardinal number increases, since the energy functional depends only on the occupied orbitals.

We now use the difference between the finite basis set Hartree–Fock and OEP energies as a measure of the non-locality of the HF operator in each case. In Figure 4.4 we plot the deviation of the OEP energy from the Hartree–Fock value in the same orbital basis set. The solid horizontal line indicates the deviation of the numerical OEP energy from the numerical Hartree–Fock value. Two plots of the energy deviations are presented for two different choices of auxiliary basis.

Several conclusions are evident from Figure 4.4. Firstly for small orbital basis sets, *e.g.* cc-pVDZ the products of the functions are sufficiently linearly independent to allow the Hartree–Fock energy to be obtained. For both choices of orbital basis set type, the OEP energy approaches the numerical value as N increases. However the cc-pVNZ basis set results show much greater sensitivity to the choice of cutoff in the TSVD regularisation and even at the 6Z level are much further from the numerical OEP values than the corresponding cc-pCVNZ values. We note that except for the DZ level, the solutions of Staroverov *et al.* are not obtained as we enforce the Aufbau principle. In all cases the choice of a lower filter leads to a lower energy and hence a smaller deviation from the Hartree–Fock value, although the cc-pCVNZ values are considerably more stable than the cc-pVNZ ones.

4.6.2 Convergence of the Finite Basis Set OEP Eigenvalues

We may also consider the convergence of the orbital eigenvalues relative to the numerical values. It has been observed that such convergence is poor and can oscillate with cardinal number [196, 207]. For the Ne atom using the cc-pVNZ orbital basis sets, plots of the deviation of the HOMO eigenvalue from the Hartree–Fock value, as a function of the cardinal number, are presented in Figure 4.5. The HOMO has particular significance since the OEP and Hartree–Fock solutions are the same in the limit of a complete basis set. The deviation should therefore approach zero with increasing cardinal number. For both choices of TSVD cutoff the convergence is oscillatory, although the values with a cutoff of 10^{-4} are considerably better behaved.

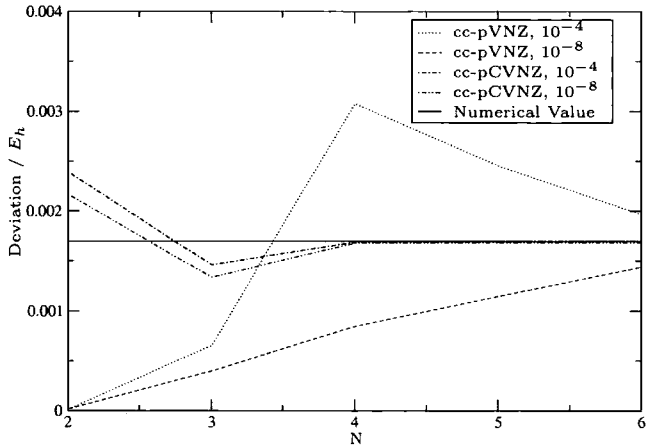

(a) $\{g_t\}$ is the orbital basis set

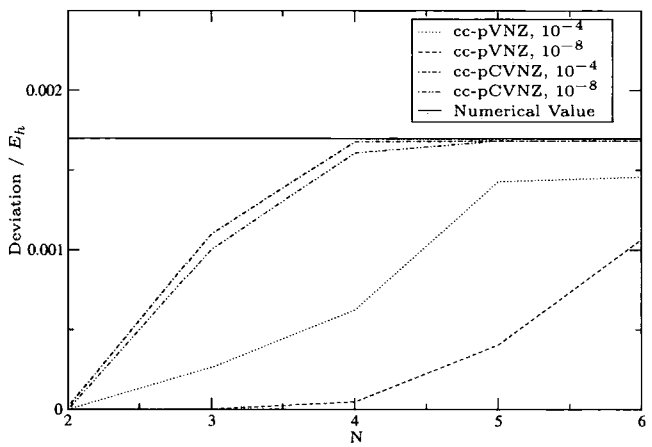

(b) $\{g_t\}$ is defined by a base of 1.8 and range of -10 to 7 for s, p, d, f, g, h, and i angular momenta

Figure 4.4: The deviation of the OEP exchange-only electronic energy from the Hartree–Fock energy, in E_h, as a function of cardinal number for the cc-pVNZ and cc-pVCNZ basis sets

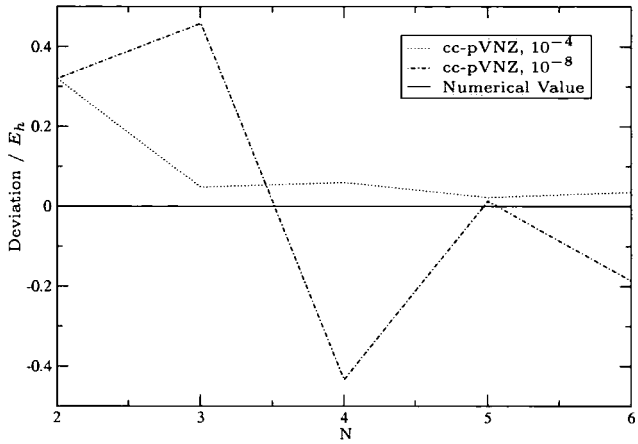

(a) $\{g_t\}$ is the orbital basis set

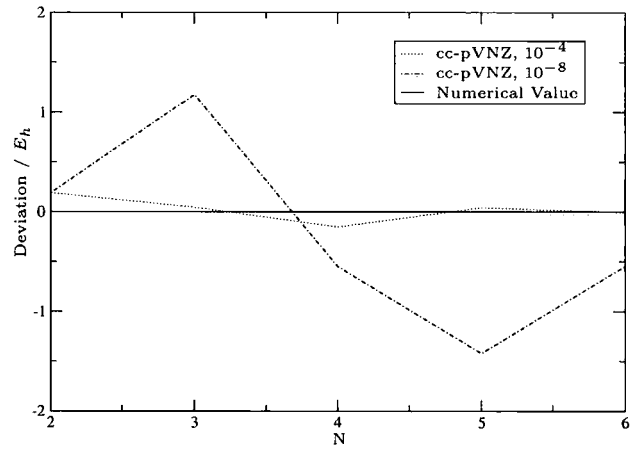

(b) $\{g_t\}$ is defined by a base of 1.8 and range of -10 to 7 for s, p, d, f, g, h, and i angular momenta

Figure 4.5: Convergence of the OEP exchange-only HOMO eigenvalue with cardinal number for each choice of auxiliary basis set for the cc-pVNZ basis sets

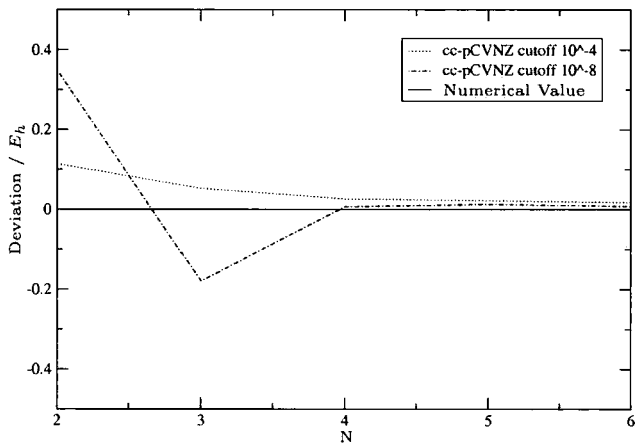

(a) $\{g_t\}$ is the orbital basis set

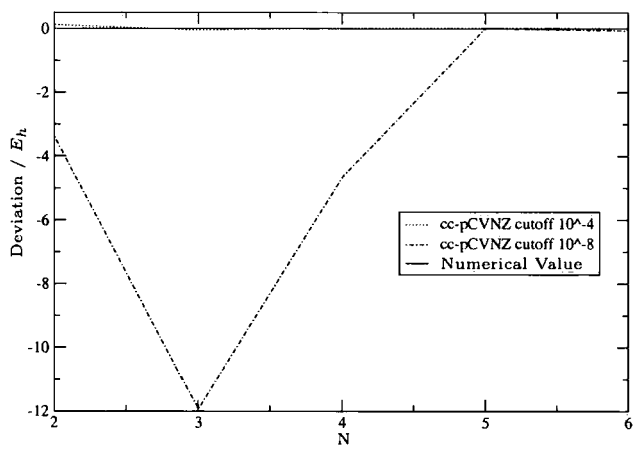

(b) $\{g_t\}$ is defined by a base of 1.8 and range of -10 to 7 for s, p, d, f, g, h, and i angular momenta

Figure 4.6: Convergence of the HOMO eigenvalue with cardinal number for each choice of auxiliary basis with the cc-pCV*N*Z orbital basis sets

For the cc-pCVNZ orbital basis set series the convergence of the orbital eigenvalues with respect to cardinal number is presented in Figure 4.6 for the different choices of auxiliary set. The convergence of the eigenvalues is much more well behaved. Although the oscillatory behaviour still remains for a cutoff of 10^{-8}.

It is notable that smooth convergence is only obtainable when the cc-pCVNZ orbital basis functions are used, which have greater linear dependence in their products, and a reasonably high filter is employed. The smoothest convergence is obtained when the orbital basis set is used as auxiliary, again reflecting the need for balance to ensure a reasonable level of product linear dependence can be obtained. Similar observations can be made for the other occupied orbitals.

The addition of core correlating functions is likely to be most significant for the occupied orbitals. The effect of adding lower exponent functions remains to be investigated. Whilst it is unlikely that this would have significant effect on the electronic energy calculated for the Hartree–Fock functional it may effect the convergence of the higher virtual eigenvalue spectrum, which could have significant implications in the application of the OEP method to the calculation of excitation energies. This could also have significant implications for the use of other orbital dependent energy expressions which depend explicitly on the unoccupied orbitals, such as those resulting from many body perturbation theory. The convergence of the eigenvalue spectrum is very sensitive to the quality of the exchange potential obtained and so we now examine its behaviour.

4.6.3 Convergence of the Finite Basis Set OEP Potentials

The presence of oscillations in the finite basis set OEP potentials was observed in the previous section and has been reported in the literature [107, 204, 208]. The eigenvalues obtained reflect the quality of the exchange potential closely. We now examine how the Ne exchange potentials change with cardinal number, auxiliary set and TSVD cutoff in Figures 4.7 and 4.8.

In Figure 4.7 the potentials calculated with the orbital basis sets as the auxiliary basis are presented. On the left are the potentials calculated with a TSVD cutoff of 10^{-4} and on the right those with a TSVD cutoff of 10^{-8}. For both the cc-pVNZ and cc-pCVNZ orbital basis sets the potentials are smooth and well behaved with the larger cutoff, reflecting the eigenvalue convergence in Figures 4.5(a) and 4.6(a). Only the DZ potentials show small amounts of unphysical behaviour, as may be expected since for this small basis set the orbital basis set products cannot approach linear dependence. As the TSVD cutoff is reduced the potentials display more oscillatory structure, how-

ever this is much less pronounced in the cc-pCVNZ case, with the potentials using this basis set becoming smooth at QZ level and higher. Again this reflects the eigenvalue observations.

In Figure 4.8 exchange potentials are presented calculated using the large auxiliary basis set. When a small TSVD cutoff is applied the potentials obtained are oscillatory, reflecting the eigenvalue convergence in Figures 4.5(b) and 4.6(b). This is consistent with the imbalance of the orbital and auxiliary basis sets. Applying a larger TSVD cutoff improves the potentials considerably. It has been confirmed that removing the auxiliary basis functions with angular momenta not present in the orbital basis set results in smooth potentials when a large cutoff is used.

In summary, problems with unphysical structure in the optimized effective potentials calculated using the Yang–Wu procedure have been highlighted. These can be traced to an imbalance between the orbital and potential basis sets. For a given choice of orbital and auxiliary basis set these oscillatory potentials are however the true finite basis set OEP solutions, as highlighted by the condition number analysis. The use of TSVD regularisation with a large cutoff significantly reduces the structure and enables the combination of standard orbital basis sets with large auxiliary basis sets for the potential expansion. When applying the OEP approach it is therefore important to balance the need for flexibility in the representation of the potential with the requirement that the resulting solutions are physically sensible.

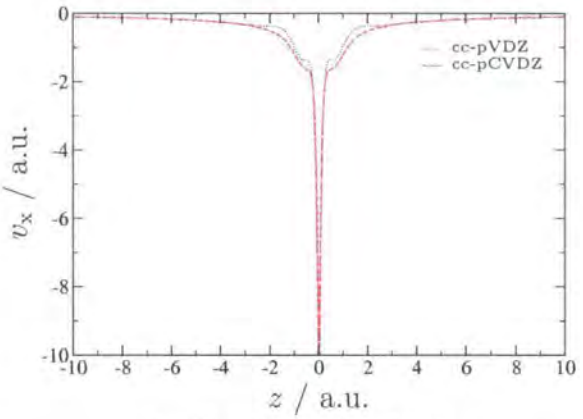

(a) N = 2, cutoff = 10^{-4}

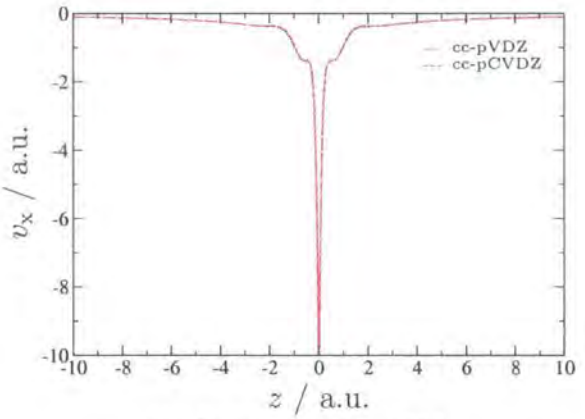

(b) N = 2, cutoff = 10^{-8}

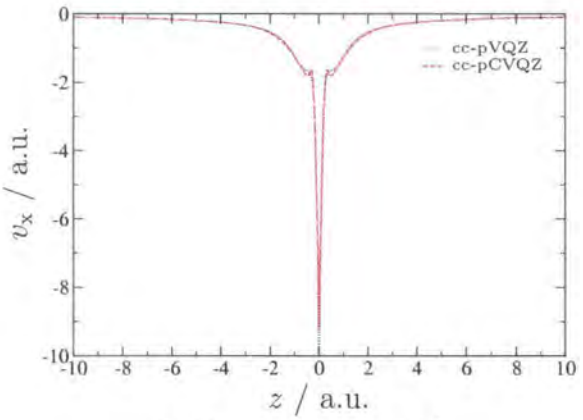

(c) N = 4, cutoff = 10^{-4}

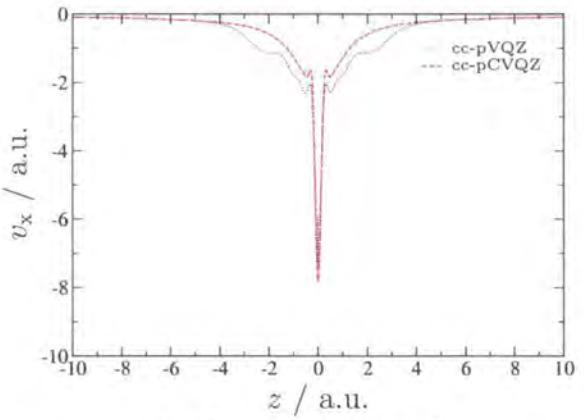

(d) N = 4, cutoff = 10^{-8}

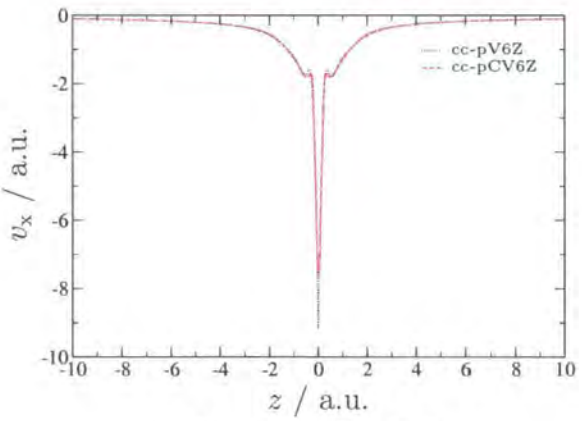

(e) N = 6, cutoff = 10^{-4}

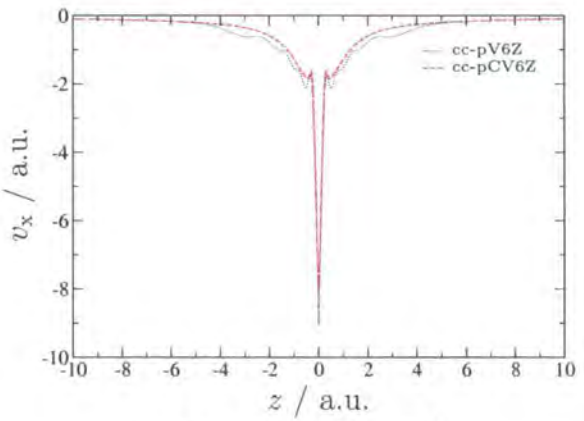

(f) N = 6, cutoff = 10^{-8}

Figure 4.7: Convergence of the OEP exchange potential with cc-pVNZ and cc-pCVNZ orbital basis sets when $\{g_t\}$ is chosen to be the same as the orbital basis set

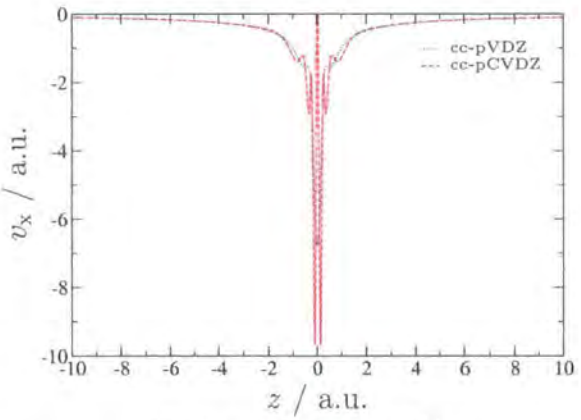

(a) N = 2, cutoff = 10^{-4}

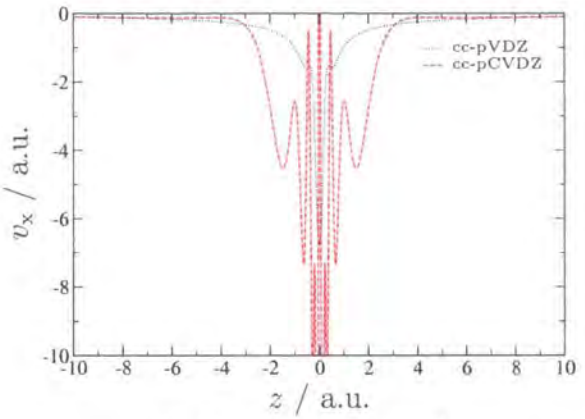

(b) N = 2, cutoff = 10^{-8}

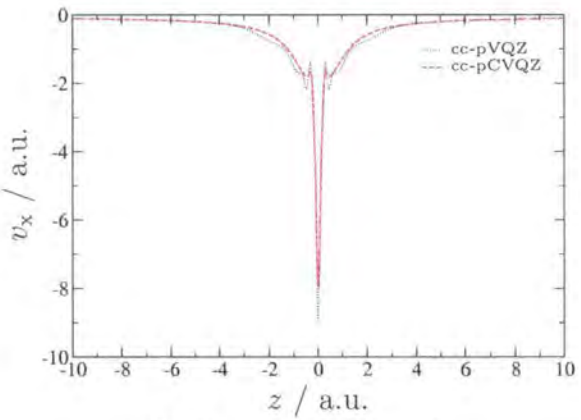

(c) N = 4, cutoff = 10^{-4}

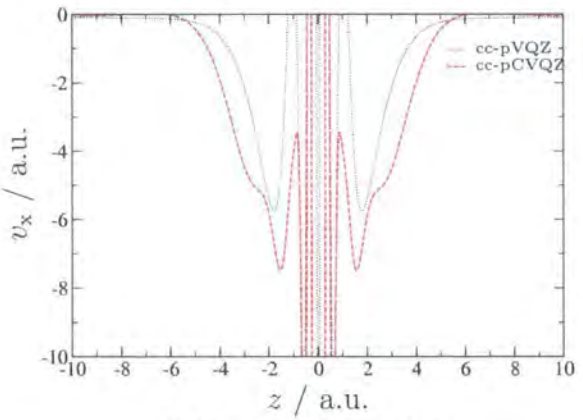

(d) N = 4, cutoff = 10^{-8}

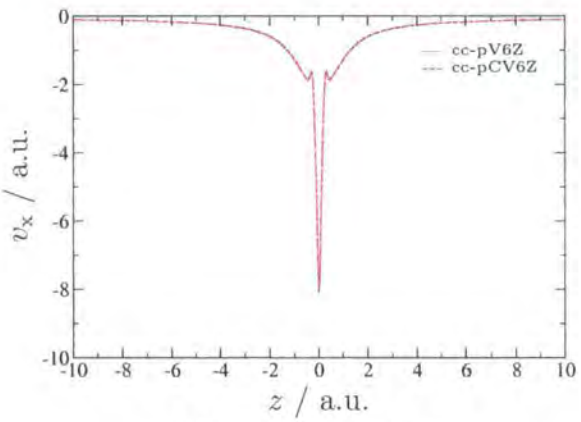

(e) N = 6, cutoff = 10^{-4}

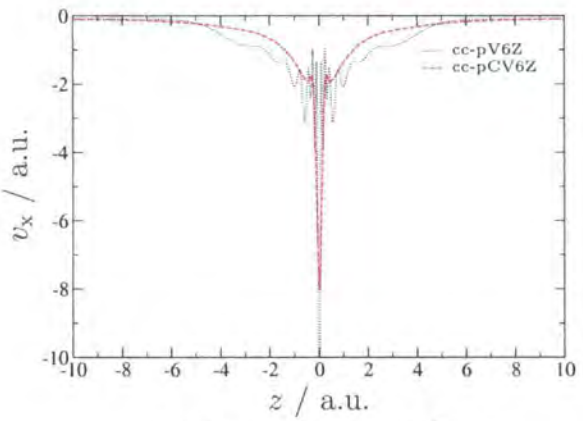

(f) N = 6, cutoff = 10^{-8}

Figure 4.8: Convergence of the OEP exchange potential with cc-pVNZ and cc-pCVNZ orbital basis sets when $\{g_t\}$ is defined by a base of 1.8 and a range of -10 to 7 for s, p, d, f, g, h, and i angular momenta

4.7 The Wu–Yang Constrained Search Method

In Chapter 1 we outlined the ZMP method in which the Levy constrained search is applied to the Kohn–Sham equations. We now consider an alternative implementation of the constrained search method, suggested by Wu and Yang (WY), which is computationally very similar to the direct optimization method used to calculate optimized effective potentials. The method provides the inverse mapping, $\rho_w(\mathbf{r}) \rightarrow w(\mathbf{r})$, compared to the OEP procedure, under the assumption that the exchange–correlation energy is an explicit functional of the density. For closed shells the Kohn–Sham non-interacting kinetic energy is defined as

$$T_s[\rho_{\text{in}}] = \min_{\Psi_{\text{det}} \rightarrow \rho_{\text{in}}} T[\Psi_{\text{det}}] \tag{4.7.1}$$

which is the minimum over all possible determinantal wavefunctions, constructed from doubly occupied orbitals $\{\varphi_i\}$, which yield the input density ρ_{in}. As mentioned in Section 1.6.4, minimising T_s for a given density minimises the corresponding Kohn–Sham energy under the assumption that all other contributions to the electronic energy are explicit functionals of ρ. The evaluation of $T_s[\rho]$ is therefore a minimisation problem with the constraint that $\rho(\mathbf{r}) = \rho_{\text{in}}(\mathbf{r})$. By introducing the Lagrange multiplier function $v(\mathbf{r})$ for this constraint, we may define the functional

$$W_s[\Psi_{\text{det}}, v(\mathbf{r})] = 2\sum_{i}^{N/2} \left\langle \varphi_i \left| \hat{T} \right| \varphi_i \right\rangle + \int d\mathbf{r}\; v(\mathbf{r}) \left\{ \rho(\mathbf{r}) - \rho_{\text{in}}(\mathbf{r}) \right\} \tag{4.7.2}$$

In order to minimise $T[\{\varphi_i\}]$ and ensure that $\rho(\mathbf{r}) = \rho_{\text{in}}(\mathbf{r})$ the orbitals must make W_s stationary and be normalised. The normalisation can be imposed by a set of Lagrange multipliers $\{\varepsilon_i\}$ and the orbitals are then defined by the solution of the equations

$$\left[\hat{T} + v(\mathbf{r})\right] \varphi_i(\mathbf{r}) = \varepsilon_i \varphi_i(\mathbf{r}) \tag{4.7.3}$$

where the orbitals, φ_i, are eigenfunctions of a Hermitian operator and hence already orthogonal. The requirement that $T[\Psi_{\text{det}}]$ be minimised means that $N/2$ eigenfunctions must be chosen from the solutions to Eqn. (4.7.3). In the normal Kohn–Sham scheme the lowest $N/2$ orbitals are chosen. This limits our scope of application to ground state non-interacting v-representable densities. For such densities the orbitals are eigenstates of $v(\mathbf{r})$ as defined by Eqn. (4.7.3) and hence the determinantal wavefunction Ψ_{det} is an implicit function of $v(\mathbf{r})$,

$$\Psi_{\text{det}} = \Psi_{\text{det}}[v(\mathbf{r})] \tag{4.7.4}$$

and so

$$W_s[\Psi_{\rm det}[v(\mathbf{r})], v(\mathbf{r})] = \min_{\varphi_i, \langle\varphi_i|\varphi_i\rangle=1} W_s[\Psi_{\rm det}, v(\mathbf{r})] \tag{4.7.5}$$

The first functional derivative of $W_s[\Psi_{\rm det}[v(\mathbf{r})], v(\mathbf{r})]$ is then

$$\frac{\delta W_s[\Psi_{\rm det}[v(\mathbf{r})], v(\mathbf{r})]}{\delta v(\mathbf{r})} = \rho(\mathbf{r}) - \rho_{\rm in}(\mathbf{r}) \tag{4.7.6}$$

which at the minimum of $T[\Psi_{\rm det}]$ is zero and represents the constraint condition on the density. The second functional derivative is

$$\frac{\delta^2 W_s[\Psi_{\rm det}[v(\mathbf{r})], v(\mathbf{r})]}{\delta v(\mathbf{r}')\delta v(\mathbf{r})} = \frac{\delta\rho(\mathbf{r})}{\delta v(\mathbf{r}')} = 2\sum_i \sum_a \frac{\varphi_i^*(\mathbf{r})\varphi_a(\mathbf{r})\varphi_a^*(\mathbf{r}')\varphi_i(\mathbf{r}')}{\varepsilon_i - \varepsilon_a} + \text{c.c.} \tag{4.7.7}$$

which can be shown to be negative at any $v(\mathbf{r})$ for any arbitrary change $\delta v(\mathbf{r})$ and hence the stationary point of $W_s[\Psi_{\rm det}[v(\mathbf{r})], v(\mathbf{r})]$ is a maximum [58]. The Kohn–Sham non-interacting kinetic energy is then returned from the unconstrained maximisation

$$T_s[\rho_{\rm in}] = \max_{v(\mathbf{r})} W_s[\Psi_{\rm det}[v(\mathbf{r})], v(\mathbf{r})] \tag{4.7.8}$$

which establishes a variational principle over the potential for the calculation of T_s corresponding to an input density. For practical implementation of this scheme we follow a route similar to the one used for the optimized effective potential. The potential $v_s(\mathbf{r})$ is constructed according to Eqn. (4.2.2) and again the Fermi–Amaldi potential [197] is used for the reference potential $v_0(\mathbf{r})$ which provides the correct long range behaviour for an exact exchange–correlation potential. Substituting the expansion into Eqn. (4.7.2) for W_s we obtain

$$\begin{aligned} W_s[\Psi_{\rm det}, v(\mathbf{r})] &= 2\sum_i^{N/2} \left\langle \varphi_i \left| \hat{T} \right| \varphi_i \right\rangle + \int d\mathbf{r}\, \{v_{\rm ext}(\mathbf{r}) + v_0(\mathbf{r})\}\, \{\rho(\mathbf{r}) - \rho_{\rm in}(\mathbf{r})\} \\ &+ \int d\mathbf{r} \sum_t b_t g_t(\mathbf{r})\, \{\rho(\mathbf{r}) - \rho_{\rm in}(\mathbf{r})\} \end{aligned} \tag{4.7.9}$$

and the first and second derivatives become

$$\frac{\partial W_s[\Psi_{\rm det}[v(\mathbf{r})], v(\mathbf{r})]}{\partial b_t} = \int d\mathbf{r}\, [\rho(\mathbf{r}) - \rho_{\rm in}(\mathbf{r})]\, g_t(\mathbf{r}) \tag{4.7.10}$$

$$\frac{\partial^2 W_s[\Psi_{\rm det}[v(\mathbf{r})], v(\mathbf{r})]}{\partial b_u \partial b_t} = 2\sum_i \sum_a \frac{\langle\varphi_i\,|g_u(\mathbf{r})|\,\varphi_a\rangle\,\langle\varphi_a\,|g_t(\mathbf{r})|\,\varphi_i\rangle}{\varepsilon_i - \varepsilon_a} \tag{4.7.11}$$

These are the key expressions required for the practical implementation of the WY scheme. The problem is now an unconstrained maximisation of $W_s[\Psi_{\rm det}[v(\mathbf{r})], v(\mathbf{r})]$ with respect to the set of coefficients $\{b_t\}$. Both first and second derivatives can be employed with the same optimization procedures as in Section 4.3. To carry out the maximisation the same algorithms are used and $-W_s$ is minimised using the negatives of the derivatives.

To demonstrate the usefulness of this procedure, in Table 4.5 we present values of the non-interacting kinetic energy, T_s, calculated using the WY procedure for several choices of orbital basis set. Relaxed density matrices were calculated at the CCSD level using the Gaussian 03 program [209] and then re-ordered appropriately and read into our CADPAC implementation of the WY scheme. Also given are the corresponding values of the CCSD kinetic energy, T. The difference between T and T_s is the kinetic energy contribution to the DFT exchange–correlation energy T_c. Also presented are the CCSD and Hartree–Fock electronic energies, along with the CCSD correlation energy computed as the difference between these two quantities.

The observations related to the required linear dependence of the basis function products made for the OEP procedure also hold for the WY method. As such, to ensure balance between the orbital and auxiliary basis sets, we consider only the case where the same basis set is used throughout. Our best estimate values for T, T_s, and T_c are thus the cc-pV5Z values at the bottom of Table 4.5. There has been interest in calculating T_c using various approximate functional forms [210, 211] and the values in Table 4.5 may provide a way to assess the performance of these T_c functionals.

The key feature of the WY scheme is that it allows the calculation of Kohn–Sham orbitals and eigenvalues from high quality *ab initio* input densities without the need for a knowledge of the exchange–correlation potential. We will see in later chapters how this procedure may be used to calculate accurate response properties and provide insight into the characteristics of various Kohn–Sham exchange–correlation approximations.

Table 4.5: Energy contributions calculated using the CCSD and WY(CCSD) methods, in E_h

Molecule	No. Func.	T(CCSD)	T_s (WY(CCSD))	T_c	E(CCSD)	E(HF)	E_c
aug-cc-pVDZ							
He	9	2.85593766	2.82280384	0.03313383	-2.88954849	-2.85570467	-0.03384382
Ne	25	128.47733281	128.30381207	0.17352074	-128.71643986	-128.49713423	-0.21930563
HF	34	100.07029795	99.93756055	0.13273740	-100.26880412	-100.03441998	-0.23438414
N_2	50	109.07187231	108.88542529	0.18644702	-109.29566965	-108.96110126	-0.33456839
F_2	50	198.83432538	198.55466884	0.27965655	-199.15258871	-198.70030953	-0.45227918
CO	50	112.87296489	112.70635504	0.16660985	-113.07741679	-112.75562356	-0.32179323
CH_4	61	40.27418645	40.14293159	0.13125486	-40.39841478	-40.19964961	-0.19876517
aug-cc-pVTZ							
He	25	2.89753860	2.86188449	0.03565411	-2.90083640	-2.86122253	-0.03961387
Ne	55	128.71191936	128.50473735	0.20718202	-128.83847561	-128.53400977	-0.30446584
HF	80	100.24934149	100.03092229	0.21841920	-100.36710981	-100.06186612	-0.30524369
N_2	110	109.23783742	108.98067231	0.25716511	-109.40715648	-108.98557167	-0.42158481
F_2	110	199.09689144	198.71364774	0.38324370	-199.34353367	-198.75679514	-0.58673853
CO	110	113.03006416	112.76782344	0.26224072	-113.19131332	-112.78243902	-0.40887430
CH_4	155	40.40508325	40.21956845	0.18551480	-40.46376207	-40.21382859	-0.24993348
aug-cc-pVQZ							
He	55	2.90148768	2.86529798	0.03618970	-2.90272034	-2.86153946	-0.04118088
Ne	75	128.80117755	128.53864766	0.26252989	-128.87040124	-128.54465258	-0.32574866
HF	130	100.33070061	100.07043199	0.26026861	-100.39992896	-100.06894445	-0.33098451
N_2	150	109.33778542	109.00149469	0.33629073	-109.45638636	-108.99145121	-0.46493515
F_2	150	199.24724983	198.77147086	0.47577897	-199.40208501	-198.76974076	-0.63234425
CO	150	113.12590287	112.79635270	0.32955017	-113.23790542	-112.78905452	-0.44885090
CH_4	295	40.44437726	40.23499168	0.20938558	-40.48493931	-40.21642899	-0.26851032
aug-cc-pV5Z							
He	75	2.90274553	2.86631085	0.03643468	-2.90314388	-2.86163454	-0.04150934
Ne	95	128.84860896	128.56442859	0.28418037	-128.88841636	-128.54682276	-0.34159360
HF	160	100.33751986	100.07182906	0.26569081	-100.40647043	-100.07058094	-0.33588949
N_2	190	109.38495320	109.02669210	0.35826109	-109.47704694	-108.99262467	-0.48442227
F_2	190	199.32666632	198.81450581	0.51216051	-199.43404759	-198.77284154	-0.66120605
CO	180	113.14896494	112.80194875	0.34701619	-113.24860992	-112.79025297	-0.45835695
CH_4	395	40.46038515	40.24235146	0.21803369	-40.49140964	-40.21701442	-0.27439522

Chapter 5

Comparison of Exchange Methods

In this chapter we compare the various Kohn–Sham exchange potentials we have implemented. Exchange only optimized effective potential results are compared with Wu–Yang (WY) results using a Hartree–Fock density as input; with the Localized Hartree–Fock (LHF) and Krieger–Li–Iafrate (KLI) approximations; as well as with the B88X GGA exchange functional. NMR shielding constants are used as a sensitive probe of differences in the exchange representations. The trends in these values are rationalised in terms of the associated HOMO–LUMO eigenvalue differences. The exchange potential, electron density, HOMO and LUMO probability density functions and electronic energies are compared with the OEP analogues.

5.1 Exchange Approximations

If approximate exchange approaches based on the non-local Hartree–Fock energy functional are to be used successfully in future DFT exchange–correlation approximations, then it is important to quantify their accuracy and investigate differences between them. We now compare the results of finite basis set Yang–Wu [112] OEP calculations with the approximate exchange potentials due to Krieger, Li and Iafrate (KLI) [124] and the Localized Hartree–Fock method of Della Sala and Görling [114]. We also use the constrained search implementation of Wu and Yang [58] (based on the Levy constrained search [54, 57]) and compare results obtained when a Hartree–Fock density is used as input. Results determined using the B88X GGA functional are also examined. Finally to assess the differences between exact exchange-only and near exact correlated Kohn–Sham calculations, we also apply the WY approach to accurate Brueckner-Doubles coupled cluster densities.

The calculation of NMR shielding constants is a sensitive probe of the differences

in the exchange potentials owing to the inverse dependence of the paramagnetic contribution in Eqn. (2.7.4) on the occupied–virtual eigenvalue differences. In Chapter 2, analysis of such results highlighted differences between the ZMP and LHF exchange-only potentials, with LHF results being significantly closer to experimental values, despite the exchange only nature of the theory. In the present chapter we further investigate these differences by comparing the electronic energies, eigenvalues, NMR shielding constants, potentials, densities and frontier orbitals, with reference to the corresponding OEP quantities.

5.2 The Calculation of Exchange Energies, Eigenvalue Differences and NMR Shielding Constants

The ultimate criterion to quantify the quality of an approximate exchange potential is the electronic energy evaluated using the Hartree–Fock energy functional of Eqn. (1.3.6). This energy is rigorously minimised for a single determinant wavefunction by the Hartree–Fock approach. However in the Kohn–Sham formalism, the orbitals must be determined subject to the constraint that they arise from the solution of an equation of the form of (2.1.2), which contains a multiplicative potential. This means that energies higher than those of the Hartree–Fock scheme are obtained (assuming the Aufbau principle is enforced — see Section 4.6). For the OEP, LHF and KLI methods this energy expression is evaluated during the course of the calculation. In the WY procedure the functional of Eqn. (4.7.9) is maximised and the energy expression is unknown. As such we evaluate the orbital Hartree–Fock energy functional of Eqn. (1.3.6) in a separate calculation after convergence. We use the WY approach here in place of the ZMP [59] method of Chapter 2, since it offers greater numerical stability and does not require a specific choice of Lagrange multiplier. A similar procedure is followed for B88X, since the energy expression is defined as a functional of the density rather than the orbitals.

All calculations use an uncontracted version of the Huzinaga IV Gaussian orbital basis set [144, 145]. This extensive basis set is important for the KLI and LHF calculations due to the resolution of the identity used in their implementation. The problem of gauge invariance is minimised by use of the LORG [141] method in calculating the NMR shielding constants. The WY and OEP calculations use second order optimizations as described in Chapter 4, with a cutoff of 10^{-4} for the truncated singular value decomposition (TSVD) regularisation. This cutoff ensures smooth potentials, with HOMO eigenvalues close to those of the Hartree–Fock method. In light of the obser-

vations in Section 4.6 we choose an auxiliary basis defined by a base of 1.8^N where $N = -5$ to 6 for s, p, d and f type functions. The Fermi–Amaldi potential is used as the reference potential of Eqn. (4.2.2) in these procedures and has the correct $-1/r$ asymptotic behaviour, since the molecules considered here do not exhibit nodal surfaces in their highest occupied molecular orbitals. The exchange potentials calculated for the N_2 molecule using each method are shown in Figure 5.1.

Table 5.1 presents the electronic energies for each approach evaluated using the Hartree–Fock energy functional, for the CO, N_2 and PN molecules. The geometries used are the near experimental geometries of Ref. [164], which are 1.128, 1.098, and 1.491 Å respectively. The Hartree–Fock energy for each molecule is included for comparison and, as required, is lower than that of the any of the Kohn–Sham methods. The OEP energies are the next lowest as should be the case, with a maximum deviation of 4 mE_h from the Hartree–Fock values, and are closely followed by the WY energies, which are only slightly higher. This may be expected by consideration of the constrained search method which minimises the non-interacting kinetic energy to determine a set of orbitals corresponding to an input density. The OEP approach on the other hand minimises both the non-interacting kinetic and exchange energy components. Since the kinetic energy accounts for the largest part of the electronic energy the WY and OEP energies and hence densities and eigenvalues may be expected to be close. The LHF and KLI energies are close to each other as expected from the similarity in their construction as discussed in Chapter 2, and are both above the WY and OEP approaches. The B88X energy is significantly higher reflecting the shortcomings of this exchange potential relative to the exact Kohn–Sham exchange potential.

Also presented, in Table 5.1, are the uncoupled isotropic shielding constants of the three molecules. The differences between the methods are very evident, highlighting the sensitivity of NMR shielding constant calculations to the potential. In line with the observations of Cohen *et al.* [212], the OEP and WY shieldings are very similar. The differences in the absolute values of Ref. [212] with those in Table 5.1 are due to different choices of orbital and auxiliary basis sets, and the use of Slater functions in the calculations of Ref. [212]. The LHF and KLI results are similar as expected, and are significantly lower than those of WY and OEP. This is consistent with the differences observed in Chapter 2 between the ZMP and LHF potentials. The shieldings from the B88X GGA functional are lower still. It is useful to compare these exchange only shielding constants with values including the effects of electron correlation. We therefore make use of the WY procedure of Chapter 4 to calculate shielding constants from Kohn–Sham orbitals and eigenvalues determined from a high quality Brueckner Doubles (BD) coupled cluster density. These shieldings are denoted WY(BD) and are

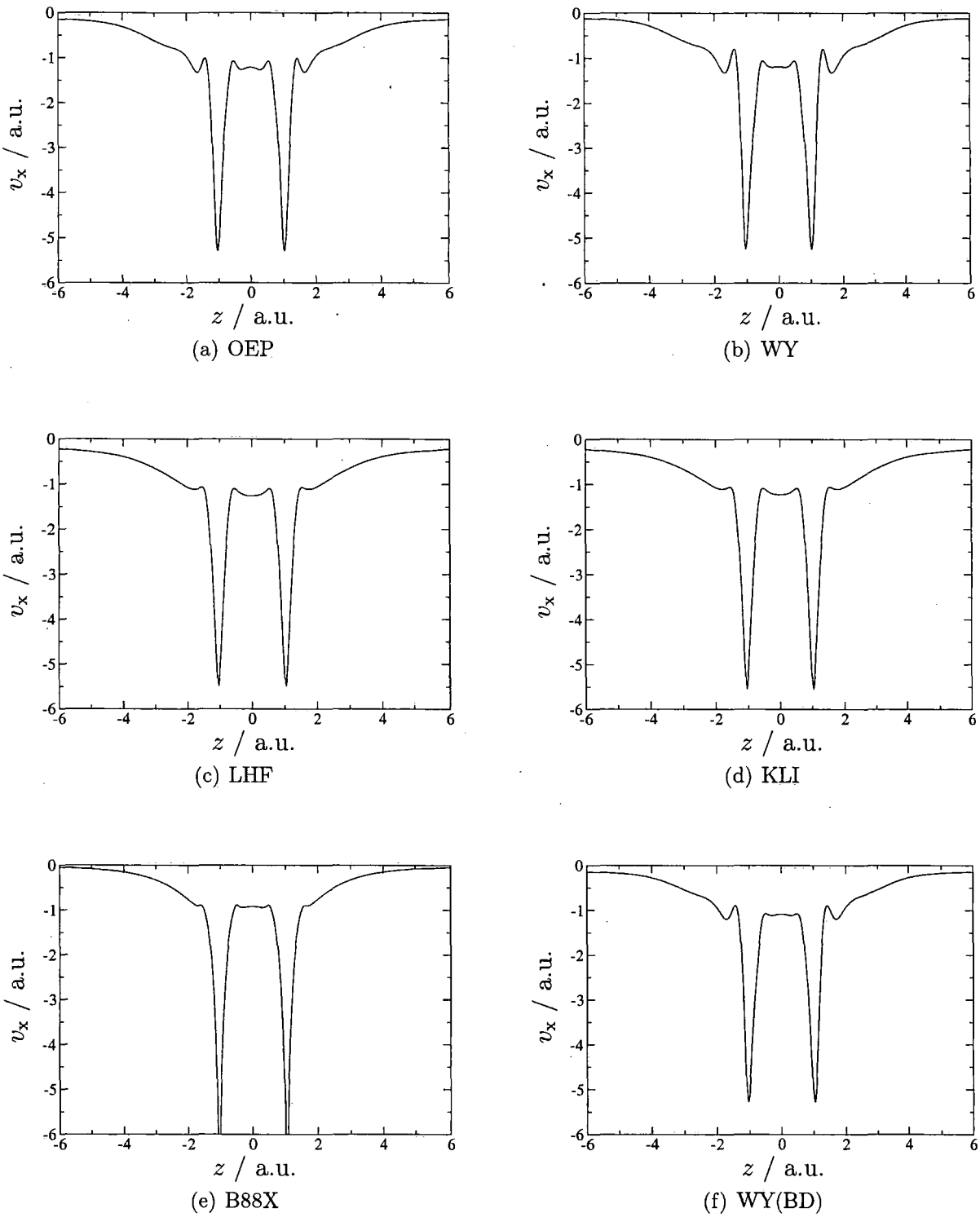

Figure 5.1: Exchange potentials of the N_2 molecules calculated using a variety of exchange-only methods

Table 5.1: Electronic energies (Hartree–Fock expression), uncoupled isotropic NMR shielding constants, and HOMO–LUMO gaps determined using various exchange methods.

	CO		N_2	PN	
Total Electronic Energies/E_h					
OEP	-112.7828		-108.9848	-395.1692	
WY	-112.7827		-108.9848	-395.1692	
LHF	-112.7802		-108.9819	-395.1653	
KLI	-112.7802		-108.9819	-395.1647	
B88X	-112.7637		-108.9677	-395.1468	
HF	-112.7881		-108.9902	-395.1777	
Isotropic Shieldings/ppm					
	C	O	N	P	N
OEP	21.8	35.4	-15.4	215.1	206.0
WY	21.1	34.6	-16.0	212.8	-209.5
LHF	2.5	-5.1	-49.3	79.3	-284.7
KLI	-1.9	-7.8	-54.3	80.9	-262.4
B88X	-10.4	-76.0	-80.8	-20.2	-403.8
WY(BD)[a]	-0.7	-42.6	-64.9	47.5	-340.5
Expt.[b]	2.8	-36.7	-59.6	53	-349
HOMO–LUMO Gaps/E_h					
OEP	0.287		0.345	0.198	
WY	0.286		0.344	0.198	
LHF	0.267		0.319	0.175	
KLI	0.266		0.317	0.179	
B88X	0.260		0.307	0.162	
WY(BD)[a]	0.268		0.316	0.172	

[a] Determined from a correlated BD density
[b] Ref. [153] and references therein.

associated with some unknown exchange–correlation functional that is assumed to be an explicit functional of the density and yields the BD density. They are formally equivalent to the MKS(BD) values of Ref. [143] and give very good agreement with the experimental values, which are also presented. Compared with these reference values, OEP and WY give shieldings that are much too high whilst LHF, KLI and B88X values are much closer; particularly those of LHF and KLI.

The variations in the uncoupled NMR shielding constant quality can be interpreted in terms of the paramagnetic component of the shielding constant [149–152], as discussed in Section 2.7.2. When comparing methods, those that give large occupied–virtual eigenvalue differences typically give larger shieldings than those that give smaller gaps. The most significant of these is the HOMO–LUMO gap and as such these eigenvalue differences are also summarised in Table 5.1. The results correlate well with the shielding constant calculations. Again the results follow the trend OEP $\approx$ WY > LHF $\approx$ KLI > B88X. We may compare these values with the WY(BD) HOMO–LUMO gaps, which represent near exact DFT results. In line with the shielding constants, the OEP and WY methods significantly overestimate the gaps. The LHF KLI and B88X gaps are more accurate, again particularly those of LHF and KLI. The underestimation of the gap by the B88X GGA functional is typical of all GGA approximations.

The calculations summarised in Table 5.1 show clearly that OEP and WY give similar results. The LHF and KLI results are also similar, but are significantly different to OEP and WY. The B88X approximation is fully local and gives different results again. This reflects differences in the Kohn–Sham eigenvalues and orbitals arising in each approach due to differences in their exchange potentials. We now investigate the differences between the approaches by examining the potentials, densities and frontier orbital probability densities associated with each method

5.3 Potentials, Densities and Frontier Orbitals

Since the OEP exchange only method represents the rigorous way to handle orbital dependent functionals within the Kohn–Sham DFT formalism, we present differences of the other approaches relative to the OEP quantities. For the N_2 molecule with nuclear coordinates $x = 0, y = 0, z = \pm 0.549$ Å we begin by defining the potential difference

$$\Delta v_{\mathrm{x}} = v_{\mathrm{x}} - v_{\mathrm{x}}^{\mathrm{OEP}} \tag{5.3.1}$$

where v_{x} is the potential of the method under consideration and $v_{\mathrm{x}}^{\mathrm{OEP}}$ is the OEP exchange only potential. Part (a) of Figures 5.2 to 5.5 present contour plots of the potential difference Δv_{x} for the WY, LHF, KLI and B88X methods respectively. All plots are presented in the xz plane. Any plane containing the two nuclei is the same due to cylindrical symmetry. Regions in red indicate values above that of the OEP potential and regions in blue indicate values below. White areas represent essentially zero difference. The OEP, WY, LHF and KLI potentials all asymptotically behave as $-1/r$ and so may be compared directly. However the B88X GGA exchange potential averages over the discontinuity as discussed in Section 1.7.3. In order to make this potential comparable with the others we must apply a negative shift, the magnitude of which may be calculated as $\varepsilon_{\mathrm{HOMO}} + I$, where I is the B88X ionisation potential. This shift has been calculated and included in Figure 5.5(a). The potential difference plots mirror the trends in Table 5.1. The WY plot shows very few features, highlighting the similarity of the OEP and WY potentials. The LHF and KLI plots exhibit more features but are similar to each other. The B88X plot shows substantial differences with OEP, reflecting the large differences between the methods.

The potentials give rise to the orbitals in each method through the solution of the Kohn–Sham equation and the squares of the occupied orbitals contribute to the density. It is therefore of interest to examine the density differences. Part (b) of Figures 5.2 to

5.5 present the quantity

$$\Delta\rho = \rho - \rho^{\mathrm{OEP}} \tag{5.3.2}$$

For each method there is a spatial correlation between the density difference and potential difference plots. Red areas on the density difference plots indicate regions where the density is greater than that of the OEP. These generally correspond to blue areas in the potential difference plots where the potential is lower than OEP, and vice versa. This is consistent with chemical intuition that a region of lower/higher potential will correspond to a region of higher/lower density. Similar observations were made for the correlation potential in the dispersion study of Ref. [213]. The plots show that the WY density is close to that of the OEP. Again the LHF and KLI plots are similar but exhibit differences relative to the OEP. The B88X plot exhibits the largest differences relative to OEP; the spatial correlation between the potential and density differences is particularly noticeable in this case.

The NMR shielding constant results were rationalised in terms of the HOMO–LUMO gaps. It is therefore of interest to compare the HOMO and LUMO frontier orbitals from the various methods with those of the OEP. We consider the square of the orbital, which is a probability density. For all of the approaches the N_2 HOMO orbital is of σ_g symmetry and so is cylindrically symmetric as required for the plot in the xz plane to be meaningful. We therefore define the quantity

$$\Delta\varphi^2_{\mathrm{HOMO}} = (\varphi_{\mathrm{HOMO}})^2 - (\varphi^{\mathrm{OEP}}_{\mathrm{HOMO}})^2 \tag{5.3.3}$$

which is plotted in part (c) of Figures 5.2 to 5.5. The LUMO orbital however is degenerate and has π_g symmetry. In order to ensure cylindrical symmetry required for the contour plots we consider half of the sum of the squares of the LUMO and degenerate LUMO+1 orbitals

$$\Delta\varphi^2_{\mathrm{LUMO}} = \frac{(\varphi_{\mathrm{LUMO}})^2 + (\varphi_{\mathrm{LUMO+1}})^2 - (\varphi^{\mathrm{OEP}}_{\mathrm{LUMO}})^2 - (\varphi^{\mathrm{OEP}}_{\mathrm{LUMO+1}})^2}{2} \tag{5.3.4}$$

which is plotted in part (d) of Figures 5.2 to 5.5. The most striking feature of the HOMO and LUMO probability density plots is the contraction of the LUMO orbitals of LHF and KLI compared with OEP. This is consistent with the observed reduction in the HOMO–LUMO gaps for these methods. The contraction is also present for B88X but positive regions are observed at long range due to the incorrect asymptotic behaviour of the B88X potential. The WY plot even exhibits a similar contraction, although the magnitude is much smaller. This is consistent with the very small decrease in the HOMO–LUMO gap in moving from OEP to WY (for CO and N_2 the gaps reduce

by $1 \times 10^{-3} E_h$).

The plots in Figures 5.2 to 5.5 show that the LHF, KLI and B88X methods provide potentials, densities and frontier orbitals that are notably different from those of OEP. In Table 5.1 we compared the shielding constants and eigenvalue differences of these approaches with WY(BD) results which include correlation. Those results suggested the presence of some correlated character in the LHF, KLI and B88X solutions. To investigate this further we apply the WY procedure to an accurate Brueckner-Doubles coupled cluster density and plot the differences in the same quantities relative to the exchange only OEP method in Figure 5.6. That is, we subtract from near exact values, including the effects of exchange and correlation, the exchange only OEP values. The features in Figure 5.6 are therefore directly attributable to the effects of correlation. The plots show the same qualitative differences as those observed for LHF, KLI and B88X, confirming the presence of correlated character in these approximate exchange methods. The introduction of correlation by the B88X functional for multicentre systems is well known and arises due to its purely local nature [148]. The observation of correlated character in the LHF and KLI solutions arises due to the common-energy-denominator closure approximation which can be employed to derive their equations (see Section 2.5). These results are consistent with the observations of Table 5.1 and also with the excitation energy observations of Della Sala and Görling [128].

The investigation of the exchange only approximations has highlighted their deficiencies, relative to the exchange only OEP. These deficiencies can mimic the effects of electron correlation. This has important implications for the construction of multiplicative hybrid functionals. In the next chapter, we consider the application of the OEP method to hybrid energy functionals which contain fractions of orbital dependent exchange and include the effects of electron correlation.

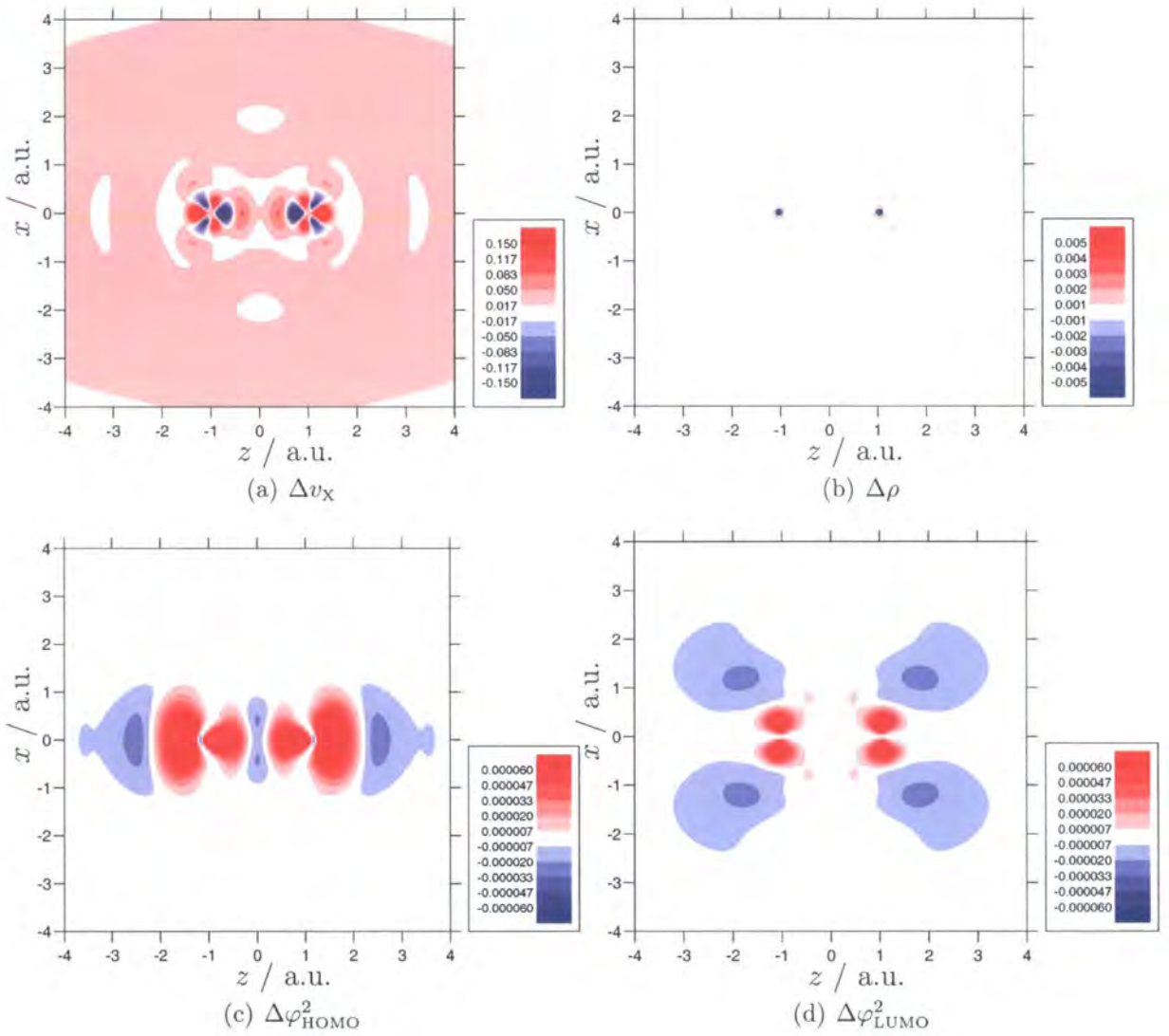

Figure 5.2: Contour plots for N_2: WY minus OEP. (a) potential, (b) electron density, (c) HOMO probability density, (d) LUMO probability density. All quantities are in atomic units.

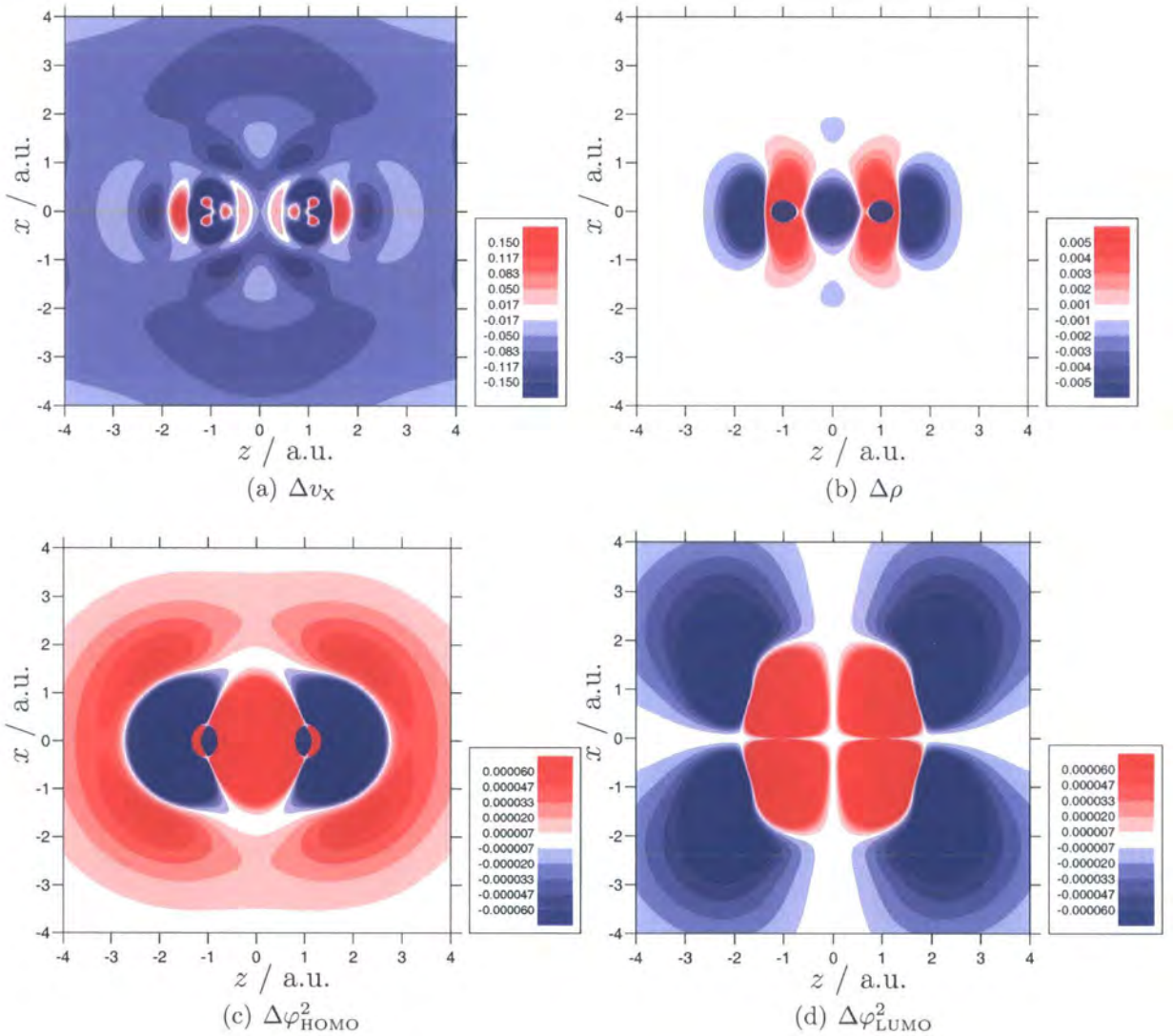

(a) Δv_{X} (b) $\Delta\rho$

(c) $\Delta\varphi^2_{\mathrm{HOMO}}$ (d) $\Delta\varphi^2_{\mathrm{LUMO}}$

Figure 5.3: Contour plots for N_2: LHF minus OEP. (a) potential, (b) electron density, (c) HOMO probability density, (d) LUMO probability density. All quantities are in atomic units.

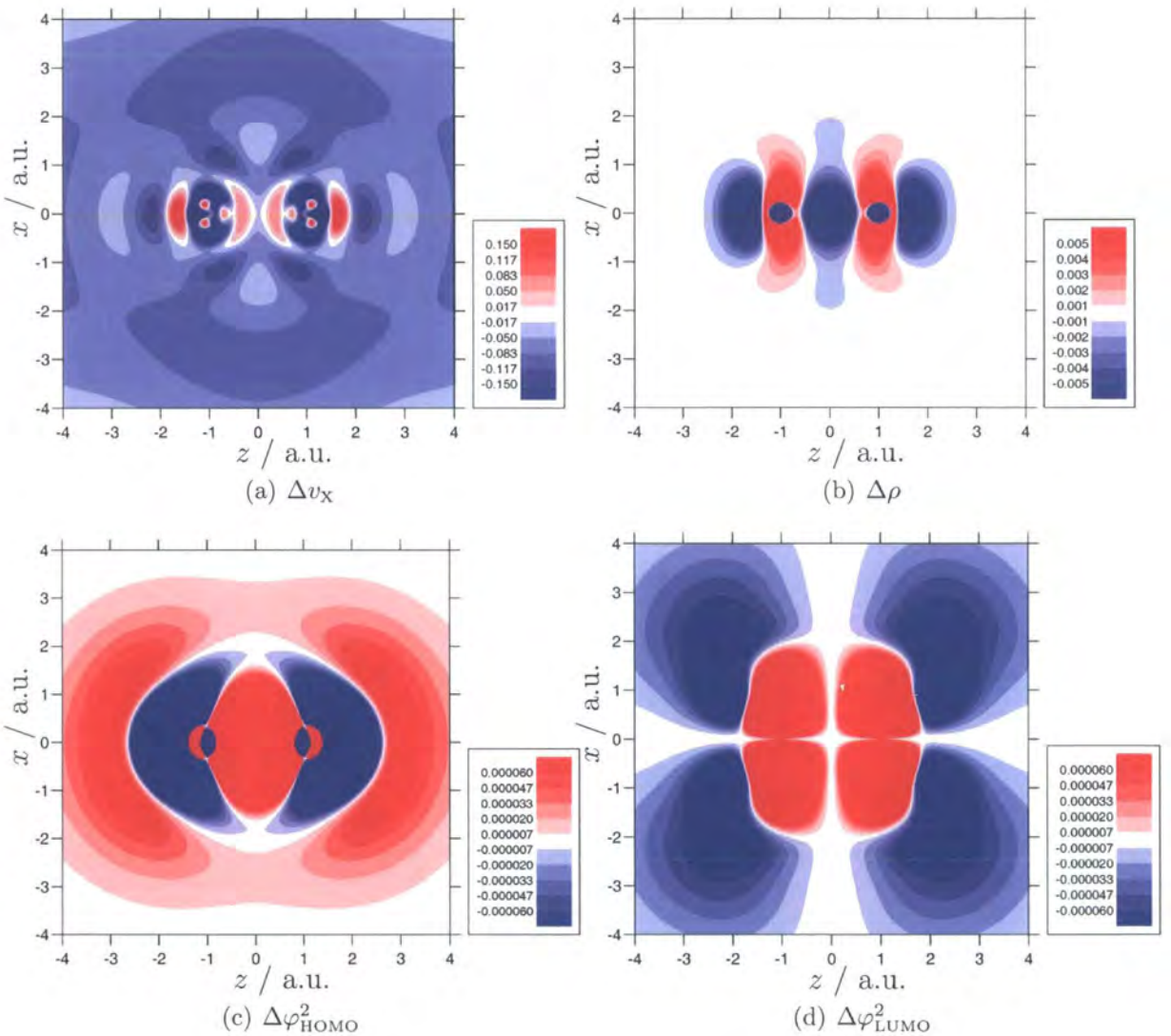

Figure 5.4: Contour plots for N_2: KLI minus OEP. (a) potential, (b) electron density, (c) HOMO probability density, (d) LUMO probability density. All quantities are in atomic units.

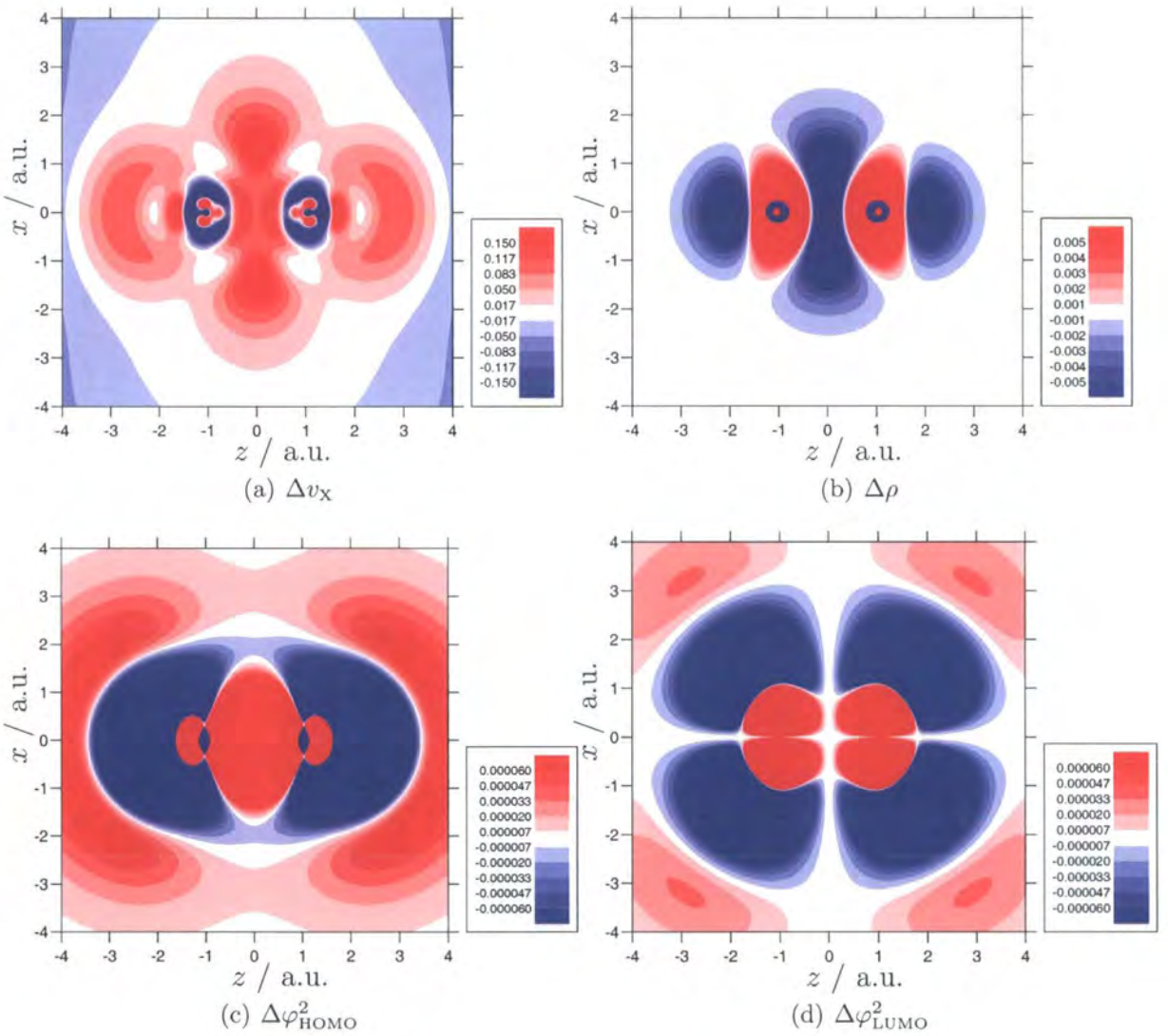

Figure 5.5: Contour plots for N_2: B88X minus OEP. (a) potential, (b) electron density, (c) HOMO probability density, (d) LUMO probability density. All quantities are in atomic units.

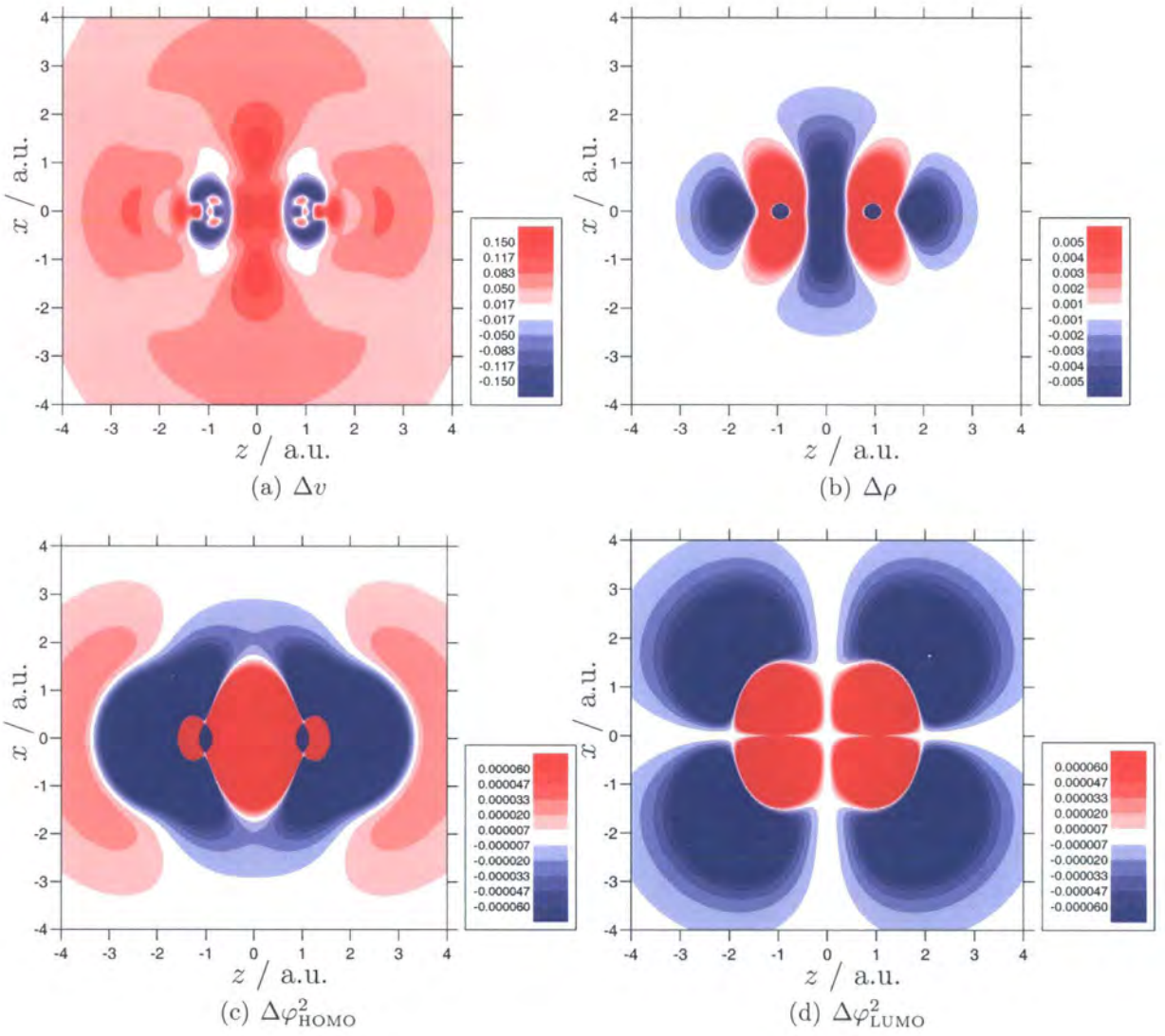

Figure 5.6: Contour plots for N_2: WY(BD) minus OEP. (a) potential, (b) electron density, (c) HOMO probability density, (d) LUMO probability density. All quantities are in atomic units.

Chapter 6

Applications of OEP-based Hybrid Functionals

In this chapter we apply our implementation of the Yang–Wu OEP method to hybrid energy functionals, which contain a fraction of orbital dependent exchange and include the effects of electron correlation. These functionals are used to calculate main group NMR shielding constants, rotational g tensors and as a particularly challenging test, transition metal chemical shifts. The quality of the results is assessed by comparison with experimental data. Notable improvements are obtained compared to conventional DFT calculations. The WY constrained search procedure is also employed with high quality Brueckner-Doubles electron densities to provide near exact KS-DFT values for comparison.

6.1 Calculating NMR Shielding Constants with the OEP and WY Methods

In this section, we apply the OEP/WY implementations of Chapter 4 to the calculation of nuclear magnetic resonance (NMR) shielding constants. The OEP implementation may be easily extended for application to any energy functional by re-writing the first derivative of Eqn. (4.2.5) as

$$\frac{\partial E_{\mathrm{xc}}[\{\varphi_{i\sigma}\}]}{\partial b_t^\sigma} = \sum_i \sum_a \left\langle \varphi_{i\sigma} \left| \hat{H}_{\mathrm{eff}}^\sigma \right| \varphi_{a\sigma} \right\rangle \frac{\langle \varphi_{a\sigma} | g_t | \varphi_{i\sigma} \rangle}{\varepsilon_{i\sigma} - \varepsilon_{a\sigma}} + \mathrm{c.c.} \tag{6.1.1}$$

where $\hat{H}_{\mathrm{eff}}^\sigma \varphi_{i\sigma}^*(\mathbf{r}) = \delta E[\{\varphi_{i\sigma}\}]/\delta\varphi_{i\sigma}(\mathbf{r})$. For the exchange-only case the first term in the product is simply elements of the Fock matrix, for a hybrid functional it is elements of the Kohn–Sham matrix with the exchange contribution evaluated as in the

Hartree–Fock scheme and for a functional which depends explicitly on the density it is the elements of the Kohn–Sham matrix. Our CADPAC implementation was modified accordingly to allow the application of the OEP procedure to any energy functional. For explicit functionals of the density the conventional and OEP evaluations are equivalent.

The WY procedure allows the calculation of an exchange–correlation potential corresponding to a supplied electron density, and when a density from a DFT functional depending explicitly on the density is employed it too should return results equivalent to the conventional evaluation. To illustrate the accuracy of the methods NMR shielding constants were calculated for 21 molecules using conventional and OEP evaluations of the LDA exchange–correlation functional. LDA relaxed density matrices were also input to the WY procedure and NMR shielding constants calculated. The results are presented in Table 6.1 with errors calculated relative to experiment. The OEP and WY results agree superbly with those of the conventional evaluation, the overall mean absolute errors relative to experiment for each method agreeing to better than 0.1 ppm.

We now consider the application of the OEP and WY procedures to the calculation of NMR shielding constants with hybrid functionals. For the same set of 21 molecules, shielding constants were calculated with the OEP/WY procedures for the HF, B3LYP, B97-2 and PBE0 energy functionals/densities. The results are presented in Tables 6.2 and 6.3. Errors are calculated relative to the experimental values. Also presented are WY(BD) values which result from the application of the WY procedure to accurate Brueckner-Doubles coupled cluster electron densities.

The OEP and WY results are clearly similar as was observed for the exchange-only case in Chapter 5 and has been shown in Ref. [212]. The WY results are formally equivalent to those of the MKS procedure of Ref. [143]. The results show a marked improvement over conventional coupled hybrid evaluations. Similar quality can be obtained with the OEP procedure but the calculations do not require the separate calculation of a relaxed density matrix. Differences between the OEP and WY results are small. The largest differences are observed for the Hartree–Fock based methods. Differences in the hybrid OEP / WY calculations are smaller since these typically contain smaller amounts of orbital exchange, ξ, in the range $0.2 - 0.3$. The key advantage of the WY procedure is that the functional form is not required and so supplying high quality electron densities can provide accurate Kohn-Sham values. The WY(BD) calculations give the highest quality results and compare well with the best *ab initio* values presented in Table 2.6.

In Chapter 2 we considered how the fraction of orbital exchange in the functional influenced the NMR shielding constants evaluated for multiplicative hybrid functionals

Table 6.1: Comparison of conventional, OEP and WY shielding constants, in ppm, calculated using the LDA energy functional / density

Mol	Nucl	LDA	O-LDA	WY(LDA)	Expt.
HF	F	416.2	416.1	416.1	419.7
H_2O	O	334.8	334.8	334.8	357.6
CH_4	C	193.1	193.2	193.2	198.4
CO	C	-20.3	-20.2	-20.2	2.8
	O	-87.6	-87.7	-87.7	-36.7
N_2	N	-91.4	-91.3	-91.3	-59.6
F_2	F	-284.2	-284.8	-285.0	-192.8
O'OO'	O'	-1532.7	-1529.5	-1528.8	-1290.0
	O	-921.8	-921.6	-920.7	-724.0
PN	P	-73.7	-73.5	-73.5	53.0
	N	-414.9	-415.2	-414.8	-349.0
H_2S	S	733.9	734.0	733.9	752.0
NH_3	N	266.3	266.3	266.3	273.3
HCN	C	65.3	65.3	65.3	82.1
	N	-56.7	-56.7	-56.7	-20.4
C_2H_2	C	100.8	100.8	100.8	117.2
C_2H_4	C	40.9	40.9	40.9	64.5
H_2CO	C	-40.0	-40.5	-40.6	-4.4
	O	-493.5	-492.8	-493.2	-375.0
N'NO	N'	87.7	87.7	87.8	99.5
	N	-2.3	-2.2	-2.2	11.3
	O	179.0	179.1	179.2	200.5
CO_2	C	50.0	50.0	50.0	58.8
	O	209.7	209.7	209.7	243.4
OF_2	O	-667.6	-669.4	-669.5	-473.1
H_2CNN'	C	164.5	164.7	164.7	164.5
	N	-61.5	-61.8	-61.8	-43.4
	N'	-166.4	-166.9	-166.9	-149.0
HCl	Cl	959.5	959.8	959.8	952.0
SO_2	S	-242.9	-242.1	-242.1	-126.0
	O	-282.0	-281.8	-281.8	-205.0
PH_3	P	583.1	583.0	583.0	599.9
d		-51.8	-51.7	-51.7	
$\|d\|$		52.3	52.2	52.2	
$\|d\|$%		89.7	90.1	90.1	
Omitting O_3					
d		-40.6	-40.6	-40.6	
$\|d\|$		41.1	41.1	41.1	
$\|d\|$%		94.2	94.6	94.6	

Table 6.2: NMR shielding constants, in ppm, calculated using the OEP method

Mol	Nucl	OEP	O-B3LYP	O-B972	O-PBE0	Expt.
HF	F	425.4	414.7	415.0	416.5	419.7
H_2O	O	338.9	330.1	330.6	332.8	357.6
CH_4	C	193.3	188.4	190.9	192.3	198.4
CO	C	21.1	-7.6	-1.8	-3.7	2.8
	O	33.8	-53.0	-45.7	-47.8	-36.7
N_2	N	-16.3	-70.1	-64.3	-65.0	-59.6
F_2	F	-51.2	-217.5	-208.0	-199.1	-192.8
O'OO'	O'	-664.2	-1231.0	-1193.5	-1169.6	-1290.0
	O	-597.7	-821.2	-790.5	-786.1	-724.0
PN	P	205.8	17.3	35.8	33.1	53.0
	N	-209.0	-357.9	-339.9	-342.0	-349.0
H_2S	S	739.2	711.3	725.8	732.5	752.0
NH_3	N	266.0	260.5	261.6	263.7	273.3
HCN	C	93.9	75.0	78.9	77.7	82.1
	N	28.0	-30.3	-21.0	-24.0	-20.4
C_2H_2	C	127.1	110.3	114.8	113.0	117.2
C_2H_4	C	76.5	51.8	58.1	56.3	64.5
H_2CO	C	10.8	-20.3	-12.9	-16.4	-4.4
	O	-164.8	-375.2	-349.1	-358.5	-375.0
N'NO	N'	127.6	96.2	101.0	101.6	99.5
	N	28.2	3.2	11.5	10.5	11.3
	O	241.2	189.8	190.8	194.5	200.5
CO_2	C	69.6	54.2	59.4	58.4	58.8
	O	265.6	224.0	226.1	226.7	243.4
OF_2	O	-311.2	-546.9	-521.3	-514.3	-473.1
H_2CNN'	C	171.8	162.0	164.5	165.9	164.5
	N	-12.0	-52.6	-43.0	-42.8	-43.4
	N'	-72.6	-148.4	-136.3	-133.6	-149.0
HCl	Cl	963.4	946.4	953.0	957.8	952.0
SO_2	S	-53.8	-185.2	-162.8	-163.0	-126.0
	O	-60.5	-222.9	-212.7	-208.5	-205.0
PH_3	P	595.3	565.4	580.8	586.2	599.9
d		69.0	-16.9	-6.4	-4.9	
$\|d\|$		72.0	20.6	15.7	15.5	
$\|d\|$%		81.2	37.5	17.7	23.1	
Omitting O_3						
d		48.5	-16.8	-7.9	-7.2	
$\|d\|$		51.7	16.8	11.3	10.4	
$\|d\|$%		84.4	39.4	18.3	24.0	

Table 6.3: NMR shielding constants, in ppm, calculated using the WY method

Mol	Nucl	WY	WY(B3LYP)	WY(B972)	WY(PBE0)	WY(BD)	Expt.
HF	F	424.8	414.6	415.0	416.4	418.2	419.7
H_2O	O	338.4	330.1	330.6	332.8	333.7	357.6
CH_4	C	193.1	188.4	190.9	192.3	191.4	198.4
CO	C	20.2	-7.6	-1.8	-3.7	-1.3	2.8
	O	33.1	-53.0	-45.7	-47.8	-42.8	-36.7
N_2	N	-16.9	-70.1	-64.3	-65.1	-65.0	-59.6
F_2	F	-52.2	-217.9	-208.4	-199.5	-207.5	-192.8
O'OO'	O'	-676.4	-1231.6	-1194.0	-1170.8	-1113.3	-1290.0
	O	-598.0	-820.2	-789.3	-785.1	-744.2	-724.0
PN	P	203.6	17.1	35.7	32.9	43.8	53.0
	N	-211.8	-358.0	-340.2	-342.4	-338.5	-349.0
H_2S	S	736.5	711.1	725.6	732.2	725.9	752.0
NH_3	N	265.6	260.5	261.6	263.7	263.2	273.3
HCN	C	93.7	75.0	78.9	77.7	78.9	82.1
	N	26.8	-30.3	-21.1	-24.1	-20.8	-20.4
C_2H_2	C	126.9	110.3	114.7	113.0	114.4	117.2
C_2H_4	C	76.3	51.8	58.0	56.3	58.3	64.5
H_2CO	C	10.6	-20.4	-13.0	-16.5	-10.8	-4.4
	O	-168.9	-375.7	-349.7	-359.3	-337.9	-375.0
N'NO	N'	126.6	96.2	101.1	101.6	101.7	99.5
	N	28.1	3.2	11.5	10.5	12.2	11.3
	O	240.7	189.8	190.8	194.5	204.5	200.5
CO_2	C	69.3	54.1	59.3	58.4	61.1	58.8
	O	264.8	224.0	226.1	226.7	235.1	243.4
OF_2	O	-316.9	-547.8	-522.2	-515.5	-491.9	-473.1
H_2CNN'	C	171.8	162.0	164.5	165.9	164.9	164.5
	N	-13.0	-52.6	-43.0	-42.9	-43.5	-43.4
	N'	-77.4	-148.6	-136.4	-133.8	-139.7	-149.0
HCl	Cl	961.8	946.3	952.9	957.7	955.0	952.0
SO_2	S	-55.2	-185.1	-162.7	-163.0	-138.3	-126.0
	O	-62.1	-222.8	-212.6	-208.4	-176.7	-205.0
PH_3	P	593.1	565.2	580.7	586.0	582.9	599.9
d		67.3	-17.0	-6.5	-5.0	2.2	
$\|d\|$		70.8	20.7	15.7	15.4	15.0	
$\|d\|$%		79.2	37.6	17.8	23.2	14.5	
Omitting O_3							
d		47.2	-16.9	-8.0	-7.3	-2.9	
$\|d\|$		50.8	16.9	11.3	10.5	9.4	
$\|d\|$%		82.3	39.5	18.4	24.2	15.0	

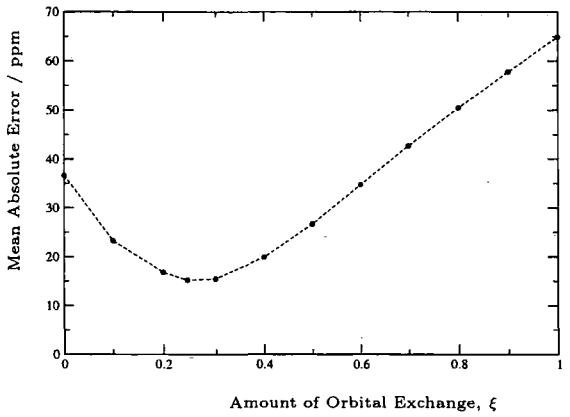

Figure 6.1: The mean absolute error, in ppm, as a function of the amount of exchange ξ in OEP hybrid functionals

containing the KLI and LHF approximations to the exchange potential. It was found that amounts around 0.5 to 0.6 were optimal which contrasts the typical amount of 0.2 to 0.3 in conventional hybrid functionals. We now consider the same variation for OEP evaluations of the hybrid functionals of Ref. [152] in order to confirm whether this difference in the optimal amount of exchange arises due to approximations inherent in the LHF/KLI procedures or if it is a feature of functionals employing multiplicative exchange potentials. The mean absolute error as a function of the amount of exchange, ξ, for the set of 21 molecules considered in Table 6.2 is plotted in Figure 6.1.

For the OEP hybrid functionals the mean absolute errors minimise around $\xi = 0.2-0.3$ in line with the amount of exchange in conventional hybrid functionals. Similar observations were made for the ZMP results in Ref. [152]. This highlights again the difference in character of the LHF/KLI and OEP/WY methods, which was discussed in detail in Chapter 5. We now move on to consider other applications of the OEP hybrid functionals.

6.2 Rotational g tensors

When a molecule rotates it acquires a magnetic moment proportional to its angular momentum. In the presence of an external magnetic field the Zeeman interaction between this magnetic moment and the external magnetic induction causes a shift in the rotational energy levels. This shift can be observed in molecular beam [216] and

microwave Zeeman experiments [217, 218], and may be written in atomic units as

$$\Delta E = -\mu_{\mathrm{N}} \mathbf{B}^{\mathrm{T}} \mathbf{g} \mathbf{J} \tag{6.2.1}$$

where μ_{N} is the nuclear magneton, $\mathbf{B}$ is the external magnetic induction, $\mathbf{J}$ is the angular momentum of the molecule with respect to its centre of mass, and $\mathbf{g}$ is the dimensionless 3×3 rotational g tensor. The g tensor can be evaluated as the second derivative of the electronic energy E with respect to $\mathbf{B}$ and $\mathbf{J}$:

$$\mathbf{g} = -\frac{1}{\mu_{\mathrm{N}}} \left. \frac{\partial^2 E(\mathbf{B}, \mathbf{J})}{\partial \mathbf{B} \partial \mathbf{J}} \right|_{\mathbf{B},\mathbf{J}=0} . \tag{6.2.2}$$

The calculation of g tensors is similar to that of other singlet second-order magnetic response properties such as nuclear magnetic resonance (NMR) shielding constants, spin rotation constants, and magnetisabilities.

The high accuracy obtained in the experimental determination of rotational g tensors makes them an excellent candidate to test the accuracy of theoretical methods. A wide range of theories have been used to calculate g tensors including Hartree–Fock (HF) theory [219–222], multiconfigurational self-consistent field (MCSCF) theory [223–230], Møller–Plesset theory to second [229, 231, 232], third [229, 231], and fourth orders [229] (MP2, MP3, MP4), linearised coupled-cluster doubles (L-CCD) theory [231], coupled cluster singles-and-doubles (CCSD) theory [229], the second-order polarization propagator approximation (SOPPA) [229, 233–235], the coupled-cluster polarization propagator approximation (CCSDPPA) [236–239], the SOPPA using CCSD amplitudes (SOPPA(CCSD)) [229, 240], full configuration-interaction (FCI) theory [241–243], and density-functional theory (DFT) [228, 244, 245].

Recently Wilson *et al.* [245] used DFT in an extensive assessment of different exchange–correlation functionals for the calculation of rotational g tensors. They considered the local density approximation (LDA), the Becke–Lee–Yang–Parr (BLYP) GGA [64, 65], and the Becke-3-parameter-Lee–Yang–Parr (B3LYP) hybrid functional [94]. Also considered was the Keal–Tozer (KT2) GGA functional [69], which was specifically designed to yield good quality magnetic response parameters. The authors observed the quality of calculated g tensors followed the trend LDA<BLYP<B3LYP<KT2. In this section we consider the application of the OEP procedure to a range of hybrid exchange-correlation functionals. Uncoupled results are compared with conventional coupled hybrid values and the KT2 functional, which provides the previous best DFT results. Where possible the effect of vibrational corrections is considered. The influence of the amount of orbital exchange on the quality of the g tensors is examined.

Rotational g tensors are also obtained directly from *ab initio* coupled electron densities using the Wu–Yang (WY) approach.

The OEP implementation described in Chapter 4 is employed and the Kohn–Sham effective potential is expanded according to Eqn. (4.2.2). For the reference potential $v_0(\mathbf{r})$ the Fermi–Amaldi potential of Eqn. (4.2.3) constructed using the Hartree–Fock density is used. In the WY calculations the same reference potential is used. In both approaches the optimization is carried out with second order quasi-Newton methods as described in Chapter 4.

The key feature of the OEP and WY implementations in Chapter 4 is that they utilise the expansion of Eqn. (4.2.2) and so $v_s(\mathbf{r})$ can be expressed as a simple sum of fixed terms and a linear combination of Gaussian functions. Once the optimal coefficients $\{b_t\}$ for the linear combination have been determined it is straightforward to reconstruct the potential in any electronic structure program. In order to calculate rotational g tensors we determine the solution of the OEP problem in CADPAC and then read the set of coefficients $\{b_t\}$ defining the effective potential into a modified version of the DALTON program [246], provided by Lutnæs [247]. The potential is then reconstructed using the same geometry, reference potential and orbital and auxiliary basis sets. The Kohn–Sham equations are solved by a single diagonalization (since $v_s(\mathbf{r})$ has no orbital dependence) and the resulting orbitals and eigenvalues are used to compute the uncoupled rotational g tensors.

The advantage of this two code approach is that it allows the exploitation of the extensive property evaluations available in the DALTON program. In the evaluation of the g tensor, rotational London atomic orbitals are used to ensure fast basis set convergence and gauge independent results [219]. These orbitals are essential for molecules of the size considered here and were not available in the CADPAC program. The implementation was checked by confirming that the converged one-electron eigenvalues in DALTON agreed with those of the corresponding OEP/WY calculations in the CADPAC code, to within numerical integration error. The property calculations were checked by comparison of single origin magnetisability calculations in DALTON and CADPAC. The London orbital calculations were checked by confirming gauge-origin invariance and comparison of large basis set single origin magnetisabilities with London orbital magnetisabilities for small molecules.

We follow the previous DFT investigation of Wilson *et al.* [245] and use the aug-cc-pVTZ orbital basis set [248–250], but with Cartesian basis functions rather than spherical since the latter are not available in the CADPAC code. The 58 molecules considered are listed in Table 6.4 and contain 67 isotopic combinations and 143 unique tensor elements. Rotational g tensors are known to be sensitive to molecular geometry

Table 6.4: The molecules for which rotational g tensors were determined

carbon monoxide [CO], carbon sulfide [CS], carbon selenide [CSe],
hydrogen cyanide [$HC^{15}N$], fluoro cyanide [$FC^{15}N$], chloro cyanide [$ClC^{15}N$],
bromo cyanide [$BrC^{15}N$], carbonyl sulfide [OCS, $OC^{34}S$, $O^{13}CS$],
nitrous oxide [$^{15}N^{15}NO$, $^{14}N^{14}NO$], carbonyl selenide [$OC^{80}Se$, $OC^{76}Se$],
methylidene phosphine [HCP, DCP], hydrogen boron sulfide [HBS],
fluoro acetylene [FCCH], chloro acetylene [$^{35}ClCCH$, $^{37}ClCCH$],
bromo acetylene [$^{79}BrCCH$, $^{81}BrCCH$], ammonia [$^{15}NH_3$],
trifluoromethane [CHF_3], methylisocyanide [$CH_3\ ^{14}NC$],
acetonitrile [$CH_3C^{15}N$, $CH_3C^{14}N$, $CD_3C^{14}N$], fluoromethane [CH_3F],
chloromethane [CH_3Cl], acrolein [CH_2CHCHO], propene [CH_2CHCH_3],
propynal [HCCCHO], dimethylether [CH_3OCH_3],
dimethylsulfane [CH_3SCH_3], acetaldehyde [CH_3CHO], formaldehyde [H_2CO],
thioformaldehyde [H_2CS], formic acid [HCOOH], formamide [$HCONH_2$],
glycoaldehyde [CH_2OHCHO], methyl formate [$HCOOCH_3$], ketene [H_2CCO],
difluoromethane [CH_2F_2], carbonic difluoride [F_2CO], formyl fluoride [HFCO],
fluoroethene [$CFHCH_2$], 1,1-difluoroethene [CF_2CH_2],
cis-difluoroethene [CFHCFH], fluoroethane [CFH_2CH_3],
trifluoroethene [CF_2CFH], ozone [O_3], sulfur dioxide [SO_2],
difluorooxide [F_2O], hypofluoros acid [HOF], Water [H_2O],
hydrogendisulfide [H_2S], methylene [C_4H_6],
cyclopropene [C_3H_4], aziridine [C_2H_5N], oxirane [C_2H_4O],
thiirane [C_2H_4S], cyclopropenone [C_3H_2O], methylcyclopropene [C_4H_6],
cyclobutene [C_4H_6], oxetane [C_3H_6O], β-propiolactone [$C_3H_4O_2$]

although the study of Wilson *et al.* showed that the relative performance of the DFT methods was unchanged whether optimized or experimental geometries are employed. In this case we consider only the experimental geometries of Ref. [245], apart from the ozone molecule for which we use $r = 1.2717$ Å and $\theta = 116.78°$ from Ref. [251]. The results are compared with the experimental g tensors compiled by Wilson *et al.* in Ref. [245] with the exception of ammonia and thioformaldehyde. For the ammonia molecule the values of Ref. [252] are used since they have smaller error bars and for thioformaldehyde a typographical error was noted in the original paper [253] – the dominant diagonal element of the tensor is -5.2602 (rather than the value of -5.6202 used in Ref. [245]).

As highlighted in Chapter 4, application of the OEP/WY procedures requires careful choice of the auxiliary basis set in Eqn. (4.2.2) and the cutoff in the TSVD regularisation. We commenced by examining the effect of these choices on the exchange–correlation potentials of the g tensors for a subset of the molecules in Table 6.4. For the auxiliary basis set we considered both eventempered basis sets and the use of the primary orbital basis. Comparison of g tensors calculated using the primary orbital basis set with converged values obtained using a large auxiliary basis set showed differences greater than 2%. The eventempered auxiliary basis sets are defined by s, p, d, and f functions on all atom centres with exponents λ^{n_s}, λ^{n_p}, λ^{n_d} and λ^{n_f} where λ is a universal base and n_s, n_p, n_d and n_f are negative and positive integers which define the range of the functions. A variety of bases were considered for a subset of the molecules and a value of 2 was found to be optimal. In line with the observations for the Ne atom

it was found that capping the highest exponent for each angular momentum function at a maximum of 2^6 removed unphysical structure in the potential at the positions of the nuclei. The effect of this capping was found to lead to no significant change in the g tensors obtained, changes being less than those observed on changing from a triple zeta to quadruple zeta orbital basis set. To choose the ranges for each angular momentum, values were chosen such that the exponents span the same range of values as those of the orbital basis set, with the lowest exponent multiplied by 0.1. To choose a value for the TSVD cutoff, values between 10^{-4} and 10^{-8} were considered and the resulting exchange–correlation potentials examined. In line with the observations of Chapter 4, a value 10^{-4} was found to be appropriate. The effect of lowering the filter on the g tensor was found to be less than the orbital basis set incompleteness error.

Having chosen an auxiliary set we tested its usefulness by applying the OEP method to the KT2 functional and calculating rotational g tensors. Since the KT2 functional is a GGA and corresponds to a rigorous Kohn–Sham equation of the form of Eqn. (4.2.1), the OEP solution, in the limit of a complete auxiliary basis set, should yield the same solution as the conventional evaluation. For the molecules CO, CSe, OCS, N_2O, NH_3, HOF, H_2O and SO_2 (15 unique tensor components) the average deviation from the KT2 values was found to be just 0.1% with a maximum deviation of 0.3%.

For the set of molecules in Table 6.4, rotational g tensors were calculated for the B3LYP, B97-2 and B97-3 [254] hybrid functionals in a coupled manner. For the KT2 functional uncoupled g tensors were evaluated. The OEP procedure was applied to each of the hybrids and the resulting potential, orbitals and eigenvalues were used to determine uncoupled rotational g tensors. The results are denoted O-B3LYP, O-B97-2 and O-B97-3. The calculated values are presented in Table 6.5. The mean absolute error (MAE), mean error (ME), percentage mean absolute error (PMAE), and standard deviation (SD) for the calculated g tensors relative to experiment are summarised in Table 6.6 both including and omitting the ozone molecule due to its significant multireference character.

Table 6.5: Rotational g tensors determined by experiment and calculated using DFT methods. Basis set used is aug-cc-pVTZ.

Molecule	KT2	B3LYP	B97-2	B97-3	O-B3LYP	O-B97-2	O-B97-3	Exp.
				Linear molecules				
CO	-0.2673	-0.2811	-0.2827	-0.2861	-0.2704	-0.2717	-0.2719	-0.2689
CS	-0.2782	-0.2923	-0.2932	-0.2989	-0.2730	-0.2740	-0.2728	-0.2702
CSe	-0.2548	-0.2733	-0.2713	-0.2793	-0.2480	-0.2463	-0.2463	-0.2431
$HC^{15}N$	-0.0912	-0.0980	-0.0983	-0.0978	-0.0936	-0.0941	-0.0924	-0.0904
$FC^{15}N$	-0.0481	-0.0515	-0.0499	-0.0502	-0.0509	-0.0493	-0.0495	-0.0504
$ClC^{15}N$	-0.0393	-0.0408	-0.0396	-0.0397	-0.0407	-0.0394	-0.0395	-0.04121
$BrC^{15}N$	-0.0331	-0.0344	-0.0334	-0.0335	-0.0339	-0.0329	-0.0330	-0.0325

Continued

Continued

Molecule	KT2	B3LYP	B97-2	B97-3	O-B3LYP	O-B97-2	O-B97-3	Exp.
OCS	-0.0287	-0.0304	-0.0290	-0.0293	-0.0299	-0.0284	-0.0285	-0.028839
$OC^{34}S$	-0.0281	-0.0298	-0.0284	-0.0287	-0.0293	-0.0278	-0.0280	-0.028242
$O^{13}CS$	-0.0286	-0.0303	-0.0288	-0.0292	-0.0298	-0.0283	-0.0284	-0.028710
$^{15}N^{15}NO$	-0.0769	-0.0797	-0.0772	-0.0774	-0.0782	-0.0756	-0.0754	-0.07606
$^{14}N^{14}NO$	-0.0796	-0.0825	-0.0799	-0.0801	-0.0810	-0.0783	-0.0780	-0.07887
$OC^{80}Se$	-0.0196	-0.0210	-0.0198	-0.0200	-0.0204	-0.0192	-0.0192	-0.01952
$OC^{76}Se$	-0.0198	-0.0212	-0.0200	-0.0202	-0.0206	-0.0194	-0.0194	-0.01969
HCP	-0.0419	-0.0468	-0.0461	-0.0458	-0.0450	-0.0442	-0.0437	-0.0430
DCP	-0.0359	-0.0400	-0.0394	-0.0391	-0.0385	-0.0378	-0.0374	-0.0353
HBS	-0.0406	-0.0433	-0.0409	-0.0428	-0.0412	-0.0388	-0.0395	-0.0414
FCCH	-0.0071	-0.0092	-0.0073	-0.0072	-0.0094	-0.0075	-0.0075	-0.0077
^{35}ClCCH	-0.0070	-0.0080	-0.0062	-0.0062	-0.0083	-0.0065	-0.0066	-0.00630
^{37}ClCCH	-0.0068	-0.0077	-0.0060	-0.0060	-0.0081	-0.0063	-0.0065	-0.00601
^{79}BrCCH	-0.0055	-0.0059	-0.0045	-0.0045	-0.0061	-0.0046	-0.0046	-0.00395
^{81}BrCCH	-0.0055	-0.0058	-0.0044	-0.0045	-0.0060	-0.0046	-0.0046	-0.00388
Symmetric top molecules								
$^{15}NH_3$	0.5508	0.5615	0.5654	0.5677	0.5592	0.5629	0.5653	0.5654
	0.4870	0.4930	0.4963	0.4977	0.4916	0.4948	0.4951	0.5024
CHF_3	-0.0394	-0.0389	-0.0375	-0.0374	-0.0394	-0.0381	-0.0381	-0.0359
CH_3 ^{14}NC	-0.0589	-0.0608	-0.0588	-0.0589	-0.0601	-0.0582	-0.0580	-0.0546
$CH_3C^{15}N$	-0.0333	-0.0351	-0.0336	-0.0335	-0.0346	-0.0331	-0.0328	-0.0317
CH_3C ^{14}N	-0.0353	-0.0371	-0.0356	-0.0355	-0.0367	-0.0351	-0.0348	-0.0338
CD_3C ^{14}N	-0.0331	-0.0347	-0.0334	-0.0333	-0.0343	-0.0330	-0.0327	-0.0315
CH_3F	-0.0657	-0.0645	-0.0596	-0.0592	-0.0660	-0.0612	-0.0609	-0.0620
	0.2494	0.2567	0.2629	0.2642	0.2522	0.2583	0.2588	0.265
CH_3Cl	-0.0186	-0.0180	-0.0137	-0.0136	-0.0196	-0.0153	-0.0155	-0.0165
Asymmetric top molecules								
acrolein	-0.5574	-0.5738	-0.5656	-0.5688	-0.5550	-0.5466	-0.5451	-0.5512
C_3H_4O	-0.0578	-0.0609	-0.0599	-0.0605	-0.0592	-0.0582	-0.0583	-0.0567
	-0.0079	-0.0079	-0.0062	-0.0061	-0.0086	-0.0069	-0.0070	-0.0080
propene	-0.0903	-0.0936	-0.0881	-0.0879	-0.0953	-0.0900	-0.0905	-0.0789
C_3H_6	-0.0441	-0.0455	-0.0430	-0.0431	-0.0449	-0.0425	-0.0424	-0.0424
	0.0101	0.0107	0.0135	0.0137	0.0096	0.0123	0.0122	0.0107
propynal	-0.5713	-0.5865	-0.5787	-0.5814	-0.5627	-0.5546	-0.5501	-0.553
C_3H_2O	-0.0398	-0.0426	-0.0416	-0.0419	-0.0409	-0.0398	-0.0397	-0.040
	-0.0147	-0.0153	-0.0139	-0.0138	-0.0156	-0.0142	-0.0141	-0.015
dimethylether	-0.0552	-0.0478	-0.0356	-0.0343	-0.0524	-0.0402	-0.0399	-0.0214
CH_3OCH_3	-0.0074	-0.0061	-0.0037	-0.0035	-0.0071	-0.0047	-0.0048	-0.0093
	-0.0238	-0.0228	-0.0205	-0.0203	-0.0240	-0.0217	-0.0218	-0.0210
dimethylsulfane	-0.0268	-0.0239	-0.0149	-0.0144	-0.0277	-0.0184	-0.0189	-0.0193
CH_3SCH_3	0.0006	0.0004	0.0038	0.0036	-0.0007	0.0026	0.0021	0.0000
	-0.0086	-0.0089	-0.0062	-0.0065	-0.0101	-0.0075	-0.0080	-0.0083
acetaldehyde	-0.3641	-0.3834	-0.3743	-0.3796	-0.3601	-0.3510	-0.3495	-0.3609
C_2H_4O	-0.0732	-0.0768	-0.0749	-0.0759	-0.0734	-0.0715	-0.0715	-0.0731
	-0.0253	-0.0251	-0.0225	-0.0225	-0.0257	-0.0232	-0.0233	-0.0245
formaldehyde	-2.9286	-3.0654	-2.9966	-3.0271	-2.9232	-2.8567	-2.8457	-2.9017
H_2CO	-0.2276	-0.2342	-0.2319	-0.2338	-0.2248	-0.2224	-0.2207	-0.2243
	-0.1101	-0.1034	-0.0939	-0.0921	-0.1057	-0.0962	-0.0949	-0.0994
thioformaldehyde	-5.4460	-5.6181	-5.4575	-5.5541	-5.4135	-5.2558	-5.2967	-5.2602
H_2CS	-0.1353	-0.1415	-0.1393	-0.1410	-0.1354	-0.1332	-0.1323	-0.1337
	-0.0280	-0.0245	-0.0170	-0.0169	-0.0271	-0.0195	-0.0200	-0.0239
formic acid	-0.3112	-0.3328	-0.3283	-0.3321	-0.3115	-0.3068	-0.3043	-0.2797
HCOOH	-0.0903	-0.0933	-0.0916	-0.0923	-0.0913	-0.0895	-0.0896	-0.0903

Continued

Continued

Molecule	KT2	B3LYP	B97-2	B97-3	O-B3LYP	O-B97-2	O-B97-3	Exp.
	-0.0292	-0.0295	-0.0277	-0.0278	-0.0294	-0.0278	-0.0278	-0.0270
formamide	-0.2843	-0.3000	-0.2939	-0.2950	-0.2857	-0.2798	-0.2770	-0.2843
$HCONH_2$	-0.0666	-0.0697	-0.0676	-0.0682	-0.0677	-0.0656	-0.0655	-0.0649
	-0.0119	-0.0124	-0.0100	-0.0101	-0.0124	-0.0102	-0.0102	-0.0117
glycoaldehyde	-0.1185	-0.1197	-0.1140	-0.1145	-0.1159	-0.1102	-0.1093	-0.1239
$C_2H_4O_2$	-0.0733	-0.0767	-0.0750	-0.0759	-0.0736	-0.0720	-0.0720	-0.0726
	-0.0130	-0.0144	-0.0125	-0.0127	-0.0148	-0.0130	-0.0132	-0.0178
methyl formate	-0.1370	-0.1394	-0.1340	-0.1347	-0.1365	-0.1311	-0.1308	-0.1267
$C_2H_4O_2$	-0.0397	-0.0413	-0.0398	-0.0402	-0.0403	-0.0389	-0.0389	-0.0391
	-0.0179	-0.0185	-0.0169	-0.0169	-0.0187	-0.0172	-0.0173	-0.0167
ketene	-0.3433	-0.3848	-0.3601	-0.3743	-0.3517	-0.3267	-0.3306	-0.4182
H_2C_2O	-0.0349	-0.0377	-0.0350	-0.0351	-0.0372	-0.0346	-0.0345	-0.0356
	-0.0247	-0.0268	-0.0250	-0.0255	-0.0256	-0.0238	-0.0238	-0.0238
difluoromethane	-0.0935	-0.0842	-0.0765	-0.0747	-0.0883	-0.0807	-0.0793	-0.0725
CH_2F_2	-0.0434	-0.0431	-0.0412	-0.0412	-0.0437	-0.0418	-0.0419	-0.0411
	-0.0413	-0.0415	-0.0401	-0.0401	-0.0419	-0.0405	-0.0405	-0.0398
carbonic difluoride	-0.0581	-0.0598	-0.0581	-0.0586	-0.0589	-0.0572	-0.0574	-0.0568
F_2CO	-0.0760	-0.0786	-0.0767	-0.0773	-0.0773	-0.0754	-0.0755	-0.0747
	-0.0331	-0.0335	-0.0323	-0.0325	-0.0337	-0.0326	-0.0328	-0.0328
formyl fluoride	-0.4276	-0.4435	-0.4377	-0.4414	-0.4247	-0.4186	-0.4165	-0.4227
HFCO	-0.0786	-0.0812	-0.0798	-0.0804	-0.0794	-0.0780	-0.0780	-0.0771
	-0.0383	-0.0384	-0.0368	-0.0369	-0.0386	-0.0372	-0.0372	-0.0371
fluoroethene	-0.1717	-0.1751	-0.1712	-0.1700	-0.1754	-0.1715	-0.1709	-0.1533
C_2H_3F	-0.0545	-0.0569	-0.0549	-0.0552	-0.0558	-0.0539	-0.0539	-0.0526
	-0.0044	-0.0042	-0.0021	-0.0021	-0.0048	-0.0028	-0.0029	-0.0037
1,1-difluoroethene	-0.0436	-0.0450	-0.0431	-0.0432	-0.0454	-0.0435	-0.0437	-0.0421
CH_2CF_2	-0.0499	-0.0523	-0.0499	-0.0501	-0.0512	-0.0488	-0.0486	-0.0466
	-0.0128	-0.0129	-0.0115	-0.0116	-0.0133	-0.0120	-0.0121	-0.0119
cis-difluoroethene	-0.1169	-0.1153	-0.1096	-0.1091	-0.1165	-0.1109	-0.1105	-0.1015
CHFCHF	-0.0303	-0.0319	-0.0309	-0.0310	-0.0313	-0.0304	-0.0303	-0.0296
	-0.0168	-0.0169	-0.0155	-0.0155	-0.0174	-0.0160	-0.0161	-0.0158
fluoroethane	-0.0106	-0.0062	0.0024	0.0034	-0.0099	-0.0013	-0.0011	0.0185
CH_3CH_2F	-0.0121	-0.0123	-0.0100	-0.0100	-0.0130	-0.0108	-0.0109	-0.0124
	-0.0255	-0.0258	-0.0238	-0.0238	-0.0264	-0.0244	-0.0246	-0.0197
trifluoroethene	-0.0550	-0.0556	-0.0531	-0.0530	-0.0558	-0.0534	-0.0532	-0.0503
$CHFCF_2$	-0.0331	-0.0342	-0.0328	-0.0330	-0.0340	-0.0327	-0.0327	-0.0321
	-0.0169	-0.0175	-0.0166	-0.0167	-0.0178	-0.0169	-0.0171	-0.0170
ozone	-2.9230	-3.6369	-3.6351	-3.7980	-2.8729	-2.8508	-2.7752	-2.9877
O_3	-0.2313	-0.2657	-0.2635	-0.2729	-0.2259	-0.2226	-0.2195	-0.2295
	-0.0792	-0.0783	-0.0751	-0.0754	-0.0782	-0.0752	-0.0754	-0.0760
sulfur dioxide	-0.6586	-0.6836	-0.6934	-0.6925	-0.6434	-0.6510	-0.6388	-0.6043
SO_2	-0.1188	-0.1207	-0.1196	-0.1200	-0.1179	-0.1168	-0.1164	-0.11634
	-0.0845	-0.0863	-0.0846	-0.0853	-0.0861	-0.0845	-0.0851	-0.08865
difluorooxide	-0.2292	-0.2202	-0.2121	-0.2075	-0.2263	-0.2187	-0.2155	-0.213
OF_2	-0.0606	-0.0606	-0.0585	-0.0580	-0.0611	-0.0590	-0.0587	-0.058
	-0.0729	-0.0738	-0.0714	-0.0715	-0.0720	-0.0698	-0.0694	-0.068
hypofluoros acid	0.6573	0.6741	0.6742	0.6796	0.6726	0.6728	0.6758	0.642
HOF	-0.1188	-0.1212	-0.1164	-0.1164	-0.1211	-0.1165	-0.1161	-0.119
	-0.0684	-0.0676	-0.0633	-0.0629	-0.0692	-0.0650	-0.0648	-0.061
water	0.6331	0.6534	0.6539	0.6591	0.6514	0.6519	0.6547	0.657
H_2O	0.7083	0.7170	0.7179	0.7238	0.7160	0.7171	0.7167	0.718
	0.6227	0.6395	0.6405	0.6445	0.6377	0.6386	0.6401	0.645
hydrogendisulfide	0.4076	0.3951	0.4083	0.4031	0.3907	0.4033	0.3992	0.355

Continued

Continued

Molecule	KT2	B3LYP	B97-2	B97-3	O-B3LYP	O-B97-2	O-B97-3	Exp.
H_2S	0.2020	0.1738	0.1952	0.1871	0.1733	0.1936	0.1849	0.195
	0.2438	0.2243	0.2389	0.2331	0.2210	0.2349	0.2288	0.209
methylenecyclopropane	-0.0754	-0.0727	-0.0672	-0.0664	-0.0752	-0.0698	-0.0696	-0.0672
C_4H_6	-0.0265	-0.0269	-0.0247	-0.0246	-0.0270	-0.0249	-0.0248	-0.0231
	0.0254	0.0261	0.0283	0.0284	0.0248	0.0269	0.0267	0.0244
cyclopropene	-0.0910	-0.0973	-0.0955	-0.0955	-0.0925	-0.0908	-0.0890	-0.0897
C_3H_4	-0.1638	-0.1606	-0.1521	-0.1517	-0.1615	-0.1532	-0.1532	-0.1492
	0.0492	0.0529	0.0558	0.0564	0.0501	0.0528	0.0529	0.0536
aziridine	-0.0466	-0.0428	-0.0350	-0.0342	-0.0464	-0.0387	-0.0387	-0.0422
C_2H_5N	0.0171	0.0212	0.0266	0.0273	0.0179	0.0231	0.0232	0.0229
	0.0527	0.0520	0.0550	0.0549	0.0500	0.0528	0.0522	0.0539
oxirane	-0.1028	-0.1007	-0.0932	-0.0924	-0.1038	-0.0964	-0.0963	-0.0946
C_2H_4O	0.0096	0.0152	0.0201	0.0209	0.0121	0.0168	0.0169	0.0189
	0.0310	0.0310	0.0337	0.0337	0.0291	0.0317	0.0312	0.0318
thiirane	-0.0190	-0.0174	-0.0097	-0.0102	-0.0211	-0.0136	-0.0151	-0.0159
C_2H_4S	-0.0296	-0.0274	-0.0221	-0.0217	-0.0301	-0.0249	-0.0249	-0.0242
	0.0489	0.0483	0.0503	0.0502	0.0468	0.0487	0.0483	0.0487
cyclopropenone	-0.2905	-0.2969	-0.2930	-0.2937	-0.2892	-0.2852	-0.2844	-0.2900
C_3H_2O	-0.1000	-0.1019	-0.0996	-0.0999	-0.1007	-0.0984	-0.0984	-0.0963
	-0.0138	-0.0111	-0.0086	-0.0084	-0.0123	-0.0098	-0.0098	-0.0121
methylcyclopropene	-0.0908	-0.0904	-0.0835	-0.0832	-0.0893	-0.0824	-0.0816	-0.0813
C_4H_6	-0.0455	-0.0461	-0.0443	-0.0444	-0.0454	-0.0436	-0.0435	-0.0261
	0.0180	0.0188	0.0206	0.0205	0.0176	0.0193	0.0189	0.0166
cyclobutene	-0.0555	-0.0575	-0.0545	-0.0547	-0.0565	-0.0535	-0.0531	-0.0516
C_4H_6	-0.0762	-0.0746	-0.0697	-0.0692	-0.0763	-0.0713	-0.0713	-0.0663
	-0.0261	-0.0217	-0.0196	-0.0187	-0.0233	-0.0212	-0.0208	-0.0219
oxetane	-0.0156	-0.0124	-0.0075	-0.0069	-0.0144	-0.0097	-0.0094	-0.0073
C_3H_6O	-0.0500	-0.0472	-0.0420	-0.0411	-0.0496	-0.0444	-0.0440	-0.0429
	-0.0847	-0.0781	-0.0749	-0.0741	-0.0795	-0.0763	-0.0758	-0.0747
beta-propiolactone	-0.0820	-0.0833	-0.0800	-0.0803	-0.0821	-0.0788	-0.0786	-0.0758
$C_3H_4O_2$	-0.0386	-0.0395	-0.0376	-0.0378	-0.0391	-0.0372	-0.0372	-0.0356
	-0.0332	-0.0331	-0.0319	-0.0320	-0.0333	-0.0322	-0.0323	-0.0319

For the hybrid functionals the uncoupled OEP evaluation gives g tensors which are a significant improvement over those from the conventional coupled evaluation. When all of the molecules are included, mean absolute errors reduce by at least a factor of 2 in moving from B3LYP, B97-2 and B97-3 to O-B3LYP, O-B97-2 and O-B97-3 respectively. The mean errors and standard deviations are reduced by more than a factor of 3. The percentage mean absolute error also reduces for the latter two functionals. When ozone is omitted the improvement is more modest, reflecting the fact that this molecule is particularly poorly described in conventional calculations. This may be expected since the method contains a fraction of the non-multiplicative Hartree–Fock exchange and the Hartree–Fock method is particularly poor for molecules with multireference character. In contrast, ozone is not particularly challenging for the OEP based calculations. The tensor elements for the ozone molecule in each approach are summarised in Table 6.7 and are compared with experimental values. The zero point vibrational corrections

of Ref. [228] are also applied to the experimental results in order to provide a more rigorous comparison. For all of the approaches the g_{zz} component is well described and application of the OEP method to the hybrid functionals leads to little change. In contrast the g_{yy} and particularly the g_{xx} components, exhibit large errors in the conventional evaluations and the OEP results give a significant improvement.

Table 6.6: Mean absolute error (MAE), mean error (ME), percentage mean absolute error (PMAE), and standard deviation (SD), for rotational g tensor elements, relative to experimental values.

	Including ozone				Excluding ozone			
	MAE	ME	PMAE	SD	MAE	ME	PMAE	SD
KT2	0.0082	−0.0043	10.9	0.0203	0.0078	−0.0048	11.1	0.0197
B3LYP	0.0153	−0.0133	11.3	0.0636	0.0107	−0.0087	11.2	0.0347
B97-2	0.0125	−0.0084	8.8	0.0583	0.0079	−0.0037	8.7	0.0224
B97-3	0.0149	−0.0107	9.2	0.0735	0.0091	−0.0049	9.1	0.0297
O-B3LYP	0.0077	−0.0037	12.0	0.0189	0.0070	−0.0046	12.2	0.0162
O-B97-2	0.0057	0.0013	7.1	0.0165	0.0048	0.0003	7.2	0.0120
O-B97-3	0.0064	0.0018	6.8	0.0214	0.0049	0.0003	6.9	0.0120

When all of the molecules are considered the quality of the methods in terms of the mean absolute errors can be summarised as,

$$\text{B3LYP} < \text{B97-3} < \text{B97-2} < \text{KT2} < \text{O-B3LYP} < \text{O-B97-3} < \text{O-B97-2} \qquad (6.2.3)$$

The best results are obtained with the O-B97-2 functional where the MAE, ME, PMAE and SD have values of just 0.0057, 0.0013, 7.1%, and 0.0165 respectively. The correlation between the O-B97-2 and experimental g tensors is presented in Figure 6.2. The slope and intercept of the linear trendline are 1.0102 and −0.0002 with $R^2 = 0.993$. If O_3 is omitted, O-B97-3 and O-B97-2 yield similar accuracy. Whether ozone is included or not, the OEP based evaluations out perform the KT2 functional which was found

Table 6.7: Rotational g tensor components for the ozone molecule.

	g_{xx}	g_{yy}	g_{zz}
KT2	−2.9230	−0.2313	−0.0792
B3LYP	−3.6369	−0.2657	−0.0783
B97-2	−3.6351	−0.2635	−0.0751
B97-3	−3.7980	−0.2729	−0.0754
O-B3LYP	−2.8729	−0.2259	−0.0782
O-B97-2	−2.8508	−0.2226	−0.0752
O-B97-3	−2.7752	−0.2195	−0.0754
Expt.	−2.9877	−0.2295	−0.0760
Expt.[a]	−2.9169	−0.2277	−0.0746

[a] Experimental results with calculated zero-point vibrational contributions (from Ref. [228]) removed.

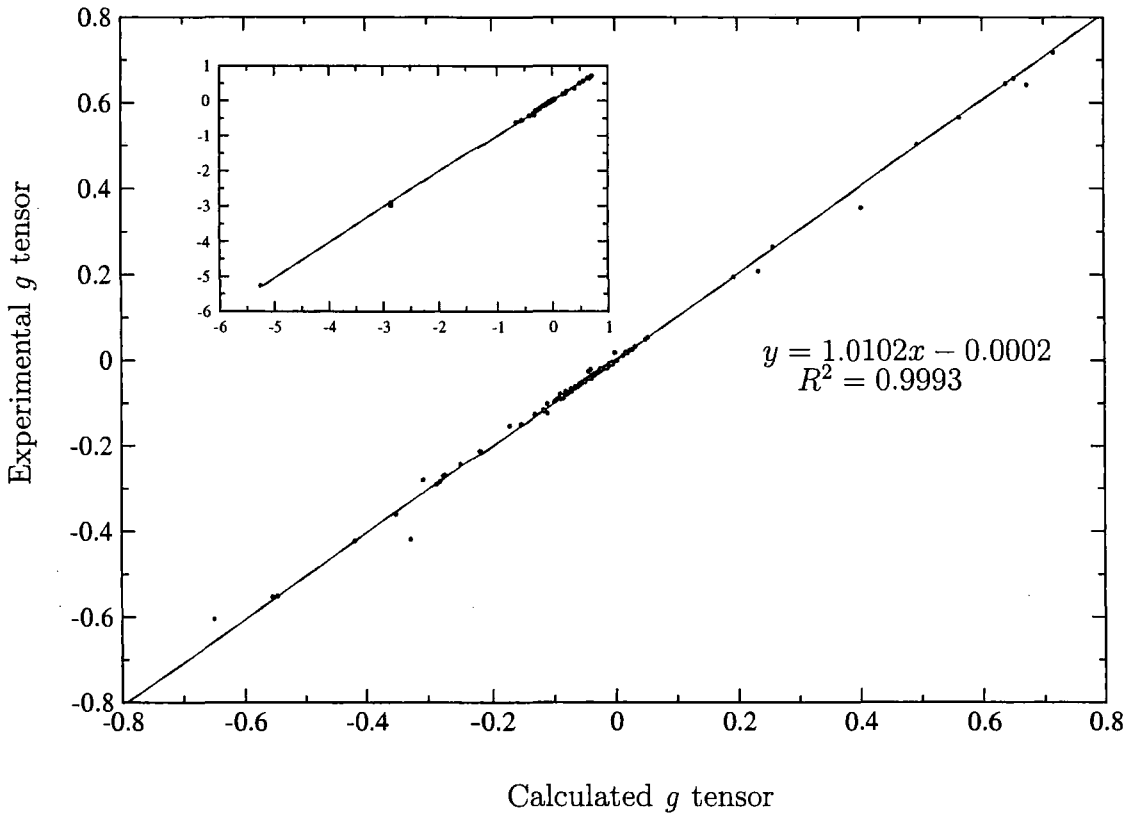

Figure 6.2: Correlation of O-B97-2 rotational g tensors with experimental values. The inset includes the entire range of g tensors.

to be most accurate DFT method in the study of Wilson *et al.* [245]

For the 22 linear molecules in Table 6.5, the errors in the calculated g tensors are particularly small. Over this subset the mean error of O-B97-3 is lowest at 0.0011 followed by O-B97-2(0.0013), KT2(0.0017), O-B3LYP(0.0018), B97-2(0.0040), B97-3(0.0049), and B3LYP(0.0050). The smallest errors approach experimental error bars. Molecules in the full set which are a particular improvement when the OEP evaluation is employed are CO, CS, CSe, HCN, thioformaldehyde, formaldehyde and sulfur dioxide. (It was the analysis of the OEP results that highlighted the error in the thioformaldehyde experimental number of Refs. [218] and [245]). One particularly difficult case is the largest component of the ketene g tensor for which the O-B97-2 value of -0.3267 is well above the experimental value of -0.4182; it is even less accurate than the B97-2 value of -0.3601. This data point is evident in Figure 6.2. The effect of changing the orbital and auxiliary basis sets was investigated and resulted in no significant improvement for this molecule. It is also notable that the KT2 GGA functional is relatively poor for ketene, with a value of -0.3433 for the largest component.

In our comparison with experiment we have not considered the effect of zero point vibrational corrections (ZPVCs) on rotational g tensors. These corrections may be used to remove the vibrational contributions from the experimental data. These quantities are difficult to compute although MCSCF values are available for NH_3, H_2O, HOF and O_3 [228–230] and a Hartree–Fock value is available for H_2S. For these molecules, errors relative to both corrected and uncorrected experimental data were computed. For the OEP methods the inclusion of ZPVCs *reduces* the MAE over this subset by an average of 6% whereas for the conventional evaluations the error is *increased* by an average of 14%. For all six methods the PMAEs actually increased slightly because of the small g tensor components, although the increase is smaller for OEP methods. The values for O_3 were given in Table 6.7. Although based on limited data, these observations lend further support to the view that the OEP hybrid functionals deliver improved predictions.

6.2.1 The Influence of Orbital Exchange

Following the observation in Section 6.1 that an amount of orbital exchange around 0.2 was optimal for the calculation of NMR shielding constants, we now investigate whether similar observations hold for g tensors determined from hybrid functionals via an OEP evaluation. The functionals of Ref. [152] with amounts of exchange, ξ, between 0 and 1 were used to determine g tensors of the representative subset of molecules CO, CSe, OCS, N_2O, NH_3, HOF, H_2O and SO_2. In Figure 6.3 the mean absolute error

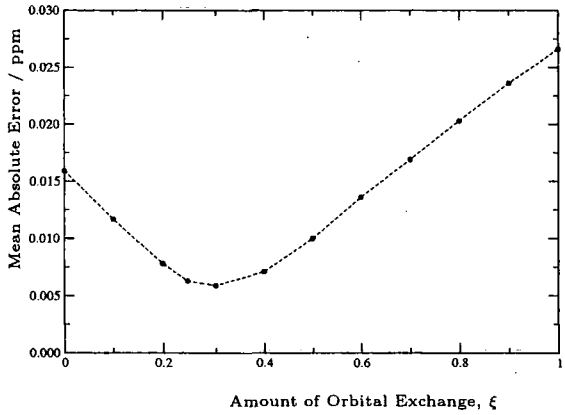

Figure 6.3: Mean absolute error for a subset of 8 molecules (see text) as a function of the amount of orbital exchange, ξ

relative to experiment is plotted as a function of ξ. In line with the NMR results of Ref. [152] and Section 6.1 the best g tensors are obtained with $\xi \approx 0.3$ which is consistent with previous observations regarding the similarity of WY/ZMP and OEP potentials.

6.2.2 Calculating g tensors from Coupled-Cluster Densities

All of the g tensor results presented up to this point have been for pure DFT calculations. We now consider the determination of g tensors directly from *ab initio* electron densities using the WY procedure. For the same subset of molecules as in Section 6.2.1, we calculated Brueckner-Doubles coupled-cluster relaxed density matrices and input them to our implementation of the WY procedure in the CADPAC code, which returns an optimal set of coefficients $\{b_t\}$. Since the same expansion is used in the WY procedure as in the OEP implementation these may again be transferred directly to the DALTON program and the uncoupled g tensors evaluated. The results are denoted WY(BD), and are presented in Table 6.8 along with results for the same subset calculated using the pure DFT methods. The mean absolute errors of conventional hybrids are in the range 0.0127(B97-2) to 0.0139(B97-3), whereas the OEP errors are between 0.0068(O-B97-3) and 0.0084(O-B3LYP). The WY(BD) results give a slightly lower error at 0.0066.

The WY(BD) results are of good quality. However they require the calculation of coupled cluster relaxed density matrices. The modest improvement in accuracy is therefore associated with a significant increase in the computational cost of the method. The WY(BD) results are not therefore applicable to larger systems.

Table 6.8: Rotational g tensors for a subset of molecules determined by experiment and calculated using DFT methods and the WY(BD) approach. The basis set used is aug-cc-pVTZ.

Molecule	KT2	B3LYP	B97-2	B97-3	O-B3LYP	O-B97-2	O-B97-3	WY(BD)	Exp.
CO	-0.2673	-0.2811	-0.2827	-0.2861	-0.2704	-0.2717	-0.2719	-0.2677	-0.2689
CSe	-0.2548	-0.2733	-0.2713	-0.2793	-0.2480	-0.2463	-0.2463	-0.2505	-0.2431
$O^{13}CS$	-0.0286	-0.0303	-0.0288	-0.0292	-0.0298	-0.0283	-0.0284	-0.0280	-0.028710
$^{15}N^{15}NO$	-0.0769	-0.0797	-0.0772	-0.0774	-0.0782	-0.0756	-0.0754	-0.0758	-0.07606
$^{15}NH_3$	0.5508	0.5615	0.5654	0.5677	0.5592	0.5629	0.5653	0.5693	0.5654
	0.4870	0.4930	0.4963	0.4977	0.4916	0.4948	0.4951	0.4988	0.5024
SO_2	-0.6586	-0.6836	-0.6934	-0.6925	-0.6434	-0.6510	-0.6388	-0.6121	-0.6043
	-0.1188	-0.1207	-0.1196	-0.1200	-0.1179	-0.1168	-0.1164	-0.1145	-0.11634
	-0.0845	-0.0863	-0.0846	-0.0853	-0.0861	-0.0845	-0.0851	-0.0854	-0.08865
HOF	0.6573	0.6741	0.6742	0.6796	0.6726	0.6728	0.6758	0.6866	0.642
	-0.1188	-0.1212	-0.1164	-0.1164	-0.1211	-0.1165	-0.1161	-0.1156	-0.119
	-0.0684	-0.0676	-0.0633	-0.0629	-0.0692	-0.0650	-0.0648	-0.0644	-0.061
water	0.6331	0.6534	0.6539	0.6591	0.6514	0.6519	0.6547	0.6632	0.657
H_2O	0.7083	0.7170	0.7179	0.7238	0.7160	0.7171	0.7167	0.7270	0.718
	0.6227	0.6395	0.6405	0.6445	0.6377	0.6386	0.6401	0.6474	0.645
MAE	0.0123	0.0132	0.0127	0.0139	0.0084	0.0079	0.0068	0.0066	
ME	-0.0094	-0.0086	-0.0075	-0.0067	-0.0040	-0.0028	-0.0013	0.0036	
PMAE	3.4	4.6	3.6	4.0	3.0	2.3	2.1	2.2	
SD	0.0162	0.0232	0.0257	0.0270	0.0136	0.0151	0.0132	0.0122	

6.3 Transition Metal NMR Chemical Shifts

In the preceding two sections we have demonstrated the applicability of the OEP hybrid functionals to the calculation of magnetic response properties for molecules consisting of main group atoms. Significant improvements over conventional DFT calculations were obtained. We now investigate the performance and limitations of the method by attempting to apply it to a set of much more challenging transition metal complexes. Specifically, we consider transition metal chemical shifts since very few absolute shielding constants for these systems are known. There has been substantial interest in using DFT for transition metal systems [255–263] due to the low computational cost of the method, and many authors have employed conventional hybrid functionals for this purpose. We now wish to determine whether the improvements in magnetic response properties observed for main group molecules extend to these more challenging systems.

We consider the chemical shifts of the transition metal nuclei in $TiCl_3CH_3$, CrO_4^{2-}, $Mn(CO)_6^+$, VF_5 and VOF_3, relative to $TiCl_4$, $Cr(CO)_6$, MnO_4^-, and $VOCl_3$ for the latter two complexes. Rather than using a two code approach for these calculations we extended the ability of our CADPAC OEP implementation to include the calculation of NMR shielding constants using the gauge-including-atomic-orbitals (GIAO) formalism, which is essential for the accurate determination of shielding constants in systems of this size. Specifically, we incorporated the GIAO implementation of Ref. [264] provided by Cohen [265] but with Gaussian rather than Slater type basis functions. All calculations

use an orbital basis set comprised of the 8s6p4d Wachters [266] basis set on the metal and 6-31G(d,p) on the ligands. For the Ti, Cr, and V complexes the calculations use the experimental geometries of Refs. [258], [259, 260] and [261] respectively. For the Mn complexes, no experimental structural data is available for $Mn(CO)_6^+$ and so following earlier studies by Bühl [263] we use the BP86 optimized geometry (r_{Mn-C} = 1.896 Å). For consistency in the calculation of the chemical shifts, we also employ the BP86 geometry of MnO_4^- (r_{Mn-O} = 1.624 Å compared with the experimental value of r_{Mn-O} = 1.629 Å). The calculated chemical shifts are compared with those of Refs. [258], [262] and [263] for Ti/V, Cr and Mn systems respectively. All conventional hybrid functional shieldings were determined using the DALTON program, since these require a coupled GIAO evaluation which is not implemented in the CADPAC code. All uncoupled values were determined using our extended CADPAC code.

6.3.1 Applying the OEP procedure to GGA Functionals

The OEP calculations require a choice of reference potential, $v_0(\mathbf{r})$, potential expansion basis set (see Eqn. (4.2.2)), and TSVD cutoff. To investigate these factors we first employed the OEP procedure to calculate potentials corresponding to GGA energy functionals. These energy functionals are explicit functionals of the density and should yield the same solution as the conventional evaluation (and hence the same uncoupled shieldings and chemical shifts), in the limit of a complete basis set with accurate convergence.

In their original implementation of the OEP method [112], Yang and Wu proposed the Fermi–Amaldi approximation [197] for the reference potential, $v_0(\mathbf{r})$, of Eqn. (4.2.2);

$$v_0^{\mathrm{FA}}(\mathbf{r}) = \left(1 - \frac{1}{N}\right) \int \frac{\rho_0(\mathbf{r}')}{|\mathbf{r} - \mathbf{r}'|} d\mathbf{r}' \tag{6.3.1}$$

where N is the number of electrons and $\rho_0(\mathbf{r})$ is a fixed reference density for the system. In the present case we use the converged B3LYP density for $\rho_0(\mathbf{r})$. The use of this reference potential ensures an asymptotic $-1/r$ dependence. This is appropriate when the Hartree–Fock energy functional is used, as in Chapters 4 and 5. However when the OEP procedure is applied to GGA functionals the potential must not exhibit this asymptotic behaviour, but instead should decay exponentially. It is therefore natural to omit the $-1/N$ term from the Fermi–Amaldi potential, leaving the bare Coulomb potential. Unfortunately calculations of NMR shielding constants using the Coulomb potential as reference gave undesirably large discrepancies between the conventional and OEP evaluations. Although these were reduced by using a large auxiliary set

Table 6.9: Transition metal NMR shielding constants and chemical shifts, in ppm, calculated using the BLYP and HCTH GGA functionals. All calculations use an uncoupled formalism. The OEP calculations use the reference potential in Eqn. (6.3.2).

Molecule	BLYP	O-BLYP [orb][a]	O-BLYP [large][b]	HCTH	O-HCTH [orb][a]	O-HCTH [large][b]	δ_{exp}
$TiCl_4$	−993	−988	−993	−1017	−1010	−1018	
$TiCl_3CH_3$	−1445	−1489	−1464	−1480	−1505	−1488	
δ	**453**	**501**	**471**	**464**	**495**	**471**	**613**
$Cr(CO)_6$	−672	−696	−676	−714	−723	−715	
CrO_4^{2-}	−2524	−2533	−2523	−2542	−2542	−2541	
δ	**1852**	**1837**	**1848**	**1828**	**1819**	**1826**	**1795**
MnO_4^-	−3693	−3733	−3692	−3698	−3732	−3695	
$Mn(CO)_6^+$	−1804	−1877	−1814	−1863	−1893	−1866	
δ	**−1889**	**−1856**	**−1877**	**−1834**	**−1839**	**−1830**	**−1445**
$VOCl_3$	−1919	−1918	−1921	−1956	−1949	−1957	
VF_5	−1183	−1177	−1182	−1217	−1204	−1217	
δ	**−736**	**−742**	**−739**	**−739**	**−744**	**−740**	**−895**
VOF_3	−1201	−1198	−1201	−1235	−1220	−1236	
δ	**−718**	**−720**	**−720**	**−721**	**−728**	**−721**	**−757**
$\|d\|$	172	151	164	153	143	150	
RMS	224	203	216	200	196	197	

[a] SVD cutoff of 10^{-8}
[b] SVD cutoff of 10^{-10}

they still remained unacceptable. Several choices of TSVD cutoff were considered but sufficiently accurate results could not be obtained and for some systems convergence problems were encountered.

To reduce the burden on the linear combination of Gaussian functions in Eqn. (4.2.2) and allow accurate results to be obtained with more modest basis sets, we require a reference potential that more closely resembles that of the true Kohn–Sham effective potential. As such, we note that the potentials of all GGA functionals are dominated by Dirac exchange and so we consider the addition of a Dirac type contribution to $v_0(\mathbf{r})$

$$v_0^D(\mathbf{r}) = \int \frac{\rho_0(\mathbf{r}')}{|\mathbf{r}-\mathbf{r}'|} d\mathbf{r}' - \frac{4C_x}{3}\rho_0^{\frac{1}{3}}(\mathbf{r}) \tag{6.3.2}$$

where

$$C_x = \frac{3}{4}\left(\frac{3}{\pi}\right)^{\frac{1}{3}} \tag{6.3.3}$$

Spin labels are not included since we consider only closed shell complexes. In Table 6.9 we present the conventional uncoupled BLYP shielding constants and chemical shifts along with those determined using the OEP procedure on the BLYP functional, denoted O-BLYP, using the reference potential of Eqn. (6.3.2). The mean absolute and RMS errors of the chemical shifts relative to experiment are also listed.

Two choices of auxiliary basis set are considered, firstly the column denoted O-BLYP[orb] considers the case where the primary orbital Wachters/6-31G(d,p) basis is used in the expansion of $v_s(\mathbf{r})$. This ensures perfect balance between the orbital and

auxiliary basis sets which is beneficial in the OEP procedure (see Section 4.6). For all choices of auxiliary basis set we chose a TSVD cutoff which was as small as possible, without introducing unphysical shifts or structure into the exchange–correlation potential which is obtained via

$$v_{\mathrm{xc}}(\mathbf{r}) = v_0(\mathbf{r}) - v_{\mathrm{J}}(\mathbf{r}) + \sum_t b_t g_t(\mathbf{r}) \tag{6.3.4}$$

Figure 6.9 presents plots of the potential for the representative complex CrO_4^{2-}. The exchange–correlation potential is plotted along the z axis, which is the principle axis in this tetrahedral molecule and the Cr atom is at z=0. For O-BYLP[orb] calculations it was found that a TSVD cutoff of 10^{-8} was optimal, reducing the value further introduced an unphysical shift in the exchange–correlation potential, which can be traced to the most diffuse basis functions in the potential expansion [196]. Considering the modest size of the orbital basis set used in the expansion, the chemical shifts obtained are in relatively good agreement with the conventional BLYP values. The average absolute discrepancies between BLYP and O-BLYP[orb] shieldings and chemical shifts are 23 and 21 ppm respectively. The corresponding exchange–correlation potentials for CrO_4^{2-} are compared in Figure 6.4(a) and 6.4(b). The agreement is generally good although the OEP potential smooths over much of the characteristic intershell structure and does not reproduce the divergence at the nuclei [267].

It is desirable to reduce the discrepancy between the BLYP and O-BLYP chemical shifts further. Test calculations for $TiCl_3CH_3$ were performed but no significant improvement was obtained by i) adding an f function to the metal basis, ii) partial uncontraction of the metal basis, and iii) increasing the size of the ligand basis set. In order to investigate this issue we chose to expand the potential in an extensive eventempered basis set. Initially a large basis independent of the nuclear charge, Z, was employed. However unphysical structure in the potential around the ligand atoms was observed, reflecting an imbalance between the 6-31G(d,p) orbital basis sets on those atoms and the large auxiliary set. The exchange–correlation potential around the metal was found to be much better behaved, since for this atom the more extensive Wachters basis provided a better balance with the large auxiliary set. It was therefore concluded that the auxiliary basis should be chosen to be Z-dependent and thus different on the different atoms. After extensive investigation and examination of the exchange–corelation potentials, it was decided that a suitable set could be derived by multiplying the Wachters metal contraction scheme by two and the 6-31G(d,p) ligand contraction scheme by three. The ranges were chosen to span the orbital basis and a universal base of 2.0 was employed. In order to avoid unphysical shifts in the potential

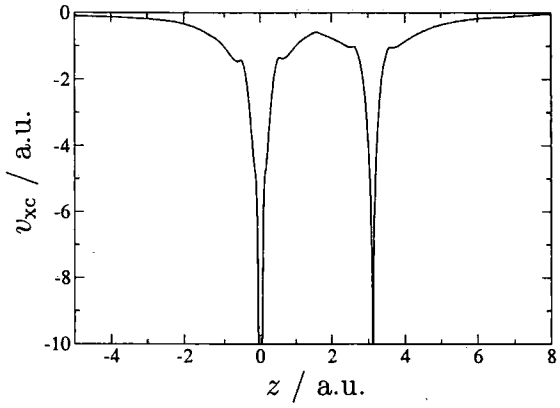

(a) BLYP

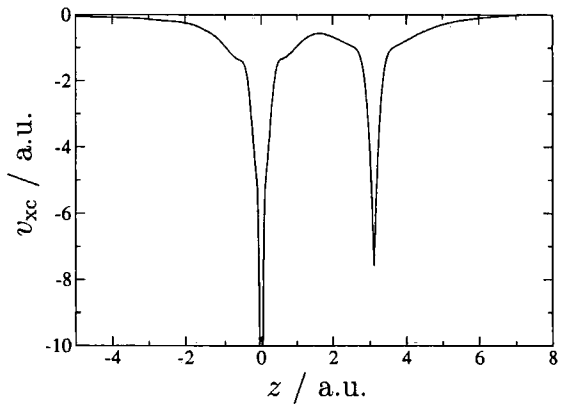

(b) O-BLYP, orb, cutoff 10^{-8}

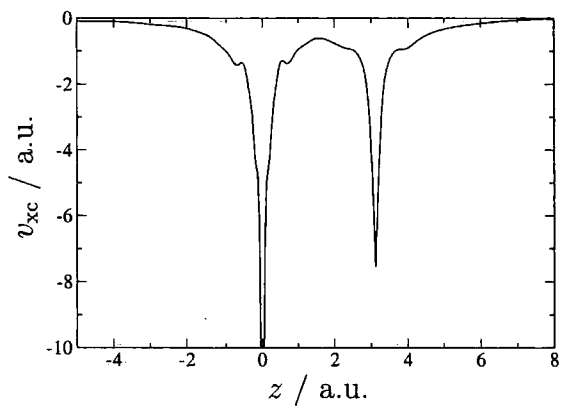

(c) O-BLYP, large, cutoff 10^{-10}

Figure 6.4: Exchange–correlation potentials for CrO_4^{2-} calculated using GGA energy functionals

Table 6.10: Ranges used to specify the exponents of eventempered basis sets

	K-Kr		Na-Ar		Li-Ne		H-He	
Ang. Mom.	min	max	min	max	min	max	min	max
s	-3	9	-3	7	-3	5	-2	3
p	-3	6	-3	4	-2	3	-1	1
d	-3	3	-1	1	-1	1	-	-

when using low TSVD cutoffs, exponents below 2^{-3} were discarded. The resulting basis set has the structure; 13s10p7d for the transition metals; 11s8p3d for Cl; 9s6p3d for C, O and F; and 6s3p for H. The ranges used are given in Table 6.10. In order to maximise agreement of the O-BLYP values with those of the BLYP functional reasonably high exponents must be included in the potential expansion. The introduction of higher angular momentum functions to the auxiliary set was found to lead to little improvement in the agreement.

The column in Table 6.9 denoted O-BLYP[large] lists the chemical shieldings and shifts obtained with this auxiliary basis set. It was found that a lower TSVD cutoff of 10^{-10} could be used, reflecting the fact that the lowest exponents of 2^{-3} are slightly higher than those of the orbital basis set. The most striking observation from these values is the improvement of the absolute shielding values which now reproduce the conventional BLYP values to within 1 ppm for the majority of compexes, demonstrating the need for a flexible potential expansion to determine these quantities precisely. For the largest complexes considered, namely $TiCl_3CH_3$, $Cr(CO)_6$ and $Mn(CO)_6^+$, the discrepancies are slightly larger. The average absolute discrepancy between BLYP and O-BLYP[large] shieldings and chemical shifts is just 4 and 8 ppm respectively. This is impressive considering the size of the molecules considered and the sensitivity of NMR parameters to the fine details of the exchange–correlation potential. The exchange–correlation potential of CrO_4^{2-} calculated using this larger auxiliary basis set is presented in Figure 6.4(c); the intershell structure is recovered.

The key idea of the OEP procedure is to find the multiplicative potential which gives rise to orbitals that minimise the total electronic energy. Since the BLYP functional is an explicit functional of the density, the energy and orbitals obtained should be equal to those of the conventional evaluation in the limit of a complete basis set. for the nine complexes considered the O-BLYP[orb] energies are higher by an average of just $2.5 \times 10^{-4} E_h$. Increasing the auxiliary basis set gives O-BLYP[large] values which have energies higher by an average of just $1.8 \times 10^{-6} E_h$.

To further test our choices of reference potential, auxiliary basis sets, and TSVD cutoffs we repeated similar OEP calculations with the HCTH GGA functional, which has previously been shown to provide good quality transition metal chemical shifts [257]. These values are also presented in Table 6.9. Conventional values are denoted HCTH

and the OEP values are denoted O-HCTH[orb] and O-HCTH[large] for each choice of auxiliary basis set. The reference potential used was again that of Eqn. (6.3.2) constructed using a B3LYP density and TSVD cutoffs of 10^{-8} and 10^{-10} were used for [orb] and [large] values respectively. The performance for this choice of GGA functional is even better, with discrepancies between HCTH and O-HCTH[orb] shielding and chemical shifts of 15 and 12 ppm. When the large auxiliary set is employed these errors reduce to just 2 and 3 ppm.

In summary, the use of a primary orbital basis set with appropriate reference potentials and TSVD cutoffs can give reasonably accurate chemical shifts, although these may benefit from some error cancellation when subtracting the calculated absolute shielding constants. The absolute shielding constants can be improved by use of a much more extensive potential expansion, providing care is taken to ensure reasonable balance with the primary orbital basis.

6.3.2 OEP Calculations using Hybrid Functionals

Following our investigation of the variables in the OEP method in the context of GGA functionals, for which the Kohn–Sham exchange–correlation potentials may be easily calculated and compared with those of the OEP evaluation, we return to the question of whether OEP hybrid functionals offer improvements over the conventional chemical shifts similar to those observed for main group molecules. Following the GGA observations a natural choice for the reference potential to be used with a hybrid energy functional is

$$v_0^{\mathrm{Hyb}}(\mathbf{r}) = \left(1 - \frac{\xi}{N}\right) \int \frac{\rho_0(\mathbf{r}')}{|\mathbf{r} - \mathbf{r}'|} d\mathbf{r}' - (1 - \xi)\frac{4C_{\mathrm{x}}}{3}\rho_0^{\frac{1}{3}}(\mathbf{r}) \qquad (6.3.5)$$

where ξ is the amount of orbital exchange in the functional. This choice provides the natural interpolation between the forms of Eqns. (4.2.3) and (6.3.2), which are appropriate for $\xi = 1$ and $\xi = 0$ respectively. This reference potential provides the correct asymptotic behaviour for all ξ, which is one of the key functions of the reference potential in the OEP procedure. We have calculated NMR chemical shifts and shielding constants with the conventional coupled B3LYP evaluation and uncoupled shielding constants using the OEP procedure with the same auxiliary basis sets as used for the GGA functionals; results are denoted O-B3LYP[orb] and O-B3LYP[large] and are presented in Table 6.11.

We first consider the O-B3LYP[orb] results. In each case moving from B3LYP to O-B3LYP[orb] the chemical shift moves in the direction of experiment, leading to no-

Table 6.11: Transition metal NMR shielding constants and chemical shifts, in ppm, calculated using the B3LYP and PBE0 hybrid functionals. Conventional/OEP calculations use a coupled/uncoupled formalism, respectively. The OEP calculations use the reference potential in Eqn. (6.3.5).

Molecule	B3LYP	O-B3LYP [orb][a]	O-B3LYP [large][b]	PBE0	O-PBE0 [orb][a]	O-PBE0 [large][b]	δ_{exp}
$TiCl_4$	−985	−831	−837	−934	−758	−764	
$TiCl_3CH_3$	−1462	−1353	−1348	−1421	−1272	−1267	
δ	**477**	**522**	**511**	**488**	**514**	**503**	**613**
$Cr(CO)_6$	−1018	−588	−602	−1021	−480	−497	
CrO_4^{2-}	−3038	−2429	−2431	−3106	−2346	−2358	
δ	**2020**	**1841**	**1829**	**2086**	**1866**	**1861**	**1795**
MnO_4^-	−4822	−3657	−3628	−5068	−3542	−3549	
$Mn(CO)_6^+$	−2636	−1771	−1799	−2748	−1612	−1645	
δ	**−2186**	**−1887**	**−1829**	**−2320**	**−1930**	**−1905**	**−1445**
$VOCl_3$	−2214	−1766	−1773	−2223	−1679	−1685	
VF_5	−1234	−1015	−1030	−1207	−948	−970	
δ	**−980**	**−752**	**−743**	**−1016**	**−732**	**−715**	**−895**
VOF_3	−1340	−1058	−1063	−1343	−993	−1004	
δ	**−873**	**−709**	**−710**	**−881**	**−687**	**−681**	**−757**
$\|d\|$	261	154	144	307	178	178	
RMS	354	213	191	420	235	228	

[a] SVD cutoff of 10^{-8}
[b] SVD cutoff of 10^{-4}

table improvement. The mean absolute error reduces from 261 ppm to 154 ppm, and the root mean square (RMS) error reduces from 354 ppm to 213 ppm. As in the GGA case a TSVD cutoff of 10^{-8} was used for all calculations with this auxiliary set. The exchange–correlation potential for CrO_4^{2-} is presented in Figure 6.5(a). Moving to the larger auxiliary basis set yields chemical shifts and shieldings which are close to those obtained using the primary orbital basis set, with mean absolute and RMS errors of just 144 ppm and 191 ppm respectively, a marginal improvement over the conventional HCTH GGA functional results. The O-B3LYP[large] exchange–correlation potential for CrO_4^{2-} is presented in Figure 6.5(b). In contrast to the GGA case, where smooth potentials could be obtained with a TSVD cutoff as low as 10^{-10}, a larger cutoff of 10^{-4} must be employed to ensure a smooth physical potential. To illustrate this the exchange–correlation potential for CrO_4^{2-} with the large auxiliary set and a TSVD cutoff of 10^{-6} is presented in Figure 6.5(c). The potential exhibits unphysical undulations between the nuclei and the intershell structure on oxygen is exaggerated. Reducing the cutoff causes further degradation of the potential, and with it the shielding constants and chemical shifts reduce in quality relative to experiment. These observations are consistent with those in Chapter 4 and of previous studies [107, 204, 208], which highlight the problem of unphysical structure when the orbital and auxiliary basis sets are unbalanced. This structure is eliminated in the present case by the choice of a large TSVD cutoff. It is noteworthy that the results then agree well with those using the primary orbital basis set for which there is no imbalance. Recent observations of

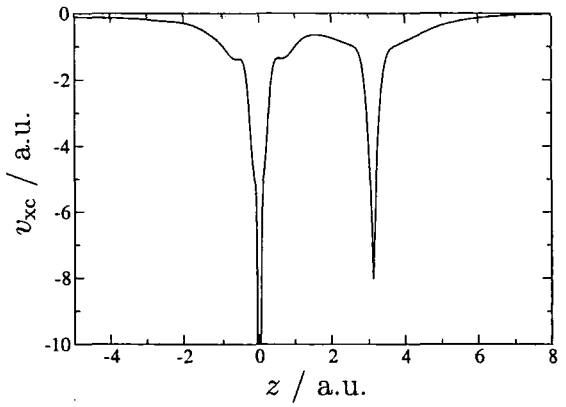

(a) O-B3LYP, orb, cutoff 10^{-8}

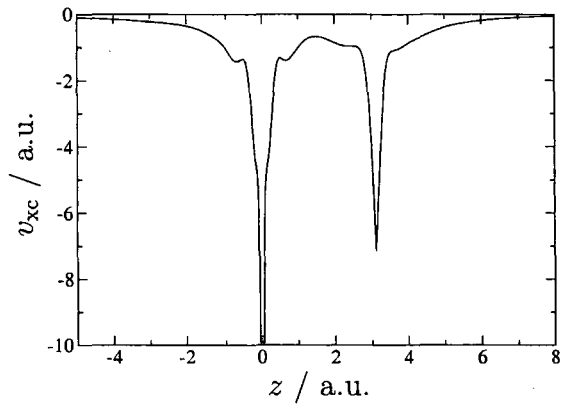

(b) O-B3LYP, large, cutoff 10^{-4}

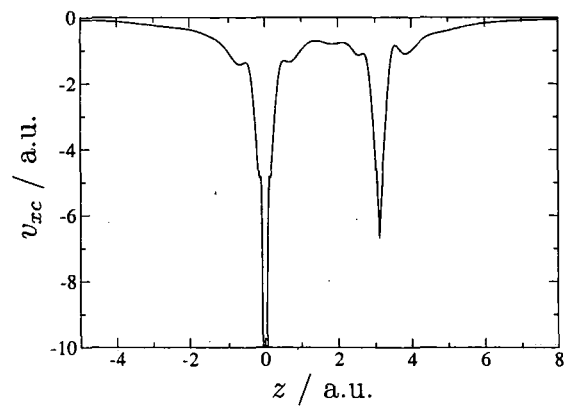

(c) O-B3LYP, large, cutoff 10^{-6}

Figure 6.5: Exchange–correlation potentials of CrO_4^{2-} calculated using hybrid energy functionals

Staroverov *et al.* are related and were discussed in detail in Section 4.6. We avoid their solutions by enforcing the Aufbau principle, choosing a large TSVD cutoff and carefully tailoring the auxiliary basis set, taking care to ensure a smooth exchange–correlation potential is obtained. As such we regard our solutions as approximations to the numerical OEP solutions. The O-B3LYP[orb] and O-B3LYP[large] total electronic energies are on average $2.8 \times 10^{-3} E_h$ and $1.8 \times 10^{-3} E_h$ higher than those of B3LYP and so despite the larger cutoff the use of a larger more flexible potential expansion yields lower energies. Also presented in Table 6.11 are PBE0 [214] ($\xi = 0.25$) values for which similar observations are made.

Throughout this chapter we have considered the application of the Yang–Wu OEP method to the calculation of magnetic response properties using OEP hybrid functionals. In all cases significant improvements over the conventional hybrid evaluations are obtained as a result of the improved orbital eigenvalue spectrum obtained with multiplicative potentials. For main group compounds the results obtained are also a significant improvement over those of widely used GGA functionals. For more challenging systems containing transition metal atoms the performance is only competitive with that of GGA functionals, however as improved orbital dependent functional forms are developed OEP based calculations are likely to become increasingly important.

Chapter 7

Chemical Application of Density Functional Theory

In Chapters 1–6 we have compared the results of calculations with results known from experiments since our aim was to quantify the improvements offered by new methodology. From a practical point of view the most important use of modern DFT calculations is their application to real chemical problems to offer insight into experimental observations. In this chapter we apply DFT to a problem of direct relevance to organic chemistry and crystal engineering. Specifically, we consider the interaction of an ammonium group and fluorine oriented β to it. Since relative energies and optimized geometries of molecules are insensitive to whether or not OEP based hybrid functionals are used, we use the computationally simple, conventional (non-Kohn–Sham) approach for the present calculations.

7.1 The Intramolecular β-Fluorine$\cdots$Ammonium Interaction in 4- and 8- Membered Rings

It has been reported [268] that 3-fluoropiperidinium **1** has a strong preference for the fluorine to be axial **1a** rather than in the equatorial conformation **1b**, as shown in Figure 7.1. The conformational preference of cis-3,5-difluoropiperidine **2** has also been explored and a similar preference for both fluorines to be axial **2a** rather than equatorial **2b** has been observed [269–271].

In neutral vicinal difluoro systems, for example 1,2-difluoroethane [272–274], β-fluoroethylamine [275], and esters of fluoroethanal [276] the stereoelectronic gauche effect is observed. This gives a preference for the the gauche conformation of the molecule and energy differences between the anti and gauche conformers in these neutral systems

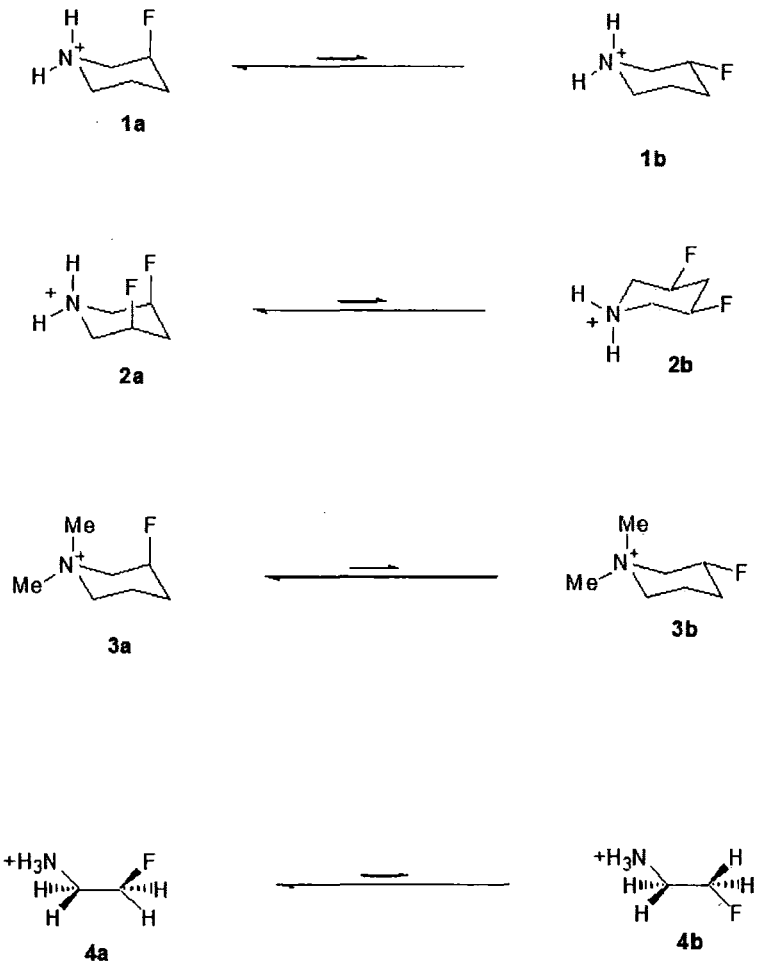

Figure 7.1: Vicinal C–F$\cdots$N$^+$ axial / gauche conformations are significantly favoured over the corresponding equatorial / trans relationships

are in the range $1.0-2.0$ kcal mol^{-1}. However in the charged 3-fluoropyrimidinium ring systems **1**–**3** the energy differences between the axial and equatorial conformations is much larger, and the stabilisation is in the range $4.0-5.0$ kcal mol^{-1} in favour of the axial conformation. Previously the conformation of the aliphatic β-fluoroethylamine hydrochloride system **4** was investigated [277]. The X-ray derived structure of **4** shows a clear gauche conformational preference as in **4a** over the anti conformer **4b**. The use of density functional theory (DFT) calculations indicated a gauche over anti preference of ~ 5.8 kcal mol^{-1}. In all of the systems **1**–**4**, the influence of intramolecular hydrogen bonding between the ammonium and β-fluorine groups is not dominating; both X-ray and theoretical structures do not reveal any short H$\cdots$F contacts. Also, in general fluorine forms only weak hydrogen bonding interactions [278–280]. To account for the higher stabilisation energies of the charged systems **1**–**4** relative to that observed due to the steroelectronic gauche effect in neutral systems, such as 1,2-difluoroethane, Snyder and Lankin proposed a C–F$\cdots$N$^+$ electrostatic orientating effect as the dominant interaction in these systems.

We now investigate the significance of this interaction to the molecular conformations of the 4-membered 3-fluoroazetidinium ring system **5** [281, 282] - which is the smallest possible β-fluoroammonium ring - and an 8-membered 1,5-diaza-ammonium-cyclooctane ring system **6**. This study was carried out in collaboration with group of O'Hagan (University of St. Andrews, UK), who provided the X-ray data for cation **5**. They also prepared a sample of the 3-fluoro-1,5-diazacyclooctane HBr salt **6** and determined its structure by X-ray crystallography. These structures are shown in Figure 7.2.

In order to quantify and investigate the intramolecular effect, calculations were carried out on the isolated systems using the B97-2 hybrid exchange–correlation energy functional [96]. Qualitatively similar results are obtained with the widely used B3LYP density functional and the more computationally demanding MP2 correlated wavefunction based method. Following the study of Ref [277], all calculations were performed with the TZ2P basis set [147], augmented with an additional s and p diffuse function on the non-hydrogen atoms. For the geometry optimizations the Gaussian 03 program was used [209] and analytic harmonic frequencies were calculated to confirm that the located stationary points are minima on the potential energy surface. The harmonic frequencies were also used to calculate zero point vibrational corrections, which are included in all quoted energy differences.

In Ref [277], the gauche and anti conformations of **4** were considered and the influence of the C–F$\cdots$N$^+$ interaction was quantified by comparing their electronic energies. For the 4-membered cationic ring system **5** it is no longer possible to establish gauche

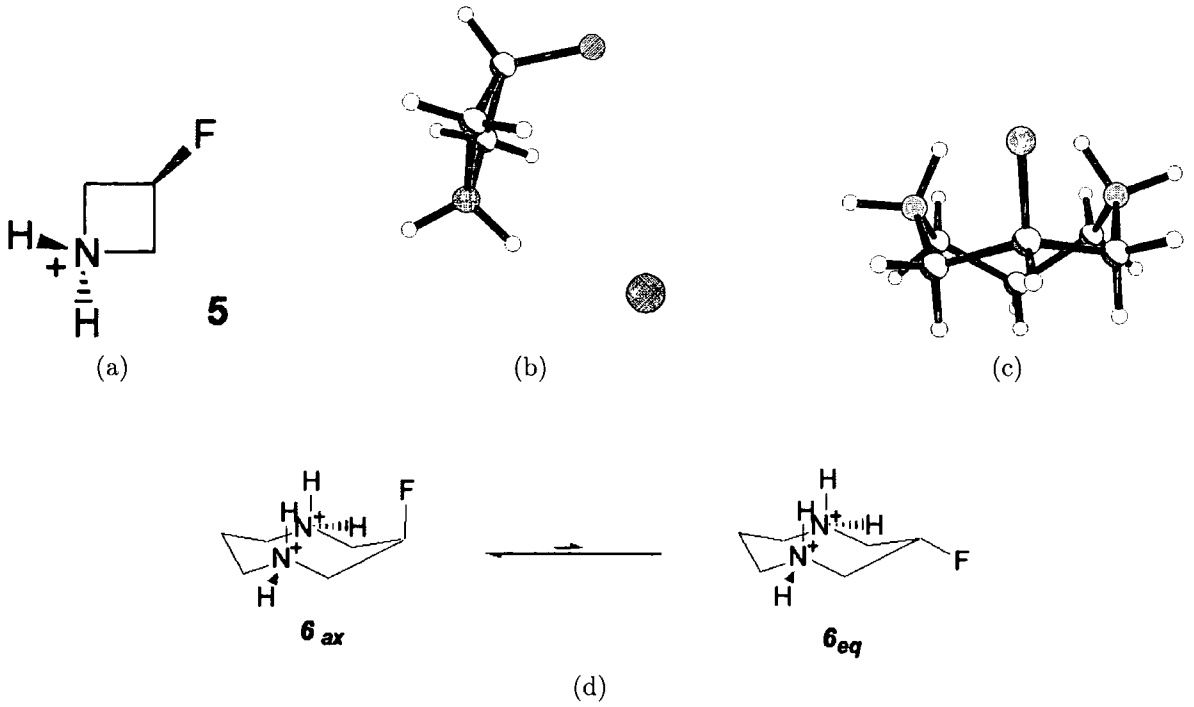

Figure 7.2: X-ray crystal structures of the compounds studied

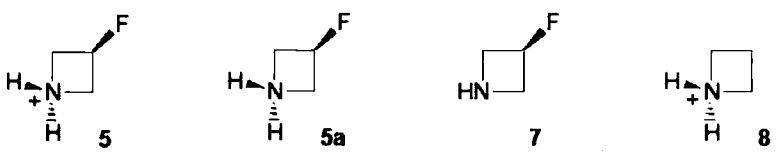

Figure 7.3: Species considered in DFT calculations

and anti conformations due to ring constraints. As an alternative, we suppress the interaction be removing the charge and/or replacing the fluorine atom by a hydrogen atom. The species on which calculations were performed are shown in Figure 7.3. The effect of the chloride counterion is also considered.

To investigate the influence of the net positive charge, the structure of β-fluoroazetidinium cation **5** was first compared with the corresponding neutral amine **7**. For the amine, stationary points were determined commencing from a range of conformations. Three stationary points were located. The lowest energy conformation is presented in Figure 7.4(a). The C–F and N–H groups are spatially well separated, with F$\cdots$H and F$\cdots$N distances of 3.96 Å and 3.28 Å respectively. The N–C–C–F torsion angle is 137.2°.

Adding a proton to amine **7** gives a chemical structure the same as cation **5** and this

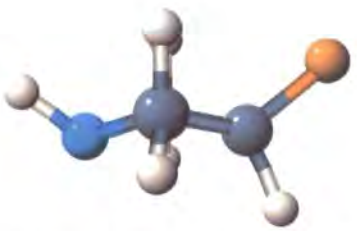

(a) DFT structure of amine **7**

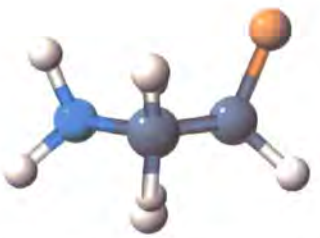

(b) DFT structure of cation **5**

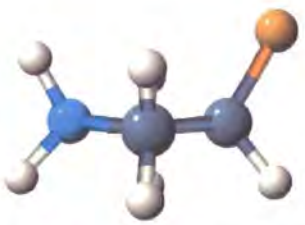

(c) X-ray structure of cation **5**

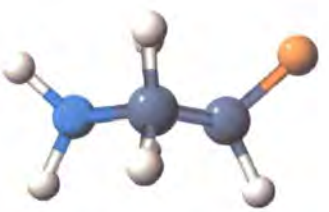

(d) DFT structure of neutral **5a**

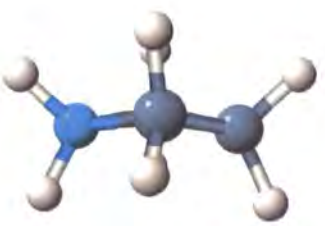

(e) DFT structure of cation **8**

Figure 7.4: X-ray and DFT optimized molecular conformations

geometry was used as a starting point for the optimization of the β-fluoroazetidinium cation. In the course of this optimization the ring pucker inverted relative to the F atom, causing the C–F and $^{+}$NH groups to approach each other more closely. This is consistent with an attractive electrostatic interaction between the groups. The optimized structure is presented in Figure 7.4(b), together with the corresponding X-ray structure in Figure 7.4(c). The calculated F$\cdots$H and F$\cdots$N distances reduce to 3.10 Å and 2.95 Å respectively and the N–C–C–F torsion angle reduces to 100.0°. Only one optimized geometry could be located for cation **5**; calculations staring from a range of other structures all converged to the same geometry.

So far we have suppressed the C–F$\cdots$N^{+} interaction by removing a proton from the cation **5** to produce the amine **7**. We next consider the addition of an extra electron to the LUMO of cation **5**, resulting in the chemically non-intuitive neutral species **5a**. The interaction is thus again suppressed but this time by the addition of an electron to the molecule. The structure of **5a** was then optimized beginning from an initial geometry equal to that of the optimized structure of **5**. During the course of this optimization the ring pucker inverted to give a structure similar to that of the neutral amine **7**. The optimized structure of **5a** is shown in Figure 7.4(d). All of these calculations clearly demonstrate the positive charge has a pronounced effect on the structure and are fully consistent with a dominant C–F$\cdots$N^{+} interaction.

As an alternative way to suppress the C–F$\cdots$N^{+} interaction we also replaced the fluorine atom in **5** by a Hydrogen atom. The optimized structure of this azetidinium ring **8** is presented in Figure 7.4(e). The dihedral angle, which was 100.0° in **5**, widens slightly to 102.3° in **8**. This is consistent with the removal of the C–F$\cdots$N^{+} interaction.

In the crystalline state the β-fluoroazetidinium molecules are obtained as the chloride salt. Each unit cell consists of four molecules and four counterions arranged as shown in Figure 7.5. To determine the effect of the Cl^{-} ion on the C–F$\cdots$N^{+} interaction, an unconstrained optimization was performed on one molecule with the Cl^{-} ion closest to it in the unit cell present, commencing from the experimental X-ray geometry. Unfortunately, in the course of this optimization the N–H bond closest to the counter ion became exceptionally long. A second optimization was also performed in which the positions of the hydrogen on nitrogen and the Cl^{-} ion were constrained to remain at their positions in the X-ray derived structure. The ring then puckered in a similar way to **7** and has a similar N–C–C–F torsion angle (134.1°), reflecting the strong electrostatic influence of the counterion, which clearly attenuates the C–F$\cdots$N^{+} interaction, consistent with an intramolecular electrostatic interaction. Both structures are presented in Figure 7.6.

The optimized structures of isolated molecules presented in Figure 7.4 are not di-

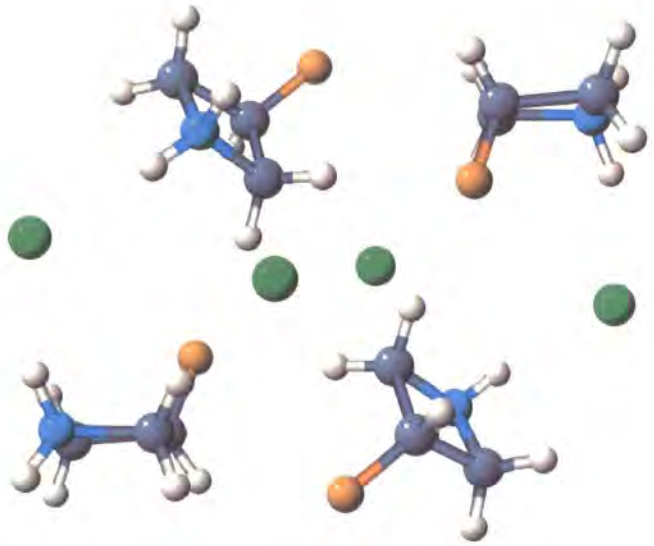

Figure 7.5: The contents of the unit cell for 3-fluoroazetidinium chloride

(a) Unconstrained Optimization

(b) Constrained Optimization

Figure 7.6: Optimized geometries in the presence of the Cl^- counter ion

(a) Axial Conformation

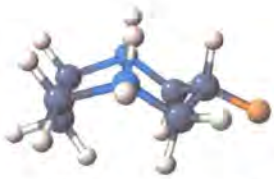

(b) Equatorial Conformation

Figure 7.7: Optimized Structures of the 3-fluoro-1,5-diazacyclooctane system

rectly comparable with the X-ray structures, since they take no account of the intermolecular effects. Even so, the X-ray structure of **5** in Figures 7.2(b) and 7.4(c) is intermediate between our optimized structures with and without the Cl^- counterion. The ring puckering more closely resembles that of the free cation **5**.

We now consider the 3-fluoro-1,5-diazacyclooctane HBr salt **6**. This 8-membered ring is much more conformationally flexible and the fluorine can potentially participate in two intramolecular C–F$\cdots$N$^+$ interactions simultaneously. The X-ray structure of the compound (Figure 7.2(c)) shows that the C–F bond occupies an axial orientation. There was no evidence of any disorder in the X-ray structure and of any molecules with the C–F bond lying in an equatorial conformation. DFT optimized geometries of both the axial and equatorial conformations of **6** were calculated and are presented in Figure 7.7.

The energy difference between the axial and equatorial conformations was computed, resulting in a preference for the axial conformer of 9.2 kcal mol^{-1}. This energy difference is consistent with that found for **2a** [269] and reflects the presence of two C–F$\cdots$N$^+$ interactions.

In summary, we have investigated the C–F$\cdots$N$^+$ interaction in two ring systems, with and without conformational flexibility. In both cases the interaction is significant in influencing the conformation adopted. The C–F$\cdots$N$^+$ interaction is similar in magnitude to that of a good hydrogen bond and so is worthy of consideration in the design of biologically relevant amine analogues. Since most aliphatic amines are protonated at physiological pH a fluorine incorporated β to an amine could be used as a tool to influence molecular conformation. The significance of the interaction could be controlled by the pK_a modulation. The fact that introduction of a fluorine leads to such an interaction without vastly altering the steric profile of the molecule may be of use in future drug design. An intermolecular analogue of the interaction may also find utility in the field of crystal engineering.

Chapter 8

Conclusions

The low computational cost and good accuracy of modern density functional theory calculations has led to their enormous popularity in chemistry. The quality of the results that can be obtained is determined by the accuracy of the approximation to the exchange–correlation energy. The most widely used functionals are the so called 'hybrid' functionals, which include a fraction of Hartree–Fock exchange, such as the ubiquitous B3LYP approximation. However, in virtually all implementations these functionals do not have a potential defined as a local multiplicative operator and so they are formally outside the Kohn–Sham scheme.

To bring these (and other orbital dependent) functionals back into the Kohn–Sham scheme, the optimized effective potential (OEP) method must be employed. The solution to this problem is, however, difficult and so in Chapter 2 we implemented and examined the performance of a number of methods to approximate it. These procedures were applied to the calculation of NMR shielding constants. It was found that the exchange-only localized Hartree–Fock (LHF) and Krieger-Li-Iafrate (KLI) procedures offer surprisingly accurate results relative to experiment, considering they contain no explicit electron correlation contributions. These potentials are notably different from those obtained using the Zhao-Morrison-Parr (ZMP) procedure. The use of these approximate exchange potentials in multiplicative hybrid functionals was also investigated and it was found that whilst in conventional functionals the optimal amount of orbital dependent exchange for the calculation of NMR shielding constants is approximately 0.2, the amount suitable for use in LHF/KLI based hybrids is higher, at approximately 0.6.

The performance of DFT methods utilising these approximate exchange potentials was then investigated further in Chapter 3 by considering excitation energies and properties related to structural perturbations. It was found that properties depending on the energy of the ground state were relatively insensitive to the representation of exchange

used. The properties of excited states were found to be much more sensitive, reflecting the importance of the virtual eigenvalue spectrum in their calculation, which is substantially different when multiplicative potentials are employed. The LHF method with no correlation functional was again found to be surprisingly accurate. As is commonly observed, the errors in the excitation energies for hybrid and GGA functionals were dominated by the Rydberg excitations which require an accurate description of the asymptotic exchange–correlation potential. To improve the quality of the results an asymptotic correction was applied, where required. Potential energy curves of the CO and N_2 molecules were then calculated and optimized geometries and vibrational frequencies of the ground and excited states calculated from them. The quality of the results was compared with those obtained using curves determined by application of the RKR procedure to experimentally determined Dunham coefficients. For all of the methods it was observed that as the energy of the states increases, the quality of the results degrades. The best overall quality was obtained with the HCTH(AC) GGA functional.

An implementation of the OEP methodology was then described in Chapter 4, which rigorously minimises the energy of orbital dependent functionals under the constraint that the orbitals are eigenstates of a local multiplicative potential. The procedure was implemented with both first and second order optimization schemes. Unexpected difficulties were encountered owing to the use of finite basis sets; the OEP potentials in a finite basis were found to be oscillatory. The magnitude of the oscillations can be related to the choices of orbital and potential expansion basis sets and the balance between them. To achieve smooth physical potentials along with smooth convergence of the energy and eigenvalues with respect to the choice of basis set, it is best to use second order optimization schemes with TSVD regularisation of the approximate Hessian and a relatively high cutoff of the singular values. A computationally similar procedure allowing the determination of the Kohn–Sham exchange–correlation potential corresponding to an input density was also implemented. Similar requirements for the calculation of smooth physical potentials apply. When this method is used with accurate *ab initio* coupled cluster electron densities then near exact Kohn–Sham orbitals, eigenvalues and exchange–correlation potentials can be obtained.

In light of the observations in Chapter 2, we further investigated differences between the exchange representations in Chapter 5, with reference to the essentially exact OEP quantities. Nuclear magnetic resonance (NMR) shielding constants were used as a sensitive probe of differences in the exchange potentials, since this quantity has explicit dependence on the Kohn–Sham orbitals and eigenvalues. The KLI and LHF methods give essentially the same results and the OEP and WY methods are also very similar to

each other. However, the KLI/LHF and OEP/WY methods are substantially different, the former giving values much closer to experiment. The quality of the NMR shielding constants obtained was rationalised by the accuracy of the HOMO–LUMO eigenvalue differences obtained from each method. The potentials, densities and HOMO/LUMO probability densities were then compared with the OEP equivalents for each method. For the WY procedure only small differences were observed although substantial differences were observed for the KLI/LHF methods. A spatial correlation between the density and potential differences was observed and a contraction of the LUMO orbital, consistent with the reduction in the HOMO–LUMO gap, was also evident. The OEP exchange only quantities were also compared with near exact quantities obtained from the application of the WY procedure to Brueckner-Doubles coupled cluster densities. The features observed are qualitatively similar to those observed for the LHF and KLI methods, indicating a degree of correlated character in the LHF and KLI procedures, which rationalises their unexpected accuracy in the determination of response properties. This character has implications for the use of these approximations in multiplicative hybrid functionals.

The OEP procedure was then applied to hybrid exchange–correlation functionals in Chapter 6 and these functionals were used to calculate a variety of magnetic response properties. To begin with, NMR shielding constants were calculated for main group molecules. The results obtained were a substantial improvement over conventional evaluations and approach the quality of the best *ab initio* calculations. The optimal amount of orbital dependent exchange to be used in the calculation of the shielding constants with these methods was also investigated. It was found that an amount of approximately 0.2 was optimal, in line with the amount found in conventional hybrid functionals. The OEP hybrid functionals were then applied to the calculation of rotational g tensors for which the results improved upon the conventional evaluations by a factor of 2 and are an improvement over the best DFT values reported in the literature. As a challenging test of the OEP procedure the method was then applied to the calculation of NMR chemical shifts for a series of transition metal complexes. Again the calculations provided a substantial improvement over the conventional calculation, and highlighted a number of important issues with the calculation of finite basis set optimized effective potentials.

In the final chapter we considered the application of density functional theory, as a predictive tool, to a problem of direct relevance to organic chemistry. The β-fluorine$\cdots$ammonium interaction was considered and its effect quantified by comparing optimised structures in which the interaction was present with similar structures in which it was suppressed. Results were also compared with X-ray structures. The

strength of the interaction was found to be on the order of a good hydrogen bond and significant in determining the molecular conformation. As such it may be of future use in the design of biologically active compounds and an intermolecular analogue of the interaction may be useful in the field of crystal engineering.

The main focus of this thesis has been the implementation and application of the OEP procedure and approximations to it. Since orbital dependent functionals provide a way to include non-local information in DFT, the importance of the OEP method in DFT is likely to grow in the coming years as the quest for improved exchange–correlation functionals continues.

Appendix A

Publications

Much of the work presented in this thesis has been published in peer-reviewed journals.

1. A. M. Teale and D. J. Tozer, 'Exchange Representations in Kohn-Sham NMR Shielding Calculations', *Chem. Phys. Lett.*, 2004, **383**, 109 [Ch. 2]

2. A. M. Teale and D. J. Tozer, 'Ground- and Excited-State Diatomic Bond Lengths, Vibrational Levels, and Potential Energy Curves from Conventional and Localised-Hartree-Fock-Based Density-Functional Theory', *J. Chem. Phys.*, 2005, **122**, 034101 [Ch. 3]

3. A. M. Teale and D. J. Tozer, 'Exchange Methods in Kohn–Sham Theory', *Phys. Chem. Chem. Phys.*, 2005, **7**, 2991 [Ch. 5]

4. O. B. Lutnæs, A. M. Teale, T. Helgaker and D. J. Tozer, 'Rotational g tensors Calculated using Hybrid Exchange–Correlation Functionals with the Optimized Effective Potential Approach', *J. Chem. Theory Comput.*, 2006, **2**, 827 [Ch. 6]

5. N. E. J. Gooseman, D. O'Hagan, A. M. Z. Slawin, A. M. Teale, D. J. Tozer and R. J. Young, 'The Intramolecular β-Fluorine$\cdots$Ammonium Interaction in 4- and 8- Membered Rings', *Chem. Comm.*, 2006, **30**, 3190 [Ch. 7]

6. A. M. Teale, A. J. Cohen and D. J. Tozer, 'Transition Metal NMR Chemical Shifts from Optimized Effective Potentials', submitted to *J. Chem. Phys.*, October, 2006 [Ch. 6]

Appendix B

Conferences and Courses Attended

1. 24 - 29 July, 2004
   Molecular Quantum Mechanics: The No Nonsense Path to Progress. An International Conference in Honour of Professor Nicholas C. Handy
   University of Cambridge, UK

2. 24 September, 2004
   CCP1 special interest group meeting on DFT response properties
   CCLRC Daresbury Laboratory, UK

3. 13 April, 2005
   25th Anniversary Graduate Student Meeting of the Royal Society of Chemistry's Theoretical Chemistry Group
   University of Nottingham, UK

4. 11 - 15 September, 2005
   11th International Conference on the Applications of Density Functional Theory in Chemistry and Physics
   Université de Genève, Geneva, Switzerland

5. 25 June - July 7, 2006
   The 9th Sostrup Summer School: QUANTUM CHEMISTRY and MOLECULAR PROPERTIES
   Himmelbjergegnens Natur- og Idrtsefterskole, Denmark

Bibliography

[1] E. Schrödinger, *Ann. d. Phys.*, 1926, **79**, 361

[2] E. Schrödinger, *Ann. d. Phys.*, 1926, **79**, 489

[3] E. Schrödinger, *Die Naturwissenschaften*, 1926, **28**, 664

[4] E. Schrödinger, *Ann. d. Phys.*, 1926, **79**, 734

[5] E. Schrödinger, *Ann. d. Phys.*, 1926, **80**, 437

[6] E. Schrödinger, *Collected Papers on Wave Mechanics*, Blackie and Son Limited, London and Glasgow, 1928

[7] M. Born, *Z. Physik*, 1926, **38**, 803

[8] P. A. M. Dirac, *Proc. Roy. Soc.*, 1928, **A117**, 610

[9] P. A. M. Dirac, *Proc. Roy. Soc.*, 1928, **A118**, 351

[10] W. Pauli, *Z. Physik*, 1925, **31**, 765

[11] M. Born and J.R. Oppenheimer, *Ann. d. Phys.*, 1927, **84**, 457

[12] D. R. Hartree, *Proc. Camb. Phil. Soc.*, 1928, **24**, 89

[13] D. R. Hartree, *Proc. Camb. Phil. Soc.*, 1928, **24**, 111

[14] D. R. Hartree, *Proc. Camb. Phil. Soc.*, 1928, **24**, 426

[15] J. C. Slater, *Phys. Rev.*, 1929, **34**, 1293

[16] J. C. Slater, *Phys. Rev.*, 1930, **35**, 509

[17] V. Fock, *Z. Phys.*, 1930, **61**, 126

[18] V. Fock, *Z. Phys.*, 1930, **62**, 765

[19] J. C. Slater, *Phys. Rev.*, 1930, **36**, 57

[20] S. F. Boys, *Proc. Roy. Soc.*, 1950, **A200**, 542

[21] T. H. Dunning, *J. Chem. Phys.*, 1970, **53**, 2823

[22] R. Ditchfield, W. J. Hehre and J. A. Pople, *J. Chem. Phys.*, 1971, **54**, 724

[23] W. J. Hehre, R. Ditchfield and J. A. Pople, *J. Chem. Phys.*, 1972, **56**, 2257

[24] P. C. Hariharan and J. A. Pople, *Theor. Chim. Acta.*, 1973, **28**, 213

[25] J. A. Pople and R. K. Nesbet, *J. Chem. Phys.*, 1954, **22**, 571

[26] P. Pulay, *J. Comput. Chem.*, 1982, **3**, 556

[27] M. F. Guest and V. R. Saunders, *Mol. Phys.*, 1974, **28**, 819

[28] C. C. J. Roothaan, *Rev. Mod. Phys.*, 1960, **32**, 179

[29] C. G. Hall, *Proc. Roy. Soc.*, 1951, **A205**, 541

[30] P-O. Löwdin, *Adv. Chem. Phys.*, 1959, **2**, 207

[31] J. A. Pople, J. S. Binkley and R. Seeger, *Int. J. Quant. Chem.*, 1976, **S10**, 1

[32] R. Krishnan and J. A. Pople, *Int. J. Quant. Chem.*, 1978, **14**, 91

[33] S. F. Boys, *Proc. Roy. Soc.*, 1950, **A201**, 125

[34] S. R. Langhoff and E. R. Davidson, *Int. J. Quant. Chem.*, 1974, **8**, 61

[35] J. A. Pople, M. Head-Gordon and K. Raghavachari, *J. Chem. Phys.*, 1987, **87**, 5968

[36] J. Čižek, *J. Chem. Phys.*, 1966, **45**, 4256

[37] J. Čižek, *Adv. Chem. Phys.*, 1969, **14**, 35

[38] G. D. Purvis and R. J. Bartlett, *J. Chem. Phys.*, 1982, **76**, 1910

[39] K. A. Brueckner, *Phys. Rev.*, 1954, **96**, 508

[40] R. K. Nesbet, *Phys. Rev.*, 1958, **109**, 1632

[41] N. C. Handy, J. A. Pople, M. Head-Gordon, K. Raghavachari and G. W. Trucks, *Chem. Phys. Lett.*, 1989, **164**, 185

[42] C. Møller and M. S. Plesset, *Phys. Rev.*, 1934, **46**, 618

[43] L. H. Thomas, *Proc. Camb. Phil. Soc.*, 1927, **23**, 542

[44] E. Fermi, *Z. Phys.*, 1928, **48**, 73

[45] E. Teller, *Rev. Mod. Phys.*, 1962, **34**, 627

[46] N. L. Balazs, *Phys. Rev.*, 1967, **156**, 42

[47] P. A. M. Dirac, *Proc. Camb. Phil. Soc.*, 1930, **26**, 376

[48] C. F. von Weizsacker, *Z. Physik*, 1935, **96**, 431

[49] C. H. Hodges, *Can. J. Phys.*, 1973, **51**, 1428

[50] K. Yonei and Y. Tomishima, *J. Phys. Soc. Jpn.*, 1965, **20**, 1051

[51] J. C. Slater, *Phys. Rev.*, 1951, **81**, 385

[52] P. Hohenberg and W. Kohn, *Phys. Rev. B.*, 1964, **136**, 864

[53] L. J. Sham and W. Kohn, *Phys. Rev. A.*, 1965, **140**, 1133

[54] M. Levy, *Phys. Rev. A.*, 1982, **26**, 1200

[55] E. H. Lieb, *Int. J. Quant. Chem.*, 1983, **24**, 243

[56] M. Levy, *Proc. Natl. acad. Sci. USA*, 1979, **76**, 6062

[57] M. Levy and J. P. Perdew in, *Density Functional Methods in Physics*, ed. R.M. Dreizler and J. da Providencia, Plenum, New York, 1985

[58] Q. Wu and W. Yang, *J. Chem. Phys.*, 2002, **118**, 2498

[59] Q. Zhao, R. C. Morrison and R. G. Parr, *Phys. Rev. A*, 1994, **50**, 2138

[60] D. J. Tozer, V. E. Ingamells, and N. C. Handy, *J. Chem. Phys.*, 1996, **105**, 9200

[61] D. M. Ceperley and B. J. Alder, *Phys. Rev. Lett.*, 1980, **45**, 566

[62] S. J. Vosko, L. Wilk and M. Nusair, *Can. J. Phys.*, 1980, **58**, 1200

[63] M. Ernzerhof, J. P. Perdew and K. Burke, *Top. Curr. Chem.*, 1996, **180**, 1

[64] A. D. Becke, *Phys. Rev. A.*, 1988, **38**, 3098

[65] C. Lee, W. Yang and R. G. Parr, *Phys. Rev. B.*, 1988, **37**, 785

[66] F. A. Hamprecht, A. J. Cohen, D. J. Tozer and N. C. Handy, *J. Chem. Phys.*, 1998, **109**, 6264

[67] J. P. Perdew, *Unified Theory of Exchange and Correlation Beyond the Local Density Approximation*, in Electronic Structure of Solids '91, edited by P. Ziesche and H. Eschrig, pages 11-20, 1991

[68] J. P. Perdew, K. Burke and M. Ernzerhof, *Phys. Rev. Lett.*, 1996, **77**, 3865

[69] T. W. Keal and D. J. Tozer, *J. Chem. Phys.*, 2003, **119**, 3015

[70] T. W. Keal and D. J. Tozer, *J. Chem. Phys.*, 2004, **121**, 5654

[71] J. P. Perdew and A. Zunger, *Phys. Rev. B.*, 1981, **23**, 5048

[72] J. P. Perdew, R. G. Parr, M. Levy and J. L. Balduz Jr., *Phys. Rev. Lett*, 1982, **49**, 1691

[73] D. J. Tozer and N. C. Handy, *J. Chem. Phys.*, 1998, **109**, 10180

[74] M. E. Casida, K. C. Casida, and D. R. Salahub, *Int. J. Quantum Chem.*, 1998, **70**, 933

[75] M. Grüning, O. V. Gritsenko, S. J. A. van Gisbergen, and E. J. Baerends, *J. Chem. Phys.*, 2001, **114**, 652

[76] Q. Wu, P. W. Ayers, and W. Yang, *J. Chem. Phys.*, 2003, **119**, 2978

[77] M. Mundt and S. Kümmel, *Phys. Rev. Lett.*, 2005, **95**, 203004

[78] D. J. Tozer, *J. Chem. Phys.*, 2003, **119**, 12697

[79] A. Dreuw, J. L. Weisman, and M. Head-Gordon, *J. Chem. Phys.*, 2003, **119**, 2943

[80] E. I. Proynov, A. Vela and D. R. Salahub, *Chem. Phys. Lett.*, 1994, **230**, 419

[81] M. Filatov and W. Thiel, *Phys. Rev. A.*, 1998, **57**, 189

[82] H. L. Schmider and A. D. Becke, *J. Chem. Phys.*, 1998, **109**, 8188

[83] R. Neumann and N. C. Handy, *Chem. Phys. Lett.*, 1997, **266**, 16

[84] J. P. Perdew, S. Kurth, A. Zupan and P. Blaha, *Phys. Rev. Lett.*, 1999, **82**, 2544

[85] J. Tao, J. P. Perdew, V. N. Staroverov and G. E. Scuseria, *Phys. Rev. Lett.*, 2003, **91**, 146401

[86] T. van Voorhis and G. E. Scuseria, *J. Chem. Phys.*, 1998, **109**, 400

[87] G. K. L. Chan, D. J. Tozer and N. C. Handy, *J. Chem. Phys.*, 1997, **107**, 1536

[88] A. D. Becke, *J. Chem. Phys.*, 2005, **122**, 064101

[89] J. Harris and R. O. Jones, *J. Phys. F.*, 1974, **4**, 1170

[90] O. Gunnarsson and B. I. Lundquist, *Phys. Rev. B.*, 1976, **13**, 4274

[91] D. C. Langreth and J. P. Perdew, *Phys. Rev. B.*, 1977, **15**, 2884

[92] J. Harris, *Phys. Rev. A.*, 1984, **29**, 1648

[93] A. D. Becke, *J. Chem. Phys.*, 1993, **98**, 1372

[94] P. J. Stevens, J. F. Devlin, C. F. Chabalowski, and M. J. Frisch, *J. Phys. Chem.*, 1994, **98**, 11623

[95] A. D. Becke, *J. Chem. Phys.*, 1997, **107**, 8554

[96] P. J. Wilson, T. J. Bradley and D. J. Tozer, *J. Chem. Phys.*, 2001, **115**, 9233

[97] K. Burke, M. Ernzerhof and J. P. Perdew, *Chem. Phys. Lett.*, 1997, **265**, 115

[98] R. T. Sharp and G. K. Horton, *Phys. Rev.*, 1953, **90**, 317

[99] J. D. Talman and W. F. Shadwick, *Phys. Rev. A.*, 1976, **14**, 36

[100] V. Sahni, J. Gruenebaum and J. P. Perdew, *Phys. Rev. B.*, 1982, **26**, 4371

[101] A. Görling and M. Levy, *Phys. Rev. A.*, 1994, **50**, 196

[102] A. Görling, *Phys. Rev. B.*, 1996, **53**, 7024; Errata 1999,**59**, 10370(E)

[103] M. Städele, J. A. Majewski, P. Vogl and A. Görling, *Phys. Rev. Lett.*, 1997, **79**, 2089

[104] M. Städele, M. Moukara, J. A. Majewski, P. Vogl and A. Görling, *Phys. Rev. B.*, 1999, **59**, 10031

[105] S. Ivanov, S. Hirata and R. J. Bartlett, *Phys. Rev. Lett.*, 1999, **83**, 5455

[106] A. Görling, *Phys. Rev. Lett.*, 1999, **83**, 5459

[107] S. Hirata, S. Ivanov, I. Grabowski, R. J. Bartlett, K. Burke and J. D. Talman, *J. Chem. Phys.*, 2001, **115**, 1635

[108] S. Hamel, M. E. Casida and D. R. Salahub, *J. Chem. Phys.*, 2002, **116**, 8276

[109] S. Kümmel and J. P. Perdew, *Phys. Rev. Lett.*, 2003, **90**, 043004

[110] L. Fritsche and J. Yuan, *Phys. Rev. A.*, 1998, **57**, 3425

[111] R. Colle and R. K. Nesbet, *J. Phys. B.*, 2001, **34**, 2475

[112] W. Yang and Q. Wu, *Phys. Rev. Lett.*, 2002, **89**, 143002

[113] L. Kleinman, *Phys. Rev. B.*, 1994, **49**, 14197

[114] F. Della Sala and A. Görling, *J. Chem. Phys.*, 2001, **115**, 5718

[115] R. D. Amos *et al.* CADPAC 6.5, *The Cambridge Analytic Derivatives Package*, 1998.

[116] H. R. Schwarz, H. Rutishauser and E. Stiefel in, *Numerical Analysis of Symmetric Matrices*, Translated by Paul Hertelendy, Prentice Hall Inc., Englewood Cliffs N.J., 1973

[117] F. Della Sala and A. Görling, *Phys. Rev. Lett.*, 2002, **89**, 033003

[118] F. Della Sala and A. Görling, *J. Chem. Phys.*, 2002, **116**, 5374

[119] A. Hesselmann and F.R. Manby, *J. Chem. Phys.*, 2005, **123**, 164116

[120] J. B. Krieger and G. J. Iafrate, *Phys. Rev. A.*, 1992, **45**, 101

[121] O. V. Gritsenko and E. J. Baerends, *Phys. Rev. A.*, 2001, **64**, 042506

[122] H. Partridge, *J. Chem. Phys.*, 1989, **90**, 1043

[123] S. Kümmel, *Private Communication*

[124] J. B. Krieger, Y. Li and G. J. Iafrate, *Phys. Rev. A.*, 1992, **46**, 5453

[125] E. Engel, A. Höck and R. M. Dreizler, *Phys. Rev. A.*, 2000, **62**, 042502

[126] Y. Li, J. B. Krieger and G. J. Iafrate, *Phys. Rev. A.*, 1993, **47**, 165

[127] T. Grabo, M. Petersilka and E. K. U. Gross, *J. Mol. Struct. (THEOCHEM)*, 2000, **501**, 353

[128] F. Della Sala and A. Görling, *Int. J. Quantum Chem.*, 2003, **91**, 131

[129] A. D. Becke, *Can. J. Chem.*, 1996, **74**, 995

[130] A. M. Lee, N. C. Handy, and S. M. Colwell, *J. Chem. Phys.*, 1995, **103**, 10095

[131] N. F. Ramsey, *Phys. Rev.*, 1950, **77**, 567

[132] N. F. Ramsey, *Phys. Rev.*, 1950, **78**, 699

[133] M. Peng, *Proc. Roy. Soc.*, 1941, **A178**, 449

[134] W. N. Lipscomb in, *Advances in Magnetic Resonance*, ed. J.S. Waugh, Academic Press, New York, 1966, Vol. 2, p137

[135] S. T. Epstein, *J. Chem. Phys.*, 1965, **42**, 2897

[136] W. Kutzelnigg, *Isr. J. Chem.*, 1980, **19**, 193

[137] M. Schindler and W. Kutzelnigg, *J. Chem. Phys.*, 1982, **76**, 1916

[138] F. London, *J. Phys. Radium*, 1937, **8**, 397

[139] H. F. Hameka, *Mol. Phys.*, 1958, **1**, 203

[140] J. A. Pople, *Mol. Phys.*, 1958, **1**, 175

[141] Aa. E. Hansen and T. D. Bouman, *J. Chem. Phys.*, 1985, **82**, 5035

[142] T. A. Keith and R. F. W. Bader, *Chem. Phys. Lett.*, 1992, **194**, 1

[143] P. J. Wilson and D. J. Tozer, *Chem. Phys. Lett.*, 2001, **337**, 341

[144] S. Huzinaga, *Approximate Atomic Functions*, University of Alberta, Edmonton, 1971

[145] W. Kutzelnigg, U. Fleischer and M. Schlindler in, *NMR-Basic Principles and Progress*, vol. 23, Springer, Heidelberg, 1990

[146] T. W. Keal, D. J. Tozer and T. Helgaker, *Chem. Phys. Lett.*, 2004, **391**, 374

[147] T. H. Dunning, *J. Chem. Phys.*, 1971, **55**, 716

[148] N. C. Handy and A. J. Cohen, *Mol. Phys.*, 2001, **99**, 403

[149] V. G. Malkin, O. L. Malkina, M. E. Casida and D. R. Salahub, *J. Am. Chem. Soc.*, 1994, **116**, 5898

[150] J. Poater, E. van Lenthe and E. J. Baerends, *J. Chem. Phys.*, 2003, **118**, 8584

[151] L. Olsson and D. Cremer, *J. Chem. Phys.*, 1996, **105**, 8995

[152] P. J. Wilson and D. J. Tozer, *J. Chem. Phys.*, 2002, **116**, 10139

[153] A. M. Teale and D. J. Tozer, *Chem. Phys. Lett.*, 2004, **383**, 109

[154] W. Hieringer, F. Della Sala and A. Görling, *Chem. Phys. Lett.*, 2004, **383**, 115

[155] A. V. Arbuznikov and M. Kaupp, *Chem. Phys. Lett.*, 2004, **386**, 8

[156] J. Gauss and J. F. Stanton, *J. Chem. Phys.*, 1996, **104**, 2574

[157] T. D. Bouman and A. E. Hansen, *Chem. Phys. Lett.*, 1990, **175**, 292

[158] K. Ruud, T. Helgaker, R. Kobayashi, P. Jørgensen, K. L. Bak, and H. J. A. Jensen, *J. Chem. Phys.*, 1994, **100**, 8178

[159] J. Gauss and J. F. Stanton, *J. Chem. Phys.*, 1995, **103**, 3561

[160] J. R. Cheeseman, G. W. Trucks, T. A. Keith, and M. J. Frisch, *J. Chem. Phys.*, 1996, **104**, 5497

[161] J. Gauss and J. F. Stanton, *J. Chem. Phys.*, 1995, **102**, 251

[162] J. Gauss, *Chem. Phys. Lett.*, 1992, **191**, 614

[163] H. Fukui, T. Baba, J. Narumi, H. Inomata, K. Miura, and H. Matsuda, *J. Chem. Phys.*, 1996, **105** 4692

[164] G. Menconi and D. J. Tozer, *Chem. Phys. Lett.*, 2002 , **360**, 38

[165] E. Runge and E. K. U. Gross, *Phys. Rev. Lett.*, 1984, **52**, 997

[166] R. van Leeuwen, *Phys. Rev. Lett.*, 1999, **82**, 3863

[167] R. van Leeuwen, *Phys. Rev. Lett.*, 1998, **80**, 1280

[168] M. E. Casida in, *Recent Developments and Applications in Density Functional Theory*, ed. J.M. Seminario, Elsevier, Amsterdam, 1996

[169] C. Van Caillie and R. D. Amos, *Chem. Phys. Lett.*, 1999, **308**, 249

[170] C. Van Caillie and R. D. Amos. *Chem. Phys. Lett.*, 2000, **317**, 159

[171] F. Furche, *J. Chem. Phys.*, 2001, **114**, 5982

[172] F. Furche and R. Ahlrichs, *J. Chem. Phys.*, 2002, **117**, 7433

[173] J. Hutter, *J. Chem. Phys.*, 2003, **118**, 3928

[174] M. Wanko, M. Garavelli, F. Bernardi, T. A. Niehaus, T. Frauenheim and M. Elstner, *J. Chem. Phys.*, 2004, **120**, 1674

[175] M. Odelius, D. Laikov and J. Hutter, *J. Mol. Struct. (THEOCHEM)*, 2003, **630**, 163

[176] S. B. Ben-Shlomo and U. Kaldor, *J. Chem. Phys.*, 1990, **92**, 3680

[177] E. S. Nielsen, P. Jørgensen and J. Oddershede, *J. Chem. Phys.*, 1980, **73**, 6238

[178] S. F. Boys and F. Bernardi, *Mol. Phys.*, 1970, **19**, 553

[179] R. Rydberg, *Z. Phys.*, 1931, **73**, 376

[180] O. Klein, *Z. Phys.*, 1932, **76**, 226

[181] A. L. G. Rees, *Proc. Phys. Soc.*, 1947, **59**, 998

[182] G. Wentzel, *Z. Phys.*, 1926, **38**, 518

[183] L. Brillouin, *Comptes Rendus*, 1926, **183**, 24

[184] H. A. Kramers, *Z. Phys.*, 1926, **39**, 828

[185] E. W. Kaiser, *J. Chem. Phys.*, 1970, **53**, 1686

[186] J. L. Dunham, *Phys. Rev.*, 1932, **41**, 721

[187] R. J. Le Roy, RKR1 2.0: A computer program Implementing the First-Order RKR method for Determining Diatomic Molecule Potential Energy Curves, University of Waterloo Chemical Physics Research Report CP-657 (2003). The source code and manual for this program may be obtained from the "Computer Programs" link at http://leroy.uwaterloo.ca

[188] R. R. Laher and F. R. Gilmore, *J. Phys. Chem. Ref. Data*, 1991, **20**, 685

[189] K. R. Lykke and B. D. Kay, *J. Chem. Phys.*, 1991, **95**, 2252

[190] T. F. Hansico and A. C. Kummel, *J. Phys. Chem.*, 1991, **95**, 8565

[191] A. Le Floch, *Mol. Phys.*, 1991, **72**, 133

[192] S. G. Tilford and J. D. Simmons, *J. Phys. Chem. Ref. Data*, 1972, **1**, 147

[193] R. J. Le Roy, LEVEL 7.5: A Computer Program for Solving the Radial Schrodinger Equation for Bound and Quasibound Levels, University of Waterloo Chemical Physics Research Report CP-655 (2002). The source code and manual for this program may be obtained from the "Computer Programs" link on the www site http://leroy.uwaterloo.ca

[194] K. P. Huber and G. Herzberg in, *Constants of Diatomic Molecules*, Van Nostrand Reinhold, New York, 1979

[195] W. Yang, P. W. Ayers and Q. Wu, *Phys. Rev. Lett.*, 2004, **92**, 146404

[196] Q. Wu and W. Yang, *J. Theo. Comp. Chem.*, 2003, **2**, 627

[197] E. Fermi and E. Amaldi, *Mem. R. Acad. Italia.*, 1934, **6**, 117

[198] C. G. Broyden, *Math. Comp.*, 1965, **19**, 577

[199] S. Ivanov, S. Hirata and R. J. Bartlett, *J. Chem. Phys.*, 2002, **116**, 1269

[200] W. H. Press, S. A. Teukolsky, W. T. Vetterling and B. P. Flannery, *Numerical Recipes*, Cambridge University, Cambridge, 1992

[201] A. N. Tikhonov and V. A. Arsenin, *Solution of Ill-posed Problems*, Winston & Sons, Washington, 1977

[202] S. Ivanov and M. Levy, *J. Chem. Phys.*, 2003, **119**, 7087

[203] N. C. Handy, M. T. Marron and H. J. Silverstone, *Phys. Rev.*, 1969, **180**, 45

[204] V. N. Staroverov, G. E. Scuseria and E. R. Davidson, *J. Chem. Phys.*, 2006, **124**, 141103

[205] J. E. Harriman, *Phys. Rev. A.*, 1983, **27**, 632

[206] J. E. Harriman and D. E. Hoch, *Int. J. Quantum. Chem.*, 1997, **63**, 111

[207] D. R. Rohr, O. V. Gritsenko and E. J. Baerends, *J. Mol. Stuct. (THEOCHEM)*, 2006, **762**, 193

[208] V. N. Staroverov, G. E. Scuseria and E. R. Davidson, *J. Chem. Phys.*, 2006, **125**, 081104

[209] Gaussian 03, Revision C.02, M. J. Frisch, G. W. Trucks, H. B. Schlegel, G. E. Scuseria, M. A. Robb, J. R. Cheeseman, J. A. Montgomery, Jr., T. Vreven, K. N. Kudin, J. C. Burant, J. M. Millam, S. S. Iyengar, J. Tomasi, V. Barone, B. Mennucci, M. Cossi, G. Scalmani, N. Rega, G. A. Petersson, H. Nakatsuji, M. Hada, M. Ehara, K. Toyota, R. Fukuda, J. Hasegawa, M. Ishida, T. Nakajima, Y. Honda, O. Kitao, H. Nakai, M. Klene, X. Li, J. E. Knox, H. P. Hratchian, J. B. Cross, V. Bakken, C. Adamo, J. Jaramillo, R. Gomperts, R. E. Stratmann, O. Yazyev, A. J. Austin, R. Cammi, C. Pomelli, J. W. Ochterski, P. Y. Ayala, K. Morokuma, G. A. Voth, P. Salvador, J. J. Dannenberg, V. G. Zakrzewski, S. Dapprich, A. D. Daniels, M. C. Strain, O. Farkas, D. K. Malick, A. D. Rabuck, K. Raghavachari, J. B. Foresman, J. V. Ortiz, Q. Cui, A. G. Baboul, S. Clifford, J. Cioslowski, B. B. Stefanov, G. Liu, A. Liashenko, P. Piskorz, I. Komaromi, R. L. Martin, D. J. Fox, T. Keith, M. A. Al-Laham, C. Y. Peng, A. Nanayakkara, M. Challacombe, P. M. W. Gill, B. Johnson, W. Chen, M. W. Wong, C. Gonzalez, and J. A. Pople, Gaussian, Inc., Wallingford CT, 2004.

[210] S. Liu and R. G. Parr, *Phys. Rev. A.*, 1996, **53**, 2211

[211] S. Liu, V. Karasiev, R. López-Boada and F. de Proft, *Int. J. Quant. Chem.*, 1998, **69**, 513

[212] A. J. Cohen, Q. Wu, and W. Yang, *Chem. Phys. Lett.*, 2004, **399**, 84

[213] M. J. Allen and D. J. Tozer, *J. Chem. Phys.*, 2002, **117**, 11113

[214] M. Ernzerhof and G. E. Scuseria, *J. Chem. Phys.*, 1999, **110**, 5029

[215] M. S. Miao, *Phil. Mag. B.*, 2000, **80**, 409

[216] N. F. Ramsey, *Molecular Beams*; Clarendon Press: Oxford, 2000.

[217] W. H. Flygare and C. H. Benson, *Mol. Phys.*, 1971, **20**, 225

[218] W. H. Flygare, *Chem. Rev.*, 1974, **74**, 653

[219] J. Gauss, K. Ruud and T. Helgaker, *J. Chem. Phys.*, 1996, **105**, 2804

[220] R. M. Stevens, R. M. Pitzer and W. N. Lipscomb, *J. Chem. Phys.*, 1963, **38**, 550

[221] H. M. Kelly and P. W. Fowler, *Chem. Phys. Lett.*, 1993, **206**, 568

[222] K. Ruud and T. Helgaker, *Chem. Phys. Lett.* 1997, **264**, 17

[223] J. F. Ogilvie, S.-L. Cheah, Y.-P. Lee and S. P. A. Sauer, *Theor. Chem. Acc.*, 2002, **108**, 85

[224] P.-O. Åstrand, K. Ruud, K. V. Mikkelsen and T. Helgaker, *Mol. Phys.*, 1997, **92**, 89

[225] P.-O. Åstrand, K. Ruud, K. V. Mikkelsen and T. Helgaker, *J. Chem. Phys.*, 1999, **110**, 9463

[226] K. Ruud, T. Helgaker and P. Jørgensen, *J. Chem. Phys.*, 1997, **107**, 10559

[227] K. Ruud, J. Vaara, J. Lounila and T. Helgaker, *Chem. Phys. Lett.*, 1998, **297**, 467

[228] C. E. Mohn, D. J. D. Wilson, O. B. Lutnæs, T. Helgaker and K. Ruud, *Adv. Quant. Chem.*, 2005, **50**, 77

[229] S. P. A. Sauer, *Adv. Quant. Chem.*, 2005,**48**, 319

[230] K. Ruud, P.-O. Åstrand and P. R. Taylor, *J. Chem. Phys.*, 2000, **112**, 2668

[231] S. M. Cybulski and D. M. Bishop, *J. Chem. Phys.*, 1997, **106**, 4082

[232] S. M. Cybulski and D. M. Bishop, *J. Chem. Phys.*, 1993, **100**, 2019

[233] J. Oddershede and J. R. Sabin, *Chem. Phys.*, 1988, **122**, 291

[234] S. P. A. Sauer, V. Špirko, I. Paidarová and J. Oddershede, *Chem.Phys.*, 1994, **184**, 1

[235] S. P. A. Sauer, V. Špirko, and J. Oddershede, *Chem. Phys.*, 1991, **153**, 189

[236] S. P. A. Sauer and J. F. Ogilvie, *J. Phys. Chem.*, 1994, **98**, 8617

[237] J. F. Ogilvie, J. Oddershede and S. P. A. Sauer, *Chem. Phys. Lett.*, 1994, **228**, 183

[238] J. Geertsen and G. E. Scuseria, *J. Chem. Phys.*, 1989, **90**, 6486

[239] S. P. A. Sauer, J. Oddershede and J. Geertsen, *Mol. Phys.*, 1992, **76**, 445

[240] S. P. A. Sauer, *Chem. Phys. Lett.*, 1996, **260**, 271

[241] K. Ruud, P.-O. Åstrand, T. Helgaker and K. V. Mikkelsen, *J. Mol. Struct. (THEOCHEM)*, 1996, **388**, 231

[242] P.-O. Åstrand, K. Ruud, K. V. Mikkelsen and T. Helgaker, *Chem. Phys. Lett.*, 1997, **271**, 163

[243] K. L. Bak, S. P. A. Sauer, J. Oddershede, and J. F. Ogilvie, *Phys. Chem. Chem. Phys.*, 2005, **7**, 1747

[244] P. J. Wilson, R. D. Amos and N. C. Handy, *J. Mol. Struct.*, 2000, **506**, 335

[245] D. J. D. Wilson, C. E. Mohn and T. Helgaker, *J. Chem. Theory Comput.*, 2005, **1**, 877

[246] DALTON, a molecular electronic structure program, Release 2.0 (2005), see http://www.kjemi.uio.no/software/dalton/dalton.html

[247] O. B. Lutnæs, *Private Communication*

[248] R. A. Kendall and T. H. Dunning Jr., *J. Chem. Phys.*, 1992, **96**, 6796

[249] D. E. Woon and T. H. Dunning Jr., *J. Chem. Phys.*, 1993, **98**, 1358

[250] A. K. Wilson, D. E. Woon, K. A. Peterson and T. H. Dunning, *J. Chem. Phys.*, 1999, **110**, 7667

[251] T. Tanaka and Y. Morino, *J. Mol. Spectrosc.*, 1970, **33**, 538

[252] W. Hüttner, U. E. Frank, W. Majer, K. Mayer, and V. Špirko, *Mol. Phys.*, 1988, **64**, 1233

[253] S. L. Rock and W. H. Flygare, *J. Chem. Phys.*, 1972, **56**, 4723

[254] T. W. Keal and D. J. Tozer, *J. Chem. Phys.*, 2005, **123**, 121103

[255] M. Bühl, *Magn. Reson. Chem.*, **44**, 2006, **44**, 661

[256] M. Bühl and F. T. Mauschick, *Magn. Reson. Chem.*, 2004, **42**, 737

[257] P. J. Wilson, R. D. Amos and N. C. Handy, *Phys. Chem. Chem. Phys.*, 2000, **2**, 187

[258] S. Grigoleit and M. Bühl, *Chem. Eur. J.*, 2004, **10**, 5541

[259] M. Kaupp, O. L. Malkina and V. G. Malkin, *J. Chem. Phys.*, 1997, **106**, 9201

[260] J. Li, G. Schreckenbach and T. Ziegler, *J. Am. Chem. Soc.*, 1995, **117**, 486

[261] M. Bühl and F. A. Hamprecht, *J. Comput. Chem.*, 1998, **19**, 113

[262] R. Bouten, E. J. Baerends, E. van Lenthe, L. Visscher, G. Schreckenbach and T. Ziegler, *J. Phys. Chem. A.*, 2000, **104**, 5600

[263] M. Bühl, *Theor. Chem. Acc.*, 2002, **107**, 336

[264] M. A. Watson, N. C. Handy, A. J. Cohen and T. Helgaker, *J. Chem. Phys.*, 2004, **120**, 7252

[265] A. J. Cohen, *Private Communication*

[266] A. J. H. Wachters, *J. Chem. Phys.*, 1970, **52**, 1033

[267] C. J. Umrigar and X. Gonze, *Phys. Rev. A.*, 1994, **50**, 3827

[268] J. P. Snyder, N. S. Chandrakumar, S. N. Rao, D. P. Spangler and D. C. Lankin, *J. Am. Chem. Soc.*, 1993, **115**, 3356

[269] J. P. Snyder, N. S. Chandrakumar, H. Sato and D. C. Lankin, *J. Am. Chem. Soc.*, 2000, **122**, 544

[270] A. M. Sum, D. C. Lankin, K. Hardcastle and J. P. Snyder, *Chem. Eur. J.*, 2005, **11**, 1579

[271] J. P. Snyder, G. L. Grunewald, F. A. Romero, I. Y. Oren and D. C. Lankin, *Org. Lett*, 2004, **4**, 3557

[272] S. Wolfe, *Acc. Chem. Res.*, 1972, **5**, 102

[273] S. F. Nelsen, *Acc. Chem .Res.*, 1978, **11**, 14

[274] P. R. Rablen, R. W. Hoffmann, D. A. Horvat and W. T. Borden, *J. Chem. Soc.*, Perkin Trans 2., 1999, 1719

[275] D. O'Hagan, C. Bilton, J. A. K. Howard, L. Knight and D. J. Tozer, *J. Chem. Soc.*, Perkin Trans. 2., 2000, 605

[276] C. R. S. Briggs, D. O'Hagan, H. S. Rzepa and A. M. Z. Slawin, *J. Fluorine Chem.*, 2004, **125**, 19

[277] C. R. S. Briggs, M. J. Allen, D. O'Hagan D. J. Tozer A. M. Z. Slawin, A. E. Goeta , and J. A. K. Howard, *Org. Biomol. Chem.*, 2004, **2**, 732

[278] J. A. K. Howard, V. J. Hoy, D. O'Hagan and G. T. Smith, *Tetrahedron*, 1996, **52**, 12613

[279] J. D. Dunitz and R. Taylor, *Chem. Eur. J.*, 1997, **3**, 89

[280] J. D. Dunitz, *ChemBioChem*, 2004, **5**, 614

[281] 3-Fluoroazetidinium chloride was obtained from the GSK compound collection.

[282] L. Provins, B. J. Van Keulen, J. Surtees, P. Talaga and B. Christophe, PCT Int. Appl. WO 2003 087064 A1.